



INOWAS Book Series

DISSERTATION

FELIX BARQUERO KAMRATH

Infiltration capacity assessment of managed
aquifer recharge spreading basins under
variable climates

Beiträge zu Abfallwirtschaft / Altlasten – Volume 108

Beiträge zu Abfallwirtschaft/Altlasten

Scientific series of the Institute of Waste Management and
Circular Economy
Technische Universität Dresden

Vol. 108 Dissertation

**Infiltration capacity assessment of
managed aquifer recharge
spreading basins under variable
climates**

Publisher: **Eigenverlag des Forums für
Abfallwirtschaft und Altlasten e.V.**

Forum für Abfallwirtschaft und Altlasten e.V.
Pratzschwitzer Straße 15
01796 Pirna
Germany

Print: **Reprogress GmbH**

Chemnitzer Straße 46b
01187 Dresden
info@reprogress.de
Tel.: 0351 47898 0

© All rights reserved. No part of this publication may be reproduced, stored in a retrieval system, or transmitted, in any form or by any means without the prior written permission of the publisher, nor be otherwise circulated in any form of binding or cover other than that in which it is published and without a similar condition being imposed on the subsequent purchaser.

Dissertation

Infiltration capacity assessment of managed aquifer recharge spreading basins under variable climates

Felix Barquero Kamrath

Editor

Prof. Dr.-Ing. habil. Christina Dornack

Beiträge zu Abfallwirtschaft/Altlasten

Scientific series of the Institute of Waste Management and
Circular Economy
Technische Universität Dresden

Vol. 108

ISBN 978-3-94923-01-4

2020

1st edition

INFILTRATION CAPACITY ASSESSMENT OF MANAGED AQUIFER RECHARGE SPREADING BASINS UNDER VARIABLE CLIMATES

Dissertation

for the award of the degree of

Doctor Ingenieur

(Dr. -Ing)

submitted to

the Faculty of Environmental Sciences
of the Technische Universität Dresden

by

M.Sc. Felix Barquero Kamrath

Born on April 11th, 1989 in Freiberg, Saxony

Submitted on: 21.11.2019

Defense date: 03.04.2020

Reviewers:

Dr. Catalin Stefan, Technische Universität Dresden

Prof. Dr. Rudolf Liedl, Technische Universität Dresden

Dr. Enrique Fernández Escalante, Tragsa Consultant Group, Madrid

ABSTRACT

Managed aquifer recharge (MAR) consists in the intentional recharge of water to aquifers and represents an adaptation measure to reduce vulnerability to climate change. One of the most common MAR methods is spreading surface, which requires a large area of land. However, it provides an additional treatment of the infiltrated water as it flows through the vadose zone. Recharging the aquifer via spreading methods has been successful at many sites. Nevertheless, these techniques also present some challenges, for example the development of a clogging layer in the infiltration basins that creates a reduction of the infiltration capacity of the recharge site.

This thesis determines the influence of climate related parameters (temperature and solar irradiance) in the reduction of infiltration capacity in different hydraulic scenarios. It also investigated the efficiency of a recovery method of already clogged infiltration ponds, and finally it developed methods based on soil water content to anticipate severe clogging states. For these objectives, three physical experimental models were constructed in the field and laboratory of the INOWAS research group, located in the city of Pirna, Germany.

The field rapid infiltration unit consisted in a 30 m³ trench filled with a sandy soil and contained sensors monitoring matric potential, water content, electrical conductivity, and temperature. Elbe River water was infiltrated under variable climatic conditions and hydraulic cycles. Tracer tests with Sodium chloride (NaCl) assisted the determination of the infiltration capacity reduction of the soil in each scenario. A warmer climate improved the living conditions of algae and microorganisms, resulting in the development of a biofilm layer that increased the flow resistance of the medium. On the other hand, an additional cause for the infiltration reduction, in the colder conditions, is the increase of the dynamic viscosity of water.

Since controlling solar irradiance in the field is challenging, a set of soil columns were installed in the laboratory and run in four light scenarios, including fractions of light and darkness. Water from the Elbe River water was continuously infiltrated maintaining a constant head. The main result of the infiltration experiment indicates that infiltrating during the night reduces clogging by 30 % in comparison to the scenario with daylight.

Nevertheless, no matter the given climatic conditions, clogging of the basin is not to be completely avoided. That is why the third infiltration setup investigated the effectiveness of scraping measures in the laboratory. Two infiltration tanks were filled with the same sand applied in the experiments described above. One tank was operated without any scraping, whereas scraping was performed in the second tank four times. Elbe River water was infiltrated continuously in both units. After the basin surface was scraped for the first time (about 1 cm depth), the infiltration capacity recovered completely, but not for a long period. The decrease of the infiltration capacity occurred every time faster, and after the fourth scraping, the recovery of the infiltration capacity represented only 60 % of the initial conditions.

The last investigation conducted in this thesis corresponds to the development of techniques to monitor the infiltration capacity in MAR basins. Water content data can identify changing conditions of the infiltration capacity of the medium. Linear regression equations using the methods of "*Root mean square displacement*" (D_{RMS}) and "*Mean water content*" (WC) can simulate a good fit with the results of the tracer tests.

The obtained results enable operators of recharge sites to better prepare for future climatic conditions. According to the IPCC (Intergovernmental Panel on Climate Change) simulations, operators can expect higher or lower favorable conditions for clogging development in the future. The site operators can increase the hydraulic loading rate of their basin or also increase the frequency of clogging management procedures (e.g. scraping). However, it must be considered that with more frequent scraping events, the recovery of the infiltration capacity will be less efficient, so that alternative methods (e.g. plowing techniques) should be applied after a certain period. Finally, the best time to scrape the basin and maximize the amount of recharged water can be determined using the developed water content-based methods.

ZUSAMMENFASSUNG

Die künstliche Grundwasseranreicherung (engl. managed aquifer recharge, MAR) ist eine Maßnahme gegen die negativen Auswirkungen einer Übernutzung der Grundwasserressourcen und umfasst die gezielte Versickerung von Oberflächenwasser in den Grundwasserleiter. Die Oberflächeninfiltrationsmethoden (engl. spreading methods) gehören zu den am häufigsten eingesetzten MAR-Methoden. Sie benötigen größere Flächen, ermöglichen aber die Qualität des infiltrierten Wassers auf dem Weg durch die ungesättigte Bodenzone zu verbessern. Die Grundwasseranreicherung mittels Oberflächeninfiltrationsmethoden ist an vielen Standorten erfolgreich. Sie ist aber auch mit Problemen verbunden, wie z.B. die Bildung einer Kolmationsschicht in den Infiltrationsbecken, die eine Reduzierung der Infiltrationskapazität bewirkt.

In der vorliegenden Arbeit wurde der Einfluss klimarelevanter Parameter (Temperatur und Sonneneinstrahlung) auf die Reduzierung der Infiltrationskapazität untersucht. Des Weiteren wurde getestet, inwieweit sich die Infiltrationskapazität nach Entfernen der oberen, kolmatierten Bodenschicht im Infiltrationsbecken wiederherstellen lässt. Darüber hinaus wurden Methoden auf Grundlage des Bodenwassergehaltes entwickelt, mit denen eine Abschätzung des fortschreitenden Kolmatierungszustandes möglich ist. Um diese Ziele zu erreichen, wurden drei Versuchseinheiten im Feld und Labor aufgebaut.

Für die Simulation einer Infiltrationsbeckenanlage im Feldmaßstab erfolgte der Einbau einer Infiltrationseinheit (30 m³). Zur Überwachung von Matrixpotenzial, Wassergehalt, elektrischer Leitfähigkeit und Temperatur erfolgte der Einbau von Sensoren in drei verschiedenen Tiefen. Elbwasser wurde unter wechselnden klimatischen Bedingungen (kalt, mild und warm) und mit verschiedenen hydraulischen Beladungszyklen (1:3, 1:1, 3:1 und kontinuierlich) infiltriert. Tracer-Tests mit Natriumchlorid (NaCl) unterstützten bei der Bestimmung der Reduzierung der Infiltrationskapazität des Bodens. Die Ergebnisse zeigen, dass ein wärmeres Klima die Wachstumsbedingungen von Algen und Mikroorganismen verbessert und damit auch die Entwicklung einer Biofilmschicht fördern, was den Strömungswiderstand des Mediums erhöht. Bei kälterem Klima ist die Erhöhung der dynamischen Viskosität des Wassers ein zusätzlicher Faktor für die Reduzierung der Infiltrationskapazität.

Da die Variation der Sonneneinstrahlung unter Feldbedingungen, welche die Kolmationsprozesse entscheidend beeinflusst, schwierig ist, erfolgte die Durchführung von Säulenversuchen mit vier unterschiedlichen Lichtszenarien mit unterschiedlicher Wellenlänge entsprechend unterschiedlicher Wetterlagen sowie Dunkelheit. Die Ergebnisse zeigen, dass eine Infiltration während der Nachtstunden ohne Sonneneinstrahlung die Kolmatierung um 30 % im Vergleich zu den Szenarien mit Sonneneinstrahlung reduziert.

In einem weiteren Infiltrationsversuch im Labormaßstab wurde untersucht, welche Auswirkung das Entfernen der oberen kolmatierten Bodenschicht auf die Wiederherstellung der ursprünglichen Infiltrationskapazität hat. In zwei kleinskaligen Versuchseinheiten wurde kontinuierlich Elbwasser infiltriert. Nach Auftreten von Kolmationserscheinungen wurde jeweils die oberste kolmatierte Bodenschicht entfernt. Die Ergebnisse zeigen, dass sich die Infiltrationskapazität nach dem ersten Entfernen der Kolmationsschicht vollständig wiederherstellen lässt. Allerdings konnte festgestellt werden, dass die Infiltrationskapazität nach jedem weiteren Entfernen des kolmatierten Bodens schneller abnahm. Des Weiteren konnte nachgewiesen werden, dass nach mehrmaligem Entfernen der Kolmationsschicht eine vollständige Wiederherstellung der Infiltrationskapazität nicht mehr möglich ist.

In dem letzten Arbeitsschritt erfolgte die Entwicklung einer Methode zur Überwachung der veränderlichen Infiltrationskapazität in Infiltrationsbecken. Dabei wurden die gemessenen Wassergehaltsdaten sowie die Ankunftszeit des infiltrierten Wassers an den Sensoren genutzt, um wechselnde Infiltrationskapazitäten des Mediums darzustellen. Die Ergebnisse wurden mittels Tracertests validiert.

Die im Rahmen dieser Arbeit erzielten Ergebnisse ermöglichen es den Betreibern von Infiltrationsanlagen den Betrieb, auch im Hinblick auf zukünftige klimatische Bedingungen, effizienter zu gestalten. Entsprechend der IPCC-Simulationen (engl. Intergovernmental Panel on Climate Change) können sie Maßnahmen treffen, um die Entstehung von Kolmation zu reduzieren oder zu verzögern. Dies kann durch die Anpassung der hydraulischen Beladungsrate oder der Häufigkeit des Entferns der Kolmationsschicht erfolgen. Es ist jedoch zu beachten, dass bei häufiger Entfernung der kolmatierten Bodenschicht die Wiederherstellung der Infiltrationskapazität ineffizienter wird, sodass nach einer gewissen Zeit andere Methoden angewendet werden sollten. Der optimale Zeitpunkt, um das Becken von der Kolmationsschicht zu befreien und die Menge des infiltrierten Wassers zu maximieren, kann durch die entwickelten, wassergehaltsbasierten Methoden zur Ermittlung der veränderlichen Infiltrationskapazität abgeschätzt werden.

RESUMEN

El manejo de recarga de acuíferos (del inglés. managed aquifer recharge, MAR) consiste en la recarga intencional de agua a los acuíferos y representa una medida de adaptación para reducir la vulnerabilidad al cambio climático. Los métodos de esparcimiento (spreading methods) son uno de los métodos de MAR más comunes. Requieren mayores áreas de terreno, pero ofrecen un tratamiento adicional de filtración del agua a medida que esta fluye a través de la zona vadosa. La recarga del acuífero mediante métodos de esparcimiento ha tenido éxito en muchos sitios. Sin embargo, estas técnicas también presentan algunos desafíos como por ejemplo el desarrollo de una capa de obstrucción en las piscinas de infiltración que crea una reducción de la capacidad de infiltración del sitio de recarga.

Esta tesis investigó la influencia de los parámetros relacionados con el clima (temperatura e irradiancia solar) en la reducción de la capacidad de infiltración. También determinó la eficiencia de recuperación de piscinas de infiltración obstruidas después del raspado de la capa superior y finalmente desarrolló métodos basados en el contenido de agua en el suelo para anticipar estados de obstrucción severos. Para estos objetivos se construyeron tres modelos experimentales físicos en el campo y laboratorio del grupo de investigación INOWAS, ubicado en la ciudad de Pirna, Alemania.

La unidad de infiltración en el campo consistió en una zanja rellena con material arenoso y sensores para monitorear la tensión, el contenido de agua, la conductividad eléctrica y la temperatura en el subsuelo. El agua del río Elba se infiltró en diferentes condiciones climáticas (frío, moderado y caliente) y ciclos de carga hidráulica (1:3, 1:1, 3:1 y flujo continuo). Las pruebas de trazador con cloruro de sodio (NaCl) ayudaron a determinar la capacidad de reducción de la infiltración del suelo. Un clima cálido mejoró las condiciones de crecimiento de algas y microorganismos y por lo tanto también el desarrollo de una biopelícula que aumentó la resistividad del flujo del medio. Por otro lado, una causa adicional para la reducción de la infiltración en las condiciones más frías es el aumento de la viscosidad dinámica del agua.

Dado que el control de las condiciones de irradiancia solar en el campo es difícil, se instalaron columnas de suelo en el laboratorio, las cuales trabajaron bajo cuatro escenarios de fracciones de luz, incluyendo un escenario de oscuridad. Agua del río Elba fue continuamente infiltrada con una cabeza constante. El principal resultado del experimento de infiltración indica que la infiltración durante la noche reduce la obstrucción de los poros del suelo en un 30 % en comparación con el escenario con irradiación solar.

El tercer sistema de infiltración investigó la eficiencia de las medidas de raspado en piscinas de infiltración que ya están bloqueadas. Se llenaron dos tanques de infiltración con el mismo material arenoso. Un tanque trabajó sin raspado, mientras que en el segundo tanque el raspado se realizó en cuatro ocasiones. Después que la superficie de la piscina fue raspada por primera vez, la capacidad de infiltración se recuperó completamente, pero no por un largo período. La disminución de la capacidad de infiltración se produjo cada vez más rápido y después del cuarto raspado la recuperación de la capacidad de infiltración representó sólo el 60 % de las condiciones iniciales.

La última investigación de esta tesis corresponde a técnicas alternativas para monitorear la capacidad de infiltración en piscinas de MAR. Los datos de contenido de agua en el suelo pueden identificar las condiciones cambiantes de la capacidad de infiltración del medio. Las ecuaciones de regresión lineal utilizando los métodos de "*desplazamiento del error cuadrado medio*" (D_{RMS}) y "*contenido de agua medio*" (WC) consiguen simular satisfactoriamente los resultados obtenidos con las pruebas de trazador.

Los resultados obtenidos permiten que los operadores de los sitios de recarga puedan prepararse mejor para posibles condiciones climáticas futuras. De acuerdo con las simulaciones del IPCC (del inglés Intergovernmental Panel on Climate Change), los operadores pueden determinar la evolución de las condiciones de obstrucción de las piscinas de infiltración. Los operadores pueden variar la tasa de carga hidráulica de la piscina o aumentar la frecuencia de procedimientos de manejo de obstrucciones (por ejemplo, raspado). Sin embargo, hay que tener en cuenta que, con más eventos de raspado, la recuperación de la capacidad de infiltración será cada vez menos eficiente, por lo que se deben aplicar métodos alternativos después de un cierto período de tiempo. Finalmente, el mejor momento para raspar la piscina y maximizar la cantidad de agua de recarga, puede ser manejado por los métodos desarrollados basados en el contenido de agua.

ACKNOWLEDGMENTS

The thesis was performed in the frame of the Research Group INOWAS at the Institute of Waste Management and Circular Economy at the Technische Universität Dresden, in Pirna, Germany. First, I want to acknowledge the funding for the INOWAS Junior Research Group, grant number 01LN1311A by the German Federal Ministry of Education and Research (BMBF).

Most of all, I want to thank Dr. Catalin Stefan for accepting me in the INOWAS Research Group and giving me the one in a life opportunity to work on my PhD. Additionally, his critics, suggestions and advices helped me to improve not just my work but also myself as a person. He is for me not just the leader of the research group or my supervisor, but also a good friend!

Special thanks to Prof. Dr. Rudolf Liedl for helping me and guiding me in the design of my experiments and thesis. To Dr. Enrique Fernández Escalante my deep appreciation for accepting to be my supervisor in such a short notice.

I want to thank all my colleagues of the INOWAS family that turned very special to me within these four years of co-work. Thomas, thanks for sharing your expertise in sensors, soil and water, so as Football, Hockey and life. I really learned a lot from the “local player of Pirna”. Jana G., thanks for the critic and support to my written report. Claudia, I really appreciate the help that you gave me, especially dealing with the German public offices. Fritz, Jana S., José B., Ralf, thank you very much for your fruitful conversations in the topic of MAR.

To all my students that helped me with their research, I want to thank, especially thanks to Andreas, José H., Muqet, Rezwana, Hafsa, Nathan and Johanna.

I would not have reached this without the lovely and helpful support of my family in Germany and Nicaragua. This work is dedicated to the two most special women in my life: my mom and my wife. During my PhD. studies, both had to deal with a severe illness and as true warriors; they managed to remain victorious, even in the most adverse situation. They inspire me to keep up with my work and always give the best in me. Thanks to both of you. I love you!

LIST OF CONTENTS

Abstract.....	I
Zusammenfassung	III
Resumen.....	V
Acknowledgments	VII
List of Contents.....	1
List of Figures	X
List of Tables	XII
Acronyms.....	XIII
1 Introduction	1
1.1 Motivation.....	2
1.2 Objectives	3
1.3 Thesis structure	3
2 Theoretical background	5
2.1 Managed aquifer recharge.....	5
2.2 Clogging in MAR.....	13
2.3 Management of clogging	18
2.4 MAR-relevant soil parameters	20
2.4.1 Hydraulic conductivity	20
2.4.2 Soil water content	22
2.4.3 Electrical conductivity	23
2.5 MAR-relevant climate properties.....	25
2.5.1 Solar irradiance.....	26
2.5.2 Temperature	27
3 Site description.....	29
3.1 Study area.....	29
3.2 Climate	29
3.3 Elbe River	33
3.4 Hydrogeology	34
4 Methodology.....	40
4.1 Influence of climate on infiltration basin recharge	40
4.1.1 Temperature	40
4.1.2 Solar irradiance.....	47
4.2 Management of clogging in spreading basins.....	50
4.3 Determination of infiltration capacity using water content.....	55
4.3.1 Tracer method	55

4.3.2	Libardi method	55
4.3.3	Root mean square method.....	57
4.3.4	Water content method	57
4.3.5	Trigger time method	57
5	Results and discussion	59
5.1	Influence of climate on infiltration basins.....	59
5.1.1	Temperature	59
5.1.2	Solar irradiance.....	74
5.2	Management of clogging in spreading basins.....	80
5.2.1	Recovery of infiltration capacity by scraping in field unit	80
5.2.2	Recovery of infiltration capacity by scraping in lab units	81
5.3	Determination of infiltration capacity using water content.....	85
5.3.1	Tracer method	85
5.3.2	Libardi method	85
5.3.3	Root mean square method.....	87
5.3.4	Water content method	87
5.3.5	Trigger time method	88
5.3.6	Validation process	89
6	Conclusions.....	93
7	Limitations and outlook	95
8	Bibliography	96
A.1.	List of publications.....	109
A.1.1	List of peer reviewed journal articles	109
A.1.2	List of conference proceedings (only first author).....	109
A.2	Geology of the Elbtal Group	110
A.3	Supplementary material	114

LIST OF FIGURES

Figure 1.1. Regional warming in the decade 2006–2015	1
Figure 1.2. Overview of the thesis main investigation areas to assess clogging	3
Figure 2.1. Global evolution of MAR capacity by decade	5
Figure 2.2. Framework for the feasibility of managed aquifer recharge	6
Figure 2.3. Main components of a MAR scheme based on surface spreading basins	8
Figure 2.4. Filtration mechanisms of suspended particles	14
Figure 2.5. Dependence of the saturated hydraulic conductivity ratio.	15
Figure 2.6. Phases of growth rate of bacteria	16
Figure 2.7. Clogging mechanisms diagram of iron (III) in the saturated zone	17
Figure 2.8. Biochemically produced gas bubbles and entrapped air bubbles	17
Figure 2.9. Scraping of the top layer of clogged infiltration basins in the USA.....	18
Figure 2.10. Tillage tools used for recovery of the infiltration rate in SAT recharge basins .	19
Figure 2.11. Main components of a water-filled tensiometer lying horizontally in the soil ..	21
Figure 2.12. Soil moisture retention curve for clay, loam and sand	22
Figure 2.13. Differences in the measurement principle for TDR and FDR sensors.....	23
Figure 2.14. Main components of UMP sensor measuring WC, EC & T in soils	23
Figure 2.15. Spectra irradiance ranges at sea level	26
Figure 2.16. Photosynthesis process of 4 algae types depending on the temperature.	27
Figure 3.1. Location of investigation site in Pirna	29
Figure 3.2. Yearly average of mean monthly temperature in Pirna	30
Figure 3.3. Mean monthly temperature in Pirna in period 2009 - 2019	30
Figure 3.4. Mean monthly precipitation and solar irradiance in Pirna	31
Figure 3.5. Mean cloud cover for the period of 1991 - 2008 and daylight variation	31
Figure 3.6. Mean and maximum wind velocity for the period of 2009 - 2019 in Pirna	32
Figure 3.7. Monthly precipitation distribution for the period of 2009 to 2019 in Pirna	32
Figure 3.8. Monthly snowfall (cm) for the period of 2010 to 2019 in Pirna	33
Figure 3.9. Daily precipitation, groundwater level, and Elbe River stage in 2017	33
Figure 3.10. Geologic map of the region of Pirna	36
Figure 3.11. Correlation of the Strehlen Limestone with the Zeichen Clay	37
Figure 3.12. Layer profile determination at the INOWAS test field	37
Figure 3.13. DPIL soundings measured at location G15 and DPST K values.....	38
Figure 3.14. Groundwater elevation model and location of drilling points in Pirna	39
Figure 4.1. Excavation of topsoil at the test field and dimensions of the infiltration unit ..	41
Figure 4.2. Grain size distribution of two soil samples of selected packing material	41
Figure 4.3. Compaction of soil at 1 m depth with a vibratory plate compactor.	42
Figure 4.4. Profile view of the infiltration unit and bird view of the infiltration unit	43
Figure 4.5. Installation of measuring devices in Layer 1, Layer 2, and Layer 3.....	43
Figure 4.6. Location of monitoring wells from in a sketch view and a satellite view	44
Figure 4.7. Well design and lithology profile of wellfield at Pirna.....	44
Figure 4.8. Soil samples collected from the borehole of I-02.....	45
Figure 4.9. Simplified sketch of MAR field site components	46
Figure 4.10. Experimental setup components	48
Figure 4.11. Schematic representation of the experiment system.	50
Figure 4.12. Schematic sketch of the spreading infiltration tank.	51
Figure 4.13. Schematic sketch of the water storage and distribution system.	52
Figure 4.14. Schematic sketch of water distribution, drainage system and EC monitoring apparatus	53
Figure 4.15. Smoothed semi-log model designed for the empirical determination of K.	56

Figure 5.1.	Variation of the temperature and solar irradiance during the experiments.....	59
Figure 5.2.	Soil temperature at Scenario 1 depths in the 3 climate scenarios.	61
Figure 5.3.	Overview of the ICRC change in different climates for 4 Scenarios.....	63
Figure 5.4.	Monitoring of the solar irradiance and air temperature.....	64
Figure 5.5.	Hourly air temperature and theoretical influence of the dynamic viscosity	64
Figure 5.6.	Overview of the ICRC change in different HLC scenarios.....	65
Figure 5.7.	Water content trigger velocity for the Layer 1, Layer 2, and Layer 3 for Sc.1	67
Figure 5.8.	Water content trigger velocity for the Layer 1, Layer 2, and Layer 3 for Sc.4....	68
Figure 5.9.	Water content trigger velocity for Layer 1 (28 cm depth; Sensor 1.2)	69
Figure 5.10.	Soil temperature at depth of 28 cm, 70 cm, and 140 cm	70
Figure 5.11.	Time to reach maximum temperatures after each infiltration cycle.....	71
Figure 5.12.	TOC in the surface of the infiltration basin grouped by scenarios	72
Figure 5.13.	Clogging of the surface of the infiltration basin at the end of the Scenario 1...	72
Figure 5.14.	TOC in the surface of the infiltration basin grouped by climates	73
Figure 5.15.	Effect of recharged water in the monitoring well.....	73
Figure 5.16.	Variation in the infiltration rates of Elbe River water for 90 % salt recovery	75
Figure 5.17.	Mean infiltration rates for 90% recovery using Elbe River water	76
Figure 5.18.	Relative difference in clogging between light scenarios.....	76
Figure 5.19.	Variations in the outflow rates of the soil columns with Elbe river water	77
Figure 5.20.	Mean infiltration rates for 90% recovery of tap water	78
Figure 5.21.	Days of infiltration before occurrence of basin overflow & scraping intervals	80
Figure 5.22.	State of the basin (a) before scraping, (b) after the scraping.....	80
Figure 5.23.	Infiltration capacity reduction in Tank 1 and Tank 2.....	82
Figure 5.24.	Infiltration capacity reduction in Tank 2 after each scraping event.....	83
Figure 5.25.	Infiltration capacity curve determined by tracer experiments	85
Figure 5.26.	Water content decrease during the drying cycles in the first 100 min.....	86
Figure 5.27.	ICRC comparison between Libardi method & Tracer curve	86
Figure 5.28.	Comparison between tracer curve and LR DRMS-based curve	87
Figure 5.29.	Comparison between tracer curve and LR WC-based curve	88
Figure 5.30.	Comparison between tracer curve and LR TT-based curve	89
Figure 5.31.	Correlation between the raw data of ICRC.....	92
Figure 0.1.	Chrono-, bio and lithostratigraphy of the Saxonian Cretaceous.....	110
Figure 0.2.	Sketch of sandstone structures in the region of Pirna	111
Figure 0.3.	Legend of geologic map of the region of Pirna	112
Figure 0.4.	Isolines of the absolute height of the Quaternary basis	113

LIST OF TABLES

Table 2.1. Classification of specific MAR methods (Stefan and Ansems, 2018)	7
Table 2.2. Operational information of selected recharge basins all over the globe	9
Table 2.3. Examples for typical wet/dry ratios for SAT systems in the USA.	13
Table 3.1. Hydraulic conductivity distribution of subsurface soil a test site Pirna	39
Table 4.1. Particle size analysis of the packing material of the infiltration unit	41
Table 4.2. Definition of experimental infiltration periods	47
Table 4.3. Recharging water characteristics	48
Table 5.1. Climatic description of the 20 infiltration Runs	60
Table 5.2. Climate category's intervals	61
Table 5.3. Runs and their corresponding climate characterization.....	61
Table 5.4. Summary of iron and manganese mean concentrations	78
Table 5.5. Mean TOC and the respective standard deviation	79
Table 5.6. Total suspended solids concentration in the Elbe River Water.	81
Table 5.7. DOC data in the inflow and outflow of the infiltration tanks	81
Table 5.8. Summary of D_{RMS} (%), WC (%), TT (min) raw data and tracer test (-) values.	90

ACRONYMS

Abbreviations

ASR:	Aquifer Storage and Recovery
ASTR:	Aquifer Storage, Transfer and Recovery
DIPL:	Direct Injection Pushing Logger
DOC:	Dissolved Organic Carbon
DPST:	Direct Push Slug Test
D _{RMS} :	Displacement of Root Mean Square
EC:	Electrical Conductivity
EPS:	Extracellular Polymeric Substances
FC:	Field Capacity
FDR:	Frequency Domain Reflectometry
HLC:	Hydraulic Loading Cycle
HLR:	Hydraulic Loading Rate
HAST:	Highstand Systems Tract
IAK:	Institut für Abfall- und Kreislaufwirtschaft
ICRC:	Infiltration Capacity Reduction Curve
IPM:	Instantaneous Profile Measurement
IPCC:	Intergovernmental Panel on Climate Change
LDO:	Luminiscence Dissolve Oxygen
LR:	Linear Regression
MAR:	Managed Aquifer Recharge
masl:	Meters Above Sea Level
mbgs:	Meters Below Ground Surface
PAR:	Photosynthetically Active Radiation
POM:	Particulate Organic Matter
PWP:	Permanent Wilting Point
RMSE:	Root Mean Square Error
SAT:	Soil Aquifer Treatment
SDGs:	Sustainable Development Goals
TDG:	Total Dissolved Gas
TDR:	Time Domain Reflectometry
TOC:	Total Organic Carbon
TSS:	Total Suspended Solids
TST:	Transgressive Systems Tract
TT:	Trigger Time
US EPA:	United States Environmental Protection Agency
UV-A:	Ultraviolet Radiation - Fraction A
UV-B:	Ultraviolet Radiation – Fraction B
UV-C:	Ultraviolet Radiation - Fraction C
WC:	Water Content

Chemical nomenclature

Fe:	Iron
HCl:	Hydrochloric acid
Mn:	Manganese
NaCl:	Sodium chloride

Symbols

A_L :	Libardi fitting parameter (-)
a :	Linear regression fitting parameter (-)
α :	Initial infiltration capacity parameter (-)
α_{bio} :	Biovolume ratio (-)
B_L :	Libardi fitting parameter (-)
b :	Linear regression fitting parameter (-)
β :	Steepness parameter for decay curve (-)
c :	Linear regression fitting parameter (-)
ϵ :	Relative dielectric permittivity (-)
g :	Gravitational acceleration constant (9.81 m/s ²)
I :	Electrical current flow (A)
K :	Hydraulic conductivity (m/s)
K_o :	Initial hydraulic conductivity (m/s)
K_r :	Hydraulic conductivity generated by direct push injection logger (m/s)
κ :	Intrinsic permeability (m ²)
L :	Total foulant depth (Length units)
μ :	Dynamic viscosity (kg/(ms) or Ns/m ²)
n :	Number of measurements (-)
Q :	Percolation observed with a specific foulant load (Volume units / Time units)
Q_o :	Initial percolation rate without foulant load (Volume units / Time units)
ρ :	Fluid density of water (kg/m ³)
T :	Temperature (°C)
t :	Time of infiltration (Time units)
t_{50} :	Infiltration time to reach half of the tracer concentration (Time units)
Θ :	Volumetric water content (%vol)
Θ_o :	Initial volumetric water content (%vol)
v_{50}/v_{50o} :	Infiltration rate reduction rate (-)
x :	Infiltrated volume per basin area (m ³ /m ²)
y :	Estimated reduction of infiltration capacity (-)
z :	Depth of soil passage (Length units)

1 INTRODUCTION

The United Nations (2019) calls upon the world's societies *"to ensure the availability and sustainable management of water"* and *"to take urgent action to combat climate change and its impacts."* Therefore, they included these contents in their Sustainable Development Goals (SDGs) 6 and 13 (United Nations, 2019):

Climate change has advanced in the last century where Earth's air temperature has warmed in average by 0.6 °C, highlighting the periods between 1910 and 1945 and from 1976 onwards (Walther et al., 2002). A graphical perspective of the variation in temperature is illustrated in Figure 1.1. The major changes have been detected in the northern hemisphere of the globe, with a rise in temperature of up to 3.0 °C in comparison to 1900. Most of the variation happened during the months from December to February.

(a) Regional warming in the decade 2006-2015 relative to preindustrial

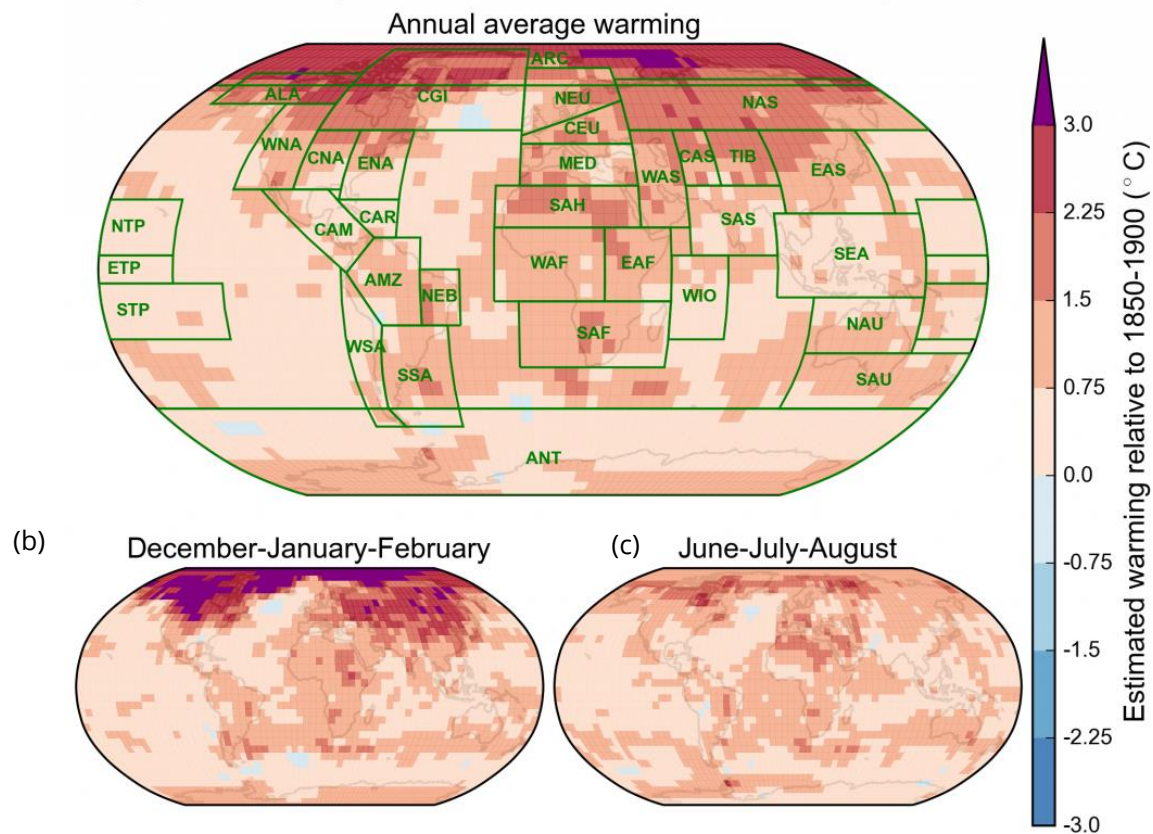


Figure 1.1. Regional warming in the decade 2006–2015 relative to 1850–1900 (Preindustrial period) for the annual mean (a), the average of December, January, and February (b), and for June, July, and August (c). Source: Allen et al. (2018)

Climate change sharpens the global problem of water scarcity and water allocation, especially facing the growing human population. Society has to shift its living style to a sustainable structure and work on technical, social, and environmentally sound solutions to remedy the overexploitation (average aquifer recharge rate is lower, or close to the average aquifer abstraction) of the world's water resources (Adger et al., 2005; Hoffmann and Sgro, 2011). Groundwater is one of the most widely used water resources which is subject to degradation and depletion. According to van der

Gun (2012), the groundwater abstraction rate has increased threefold in the last 50 years with a constant increase between 1 % and 2 % annually, leading to groundwater overexploitation. These data should strengthen the establishment of a new technological advancement to reduce and mitigate the effects of human activities and climate change (Lobell et al., 2008).

1.1 MOTIVATION

One powerful measure to address several water related problems (e.g. water scarcity in the dry season, groundwater depletion, and saltwater intrusion, among others) is managed aquifer recharge (MAR) (Dillon et al., 2019). Therefore, understanding the factors that influence the system's efficiency is a relevant investigation field. One of the key research areas in these recharge methods is the development of a blocking layer, known as clogging. It occurs either in the basin surface, in the vadose zone, or in the well filter (Martin, 2013). Thus, the determination of the most suitable conditions for clogging minimization in surface spreading methods is relevant. The accumulation of suspended solids and the biomass growth in the pore space of the soil leads to an increase of the infiltration resistance of the medium. The clogging rates depend on site-specific conditions such as soil properties, climate, water quality, and process-related parameters (Casanova et al., 2016; Martin, 2013).

MAR is an integrated tool for groundwater management that aims to alleviate the stress that the subsurface resource has been receiving in the last decades (Dillon et al., 2019). MAR's increasing importance necessitates the optimization of its processes to improve the efficiency of aquifer recharge. One of the key challenges is the formation of a zone in the surface and the subsurface that obstructs the path of infiltrating water, also called clogging. Clogging affects the screen of infiltration and exploitation wells and the surface of infiltration ponds. Physical (e.g. suspended particles), biological (e.g. algae growth), or chemical (e.g. alkalinity) factors drive the formation of clogging (Casanova et al., 2016; Martin, 2013). Spreading methods often use surface water, and the suspended solids in it either block smaller soil pores or contain microbial colonies together with organic matter (Asano et al., 2007). To optimize the operation of infiltration ponds, the clogging issue must be assessed by: (1) Minimizing/delaying its **formation**, (2) **monitoring** the infiltration capacity of the site, and (3) understanding the efficiency of the **management** of clogged layers. These three investigation areas were included as the main working axis for this thesis (see Figure 1.2) examined by field and laboratory scale experiments. The regional climate (e.g. temperature and solar irradiance) plays an important role in the formation of clogging. On one hand, it promotes or degrades the growing conditions of microorganisms (e.g. algae), and on the other hand it also results in changes in the fluid viscosity of the water (Barry et al., 2013; Dillon, 2005; Martin, 2013). Being able to anticipate the moment when the infiltration pond is completely clogged is critical to maximize the recharge volume. Once the soil pores are blocked, the low permeable layer can be scraped with heavy machinery to partially recover its infiltration capacity. The extracted material can either be exchanged or also cleaned and reinstalled in the infiltration basin (Martin, 2013).

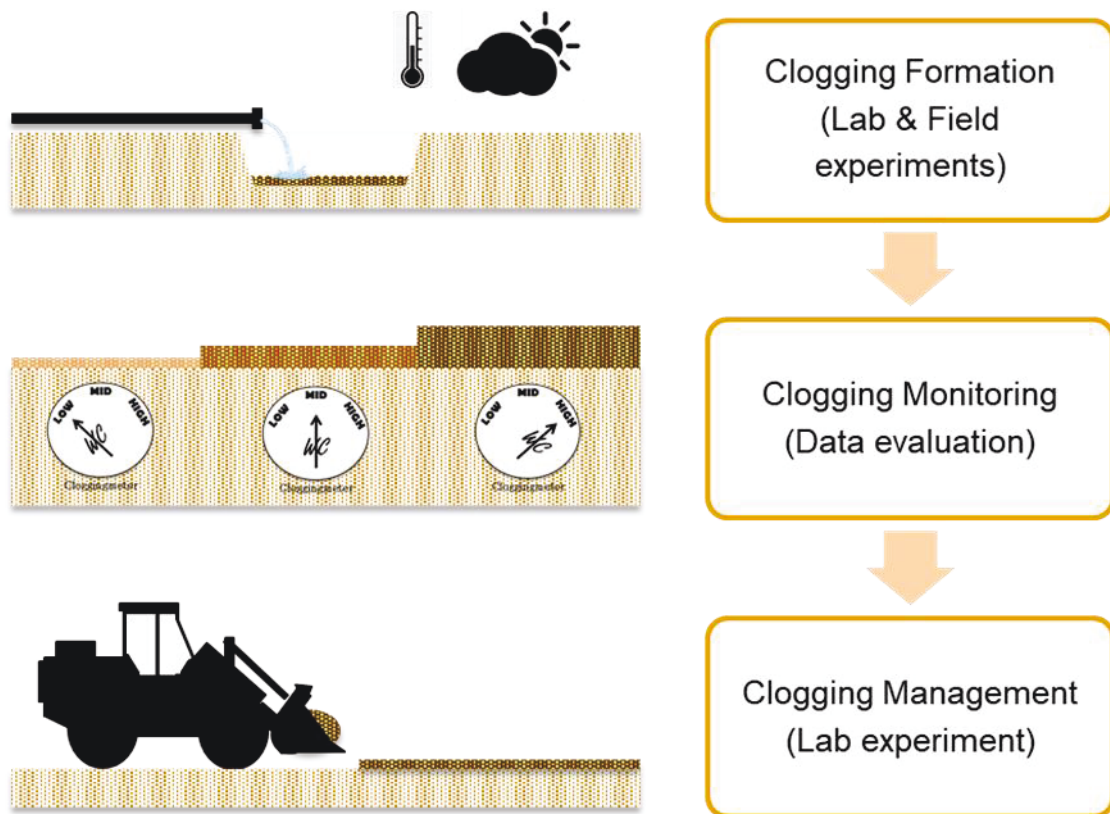


Figure 1.2. Overview of the thesis main investigation areas to assess clogging

1.2 OBJECTIVES

The main objective of this thesis is to develop tools for MAR sites with infiltration basins that eases the management of clogging, especially under consideration of the influence of the climatic variability. The specific objectives encompass:

- Understand the influence of climate related parameters (temperature and solar irradiance) in the development of the clogging layer in different hydraulic cycle scenarios.
- Determine the recovery efficiency of clogged infiltration ponds.
- Develop alternative methods based on the soil water content to anticipate severe clogging states.

1.3 THESIS STRUCTURE

The thesis is structured in the following chapters:

- Chapter 2: Encompasses the theoretical background of Managed Aquifer Recharge including possible operation of schemes, involved processes, and challenges. A description of the clogging in basins is included, mentioning the causes, consequences, and possible management options. This chapter also includes a description of climate-related parameters that have an influence on the development of a clogging layer, such as temperature and solar irradiance.
- Chapter 3: Contains the description of the site and presents the previous investigations conducted there. The description of the study area consists of an overview of the regional hydrogeology of the region of Saxonian Switzerland (ger. Sächsische Schweiz), a brief

analysis of the relation between the Elbe River and the shallow aquifer, and an analysis of the climate development in the last decade in the city of Pirna.

- Chapter 4: Describes the methodology of the study. It introduces the infiltration units that were used for the main chapters of the thesis: (1) field infiltration unit for analysis of the temperature influence in clogging, (2) laboratory infiltration soil columns for the determination of the solar irradiance influence on clogging, and (3) laboratory infiltration tanks for the evaluation of the recovery of the infiltration capacity rates of scraping procedures in clogged basins. Additionally, a description of the developed infiltration capacity monitoring methods is included.
- Chapter 5: Presents and discusses the main results of the experiments at the three different units described in Chapter 4. In addition, the selection of the most suitable water content based method is presented that can be used as an alternative for tracer tests.
- Chapter 6: Summarizes the most relevant findings of this thesis and points out the applicability of the outcomes for operators of recharge basins.
- Chapter 7: Includes the limitations and research perspectives regarding the influence of climate-related parameters and the assessment of clogging in infiltration basins.

The analysis of the alternative methods to evaluate the infiltration capacity of the soil and to determine the clogging state in the basin, was successfully published in the journal of Water 2019, 11(4), 784 (<https://doi.org/10.3390/w11040784>). The main outcomes of the results of the laboratory and field experimental units have been presented in several thematic conferences (Appendix A.1).

2 THEORETICAL BACKGROUND

2.1 MANAGED AQUIFER RECHARGE

The relevance of MAR has increased in recent decades as a potential solution to alleviate and mitigate problems of replenishment of over-exploited aquifers, intrusion of saltwater and water allocation related problems (Bekele et al., 2015). MAR is the intentional infiltration of surface water or re-injection of groundwater to an aquifer for consequent extraction or environmental benefit. Through the application of MAR, the resilience of water supply is increased, water can be provided regardless of season, and over-exploited aquifers may be replenished. Likewise, storage of water in aquifers has the benefit of minor loss through evaporation, operational efficiency and furthermore, infiltration commonly improves water quality (Dillon et al., 2009). MAR has been also considered as an ecosystem-based adaptation (EbA) technique (Ansems et al., 2014) that aims to protect the groundwater resources and has the capability to cope with the emerging extreme seasonal variability events triggered by climate change (Jilali and El Harradji, 2017).

According to Parson et al. (2012), the introduction rate of MAR techniques has been lesser than expected, despite their numerous benefits. According to Sheehan (2009), this is due to the poor awareness of MAR techniques and the lack of access to information which could encourage water supply operators to adopt and invest in MAR practices. Nevertheless, Dillon et al. (2019) did a recent exploration of the evolution of MAR capacity in 15 countries / areas around the globe (accounting for 76 % of reported MAR capacity in 2015). A summary of the MAR installed capacity (Mm^3/a) in the globe is presented in Figure 2.1. In the decade of 2000, the installed capacity doubled in comparison to the decade of 1990. This trend remains the same for the first half of the decade of 2010. The installed MAR capacity in 2015 represented 34 % of the global groundwater use in 2010 (Dillon et al., 2009).

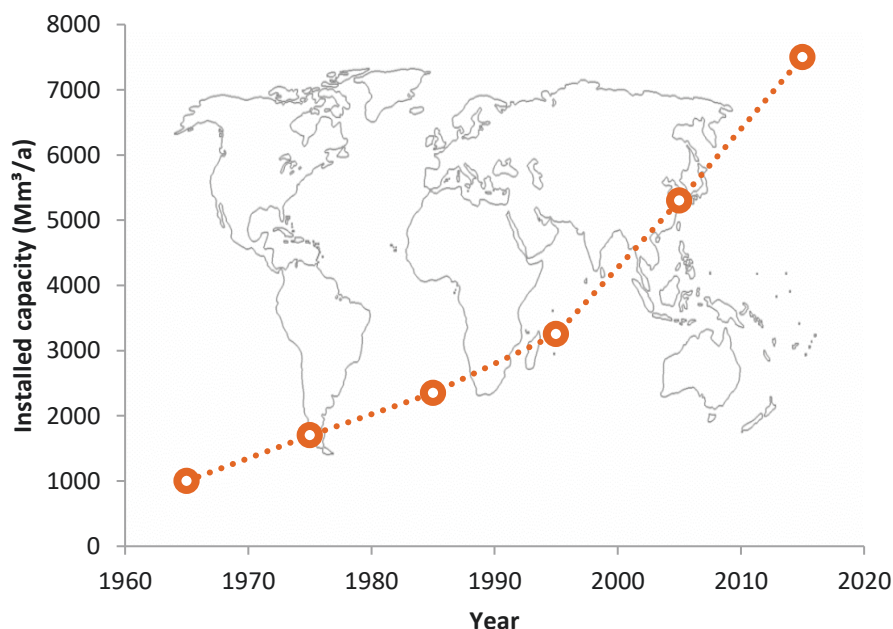


Figure 2.1. Global evolution of MAR capacity by decade since the 1960s in 15 countries/areas. Data Source: Dillon et al. (2019)

The feasibility of applying MAR can be assessed by considering different types of data from different disciplines. Figure 2.2 contains the framework of a MAR feasibility analysis. Nevertheless, it is essential to initially evaluate the feasibility of financial and technical factors (Arshad et al., 2014), to create a basis for the remaining investigation fields. The financial factors can be approached by the benefits of recharge to an individual or to a region. Assessing the latter might become complex because it englobes the public good, socio-economic and environmental benefits (Arshad et al., 2014). Maliva (2014) worked on a review of assessment methods for the total benefits from MAR. The evaluation of the technical factors should include a hydrogeological assessment, an analysis of surplus of water, and the means to convey it into the aquifer (Arshad et al., 2014).

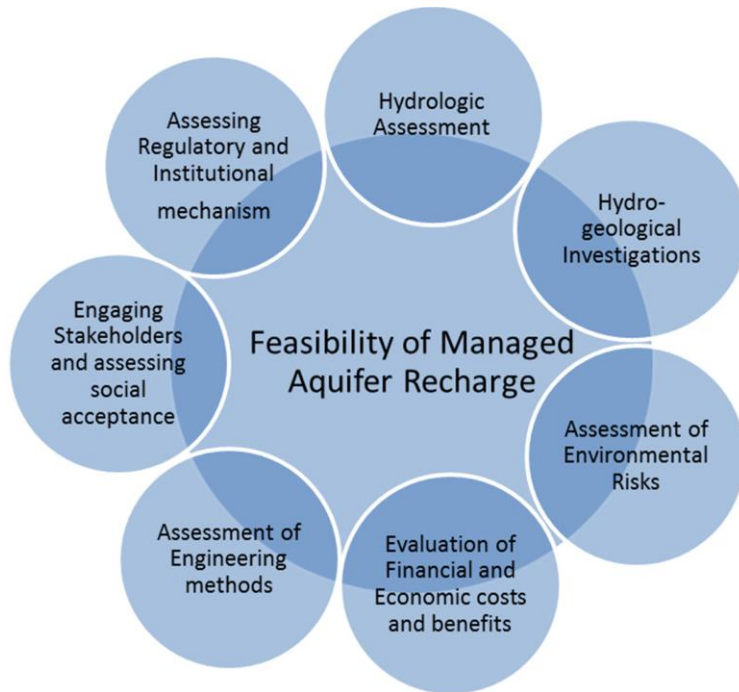


Figure 2.2. Framework for the feasibility of managed aquifer recharge. Source: Arshad (2014)

Depending on the in situ technical factors, different MAR methods can be selected. They are classified mainly in two categories: (1) referring primarily to getting water infiltrated and (2) referring to intercepting the water (see Table 2.1). Various types of MAR have been used ranging from direct injection methods (such as Aquifer Storage and Recovery (ASR) and Aquifer Storage, Transfer and Recovery (ASTR)), induced bank infiltration and surface spreading methods (Casanova et al., 2016). Besides that, some other artificial recharge methods also include sprinkle infiltration, which is relatively new in all managed aquifer recharge technologies (Jokinen et al., 2006). There are other processes not belonging to MAR that also end up in an aquifer recharge effect. These processes can be named as unintentional or unmanaged aquifer recharge methods, which refer mainly to processes where water gets to the aquifer as a side effect. Some examples are irrigation deep seepage, leakage of water pipes and sewers or mining, and industrial water disposal to sumps (Dillon et al., 2019).

Table 2.1. Classification of specific MAR methods (Stefan and Ansems, 2018)

Technique	Main MAR method	Specific MAR method
Infiltration	Spreading methods	Infiltration ponds and basins
		Flooding
		Ditch and furrow
		Excess irrigation
		Reverse drainage method
	Induced bank infiltration	
Interception	Well, shaft and borehole recharge	Deep well injection
		ASTR
		ASR
	In-channel modifications	Dug well/shaft/pit injection
		Recharge dams
		Subsurface dams
		Sand dams
Interception	Runoff and rainwater harvesting	Channel spreading
		Barriers and bunds
		Trenches
		Rooftop rainwater harvesting

This thesis focuses on spreading methods, one of the most common MAR techniques (Asano et al., 2007), with a particular focus on infiltration ponds and basins. Spreading infiltration involves diverting surface water into infiltration basins or channels allowing the water to infiltrate into the saturated zone, using the vadose zone as a filter to trap and break down organic and inorganic compounds before water reaches the aquifer (Laws et al., 2011; Stefan and Ansems, 2018). Its operation is considered a cost-effective measure compared to well injection techniques mainly because it uses gravitational forces to let water get infiltrated into the vadose zone (Arshad et al., 2014; Rupérez-Moreno et al., 2017). Figure 2.3 illustrates the main components of spreading method schemes. Depending on the source of influent (1), a pre-treatment (2) might be necessary. For instance, when using river water, a sedimentation pond is located prior to the infiltration basin. Water is supplied at a specific rate depending on its availability and the infiltration capacity of the porous media. During the water passage through the unsaturated zone (3), physical, chemical, and biological processes influence the water quality that reaches the aquifer. The subsurface storage (4) can be used during times with low availability of surface water, in which the recharged water is recovered through wells (5) located at a specific distance from the infiltration basin. Depending on the end use (7), the MAR scheme might include a post treatment (6) step.

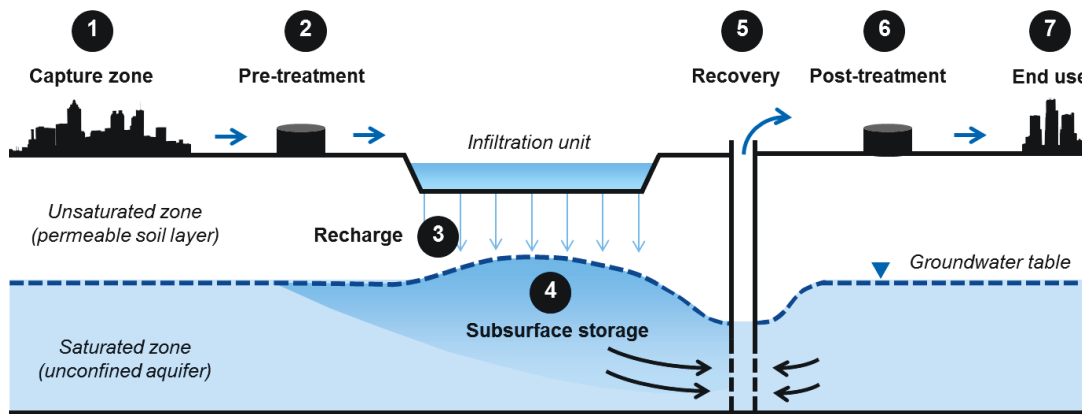


Figure 2.3. Main components of a MAR scheme based on surface spreading basins. Source: Glass (2019)

Water is infiltrated to the aquifer through an infiltration pond, and the vadose zone acts as a natural filter and an active site for the degradation of organic compounds. Interaction of infiltrated water with soil media not only allows the elimination of organic and inorganic substances but also the removal of pathogens (Casanova et al., 2016). Several water sources can be used in MAR applications. The most common sources of water for infiltration are harvested runoff and river water (Hida, 2009; Jokinen et al., 2006). The treated (reclaimed) wastewater is used in Soil Aquifer Treatment (SAT) systems, which are implemented, especially in semi-arid or arid regions where water is scarce. This alternative can be also applied to alleviate the effect of saltwater intrusion in coastal areas (Casanova et al., 2016; Council, 1994; El Ayni et al., 2011).

In infiltration ponds, large quantities of water are infiltrated at relatively low operation costs, while maintenance and anti-clogging procedures are relatively simple. However, surface spreading through infiltration basins requires a large and flat permeable surface (Dillon et al., 2009). This significantly increases the capital costs, highly depending on the land use of the site. Moreover, there is a potential for aquifer pollution depending on the water source, and the capacity of the vadose zone to assimilate, sorb, or degrade the pollutants before they reach the groundwater (Dillon et al., 2009). Furthermore, the design of the MAR basin must consider that the complete amount of water disposed in the basins will not reach the aquifer. Some fraction becomes trapped in the vadose zone as soil water, and can return to the atmosphere by evaporation and transpiration during times where the basins are empty, especially in warm regions (Racz et al., 2012).

Table 2.2 presents some examples of recharge basins in the world, giving at least one site per continent. The size of the infiltration basins complex can vary from a couple of square meters to some square kilometers. Annual recharge volumes can also be as small as 1000 m³ (Llobregat River, Spain) and expand up to 266 Mm³ (Orange County, USA), when combining a huge pond network.

Table 2.2. Operational information (recharge volume, infiltration rate, and basin area) of selected recharge basins all over the globe

#	Location	Influent Source	Recharge volume [Mm ³ /a]	Infiltration rate [m/d]	Infiltration area [ha]	Source
1	San Jacinto basin, Riverside, USA	River water	n.d.*	1.9	1.6	(Lee et al., 1992)
2	Valle San Luis, Rio Colorado, Mexico	Reclaimed water	n.d. (HLC** 1:6)	2.1	17.3	(Hernandez-Aguilar, 2017)
3	Llobregat River, Barcelona, Spain	River water	0.001	1	1.1	(Hernandez et al., 2011)
4	Cubeta de Santiuste, Segovia, Spain	River water	0.0012	n.d.	1.4	(Fernández Escalante et al., 2015)
5	Sulaibya, Kuwait City, Kuwait	Reclaimed water	0.0026	n.d.	0.09	(Al-Senafy and Sherif, 2006)
6	Floreat, Perth, Australia	Reclaimed wastewater	0.0124	n.d.	0.005	(Bekele et al., 2008)
7	Wadi Souhil, Cap Bon, Tunisia	Reclaimed wastewater	0.0420	n.d.	0.14	(Chaieb, 2014)
8	Oakes, North Dakota, USA	River water	0.0730	n.d.	0.0232	(Huff and Wald, 1989)
9	Montecchio Precalcino, Vicenza, Italy	River water	0.1000***	n.d.	n.d.	(Passadore et al., 2010)
10	Agavi, Morocco	Reclaimed Water	0.3830	1	0.750	(Bennani et al., 1992)
11	El Mida, Cap Bon, Tunisia	Reclaimed water	0.4000	n.d.	4.5	(Chaieb, 2014)

#	Location	Influent Source	Recharge [Mm ³ /a]	volume	Infiltration rate [m/d]	Infiltration area [ha]	Source
12	Atlantis, Cape Town, South Africa	Reclaimed water	2.7		n.d.	n.d.	(Murray and Harris, 2010)
13	Korba, Cap Bon, Tunisia	Reclaimed water	5.5		0.5	0.5	(Chaieb et al., 2013)
14	Khoudh Dam, ALKhod, Oman	River water	27		n.d.	n.d.	(Abdalla and Al-Rawahi, 2013)
15	Alice Springs, Northern Territory, Australia	Reclaimed water	1.3 (HLC variable)		0.14 – 1	3.8	(Barry et al., 2017)
16	Harkins Slough, Santa Cruz, USA	Lake water	2.5		0.1 – 1	3	(Racz et al., 2012)
17	Greeley, Colorado, USA	n.d.	3.7		n.d.	40	(Bouwer et al., 2009)
18	San Antonio, Texas, USA	Surface water	6.7		n.d.	n.d.	(Bouwer et al., 2009)
19	Shijiazhuang, China	River water	11.0****		1.4	600	(Su et al., 2014)
20	Ica, Villacuri, Lanchas, Peru	River water	16.0		~0.4	297	(Navarro and Fernandez, 2017)
21	Fort Dix, New Jersey, USA	Reclaimed water	16.0 (HLC 1:2)		n.d.	19	(Bouwer et al., 2009)
22	Big Fergana Canal, Uzbekistan	River water	18.0*****		2.6	0.1	(Karimov et al., 2012)
23	El Rio, Ventura, USA	River water	40		4	n.d.	(Clark et al., 2005)

#	Location	Influent Source	Recharge [Mm ³ /a]	volume	Infiltration rate [m/d]	Infiltration area [ha]	Source
24	Central Ava Valley, Tucson, Arizona; USA	River water / Reclaimed water	74 (HLC 1:1 / 5:3)		n.d.	134	(Bouwer et al., 2009)
25	Ban Nong Na, Phitsanulok, Thailand	River water	76.0		0.26	0.06	(Nadee et al., 2012)
26	The Shafdan, tel Aviv, Israel	Reclaimed water	120 (HLC 1:2 / 1:3)		175	120	(Goren et al., 2014)
27	Rio Sonora, Mexico	Reclaimed water	158.0		1.6	27	(Mendoza et al., 2012)
28	Orange County system, Anaheim, USA	River water	266.0		n.d.	43100	(Hutchinson, 2013)
* n.d. No Data ** HLC: Hydraulic loading cycle *** within two Months **** within 11 days ***** Potential value 100 Mm ³ /a assuming 250 basins along the Big Fergana Canal							

→

The soil texture at the site influences the infiltration potential and the hydraulic loading rate (HLR), which is the annual volume of water infiltrated per square meter (m/a). When designing infiltration basins, the HLR can be set as 10 % of the infiltration capacity (volume of water that can flow through the media without causing any saturation of the medium) determined by pre-tests in the field or the laboratory. Examples of HLR are 30 m/a for fine textured soils (e.g sandy loam), 100 m/a for loamy sands, 300 m/a for medium sands, and up to 500 m/a in coarse sand (Crites et al., 2014; NRMMC, 2009; US EPA, 2006).

Some MAR schemes introduce hydraulic loading cycles (HLC) or flooding and drying cycles in their infiltration schedules, especially in SAT systems (Asano et al., 2007; Casanova et al., 2016). HLC consists in an intermittent infiltration period. A temporary pause is systematically included to allow the recovery of oxygen concentration in the uppermost section of the recharge basin, which induces the maximum decomposition rate of organic matter, particularly for nitrification (Bouwer, 1996; Dutta et al., 2015; Sprenger et al., 2017). This also permits the adequate maintenance of the basin surface, because during the dry period, the low-permeability layer on the pond's surface can be scraped (Casanova et al., 2016). This improves the recovery of aerobic conditions in the topsoil and the infiltration capacity. By increasing HLR, the impact of each wetting cycle on oxygen availability, pore-fluid velocity, and retention time is higher. Assessing optimal HLC is, however, challenging because of the complexity and difficulty in measuring and mapping the spatial and temporal distribution of oxygen concentrations at the infiltration site. The oxygen concentration in the soil pores depends mainly on the simultaneously occurring transport and consumption processes. The former process is controlled by physical processes like advection and diffusion and on the other hand the latter process is regulated by chemical reactions and microbial activity (Dutta et al., 2015).

In SAT recharge sites, a common HLC is 24 hours of flooding period followed by 48 to 72 hours of drying period. After this time, a new 24 hours period of flooding starts. (Dutta et al., 2015; Haaken, 2018). The US EPA (2006) suggests for SAT projects to introduce the HLC according to the treatment stage of the influent. For influents that passed through a secondary or tertiary treatment stage the dry period can be shortened or the wet period can be adjusted to longer phases (see Table 2.3). A lack of drying cycles would reduce rapidly the infiltration rates unless submerged cleaning equipment is used to remove the clogging layer, like it is done in Anaheim Forebay in Orange County, USA (Asano et al., 2007).

Table 2.3. Examples for typical wet/dry ratios for SAT systems in the USA. Source: US EPA (2006) and Asano et al. (2007)

	Pre-treatment	Wet period [d]	Dry period [d]	Wet/dry ratio [-]
Calumet, Michigan	Untreated	2	14	1:7
Hollister, California	Primary	1	14	1:14
Barnstable, Massachusetts	Primary	1	7	1:7
Ft. Devens, Massachusetts	Primary	2	14	1:7
Vineland, New Jersey	Primary	2	10	1:5
Phoenix, Arizona site 1	Secondary	9	12	1:1.3
Phoenix, Arizona site 2	Secondary	14	14	1:1
Phoenix, Arizona site 3	Secondary	4	10	1:2.5
Mesa Northwest Plant, Arizona	Tertiary	7	21	1:3
Montebello Forebay, Los Angeles	Tertiary	28	28	1:1

Nevertheless, there are also recharge sites working without these hydraulic cycles, since the recharged water does not require further treatment through the vadose zone, and the aim of the project is mainly focused on the hydraulic restoration of the groundwater level (Council, 1994). This type of infiltration is referred in this study to as “continuous” infiltration.

Infiltration basins feature many advantages regarding the treatment capacity and the operational costs. However, the reduced efficiency of the system due to clogging is challenging. One of the most relevant factors is the development of a clogged layer in the surface of the infiltration pond.

2.2 CLOGGING IN MAR

The quality of the influent will affect the infiltration rate, due to its clogging potential. To keep high infiltration rates in the system, the quality of the water should be evaluated and monitored, and clogging of the infiltration surface should be managed. River water has a seasonally variable content of organic matter, suspended solids, and bacteria colonies. Although pre-treatment of water can considerably reduce the nutrients concentration and suspended solids in the infiltration water, periodic cleaning or management of the infiltration surfaces are typically needed (Barry et al., 2017; Bekele et al., 2013).

Clogging is one crucial issue to be considered for the design and operation of recharge basins, since it hinders the recharge capacity of spreading infiltration basins (Rice, 1974). Clogging is an unavoidable phenomenon that gradually reduces the permeability of the medium, decreasing the water volume that infiltrates into the aquifer (Du et al., 2013; Hutchinson et al., 2013; Martin, 2013; Zou et al., 2019). The factors that determine how fast clogging will develop are the fraction and shape of suspended solids, size distribution of fine soil particles, organic and inorganic materials, and microorganisms in the infiltrating water, so as hydrodynamics effects. These factors act as drivers for mechanical, chemical, biological and physical processes which eventually contribute to the reduction of the infiltration rates (Ahfir et al., 2007; Holländer et al., 2006; Zou et al., 2019).

Baveye et al. (1998) identified the most sensible areas for clogging development: basin bottoms, walls of trenches and vadose-zone wells, and well-aquifer interface in recharge wells.

There are four types of clogging:

Physical clogging is directly linked to the presence of organic and inorganic suspended particles in the source water that obstruct the flow paths through the soil media either on the surface or within the filter porous medium. The mobilization of fine particles also affects the total porosity of the soil, especially due to turbulence caused by hydraulic loading cycles. In this process, the suspended particles settle down when infiltration stops, and are remobilized with the restart of infiltration as a floc (a loosely clumped mass of fine particles) resulting in a major blockage source (Martin, 2013; Zou et al., 2019). Pavelic (2011) and Du (2013) stated that physical clogging is the most direct and dominant form of clogging controlled mainly by the amount and size of particulates present in the system. It usually leads to a slow but continuous increase of the ponding depth at a continuous infiltration rate. As the thickness of the accumulated layer increases, the infiltration rate is reduced. The lithology of the aquifer may also be important for physical clogging. Formations containing a high fraction of clays, for example some sandstones, may have pores within the soil or rock which are filled or lined with clay minerals such as kaolinite, illite, smectite, or chlorites (Martin, 2013). These fine-grained minerals may be dislodged by the infiltrating water and migrate with the flow. They may become trapped and block the pore space in narrow pathways, and thereby constrain the flow. A similar problem has been observed in muscovite and biotite rich reservoirs where the flakes of the micas were mobilized by a breakdown to smaller pieces (Martin, 2013; Rice, 1974). Additionally, Rice (1974) recommended a concentration of total suspended solids below 10 mg/L in the influent water to avoid high clogging rates.

The formation of the physical clogging layer is analogous to the mechanisms in sand filter units. Depending on the size of the suspended particles and the pore size distribution of the soil, three physical clogging mechanisms can be identified: (1) cake formation in the surface of the soil as the shallow macropores are blocked (Figure 2.4a), (2) straining as the suspended particles flow through the shallow macropores and get trapped in smaller pores in the subsoil (Figure 2.4b), and (3) bridging as smaller suspended particles (<10 μm) agglomerate via van der Waals forces and block the pores as flocs in the surface and within the soil profile (Figure 2.4c) (De Zwart, 2007).

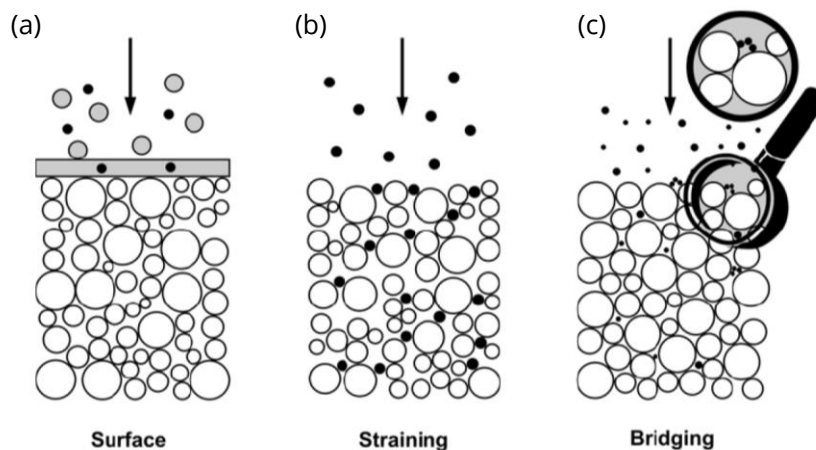


Figure 2.4. Filtration mechanisms of suspended particles flowing through a porous media. Source: De Zwart (2007)

Biological clogging occurs due to a vast spectrum of microorganism growth like bacteria and algae and accumulation of by-products from the decomposition of organic matter and polysaccharides, producing a biofilm on the infiltration surface (Martin, 2013). Biological clogging is proportional to the nutrients and free carbon available in the system (Pavelic et al., 2011). Additionally, Avnimelech

(1964) stated that biological clogging is associated with a decline in the oxidation-reduction potential in the sand. As bacteria are sensitive to shear, they tend to form stable biofilms to isolate themselves from water shear. These biofilms may inhibit fluid flow and lead to partial or complete occlusion of pore space. In infiltration wells, biological clogging usually leads a slow initial increase in the hydraulic head for a given infiltration rate, after that followed by a rapid exponential decrease (Bennion et al., 1998; Dutta et al., 2015; Martin, 2013). In a research study of Gunkel and Hoffmann (2006) in the riverbank infiltration system in the littoral zone of Lake Tegel in Berlin, Germany, the structure of the clogging biofilm and the occurrence of extracellular polymeric substances (EPS) were investigated. It was concluded that biological clogging is most likely to occur in the uppermost layer of the soil which directly correlated with the presence of higher level of dissolved organic carbon (DOC) and particulate organic matter (POM). In spreading basins with high solar incidence, algae growth is one of the main factors contributing to a reduction in infiltration rates (Asano et al., 2007). The mechanisms of biological clogging are considered more complex than physical clogging and reestablishing the infiltration rates in recharge basins may turn challenging. Furthermore, many metabolites are secreted by bacteria during their growth. The produced viscous polymers can adsorb suspended particles of the influent and accelerate the clogging process of the soil (Ruijuan et al., 2019).

Baveye et al. (1998) stated that carbon concentrated influents containing plant residues, monosaccharides, disaccharides, or alcohols have a higher potential for soil clogging, since the growth of the colony forming units increases. The most common organisms causing biological clogging are the prokaryotic forms (Baveye et al., 1998). Investigators have further classified the types of microorganisms in clogged systems into various strains of aerobic bacteria, facultative anaerobic bacteria and strict anaerobic bacteria. It can also be classified according to the main metabolic reaction of the bacteria into: denitrifying bacteria, acetogenic bacteria, sulfate-reducing bacteria, methanogenic bacteria, and photosynthetic-sulfur bacteria (Baveye et al., 1998). The correlation between the reduction of hydraulic conductivity and the biovolume ratio is dependent on the grain size distribution of the porous medium (see Figure 2.5). The biovolume ratio (α_{bio}) is defined as the bulk volume of the clogging biomass or particles per unit pore volume of unclogged soil. The reduction of the hydraulic conductivity because of biological clogging occurs faster with low biovolume ratios in soils with smaller voids size (Baveye et al., 1998).

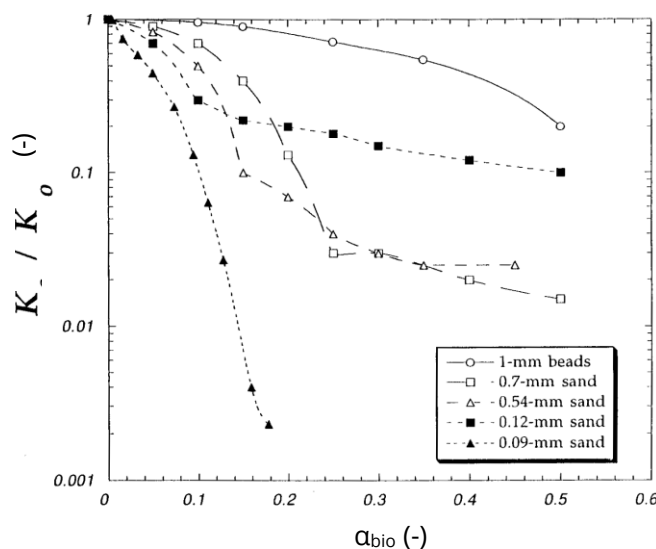


Figure 2.5. Dependence of the saturated hydraulic conductivity ratio to the biovolume ratio for *Pseudomonas aeruginosa* in 1-mm glass beads and in 0.70, 0.54, and 0.12 mm sand, and for *Arthrobacter* sp. strain AK19 in 0.09-mm sand. Source: Baveye et al. (1998)

Furthermore, Cunningham and Ross (2006) stated that the bacterial growth rate is divided into five phases (Figure 2.5): A lag phase as the amount of bacteria is still reduced. This is followed by an acceleration phase where the bacteria's reproduction exponentially increases, as long as food and oxygen are available. Once the energy sources become scarce because of the increased demand, the growth of the bacteria comes to a stationary phase and when the input is not enough, the bacteria population decreases.

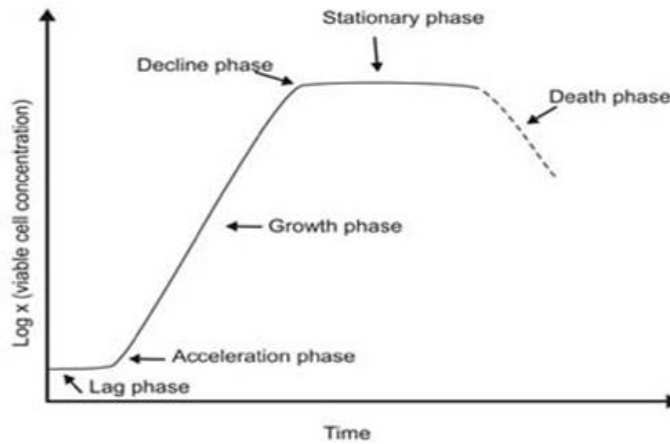


Figure 2.6. Phases of growth rate of bacteria. Source: Cunningham and Ross (2006)

Chemical clogging results from complex geochemical reactions happening in the soil pores due to mixing of water of diverse qualities. These reactions encompass mineral precipitation, dissolution, oxidation, reduction and adsorption e.g. formation of hydroxides, carbonates, and bicarbonates (Martin, 2013). These processes are mainly regulated by the type of water that is flowing through the soil media e.g. sodium-rich waters can cause a dispersion of a soil grain aggregates (Rice, 1974). Moreover, biochemical reactions due to microbial activity can also cause a biochemical clogging (Martin, 2013; Vigneswaran and Ronillo, 1987). As a consequence, precipitates may change the permeability of the porous media. Figure 2.7 illustrates how iron (III) (precipitated) can either get attached to the grains surface or get agglomerated in small cavities. Since the static adsorption force between the specific surface area of the adsorbent (soil grain) and the iron (III) is weak, the predominant blocking mechanism is the surface interception (Zhang et al., 2019). However, chemical reactions may also lead to dissolve the aquifer matrix, and thereby an increase in hydraulic conductivity may occur at MAR sites over time. Since geochemical reactions, such as redox reactions, are commonly caused by bacteria activity, it is difficult to differentiate biological and chemical processes (Martin, 2013; Rice, 1974).

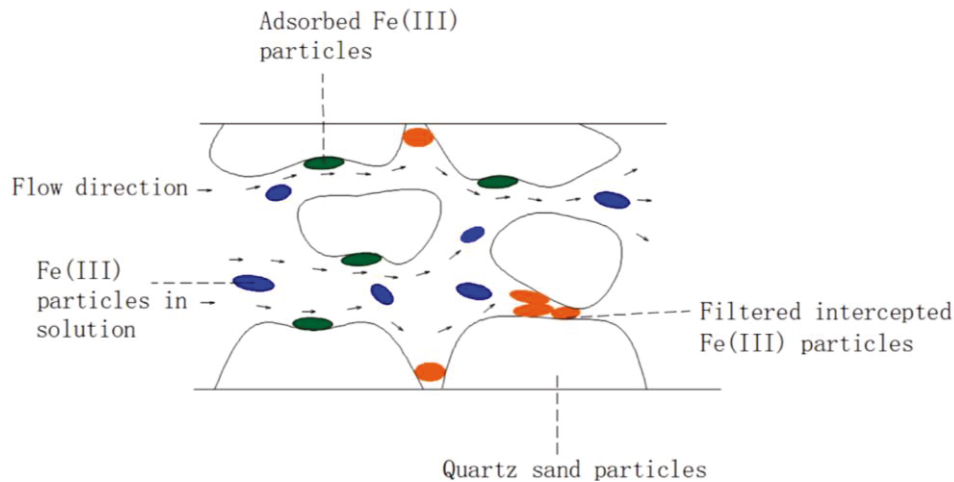


Figure 2.7. Clogging mechanisms diagram of iron (III) in the saturated zone. Source: Zhang et al. (2019)

Mechanical clogging or gas clogging is observed in spreading basins where air gets entrapped in the soil voids, reducing the infiltration and water storage capacity of the aquifer (Heilweil and Marston, 2013). This gas entrapment could also arise due to methane and nitrogen gases produced during the microbiological activity in the soil matrix (Martin, 2013). The entrapped gas bubbles typically block the largest pore pathways during the saturation phase of the infiltration, because wettability forces (adhesive and cohesive forces between the soil and liquid matrix) trap air bubbles in the center of pores. This commonly results in a sharp reduction in infiltration by restricted flow (Heilweil and Marston, 2013). Moreover, the viscosity of water changes with temperature. Therefore, lower infiltration rates are generally expected during the winter (Martin, 2013). Additionally, mechanical clogging takes place when the sand grains mobilize within the soil media. According to Pavelic (2011), mechanical clogging related to the rearrangement of soil media in sand is evident and affects the hydraulic conductivity within the first 24 hours of soil column experiments. Rice (1974) stated that long periods of intermittent infiltration cause the entrapment of gases because of the microbial activity in the soil. Figure 2.8 illustrates the different types of gas bubbles that can be found in the vicinity of the well screen in the saturated zone: Small spherical gas bubbles that ascend slowly or get attached to the grain surface, irregular gas bubbles, air bubbles in process of entrapment and entrapped air bubbles (Baveye et al., 1998).

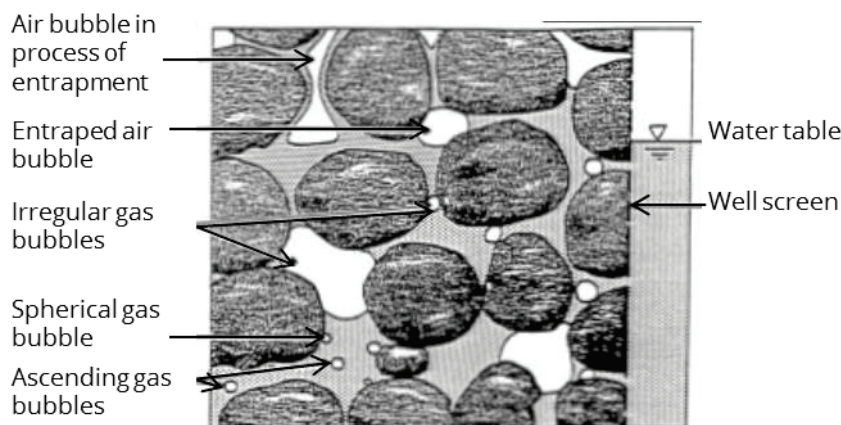


Figure 2.8. Representation of biochemically produced gas bubbles and entrapped air bubbles in the saturated zone. Source: Baveye et al. (1998)

Fernández and Sauto (2019) worked on a characterization of the different clogging processes using a multivariate geostatistical analysis in the Santiuste basin MAR site in Spain. They obtained a strong correlation between compounds dissolved in groundwater and clogging types: Physical clogging occurs with high concentrations of calcium, magnesium, total dissolved oxygen, and basic pH values. Biological clogging has the maximum correlation with pH and bicarbonate concentration. Chemical clogging increases with higher concentration of calcium, magnesium, sulphates, and nitrates. Sodium, calcium, nitrates, and dissolved oxygen are parameters influencing the development of clogging due to physical and biological processes occurring simultaneously.

Besides the quality of the influent water, other factors are also involved in developing the clogging layer such as the HLR and HLC, soil particle soil distribution, climate seasonality, temperature, and sunlight irradiance. Therefore, it is imperative to understand how different types of clogging are influenced by these factors in a MAR basin. Ponding depth also plays an important role. Pavelic et al. (2005) conducted research to understand the effects of ponding depth on infiltration rate. They concluded that an increase in ponding depth initially enhances the infiltration rate for a short time period but in the long term, it decreases the infiltration rate due to the clogging layer compaction and greater penetration of the particulate matter. Bouwer (1989) also explained that greater ponding depth results in greater detention time in the basin. Thus, the chances for regrowth of algae are higher. Moreover, higher gradients lead to filter cake compression which adversely affects the infiltration rate.

2.3 MANAGEMENT OF CLOGGING

Clogging is together with land availability, water quality and quantity, one of the main restricting factors which limits the capacity of MAR sites, it is essential to study the processes that influence its development and create mitigation strategies. Because of physical and biological clogging a thin layer of a few millimeters to a few centimeters develops on the topsoil (Martin, 2013; Zou et al., 2019). Therefore, clogging management is typically restricted to the uppermost soil layer in the infiltration basin. Examples of methods to recover basins are scraping (see Figure 2.9), scratching, tillage, or replacement of soil (Achilleos et al., 2019; Asano et al., 2007; Martin, 2013; Negev et al., 2019). Scraping of the basins consists in the mechanical or manual removal of the upper layer (Hutchinson et al., 2018).



Figure 2.9. Scraping of the top layer of clogged infiltration basins in the USA. Source: Hutchinson et al. (2018)

In a recharge site located in the Dharta watershed, Australia, clogging is controlled on infiltration basins by periodically drying the basins. The main objective is to dry the clogging layer, scrap it,

decompose it, shrink it, crack it, and finally curl it up. The removal is mechanically done in the site with front-end loaders, graders, scrapers, or manually with rakes (Soni et al., 2019).

Besides scraping, there are other techniques to deal with already clogged basins. Negev et al. (2019) worked with different tillage systems (see Figure 2.10) to recover the infiltration rates in the basin. The plowing method (Figure 2.10a) recovered the infiltration rates up to 95 %. They plow their basins in the SAT Shafdan basins, Israel, once per month and reach a depth of 40 cm. Applied subsequently, the sweep-knives cultivator (Figure 2.10b) did not improve the infiltration rates. Nevertheless, combining the later technique with the chisel-knives cultivator (Figure 2.10c) caused an extra 15 % increase in the infiltration rate. Finally, the plowing subsoiler (Figure 2.10d) resulted in an additional 70 % enhancement of the percolation rates.



Figure 2.10. Tillage tools used for recovery of the infiltration rate in SAT recharge basins: (a) Plow (b) Sweep-knives (SK) Cultivator; (c) Chisel-knives (CK) cultivator and (d) Subsoiler (paraplow type). Source: Negev et al. (2019)

San Sebastian and Fernández (2019) maintained high infiltration rates during longer periods of time by introducing vegetation into the basin in Los Arenales MAR site, in Spain. On one hand, the hydrophilic plants in the surface of the basin adsorbed micronutrients, and on the other hand their roots prevent clogging by producing new preferential flows. Additionally, the dissolved oxygen of the water flowing, through a specific vegetation type, is reduced and inhibits the potential of the occurrence of mechanical clogging.

Sometimes, it is necessary to add a treatment step to the recharge system to reduce the vulnerability to clogging. For example, the recharge sites in North China Plain suffered of clogging in their basins due to high silt concentration. The clogging potential was reduced by the construction of a desilting unit treating the influent before it entered into the infiltration basin (Liu et al., 2019).

Clogging may also develop in different rates at different sites. After seven years of operation of the MAR site in Ica, Peru, no severe impacts due to clogging were registered. Nevertheless, the infiltration ponds were redesigned to further decrease the impact of clogging. The basin walls were constructed with a stable slope (2:1) to support high lateral pressure. Additionally, the surface of the basin was carved with furrows to increase the surface area of infiltration, and simultaneously

to force a preferential sedimentation in the furrow canals, which is easier to be removed (Fernandez and Navarro, 2019).

To reduce the impacts of clogging, selected soil parameters should be monitored to evaluate and assess the best operational setup and maintenance schedule to maximize the recharge volume in time. Furthermore, the climatic boundary conditions determine the growth rate of the clogging layer, especially in infiltration basins. The following two subchapters present an overview of these soil and climatic properties.

2.4 MAR-RELEVANT SOIL PARAMETERS

This chapter contains a description of the main soil parameters in the vadose zone that can be monitored in surface spreading basins to control their functionality:

2.4.1 Hydraulic conductivity

In MAR recharge schemes, it is necessary to monitor the development of the hydraulic conductivity (K) of the soil, which indicates the infiltration capacity of a soil to permit water to flow through its pores. The determination of K in the unsaturated zone is essential to understand the soil-water transport processes such as heat transfer, mass transfer, infiltration, and runoff (Stibinger et al., 2014; Wagner et al., 2001). The in situ evaluation of K can turn into a challenge, especially if non-disturbed conditions want to be maintained. Several methods have been developed to quantify K in the field; such as auger-Hole method tension infiltrometer, single/double ring infiltrometer, and constant head well permeameter (Fodor et al., 2011; Stibinger et al., 2014; Vienken and Dietrich, 2011). However, all these techniques offer at the end only a single value representative for the complete duration of the infiltration. Moreover, all mentioned approaches are considered to be invasive, as they alterate the soil conditions in the experimental setup, which in turn influences either the matric potential, or the water content conditions or the soil compaction. The effect of these alterations can be significant for the study of K variations caused by the clogging of pores. The application of invasive methods to measure K represents a variation of the initial boundary conditions in an investigation setup working with repetitive infiltration cycles, as is the case in MAR spreading methods (Barquero et al., 2019).

K at the first infiltration layer in surface spreading operations has a key role, because it is one of the main parameters controlling the infiltration capacity of the recharge site. Commonly, a soil sampling campaign is conducted while the infiltration basin is empty to investigate the factors driving the reduction of infiltration rate produced by the clogging layer. The initial conditions for following infiltration cycles are affected by the invasive soil sampling techniques. Likewise, constant head permeameter's instrumentation changes the initial boundary conditions for the next infiltration cycle (the soil remains with higher water content due to the infiltrated water of the permeameter). Therefore, these methods are considered inappropriate for monitoring the clogging development in MAR recharge sites under specific hydraulic scenarios in laboratory experimental units, field scale units or in full size infiltration units (Barquero et al., 2019).

The hydraulic conductivity (K) is by definition the resulting flow capacity of a fluid with a specific density (ρ) and dynamic viscosity (μ) through a medium with a determined intrinsic permeability (κ) under the gravitational acceleration constant (g) (Mao, 2016):

$$K = \frac{\kappa \times \rho \times g}{\mu} \quad (1)$$

The intrinsic permeability (κ) or specific permeability (m^2) is a parameter depending solely on the soil material and is independent of the fluid that is flowing through it. The viscosity is a measure of

a fluid's resistance to flow and it is related to the ease with which the molecules can move with respect to one another (Camacho, 2017).

The dynamic viscosity (μ) has to be interpreted as the resistance required to move one horizontal layer of fluid with respect to another layer (Soares, 2015). Camacho (2017) presented a formula to determine the dependence of viscosity (Ns/m) to temperature changes from 0 °C to 370 °C:

$$\mu = 2.414 \times 10^{-5} \times 10^{\frac{247.8}{273.15 - 140 + T}} \quad (2)$$

where T is the temperature of the fluid in (°C).

The density of water (ρ) also is temperature dependent and represents the mass per unit volume (Camacho, 2017). McCutcheon et al. (1993) developed a program to calculate the density of water at variable temperatures:

$$\rho = 1000 \left(1 - \frac{(T + 288.9414)}{508929.2 \times (T + 68.12963)} \times (T - 3.9863)^2 \right) \quad (3)$$

2.4.1.1 Soil water matric potential

The soil water tension describes all existing influences exerted on the water by the soil matric and is also referred to as matric potential or pressure head. The measurement of the matric potential in a soil depends on its water content, the size of its pores, the surface tension of the soil water matric, and the properties of the surface of the soil particles. The most commonly used sensor for soil water matric potential is the water filled hydraulic tensiometer (Whalley et al., 2013). Figure 2.11 presents the main components of a water-filled tensiometer.

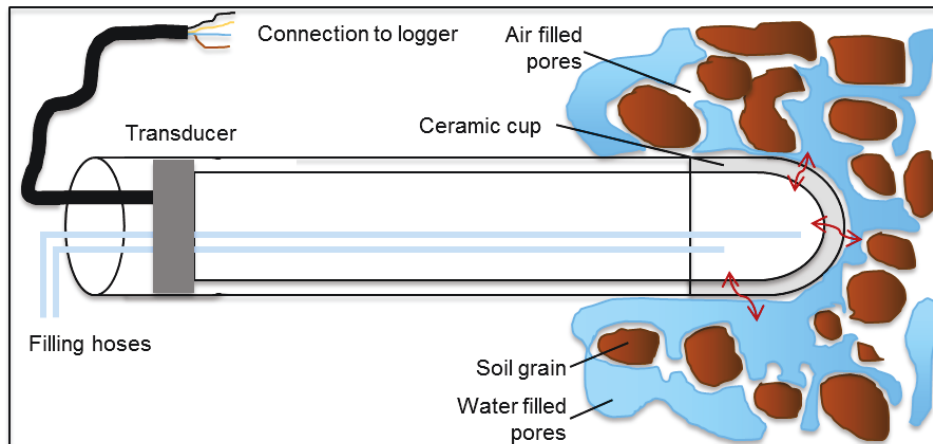


Figure 2.11. Main components of a water-filled tensiometer lying horizontally in the soil. Adapted from: UGT (2018)

The tension is closely linked to the water content of the soil: the dryer the soil, the higher the tension in the system. At the groundwater surface, the tension is considered to be zero. The relation between water content and soil tension is soil specific and highly depends on the soil properties (UGT GmbH, 2018). The soil moisture retention curve (see Figure 2.12) describes this relation and points out the field capacity (FC), and the permanent wilting point (PWP) ranges. The former concept represents the water retention force of the soil after an excess of gravitational water drained out of the soil, whereas PWP refers to the minimal soil water that the plant requires not to wilt (Assouline and Or, 2014).

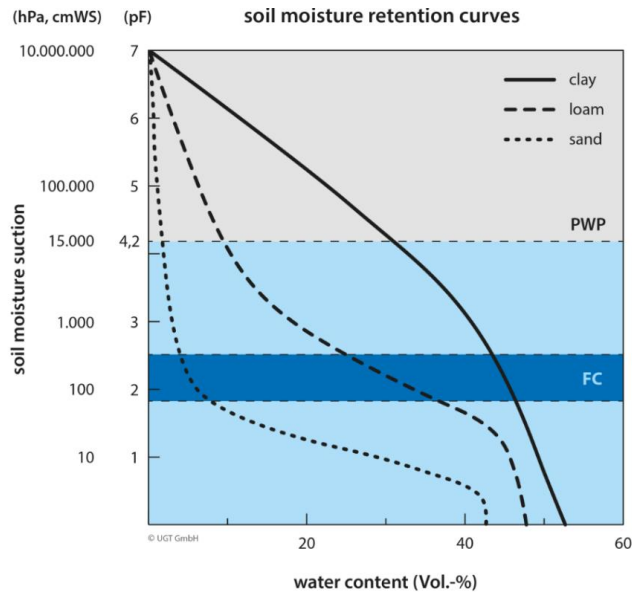


Figure 2.12. Soil moisture retention curve for clay, loam, and sand. The permanent wilting point (PWP) and the field capacity (FC) intervals are also illustrated. Source: UGT GmbH (2018)

2.4.2 Soil water content

The water content is considered to be an important variable in applied soil science (Noborio, 2001; UGT GmbH, 2014). It is used as an irrigation control parameter in the agriculture or as a decision criterion in environmental and landscape protection. Determining the water content without disturbing the sample is reached by indirect procedures that also allow a continuous observation of the water content in the field (UGT GmbH, 2014). These methods do not require a calibration of the system for almost all soil textures (Noborio, 2001).

Time domain reflectometry

The time domain reflectometry (TDR) is one of the most used systems to monitor the soil water content (Greco, 2006). It measures reliable results (including close to the surface) and does not require previous calibration, in comparison to the neutron scattering method or the gamma attenuation method. TDR does not release dangerous radiation, works with a limited interference to soil processes, and is especially suitable for automated and remote-controlled projects (Greco, 2006).

The relative dielectric permittivity, ϵ_r , and soil volumetric water content θ show strong correlation. ϵ_r indicates the velocity of propagation of electromagnetic waves through the soil pores. By longer travel times of an electromagnetic pulse in a known length passage, the smaller will be the velocity of propagation, resulting in an indication of a lower fraction of pores filled out with water (Greco, 2006).

Frequency domain reflectometry

Contrary to TDR principles, the frequency domain reflectometry (FDR) does not measure time, it rather measures an amplitude and phase of reflected pulses at each frequency window. This difference is illustrated in Figure 2.13.

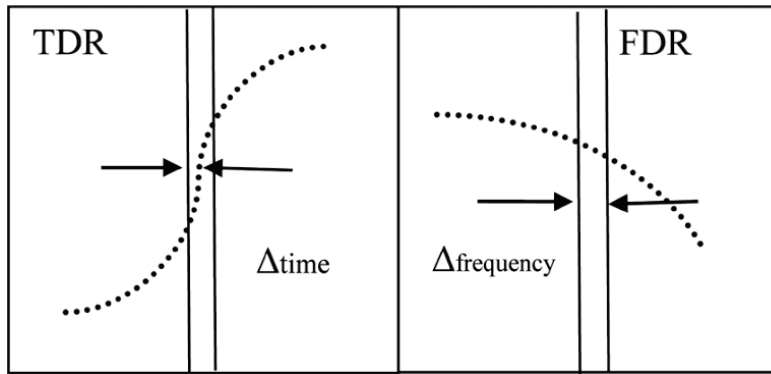


Figure 2.13. Differences in the measurement principle for TDR and FDR sensors. Source: Ilyas (2012)

UMP-1 by UGT GmbH

The system of the UMP developed by UGT GmbH (Müncheberg, Germany) cannot be assigned either to FDR or TDR. The operation principle is more familiar to the FDR process, in which the sensor works with a continuous signal at a constant frequency (60 MHz) and not with a pulse (as with FDR). However, the phase shift rather than the frequency change is taken into consideration to calculate the measurement reading. The device consists of two stainless steel rods, 10 cm in length and a diameter of 3 mm (Figure 2.14). The given dimensions and the programmed measurement frequency produce a measurement equivalent to a volume of 1 liter. The dielectric constant ϵ of the surrounding soil/water mix is determined from the phase difference of the signals running back and forth. The dielectric constant for pure water at 20 °C is $\epsilon = 80$. Dry soil has a ϵ of 2 - 5.

The dielectric constant of the soil/water mix lies between these two levels and is higher the more water is in the soil. Using the calculated dielectric constant, the water content of the soil is then determined in a unit ($[m^3]/[m^3]$) according to the Topp-Davis equation (UGT GmbH, 2014).

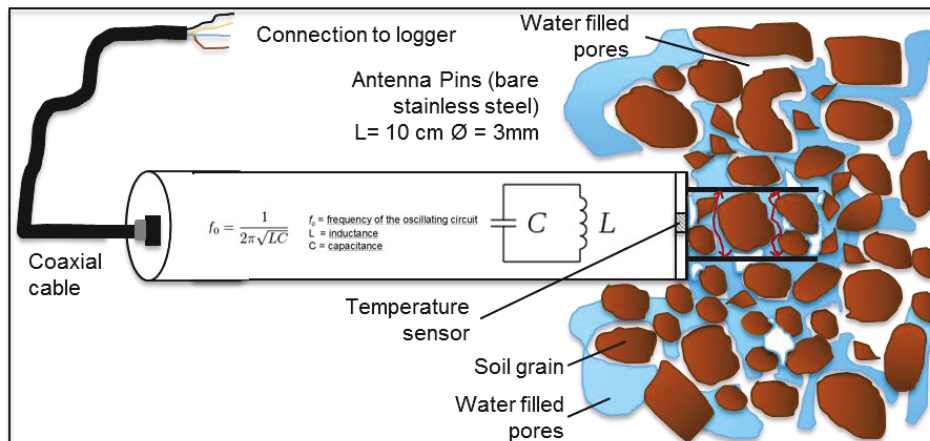


Figure 2.14. Main components of UMP sensor measuring water content, electrical conductivity, and temperature in soils. Adapted from. UGT (2014)

2.4.3 Electrical conductivity

The electrical conductivity (EC) of a soil or a solution is considered to be an efficient indicator of the concentration of a solute (cation or anion). An EC of 1 dS/m is approximately equivalent to 10 meq/L (Friedman, 2005). Electrical conductivity in water is the ability of the liquid to conduct an electric current. Water is always electrically neutral, and therefore, the overall charges of anions

and cations must counterbalance each other. All-natural waters, river waters, or urban drainage waters contain water constituents, and usually, the electrical conductivity closely reflects the total dissolved solids, which represent the total dissolved ions in the solution (Sparks et al., 1996).

When using a conductivity meter to determine the electrical conductivity of a solution, the resistance of the solution between two electrodes at a given distance is measured. This procedure can be also measured with the UMP sensor illustrated in Figure 2.14. Conductivity meters must be calibrated regularly to ensure a reliable measurement. The electrical current flow, I , is higher with increasing temperature. Therefore, EC values are typically corrected for a standard temperature of 25 °C. These corrected values are referred to as specific electrical conductivity values (Sparks et al., 1996).

Soil electrical conductivity is, similarly, the ability of the soil to transmit an electrical current. When electrical conductivity term is applied to soils, it refers to both soluble and readily dissolvable salts in the soil sample. There are three pathways of the current flow that contribute to the electrical conductivity of the soil. The first is the liquid phase pathway through dissolved solids in the large pores of the soil, the second is the solid-liquid phase pathway which is primarily dependent on exchangeable cations related to clay minerals, while the third pathway is the solid pathway which refers to conductance between soil particles which are in direct contact (Corwin and Yemoto, 2017).

Tracer experiments

Tracer hydrology is the scientific field that uses environmental and artificial tracers in modelling and assessing hydrological systems (Leibundgut et al., 2011). Tracers are substances that can maintain a flow pattern similar to that of water, and are a common method for assessing changes in the hydraulic properties of a medium, especially in laboratory experiments (Irving and Singha, 2010; Pollock and Cirpka, 2010). Tracers should have conservative behavior, low toxicity, and a high accuracy for analysis (U.S. EPA, 2002). The advantage of adding a tracer to the infiltration solution is that they are easily traceable by using substances such as sodium chloride (NaCl) to determine groundwater flow, or to study leakage from rivers or sewage pipes in the saturated and unsaturated zone (Armbruster et al., 1992; Einsiedl, 2005; Hoffmann and Dietrich, 2004; Kollmann et al., 1992; Singha and Gorelick, 2005; Zellweger, 1994). Electrical conductivity is monitored over time, which fluctuates in proportion to the concentration of salt (Abrantes et al., 2018). Normally, the tracer solution is added from the start of the infiltration event, and the conductivity peak is reached in a couple of hours (depending on the depth of the sensor and the soil properties). The linear flow velocity is calculated by monitoring the electrical conductivity from the beginning of the infiltration cycle until the sensor at a determined depth reaches the maximum measured stage. The fraction of depth over time give the linear velocity and this value represents the standard baseline state for the wet cycle. However, sometimes the development of the infiltration capacity of the basin also requires ongoing infiltration cycles, for instance in longer infiltration periods (> 3 days). In this case, tracer experiments might underestimate infiltration rates due to two main factors: (1) the higher amount of voids that are filled already with water, causing a different distribution of the flow paths, and (2) the dilution of the tracer in the ponded water above the infiltration basin surface.

The normalized linear velocity, expressed as v_{50}/v_{500} (fraction of linear velocity based on time over the initial linear velocity in the first infiltration cycle) in Equation (4), is calculated with the time it takes to reach the half of the maximum rise of electrical conductivity (t_{50}) at the depth to the sensor (z) (Leibundgut et al., 2011). The monitored changes of v_{50}/v_{500} in the infiltration experiment can be interpreted as the reduction of the infiltration rate of the medium.

$$v_{50}/v_{500} = \frac{z}{t_{50}} / \frac{z}{v_{500}} \quad (4)$$

The most widely applied salt tracer is NaCl (or “table salt”) and it stands out among other artificial tracers because of the ease of handling, low price, and ubiquitous availability. While NaCl is conservative and considered environmentally harmless in low concentrations, care needs to be taken to ensure that the salinity of the injected water does not exceed environmental limits. The maximum solubility in water is 355-360 g/L and is temperature dependent (Leibundgut et al., 2011). Limitations in using salt tracers include the high background concentrations in some water bodies, density, and local flow field changes due to large injection volumes of saline water, and cation exchange (particularly at longer flow pathways). The latter is responsible for sorption of dissociated ions in the unsaturated zone and in soils, where mineral and organic particles with large surface areas adsorb the ions onto their surfaces and remove them from the groundwater flow. However, the sorption potential of chloride is considered relatively low (Leibundgut et al., 2011).

This thesis makes use of the tracer experiments to infer the clogging state of the infiltration basin by measuring its side effect: the reduction of the vertical hydraulic conductivity. This is determined by the calculation and normalization of the linear velocity for each infiltration cycle.

2.5 MAR-RELEVANT CLIMATE PROPERTIES

Seasonality and climate effects were also considered in some studies. A study based in Australia deduced that MAR application near the deciduous forest regions showed a higher physical clogging rate in the autumn season due to higher organic loads from the leaves shedding cycle (Barry et al., 2013). In regions with huge temperature differences between summer and winter season, the viscosity of water changes accordingly. As viscosity shows an opposite and indirect relationship to the infiltration rate, the recharge rate is expected to decrease in the winter season with the colder temperatures (Casanova et al., 2016). Martin (2013) stated that the infiltration rate in winters should be reduced to half of that in summers.

Nonetheless, other researchers have contrary conclusions related to seasonality effects. A case study was carried out in Sand Hollow basin, southwestern Utah, USA, which is operated also as a MAR site from 2002 to 2011. The monitoring of hydrochemical and hydraulic records explained the effect of seasonal variability on the recharge volume of the infiltration basin. Recharge rates were observed to be higher in winter months than summer, even though colder water temperature has higher viscosity. Heilweil et al. (2013) stated that this trend could be explained by either stunt algae growth, reduced physical clogging, reduced respired gases or increased solubility or dissolution of biogenic gases due to cold water temperature. They have also associated higher Total Dissolved Gas (TDG) pressure with the presence of gas bubbles. In colder temperatures, the gas formation rate is quite low, whereas in summers (higher temperature) gas clogging is quite high as well as the TDG pressure. This gas clogging is related to algae decay and plant respiration in shallow water depths during the warmest months.

Narrowing down the factor of seasonality, researchers have also shown that the impact of temperature regulates the chemical reaction happening in soil columns and affects microorganism growth and activity (Bromly et al., 2007; Gibert et al., 2015). Xia et al. (2018) stated that biological clogging in a sand column happens 10 times faster in summer than in winter, due to the faster culturable bacteria growth rate. One study conducted in the sandy littoral zone of Lake Tegel during bank filtration assures that algae biomass values in the interstice were observed the highest in winter due to the high redox potential values. In contrast to this, in summer season enhanced mineralization and respiration rate decrease the algae production indicating a decrease in biological clogging (Gunkel and Hoffmann, 2006; Snehota et al., 2008).

Unlike temperature, the effects of sunlight on the behavior of MAR schemes are yet to be explored in greater depth. Owing to a plethora of elements involved, determining the cause of clogging represents a huge challenge. One of the factors of biological clogging is solar irradiance. Despite,

its sheer importance, literature available regarding the effect of solar irradiance on the clogging is quite scarce, which leads to poor understanding of the processes involved.

2.5.1 Solar irradiance

This chapter refers to the influence of the electromagnetic radiation coming from the sun on the operation activities of surface spreading basins. Solar irradiance is the intensity with which radiation enters Earth's atmosphere. Approximately half of the incoming solar radiation is scattered or absorbed by the atmosphere and clouds before it reaches the Earth surface (Liou, 1976). 45 % of the solar radiation is in the range of the visible light (400 - 700 nm), another 45 % consists of infrared wavelength (700 nm - 1 mm), and a 10 % ist UV radiation (100 - 400 nm) (Ryer and Light, 1997). Figure 2.15 shows each spectra irradiance ranges at sea level and outside atmosphere.

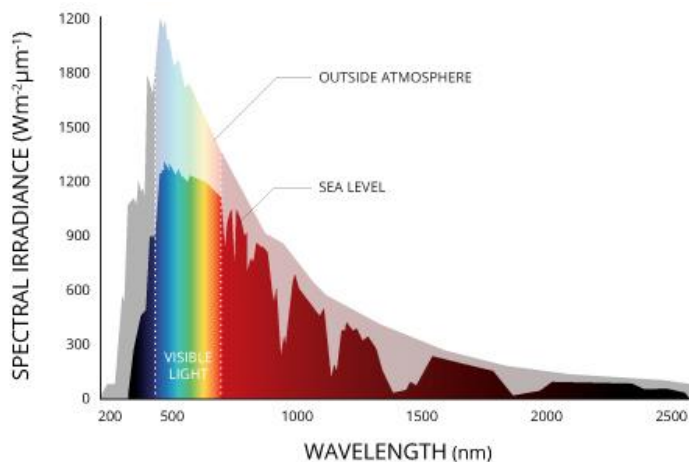


Figure 2.15. Spectra irradiance ranges at sea level, which are mainly categorized into UV radiation (100 - 400 nm), visible light (400 - 700 nm), and infrared (700 nm - 1 mm). Source: Fondriest Environmental (2014)

The ultraviolet radiation can be divided into three bands: UV-A, UV-B, and UV-C. All these short wavelengths can directly affect the DNA of water-composed organisms and also generate harmful photochemicals due to its high levels of quantum properties. Especially by shorter wavelength exposition, a greater damage can be caused. A special feature of UV-A and UV-B is its capacity to inhibit the photosynthesis process of phytoplankton by over 8 % (Fondriest Environmental, Inc., 2014; Karsten et al., 2007; Ryer and Light, 1997).

The infrared radiation contains the least amount of energy per photon and is absorbed by water and carbon dioxide, and converted to heat energy. Therefore, this radiation is responsible for the warming up of the Earth's surface. In a body of water, infrared light can only reach a certain depth below the surface: 90 % of the incoming radiation gets absorbed in the first meter of water's surface (Fondriest Environmental, Inc., 2014).

The visible light fraction is also known as photosynthetically active radiation (PAR) and is the band that provides the necessary energy for photosynthesis. Leaves of plant's communities react to different levels of PAR. For instance, most of them reflect the green wavelength and absorb the rest of the spectrum. Moreover, shade plants respond to lower PAR, whereas sun plants harvest higher level of PAR (Alados et al., 1996; Fondriest Environmental, Inc., 2014).

The distribution of ambient light intensity with a wavelength is known as irradiance spectrum. The irradiance spectrum is the sum of radiances from all light sources. Light environments depend mainly on the geometry of the light paths, the weather conditions, the time of day, altitude, azimuth

of the sun and vegetation coverage. Different regions of the world get different solar irradiance based on the above mentioned aspects (Fondriest Environmental, Inc., 2014). Nann und Riordan (1991) indicated that clouds act as a filter for some specific wavelengths: spectra ≤ 400 nm matches the irradiance received on a dark, overcast day, and 650 nm spectra can be transmitted through light clouds. The colour of ambient light changes considerably at dawn and dusk; for example light from the setting sun illuminates overhead clouds with a yellow-to-red light. After the sun sinks below the horizon, the loss of middle wavelengths (570-630 nm) becomes pronounced; the light becomes purplish. Moreover, open space (<470 nm) and humid forest areas (≈ 550 nm) have also different spectra of sunlight (Endler, 1993).

Reasons for solar irradiance variation are mainly the geographical location around the globe, because of the sun's angle towards the Earth. Additionally, cloud cover, air pollution and the hole in the ozone layer are significant sources of solar irradiance fluctuations (Bishop and Rossow, 1991).

The effective quantum yield and oxygen production (growth) of algae and photosynthetic microorganisms are higher after noon time, when the UV-A and UV-B radiation levels are reduced (Figueroa et al., 1997). This photoinhibition to UV radiation comes due to a reduction of the chlorophyll content, predominantly with higher UV-B doses (Aguilera et al., 1999; Figueroa et al., 1997). Bothwell et al. (1994) stated that solar irradiance not only influences the growth and photosynthesis of benthic diatom communities, but also inhibits algal consumers, especially due to exposure to short UV radiation.

2.5.2 Temperature

Similar to solar irradiance, the temperature is dependent on the location around the globe. Additionally, factors such as altitude, land use, water bodies, annual precipitation, wind velocity and orographic conditions are key factors that contribute to the temperature range of each region. Temperature can affect infiltration rates in MAR spreading basins, either directly due to the dependence of water viscosity on temperature, or indirectly by affecting the biological activity (Dutta et al., 2015). Solar irradiance partly influences the atmosphere temperature, which in turn increases the photosynthesis rate of algae, which is equivalent to a greater biomass blocking or reduction of the infiltration flow path (Mendoza, 2005). Looking at Figure 2.16, the algae *Scenedesmus* needs warmer conditions to reach the highest rate of photosynthesis, while *Synedra* can reach its maximum capacity at 10 °C. The photosynthesis curve has always an optimal point at which enzymes are activated and chemical reactions are sped up, whereas heat causes enzymes to be denaturated and lose its shape.

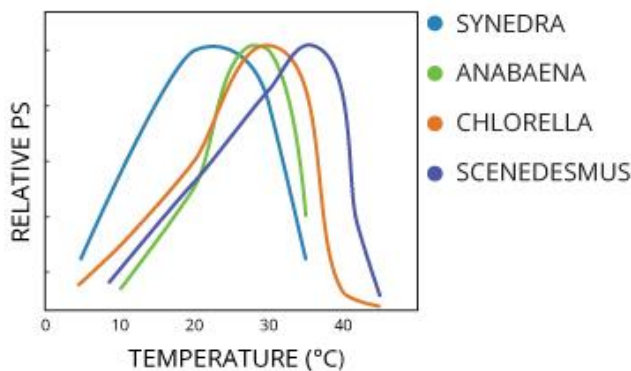


Figure 2.16. Photosynthesis process of 4 algae types depending on the temperature. Source: Fondriest Environmental (2014)

Villanueva et al. (2011) investigated the influence of temperature and nutrients on chlorophyll, bacteria, and ciliates. The nutrient's availability had a higher importance for the growth of these organisms. Nonetheless, colder temperatures hindered their reproduction capability and their enzyme's production on a small scale.

There is a shortage on the information of how solar irradiance and temperature specifically affect MAR surface spreading basins and the inherent chemical, physical, and biological processes. The experiments described in the subchapters 4.1 and 4.2 are meant to give a better perspective on this issue.

This thesis contributes to a wider understanding on the influence of these climate-related parameters on the infiltration capacity of recharge sites and proposes methods to be able to monitor clogging during the infiltration cycles. A detailed description of the designed experimental setups is presented in the next chapter.

3 SITE DESCRIPTION

In order to fulfill the objectives of this thesis, a field infiltration unit was constructed. This field unit was working under seasonal climatic changes. Criteria for the selection of the location for the infiltration unit were: closeness to a river, an aquifer that is not deeper than 20 m from ground surface, an infrastructure offering tap water and electricity connection, and most important of all, clearance that permits pumping of river water and infiltrating river water into the aquifer. The final location of this investigation site is in the vicinity of the Institute of Waste Management and Circular Economy (IAK) in the city of Pirna, Germany, as part of the INOWAS Junior Research Group of the TU Dresden.

3.1 STUDY AREA

Pirna is located 15 km southeast from Dresden, capital of the Free State of Saxony in Germany. The IAK is located on the northern riverbank side of the Elbe River (see Figure 3.1) and it features a study field area designed for groundwater-related investigations (Lehr- und Forschungsfeld Grundwasserwirtschaft) established by the TU Dresden Institute for Groundwater Management in 2007.

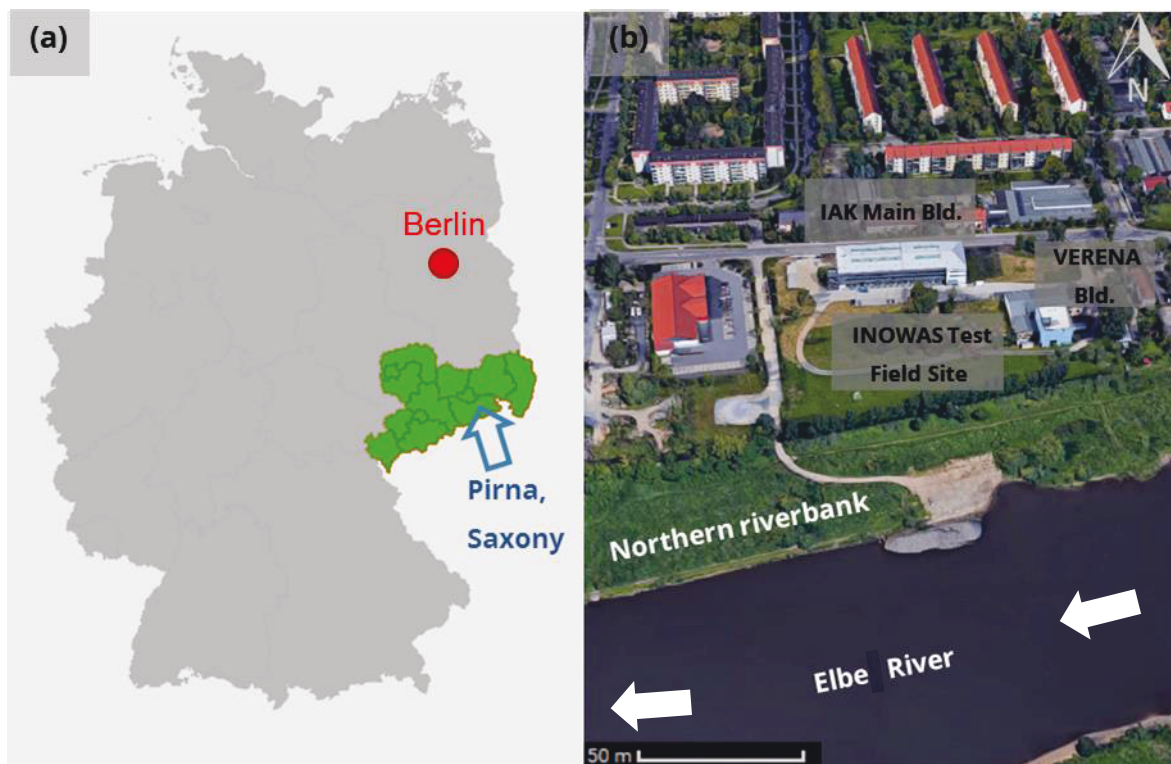


Figure 3.1. Location of investigation site in Pirna, Free State of Saxony, Germany (marked in green in a), and a satellite view of the INOWAS test site (b). Source: Google (n.d.)

3.2 CLIMATE

The regional climate is in transition between the Western European maritime climate and the Eastern European continental climate. This results in a constant exchange of supply of air masses and causes the typical Central European diversity of meteorological phenomena. The strongest influence is coming from the maritime climate (Bernhofer et al., 2009). The balancing effect of the North Atlantic (Gulf Stream) dominates in the region in comparison to other regions of the same

latitude in North America, Eastern Europe, and Asia. An example is the fact that the annual mean temperature in Dresden is about 9 °C, whereas in Winnipeg, Canada it is 2 °C, in the Volga Region (Russia) it is 5 °C and in the Western Siberia -1 °C. Additionally, the amplitude of the monthly mean temperature between the warmest and the coldest month is shorter in Dresden (Bernhofer et al., 2009).

From the data bank of the weather station in Jessen, an analysis of temperature, precipitation and solar irradiance is presented in Figure 3.2, Figure 3.3, and Figure 3.4 for the last 10 years. The mean monthly temperature ranges between 0 °C to 20 °C (Figure 3.2). July and August are the warmest months, whereas January and February register the lowest values (Data source: Mengemann, n.d.).

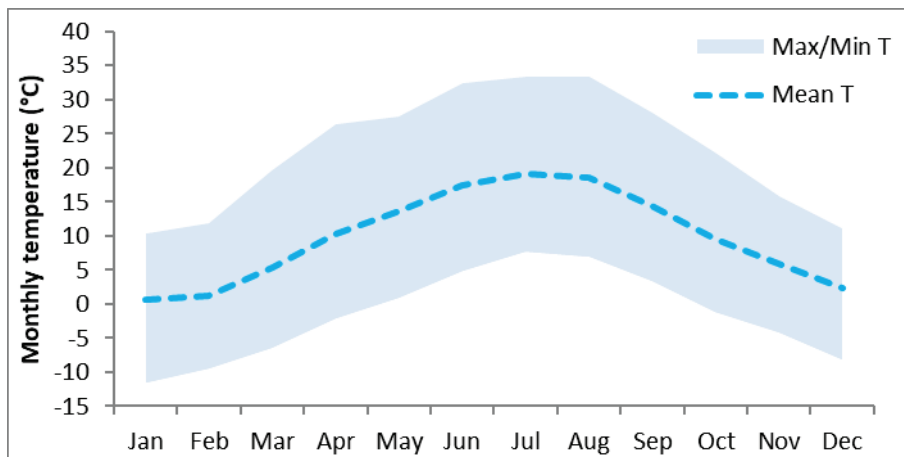


Figure 3.2. Mean monthly temperature in Pirna averaging data from 2009 - 2019. Data Source: Mengemann (n.d.)

The mean monthly temperature values (Figure 3.3) in the last decade follows a linear perspective together with its maximums and minimums, indicating rising temperatures.

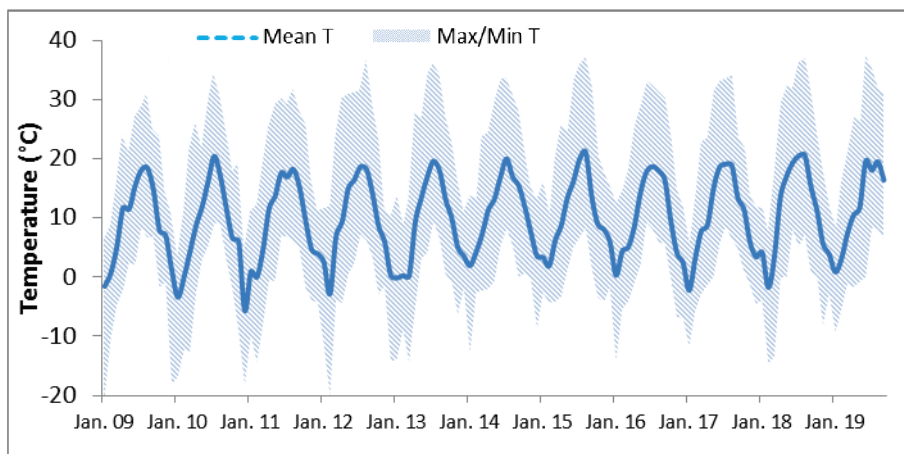


Figure 3.3. Mean monthly temperature in Pirna for the period 2009 - 2019. Data Source: Mengemann (n.d.)

The mean annual precipitation in Pirna in the last 10 years was 489 mm, distributed mostly during the summer time (June-August) as rain (see Figure 3.4). Similarly, the mean solar irradiance has its maximum in the months of June and July, mainly because of the summer solstice. Since the sun is in its highest possible position in the sky and the sunlight hours are also at their maximum during these months, the irradiance can reach values up to 1100 W/m² on clear sunny days (Mengemann, n.d.).

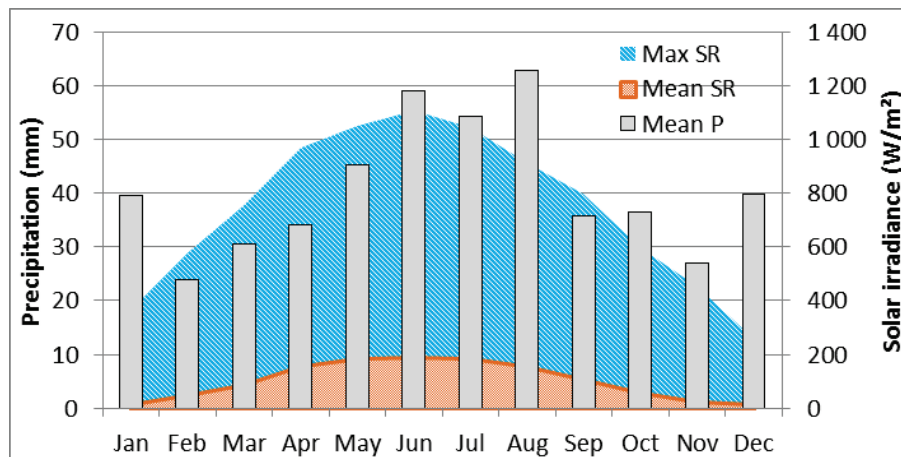


Figure 3.4. Mean monthly precipitation and solar irradiance in Pirna for the period 2009 - 2019.
Data Source: Mengemann (n.d.)

The global irradiance at a specific location depends on two factors: (1) on the length of the path the radiation travels through the atmosphere to the ground and (2) on the duration of sunshine. With increasing distance to the sea, the influence of the continental climate also increases and thus, the frequency of cloud cover is lower. This results in an increase of the Saxon global irradiance towards the east (Bernhofer et al., 2009). The annual course of the clouds is influenced by the frequency of the general weather conditions and the season (thermal stability of the atmosphere). The annual minimum can be found in August (accumulation of summer high-pressure weather conditions), and the annual maximum of cloud cover in November, as cyclones approach from the West (see Figure 3.5a) (Bernhofer et al., 2009). Moreover, the days during the months of June and July (14 hours of daylight) are the longest in Pirna (see Figure 3.5b), whereas the longest nights are during December and January (14 hours of darkness) (Weather Spark, n.d.).

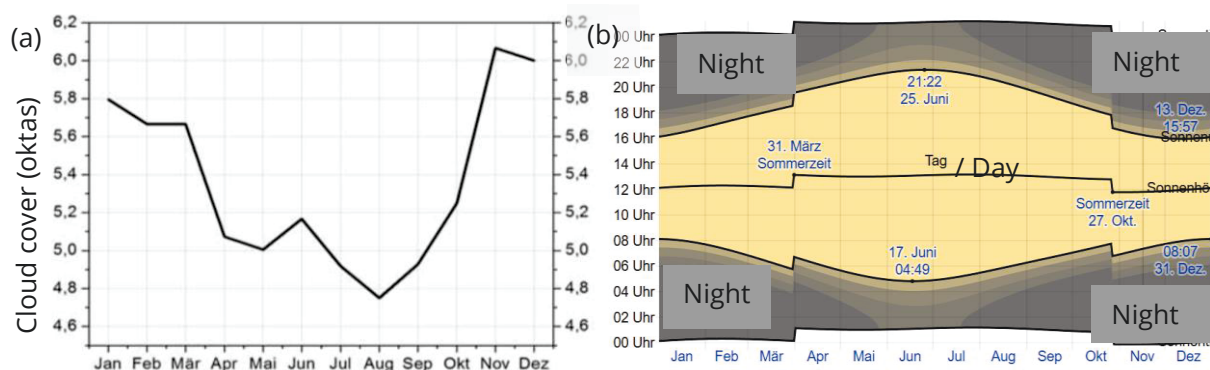


Figure 3.5. (a) Mean cloud cover for the period of 1991 - 2008 in the weather station of Dresden-Klotzsche and (b) daylight variation along the year including the time change in March and October in Pirna, Germany. Sources: Bernhofer et al. (2009) and Weather Spark (n.d.)

There are two sources that result in high wind velocities in the region: (1) the frequent South-eastern winds that occur in the Elbe Valley in every season of the year and are attributable to a channeling effect, and (2) the Bohemian Wind, which is a regional wind of the six-month wind period in South-eastern region of Saxony. The latter is caused by the outflow of cold air from the Bohemian Basin into the Elbe Valley and the Neisse Valley, combined with a simultaneous overflow of the ridges of the Osterzgebirge (ger. Eastern Ore Mountains) and Zittau Mountains (Bernhofer et al., 2009). Figure 3.6 illustrates the variation of the mean (0 - 5 km/h) and maximum (12 - 47

km/h) monthly wind velocities in the last decade at the weather station in Jessen, Pirna. The highest values are registered during the months of December to April (Mengemann, n.d.).

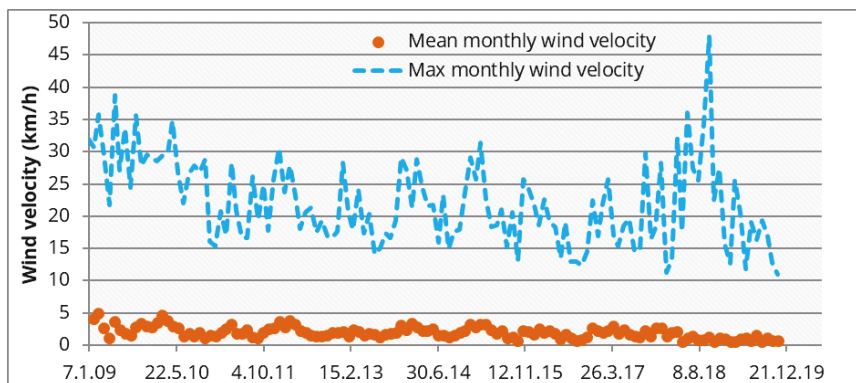


Figure 3.6. Mean and maximum wind velocity for the period of 2009 - 2019 in Pirna, Germany. Data Source: Mengemann (n.d.)

Figure 3.7 shows the distribution of the precipitation in the last decade. 2013 is the year with the highest precipitation rates, especially in the months of May and June. In the last two years (2018-2019), the precipitation has decreased in July and August to rates below 50 mm/month. February and November are the months with least precipitation in the last decade (< 10 mm/month).



Figure 3.7. Monthly precipitation distribution for the period of 2009 to 2019 in Pirna, Germany. Data Source: Mengemann (n.d.)

The months of November to April in the last decade were grouped to observe the snowfall trend. Data for the winter of 13/14 and 17/18 were unavailable. The winter from 2012/2013 experienced

the highest snowfalls (cumulative snowfall: 79 cm). Additionally, it is the only winter where it was snowing for 5 months (November-March). In the last 5 winters, the snowfall has been constrained in two months only (Figure 3.8).

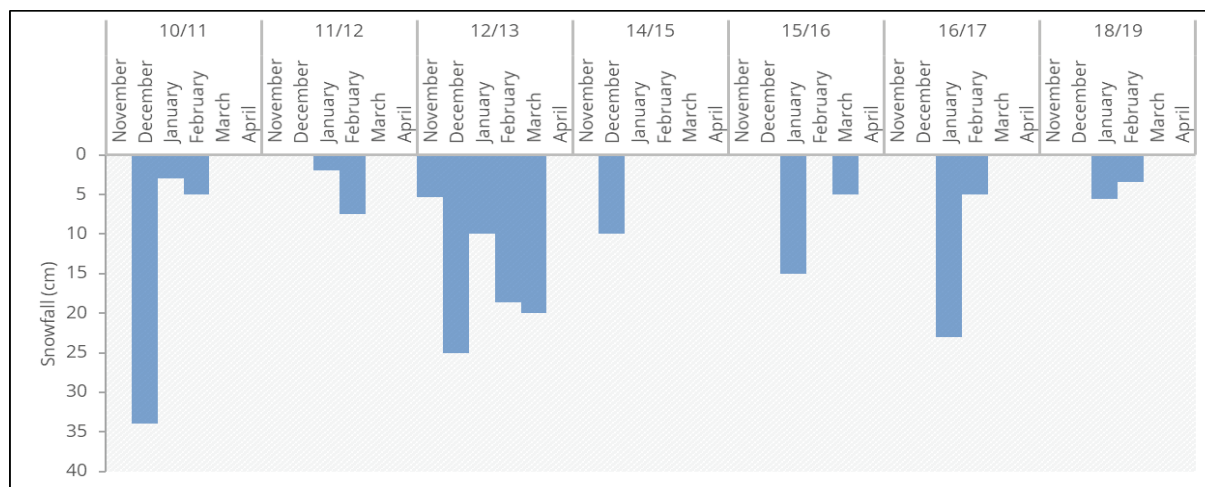


Figure 3.8. Monthly snowfall (cm) for the period of 2010 to 2019 in Pirna, Germany. Data Source: Mengemann (n.d.)

3.3 ELBE RIVER

The transnational perennial Elbe River is a waterway that originates in the Czech Republic and flows northwest through Germany (Dresden, Magdeburg, and Hamburg) into the North Sea. Its right riverbank is 150 m south of the TU Dresden wellfield in Pirna. The source of the river water is predominantly rainfall and snowmelt in the Krkonoše (Giant) Mountains in Czech Republic near the border to Poland (Yiou et al., 2006). The river is recharged primarily by direct precipitation in the Czech catchment (Markovic and Koch, 2015). The average flow rate of the river is 332 m³/s at a 1.84 m water stage in the city of Dresden. This value can fluctuate between 110 m³/s and 1700 m³/s depending on the seasons of low flow (summer) and high flow (spring). The Elbe river width ranges between 110 and 130 m with a mean flow velocity of 1 m/s (Grisczek and Bartak, 2016). A correlation was determined between groundwater levels and the nearby Elbe River, as the groundwater level fluctuations follow closely those of the Elbe River (Figure 3.9).

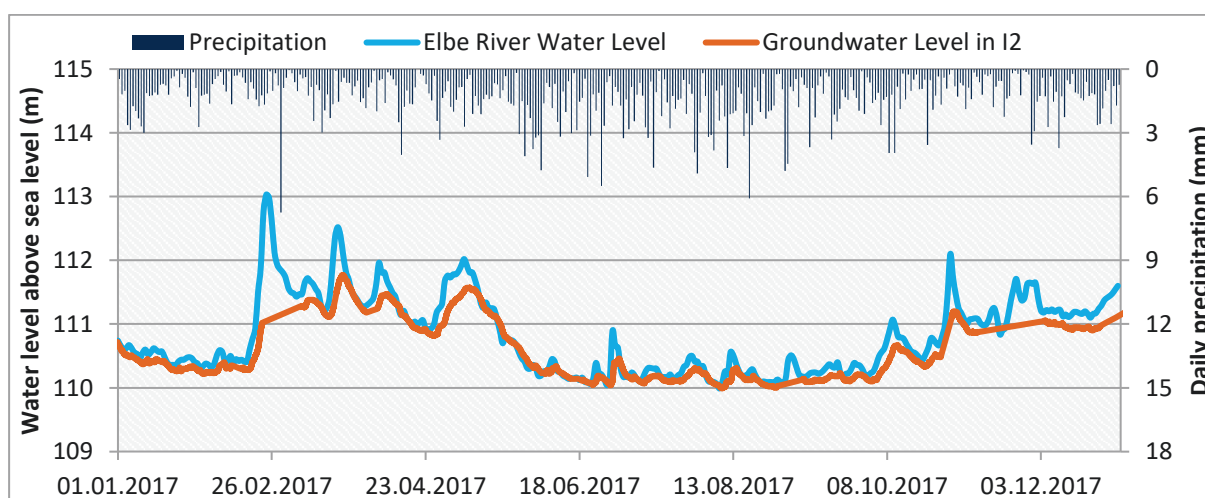


Figure 3.9. Daily precipitation, groundwater level, and Elbe River stage in 2017. Data source: Mengemann (n.d.) and Sächsisches Staatsministerium für Umwelt und Landwirtschaft (n.d.)

Elbe River has been determined as a strongly influencing water body for local groundwater level at the site and is responsible for frequent water table fluctuations within short periods (Bista, 2015; Händel et al., 2016; Kürschner, 2018; Schlamminger et al., 2014).

In the past, the Elbe River was polluted by industries, paper mills, and cellulose processing plants that dumped their effluents directly and without any treatment. Dissolved organic carbon had mean values of 24 mg/L from 1988 to 1990. Data collected from 2000 until 2010 reveal that the annual median for dissolved organic carbon concentration varies between 4.6 and 5.6 mg/L, and the mean turbidity is around 12 NTU and increases sharply up to 120 NTU in case of flood events (Grischek and Bartak, 2016). Although its quality has improved in the last decades, due to the closure of numerous industries and more widespread treatment of wastewater since the reunification of Germany and the end of the Cold War, pollution is still an ongoing problem (Lehmann and Rode, 2001). Herbicides (Nitschke and Schüssler, 1998), heavy metals (Vink et al., 1999), polyfluorinated compounds (Ahrens et al., 2009), and pharmaceuticals, such as antibiotics, diclofenac and ibuprofen (Nikolaou et al., 2007; Wiegel et al., 2004) have all been identified in the water of Elbe River.

3.4 HYDROGEOLOGY

To understand the hydrogeological context of the pilot test field, the regional geology, site lithology and surface water interactions were considered.

Pirna is located at the northwest end of the Saxon Switzerland (ger. Sächsische Schweiz) national park, known for its sandstone hills and mountains formed by the Elbe River. The Elbe Sandstones are built of shallow marine sediments of Mesozoic age, lying on the Early Paleozoic and (Late) Proterozoic crystalline bedrock. The latter is composed mostly of granites and granodiorites in the east together with phyllites, greywackes, schists, and by gneisses in the west (Vařilová, 2016). Figure 3.10 shows a geological map of the region. Pirna is only 5 km to the northwest of the mountains along the Elbe River, where the Elbe Sandstones formations are indicated in the Cretaceous age (Vařilová, 2016). Figure 0.1 and Figure 0.2 in Appendix A.2 contain more detailed information about the lithostratigraphy in Pirna and its surroundings. Pirna is located in the transition zone of the Cretaceous age, meaning that the hydraulic conductivity is lower than in the Saxonian Switzerland because of the higher content of clay and arenaceous marl sections (Niebuhr and Wilmsen, 2014).

The origin of the sandstones in the Saxonian Switzerland can be explained by two theories:

1. Sandstones originated either in a shallow sea, where sand bodies formed during the migration of large submarine sand dunes (environment corresponding to prograding sandy shoreline) (Skoček and Valečka, 1983)
2. Sandstones are remnants / sediments of offshore coarse-grained deltas (Uličný et al., 2009)

Both depositional environments indicate a well graded, coarsening downwards sequence of sand layers which would generate good hydraulic characteristics of the aquifer. From the work of Alexowsky (1997) it can be identified that the Quaternary basis at the INOWAS test field is about 100 meters below the ground surface (mbgs) (see in Appendix A.2 Figure 0.4). Subtracting the elevation of the surface level of the institute (around 115 masl), results in the depth of the unconsolidated sediments (approximately 15 m) which fits with the depth of the upper aquifer at the study site.

Figure 3.11 presents three different stratigraphies along the Elbtal Group. The "Schrammsteingebiet" is located in the nucleus of the Saxonian Switzerland and exhibits a good conductive material (sandstone), whereas in the city of Dresden a higher content of limestone is responsible for reducing the hydraulic conductivity. As it was mentioned above, the city of Pirna is located in the transition zone between the Schrammsteingebiet and Dresden, and therefore also

its hydraulic conductivity is moderate. In Pirna, a low permeable layer can be found below the unconsolidated sediments that act as bed for aquifer's formation (Niebuhr and Wilmsen, 2014). The location of the study area (northern riverbank in the western side of Copitz) is mainly composed by unconsolidated river sediments and gravel flushed by the Elbe River, resulting in a very permeable material that eases the flow of water.

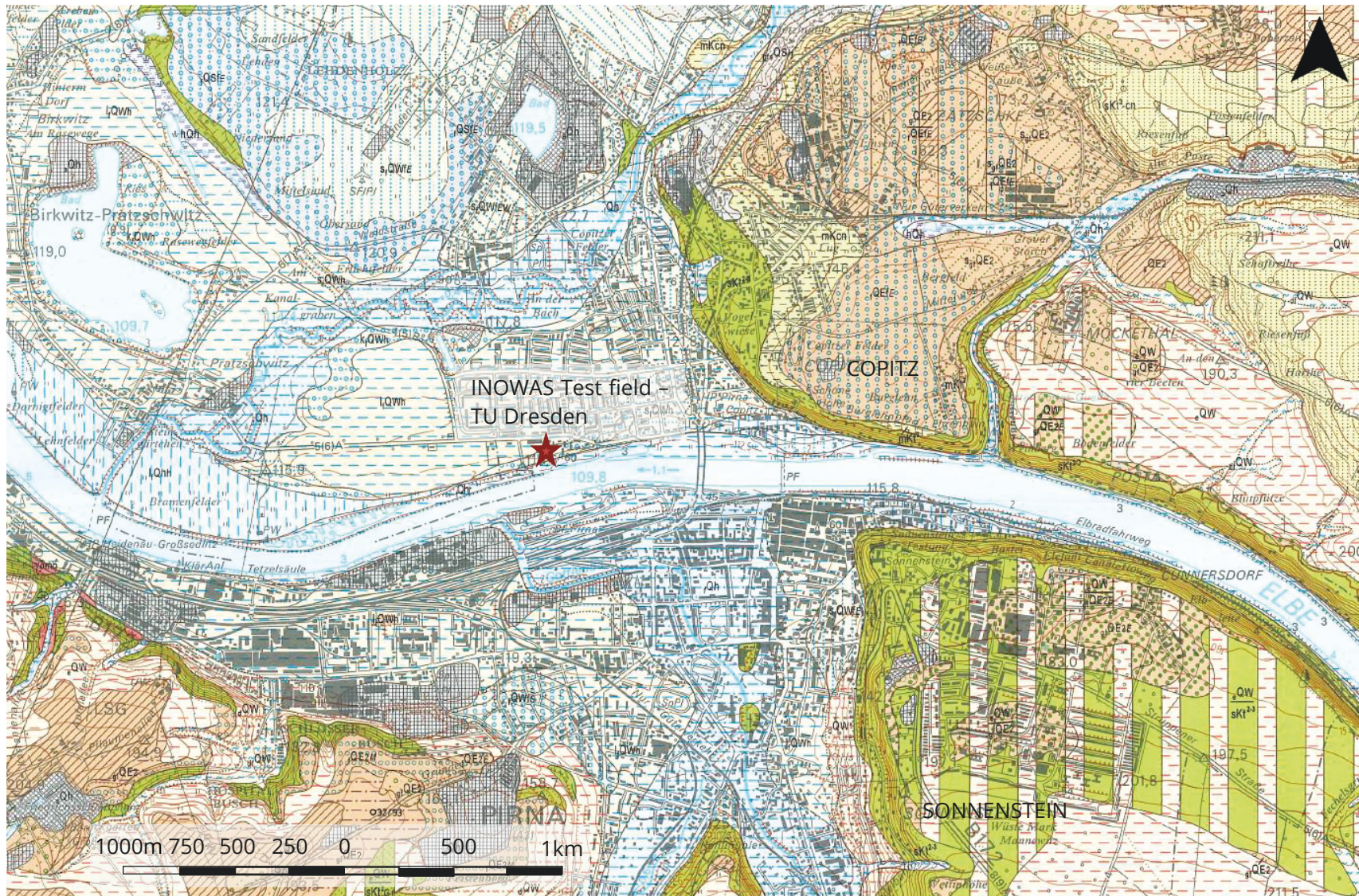


Figure 3.10. Geologic map of the region of Pirna of Free State of Saxony, Sheet 5059. Location of INOWAS test field marked with a star. Source: Alexowsky (1997). Note: The legend is attached in the Appendix A.2 (Figure 0.3)

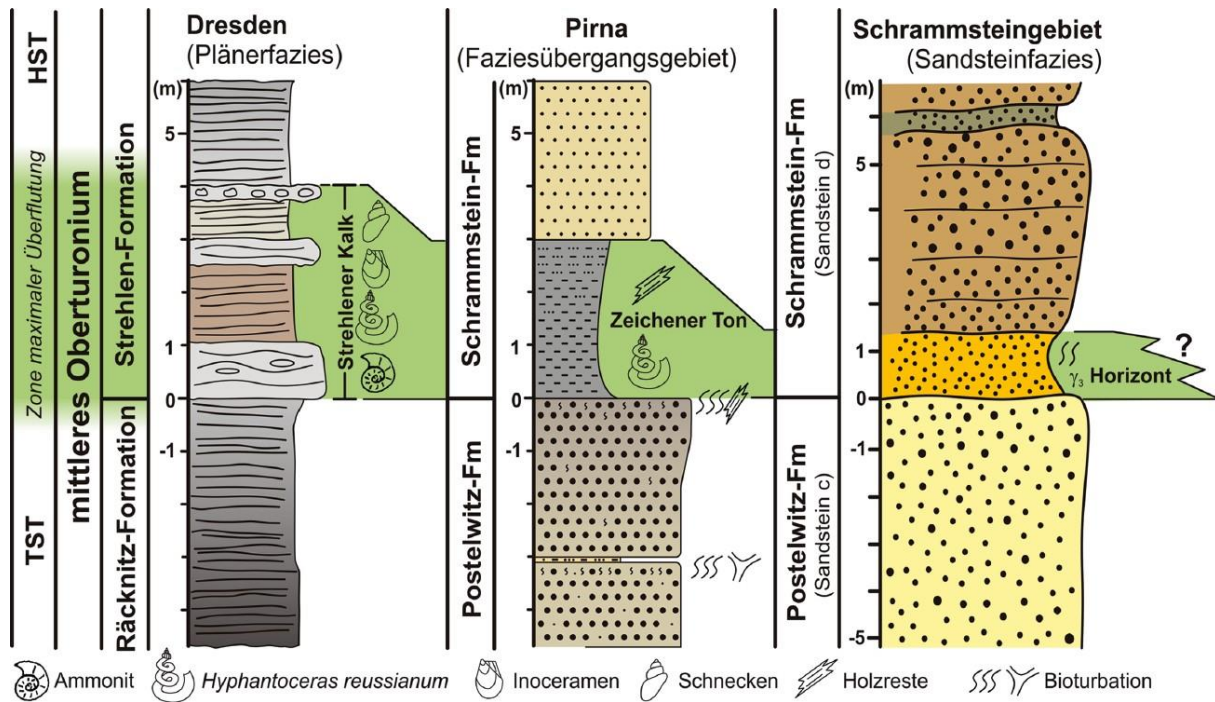


Figure 3.11. Distal – proximal correlation of the Strehlen Limestone (lower Strehlen Formation, mid-Upper Turonian) with the Zeichen Clay (facies transition zone), and the γ_3 horizon (Saxonian Switzerland) at the base of the Schrammstein Formation as a result of a maximum flooding zone; TST = transgressive system's tract, HST = highstand systems tract. Source: Niebuhr and Wilmsen (2014)

Vertical hydraulic conductivity

Dietze and Dietrich (2012) did eight perforations and performed direct push slug test (DPST) at four points (G11, G13, G15 and G17) (See location in Figure 3.14) in the INOWAS test field. 51 DPSTs helped to get detailed information of the vertical hydraulic conductivity distribution. Depths of DPST were determined in intervals with constant Direct Push Injection Log results, which can transform the radial component of K into an estimated hydraulic conductivity. G1, G2, G5, and G10 are located in an area with a higher level. This means that the distance from the land surface to the groundwater table was a couple of meters longer than the remaining wells (see Figure 3.12). The K value measured from the DPST at the investigated four locations varies from 1.85×10^{-5} m/s to 8.9×10^{-3} m/s (Figure 3.13) (Dietze and Dietrich, 2012).

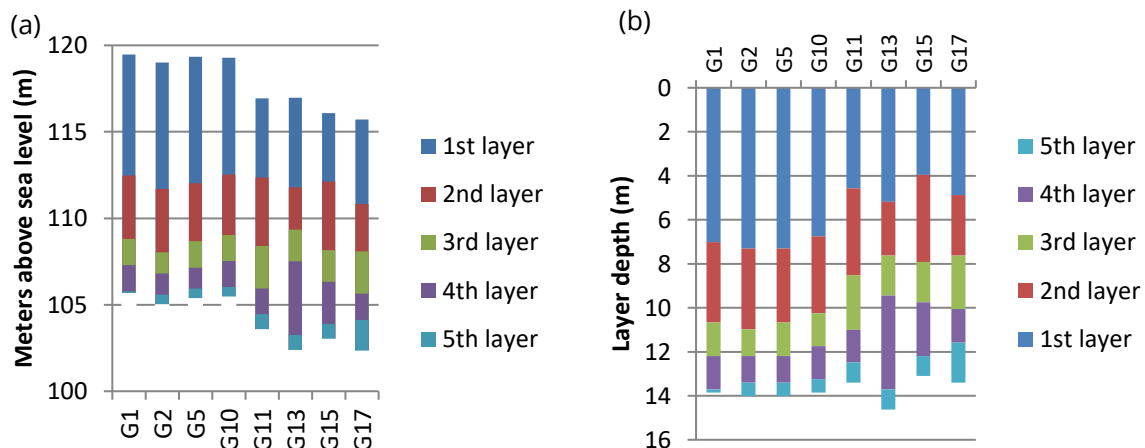


Figure 3.12. Layer profile determination at the INOWAS test field in (a) meter above sea level and (b) absolute depth. Data source: Li (2014)

Vertical variations of hydraulic conductivity

The direct push injection logger (DIPL) was developed to obtain rapid information about vertical variations in K in shallow unconsolidated settings, which uses a small diameter tool with a short screen (45 mm in test site Pirna) attached to the lower end of a pipe string and advanced into the subsurface with hammer assisted direct push technology (Dietze and Dietrich, 2012). As the tool is advancing in the subsurface, water is continually injected through the screen at a relatively high rate to prevent clogging of the screen. Advancement is stopped at the desired depth intervals; water pressure in the injection tubing is measured at different injection rates with a pressure transducer and flow controller on the surface. Based on the injections, the relative hydraulic conductivities were calculated (Dietze and Dietrich, 2012).

The DPIL was performed at 10 different locations at the test site at a depth from 0.3 m to 14.6 m below ground surface until it reached the bed rock with a depth interval of 0.3 m. At each depth interval, measurements with one high and one relatively low flow rate were performed for quality control, and the resulting pressure was measured. Accordingly, two series of relative K value were generated, K_{r1} and K_{r2} respectively. Afterwards, by analyzing and summarizing the variation intervals, layer discretization could be determined at each location (Dietze and Dietrich, 2012).

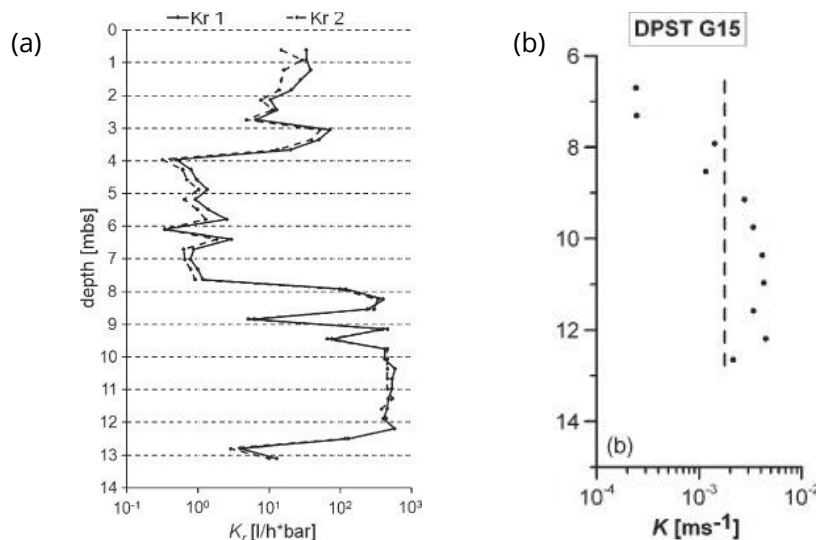


Figure 3.13. (a) Results of two DPIL soundings measured at location G15, with the injection rate of K_{r1} being larger than of K_{r2} , and (b) DPST K values (dots) obtained at G15 from 6 to 13 meters below the ground surface with geometric mean of K values (dashed line) Source: (Dietze and Dietrich, 2012)

The aquifer is mostly composed of fine to coarse sands and gravels; due to the fluvial origin, a high variability in lithology and hydraulic parameters exists. The shallow part (2-4 m below surface) consists of anthropogenic fillings and fine material of the Elbe River flood events. Between depths from 4 to 7.5 m below surface, silty sediments with hydraulic conductivity of around 5×10^{-4} m/s can be found. At 7.5 m below the surface, a highly heterogeneous layer of sand and gravel starts with a thickness of 4-5 m. This layer is highly conductive with values between 1×10^{-3} m/s and 5×10^{-3} m/s, one order of magnitude increase in hydraulic conductivity in relation to the overlying and the underlying layers. At around 11 m below surface, a significant drop in the hydraulic conductivity is measured less than 1×10^{-4} m/s (Dietze and Dietrich, 2012).

With the groundwater levels logged in October 2012 in small diameter wells, a temporal groundwater elevation model was constructed by isolines interpolation, indicating a groundwater flow to the south east, in direction to the Elbe River (Figure 3.14).



Figure 3.14. Groundwater elevation model and location of drilling points at the test field site Pirna.
Data source: Dietze and Dietrich (2012)

Numerical modelling

Li (2014) developed a numerical model of the test field site in Pirna using MODFLOW (Harbaugh, 2005). This model (grid network area: 140m by 180m; cell size: 2m x 2m) incorporated the DPST and DPIL results of the wells G11, G13, G15, and G17. The hydraulic conductivities of the layers at the different sections after the calibration of the model are presented in Table 3.1.

Table 3.1. Hydraulic conductivity distribution of subsurface soil a test site Pirna used by Li (2014)

Layer	1st layer	2nd layer	3rd layer	4th layer	5th layer
G1	7.9E-04	4.5E-04	6.5E-04	2.7E-03	1.5E-03
G2	8.1E-04	7.9E-04	2.6E-03	3.1E-03	1.6E-03
G5	7.7E-04	1.5E-04	2.7E-03	3.2E-03	9.4E-04
G10	6.7E-04	6.7E-04	2.2E-04	2.6E-03	1.6E-03
G11	8.0E-04	1.2E-04	1.3E-03	3.4E-03	2.3E-03
G13	7.8E-04	2.9E-04	2.5E-04	2.5E-03	4.4E-04
G15	7.6E-04	1.5E-04	2.4E-03	3.4E-03	2.1E-03
G17	5.4E-04	2.6E-04	3.8E-03	3.8E-03	1.7E-04

Note: Vertical cross-section of each well can be retrieved from Figure 3.12.

Bista (2015) improved this model by modifying the boundary condition's types and prolonging the simulation time period (From 152 days to 233 days). Hydraulic conductivity, specific yield and riverbed conductance were identified as the most influential flow parameters. To get the best fitted model, the specific yield was set to 0.16 and hydraulic conductivities of Layer 3 and Layer 4 were multiplied by a factor of 3 and 2, respectively.

A detailed groundwater recharge capacity of the upper layer of the soil profile (90 cm below the ground level) was modelled with HYDRUS 1D (Šimůnek et al., 2016) and determined a hydraulic conductivity ranging from 10^{-6} to 10^{-3} m/s (0.09 – 80 m/d), and a recharge rate of 0,08 cm/d (Brecht, 2015). Surface sections with big boulders and broken bricks and lime soil lenses give the soil a very heterogeneous profile with big soil hydraulic properties variations (Brecht, 2015; Moreno, 2015). The evaluated location is next to the designated area for the MAR infiltration tests of this research.

4 METHODOLOGY

The aim of the field and laboratory work was to give a valuable input to the Decision Support System of the Web Platform of the INOWAS project (www.inowas.com), to relate and validate results obtained from the laboratory work, adding to it real boundary conditions to the experiment. For more information refer to the investigation of Fichtner et al. (2019).

The MAR field test site consisted of pilot scale rapid infiltration unit and a set of 5" monitoring wells; both located in the nearby of the Elbe River banks. Infiltration scenarios were run with variable temperature ranges for the determination of the development of clogging. To quantify the influence of solar irradiance, a set of soil columns was installed in the laboratory to control the light conditions. Additionally, a physical model was constructed to determine the recovery of infiltration capacity after several scraping procedures. This consists of 2 infiltration tanks located in the laboratory. All units were packed with the same sandy material and the water source was from the Elbe River. A detailed description of each infiltration unit follows next:

4.1 INFLUENCE OF CLIMATE ON INFILTRATION BASIN RECHARGE

The climate data for the analysis of the results in the field infiltration unit were extracted from a private weather station in Jessen, Pirna, 128 m above sea level (coordinates 50° 59' 43" North - 13° 56' 54" East), which offers free access to measurements of temperature (°C), solar irradiance (W/m²), humidity (%), among others, on an hourly basis. The data can be retrieved anytime from their website www.pirna-wetter.de. Especially temperature and solar irradiance were useful for categorizing the different infiltration scenarios into warm, mild, or cold conditions.

4.1.1 Temperature

To evaluate the influence of the temperature in surface spreading basins, a rapid infiltration unit was installed in the field and different infiltration scenarios were conducted through the different climatic seasons. The infiltration capacity was assessed mainly by tracer experiments and the hydraulic processes were monitored with a network of sensors.

Setup of rapid infiltration unit

The main test unit in this research was constructed taking into account the recommendations of Sallwey et al. (2018). They worked with HYDRUS 2D/3D (Šimůnek et al., 2016) to replicate especially the conditions in the unsaturated zone and design the infiltration unit size and geometry. Modeling results helped in the determination of the optimal dimensions of the infiltration unit and the placement of measurement devices so as the hydraulic experimental scenario planning. It was determined that at depths below 1.5 m, pressure head readings do not exhibit bigger changes (Sallwey et al., 2018).

Moreover, Sallwey et al. (2018) stated that the measuring sensors should not be situated close to the infiltration unit border to avoid influence by the boundary. It was stated that the dimensions of the infiltration unit (<10 m each side) do not require more than five measuring sensors per layer, since the variation in the reading will not be significant. Finally, it was recommended to install three observation points at each level: one device in the center of the basin and two measuring tools at the side of it.

The infiltration unit site is located in the lower plane of the TU Dresden Institute in Pirna, on the south side of the main institute building. The topsoil was removed with an excavator to get a trench with the dimensions of 5.0 m at the edge of west to east and 4.0 m at the perimeter of north to

south. The depth of the trench excavation was approximately 1.50 m (Figure 4.1). This trench was afterwards filled with the experimental soil.

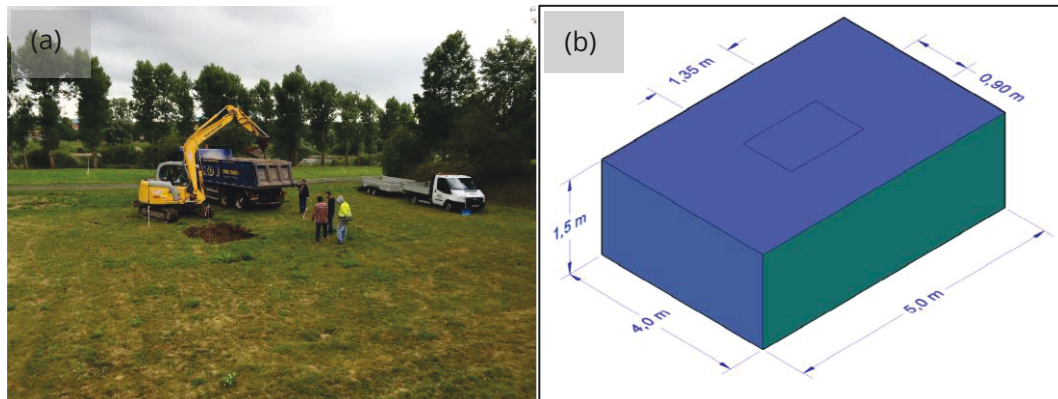


Figure 4.1. (a) Excavation of topsoil at the INOWAS test field and (b) designed dimensions of the infiltration unit, including the dimensions of the infiltration basin. (Picture by T. Fichtner 2015)

The experimental soil consisted of an industrially elaborated material from the company *Stein und Erden* (located approximately 29 km northeast of Dresden), which could be re-ordered many times to get a soil with the same hydraulic properties for the different scenarios. According to the sieve analysis (Figure 4.2) performed in the institute's laboratory, the soil has a uniformity coefficient of 4.81, and the hydraulic conductivity is 6×10^{-5} m/s (91.2 % sand, 8.0 % silt, 0.8 % clay) at 20 °C applying a mean between the empirical equations of Hazen (1892) and Zieschang (1961). Applying Equations 1, 2, and 3 the mean permeability k of the sand was determined: 6.14×10^{-12} m².

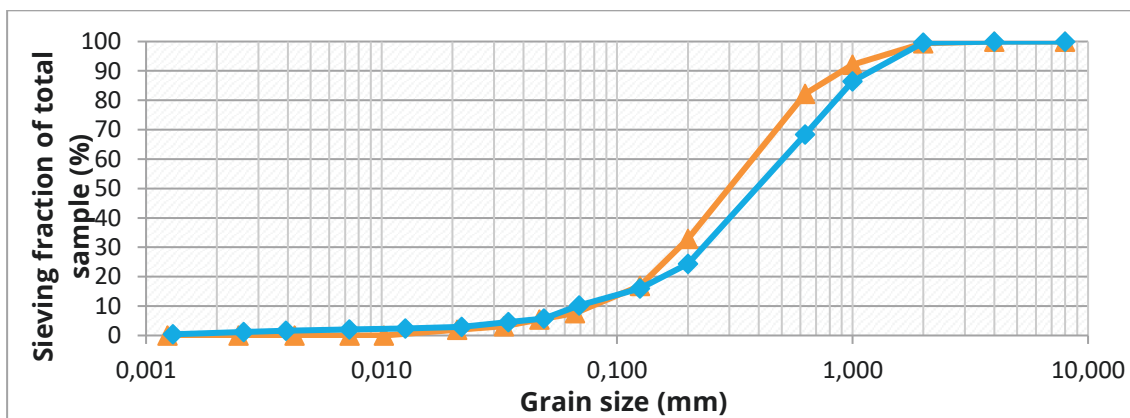


Figure 4.2. Grain size distribution of two soil samples of selected packing material

The diameter of the grain size of soil particles ranges from 0.0013 mm to 3.0 mm. Particle size analysis of the porous media is given in Table 4.1.

Table 4.1 Particle size analysis of the packing material of the infiltration unit

Grain	Diameter [mm]	Percentage
Gravel	2-8	0.48
Sand	0.0662-1	90.61
Silt	0.0025-0.0468	8.30
Clay	>0.0013	0.61
Total		100.00

The soil was introduced to the trench in weighted amounts of 50 kg. A wooden frame was constructed to control the filling height and ensure the soil compaction of 1.7 g/cm^3 in an area of 20 m^2 . In total, 51 000 kg of soil were homogenously compacted in layers of 30 cm with a Diesel-based vibratory plate compactor with a nominal pressure force of 20 kN (see Figure 4.3). Once the infiltration unit was filled, a 10 cm deep ponding basin was constructed in the center of the sand unit with the dimensions of 130 cm length and 90 cm width. The floor of the basin was flat and did not consider any inclination.



Figure 4.3. Compaction of soil at 1 m depth with a vibratory plate compactor.

In total, 12 observation points were arranged in three layers (marked in red dots in Figure 4.4). These were meant to monitor the hydraulic behavior of the system during the infiltration experiments. One observation point was located right below the infiltration basin, one 1.25 m to the east, one 1.00 m to the north and a last one 1.80 m to the northwest. The setup should cover the vertical and lateral flow patterns of the infiltration water in this half of the basin. Due to the symmetry of the homogenously packed material, it is assumed that the hydraulics will behave similarly in the other half. The depth of the first and second layer (0.3 m and 0.7 m, respectively) is directly connected with a parallel experiment that took place in an environment controlled 3D steel tank in the laboratory facilities of INOWAS (Fichtner et al., 2019). The lower observation layer was located 0.2 m above the natural soil material (1.40 m from the surface), to avoid a measurement disturbance because of the changing hydraulic conditions of the native soil.

A specific nomenclature of the observation points was designated; they are separated in two sections as can be seen in Figure 4.4. The first number indicates the layer number, the second number shows the location in the horizontal plane of the layer and both numbers are separated by a dot (".").

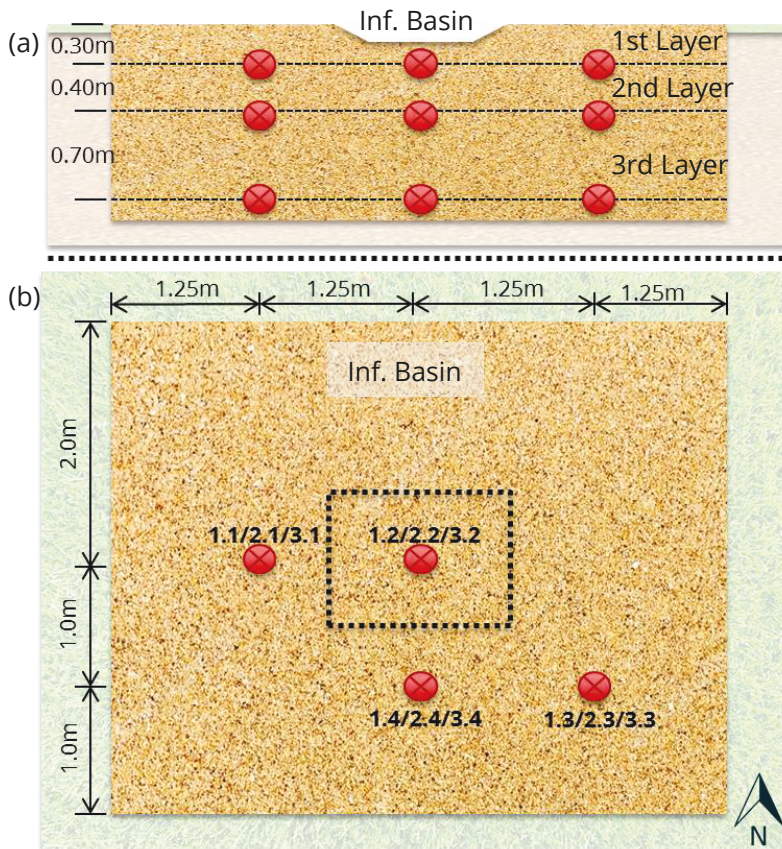


Figure 4.4. (a) Profile view of the infiltration unit and (b) bird view of the infiltration unit with the respective location of the observation points and the infiltration basin (in dashed lines)

Each observation point was equipped with multiparameter sensors that were connected to a logger (UGT GmbH, Dresden, Germany) measuring every 2 minutes. For the assessment of the spatial and temporal distribution of the infiltrated water in the vadose zone, tensiometers (tensio152, UGT GmbH, Müncheberg, Germany) and TDR-probes (UMP-1, UGT GmbH; features the measurement also of electrical conductivity and temperature) were installed. Suction cups were additionally installed in order to be able to take water samples for laboratory analysis (e.g. DOC). The installation of the sensors in the three layers is shown in Figure 4.5.



Figure 4.5. Installation of measuring devices (tensiometers, water content, temperature and electrical conductivity) in (a) Layer 1, (b) Layer 2, and (c) Layer 3

Monitoring wells

In June 2016, the company Brunnenbau Wilschdorf GmbH drilled and installed seven 5" monitoring wells at the test field of TU-Dresden in Pirna. The wells were in such a distribution that the recharge water in the rapid infiltration unit could be tracked. One monitoring well (I-01) was in the north of the infiltration basin (Figure 4.6) and I-02 in the south of it, in the groundwater flow direction. Wells I-03 to I-07 are in a strategic position to identify the path of the recharged water at different

distances. Each well case has a diameter of 219 mm, a depth of 14 m, and a 3 m screen (from interval 10 m to 13 m) as illustrated in the well design graphics of Figure 4.7.

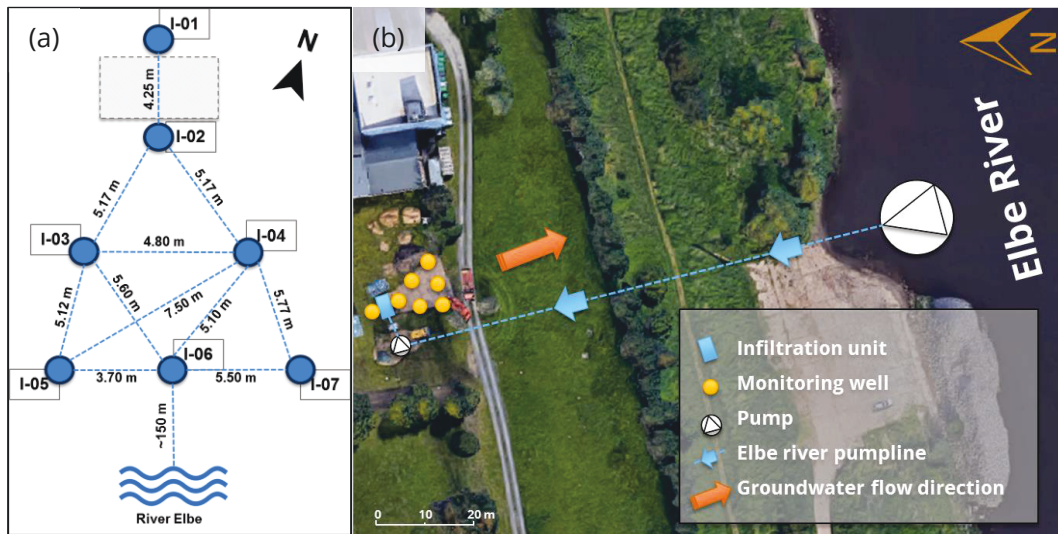


Figure 4.6. Location of monitoring wells from in a sketch view (a), and a satellite view (b)

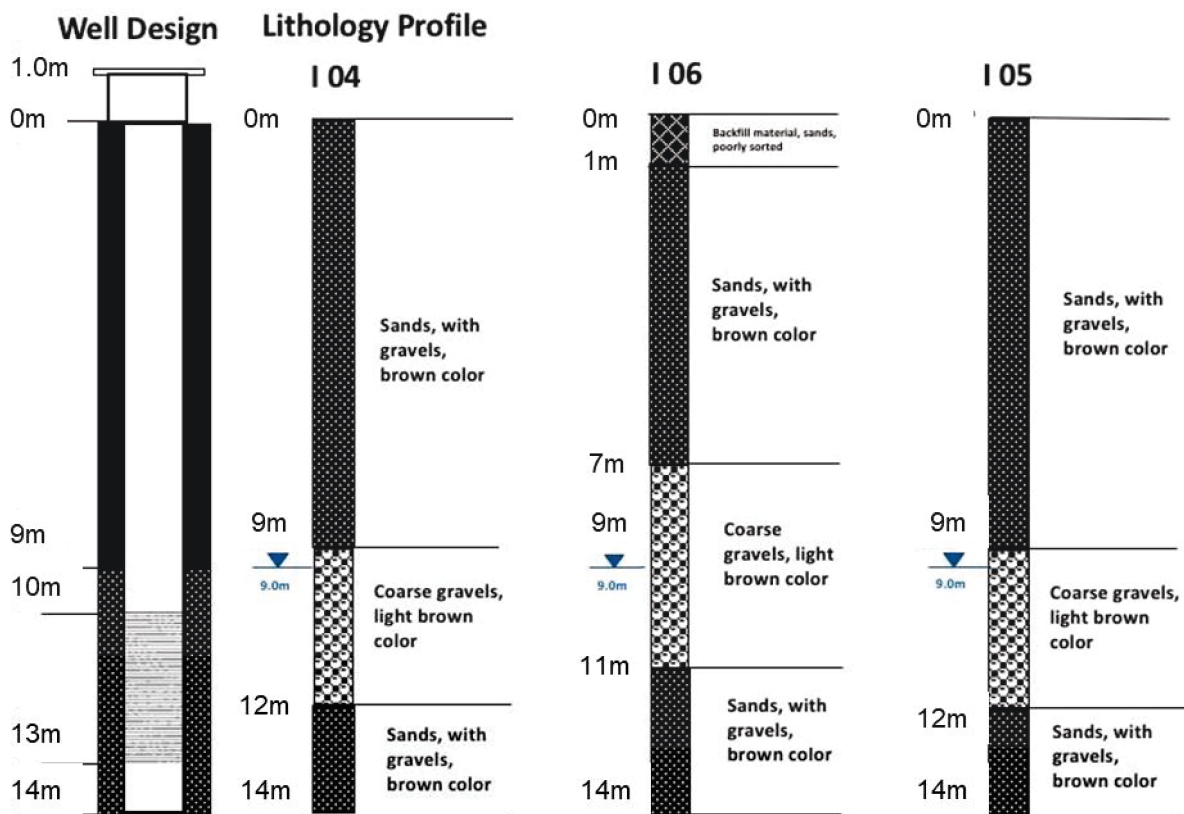


Figure 4.7. Well design and lithology profile of wellfield at Pirna

Soil samples of each drilled core were taken after each drilled meter. Since the sampling method was via Hollow Stem, the samples collected were mixed throughout the whole one-meter core. Nevertheless, clear distinctions of the main layers were easily identified. The results match approximately with the results published by Li (2014) for G11, which is the 2" well located in the vicinity of 5" wells. High organic content sand mixed with anthropogenic filling material (brick's debris) exists in the topsoil until 3 m depth, followed by a finer material with a higher content of

silt until 9 m. At this depth, the groundwater level (typical for the summertime) is reached, together with a three-meter very conductive layer of gravel. The last segment of the borehole consists of a sandy material (Figure 4.8).

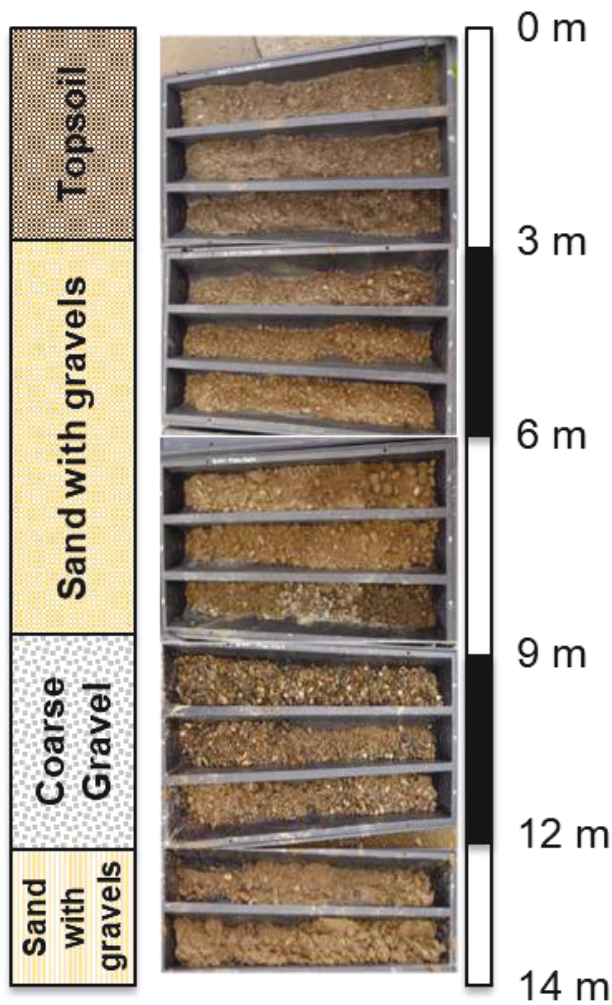


Figure 4.8. Soil samples collected from the borehole of I-02

Altogether, the MAR field complex can be simplified in a sketch presented in Figure 4.9, with all its main components: A rapid infiltration unit with a specific sensor positioning (red dots), a movable roof to avoid the influence of rain events (roof was lifted during sunny days), a pipeline from the Elbe River to the storing tanks, a network of monitoring wells equipped with groundwater sensor devices, and the control house containing the data loggers of the sensors.

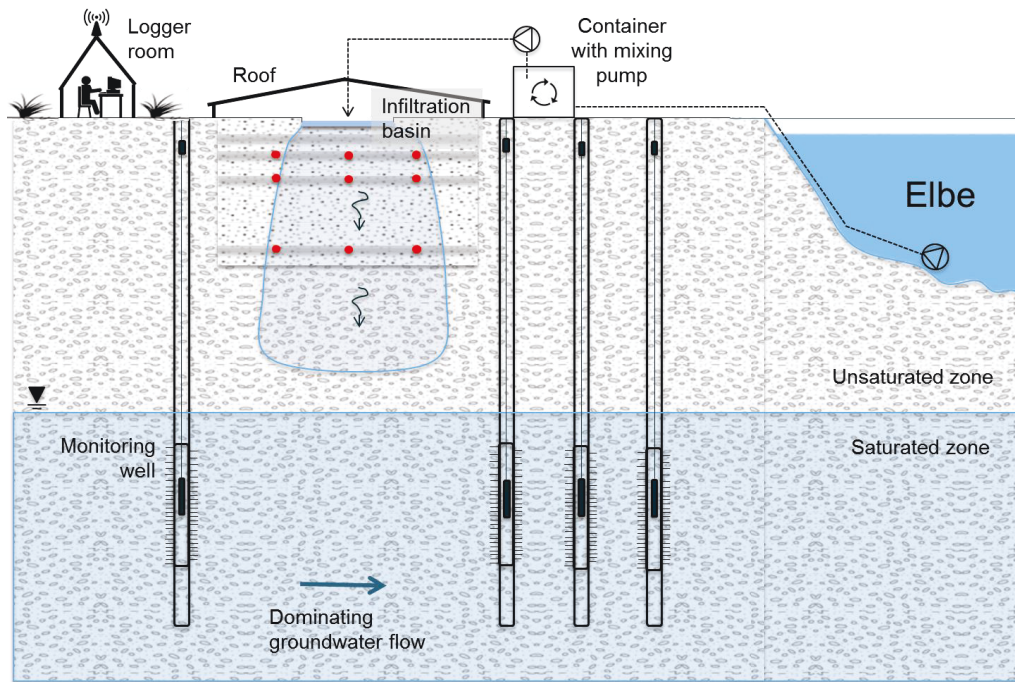


Figure 4.9. Simplified sketch (not to scale) of MAR field site components

Infiltration scenarios

The infiltration was operated in four scenarios with variable HLC and a fixed HLR of 300 m/a (reference value for other projects led by INOWAS recherche group), using Elbe River water (dissolved organic carbon (DOC) 5-7 mg/L and total suspended solids (TSS) 5-20 mg/L) that was pumped from the river and temporarily stored in a collection tank next to the basin. Infiltration pre-tests showed that the DOC of the Elbe River does not reduce significantly after 1.4 m of soil passage (sensor 3.2). The DOC was reduced from 5.82 mg/L to 5.04 mg/L; 5.38 mg/L to 4.90 mg/L, and 6.05 mg/L to 4.95 mg/L, during the pre-test infiltration in November 2016. Since the reductions were not considered significant, only the influent DOC was monitored.

The recharge rate was determined by previous infiltration column tests done in the laboratory and represents 10 % of the overall infiltration capacity of the soil. Scenario 1 simulates the HLC of a SAT site in the Dan Region, Israel, using 1 day of infiltration followed by a 3 days drying period (Goren et al., 2014). Scenario 4 represents inverted conditions with a ratio of 3:1, having a longer wet period and shorter dry phases. Scenario 2 covers a common operational mode in the USA of 1 week infiltration and 1 week pause. In order to include also sites with continuous infiltration, Scenario 3 was conducted having a continuous recharge of river water over time (Table 4.2).

The pumping rate was regulated to meet the HLR requirements. Scenarios with shorter infiltration periods have higher pumping rates, because a fixed annual volume had to be recharged in a shorter pumping period. Table 4.2 summarizes the technical hydraulic setup of each scenario. Several "runs" were conducted in order to get the reduction of the infiltration rate for every scenario with 3 climates categorized as: warm, mild, and cold. The categories were based on temperature and solar irradiance data. Some runs had to be repeated, since the climatic conditions did not meet the desired scenario.

Table 4.2. Definition of experimental infiltration periods

Scenario #	Wet Period [h]	Dry Period [h]	HLC [-]	HLR [m/a]	Pump rate [L/min]
1	24	72	1:3	300	2.77
2	168	168	1:1	300	0.69
3	Continuous	0	Continuous	300	0.35
4	72	24	3:1	300	0.92

Clogging determination by tracer tests

To quantify the effect that clogging has on the infiltration rate of spreading basins, salt tracer infiltration tests were conducted. The tests showed the change in infiltration rate over time, which is analogous to the effect of clogging. Salt tracer solutions (NaCl) with EC between 2.5 mS/cm and 5.0 mS/cm were prepared and the t_{50} times were measured for each infiltration cycle in each scenario. Infiltration velocities (m/s) were calculated using Equation (4). These linear velocities were recalculated to normalized velocities by using the initial infiltration velocity as the non-clogged original state, so that a decrease in velocity in relation to the initial value could be visualized against the volume of infiltrated water.

Additionally, at the end of each scenario, soil samples were taken from the surface of the basin surface for TOC analysis, since high carbon content in the topsoil indicates the presence of a clogging layer in the topsoil.

4.1.2 Solar irradiance

Owing to the complex dynamics of elements involved, the identification and characterisation of the cause of clogging, which in turn leads to reduced infiltration rates, represents a huge challenge. One of the factors influencing biological clogging is solar irradiance. Despite its sheer importance, literature regarding the effect of solar irradiance on the clogging rate is quite scarce, which leads to poor understanding of the processes involved.

This chapter attempts to investigate the effect of solar irradiance on clogging via column experiments and to develop a better understanding of sunlight-induced influences on the surface spreading techniques. A total of 22 sand-filled plexiglas columns were used: 12 columns for infiltration of the Elbe River water, and 10 columns for infiltration of tap water which were used as a blank. In laboratory conditions, four constrained scenarios were created: 1) sunlight, 2) blue light (450nm) 3) red light (650nm) 4) darkness. The blue and red light scenarios represent fractions of visible light that may influence the growth of photosensitive algae and bacteria. The specific objective of this work was to investigate variations in infiltration capacity, and to quantify clogging response in soil columns kept in different light conditions using tap water and Elbe River water.

Soil columns setup

The main source of water used for the experiment was Elbe River water, which was collected every second day in a 500 L container. A second source of water used for a blank test was tap water. The comparison between river water and tap water allows to identify the influence of the organic materials and suspended solids on the reduction of the infiltration capacity. Quality analyses of Elbe River water samples and tap water are presented in Table 4.3. For the DOC measurement, Whatman Puradisc Syringe Filters were used. A 50 mL sample was collected and pressed through

the filter by using a syringe, and 10 mL of hydrochloric acid (HCl) was used to inhibit further growth of bacteria. TSS were also measured using the standard method 2540-D guideline.

Table 4.3 Recharging water characteristics

Parameter	Elbe River	Tap water
DOC	5-7 mg/L	< 0.01 mg/L
EC	500-600 $\mu\text{S}/\text{cm}$	100 – 200 $\mu\text{S}/\text{cm}$
TSS	5-20 mg/L	< 1mg/L

Three artificial light sources (LED lights) were used to study the effect of different light conditions on clogging of the columns, consistent with field conditions. 650 nm (red light) and 450 nm (blue light) were chosen as the extreme spectra of visible light and a light source with all the spectrum components (IR, UV and visible light) was used as sunlight scenario. Finally, one scenario in darkness has also been conducted as the night scenario.

The laboratory experimental system included three sections: 1. water supply tanks with a circulation function (includes two submersible pumps with a maximum output of 135 L/h); 2. An upper constant-head controller for continuous water supply and drainage; and 3. the experimental seepage columns, as shown in Figure 4.10. The columns were filled with the same soil material as in the field infiltration unit in Chapter 4.1.1.

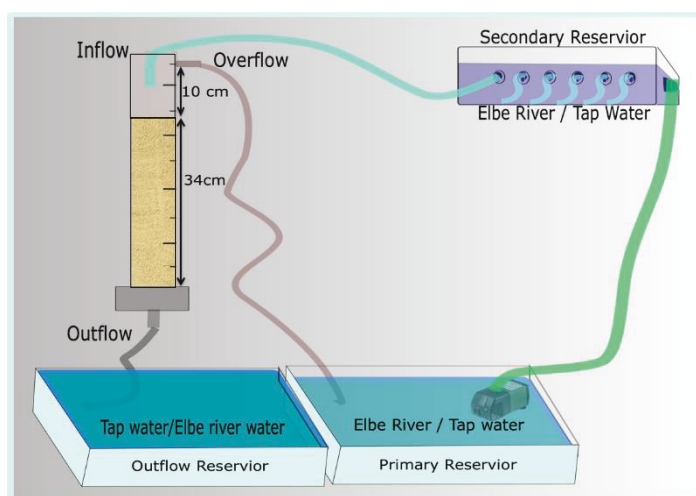


Figure 4.10. Experimental setup components. Source: Mahmood et al. (2019)

A ponding depth of 9 cm was set for all the columns. The constant head method gave the opportunity to ensure an equal input of water to all the columns in a long term. Relatively low flow rates (< 100 mL/min) and thin distribution hoses (4 mm diameter) increase the probability of having blocked hoses. Therefore, higher infiltration rates and an overflow output were considered in the experiment.

The plexiglas acrylic columns have an internal diameter of 4 cm and are supported at the base with stainless steel mesh and screens (membrane) to retain the soil in the columns and to help spreading the input water laterally throughout the columns. The total length of each column was approximately 50 cm with a packing soil depth of 34-37 cm. An empty headspace of 9 cm was left in all columns to allow surface ponding.

Using packed or monolithic columns will have a direct impact on the experimental results, as for example Bromly et al. (2007) demonstrated that it has a significant influence on the resulting solute transport behavior of the columns. The most common approach and also the one used in this experiment is dry or damp packing (Lewis and Sjöström, 2010).

It is important for the packing of the experimental vessels to produce a homogeneously filled soil column with a bulk density representative to the one in the field conditions, and simultaneously reducing the formation of stratifying layers, or preferential flow pathways along the edges (walls) of the columns and along natural fissures in the core material. Dry or damp packing involves filling small quantities of dry or damp soil into the column. Afterwards, the column is mechanically packed either by hand or with some type of compactor. Lewis and Sjöström (2010) have reviewed several studies regarding the “lifts” of dry deposition. According to their discussion, the increments could be from 0.2 cm to 15 cm depending on the objectives of the experiment. They also recommended to lightly scarify the soil surface after the compaction of one lift was done and before the addition of the next lift. This ensures a hydraulic connectivity between the layers.

For the experiment, the core material (soil) was dried in an oven at 70.0 °C for 48 hours. The oven-dried deposition was crushed, sieved manually, and larger gravels were removed. Afterwards, the dry deposition was added into the columns in a series of 10 cm lifts followed by compaction with a piston.

The soil was saturated by slowly wetting from the bottom and letting it stand flooded overnight to enable entrapped air to flow out and particles to settle. The initial saturated hydraulic conductivity was then determined from a brief (10 min) infiltration test using NaCl as tracer. The values of the initial infiltration rate of the soil columns are comparable to the values of medium to coarse sand reported in the literature (Domenico and Schwartz, 1998).

Only the porous media at the surface was exposed to the light incidence to match field prototype conditions. The outer surface of the columns was covered with aluminium foil to prevent light penetration and subsequent growth of photo-autotrophic organisms. The feed water was gravity-fed to the soil columns from a storage reservoir (primary reservoir) via a constant head tank (secondary reservoir) of 80 cm above the soil surface to assure stable hydraulic conditions and fully saturated conditions over the duration of the experiment.

To recreate actual sub-surface light-conditions and to protect the columns from surrounding air and light, a 1 meter high wooden box covered all the columns. A schematic representation of the whole experiment is shown in Figure 4.11. Four partitions were constructed inside the wooden box for the four different light scenarios and inside those partitions soil columns were triplicated for each of the water quality scenarios. Overflow from the columns was collected in storage reservoirs and recycled to the columns by pumps. An extra mixing pump was used in the reservoir of Elbe River water to avoid the deposition of suspended solids.

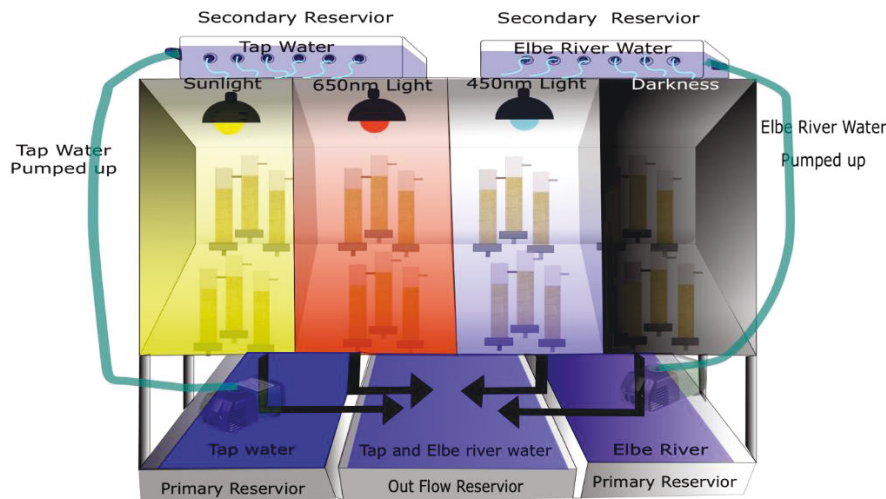


Figure 4.11. Schematic representation of the experiment system. Source: Mahmood et al. (2019)

Infiltration experiment

The experiment ran for five weeks (27 November to 30 December 2018). Tracer tests were conducted three times a week to study changes in the hydraulic properties of the porous medium due to clogging. NaCl was added as a conservative tracer at the inlet of the columns and measured at the outlet as EC to obtain the breakthrough curves. The EC measurements were manually collected every five minutes and evaluated by a probe. The reduction of the linear velocity was assessed using Equation 4.

Flow rates in the outflow of each column were also measured three times a week using a measuring cylinder and a stopwatch for more accurate and reliable measurements of hydraulic properties.

4.2 MANAGEMENT OF CLOGGING IN SPREADING BASINS

This chapter aims to investigate how scraping protocols influence infiltration rates in infiltration basins. Scraping is a common procedure in spreading basins when the infiltration rate is strongly reduced because of clogging. It consists in the removal of the upper surface of the soil and must be executed while the infiltration basin is dry. Currently, no available comprehensive summary or comparison between scraping protocols at MAR sites was found in the literature.

Setup of spreading basin infiltration tank

Two physical models were constructed for the experiment, each model represented a spreading basin infiltration unit. One unit was running without any scraping measure, whereas the second one included a scraping event every time the water level was too high. Figure 4.12 displays one of the spreading basin infiltration units in its simplest form. Each basin comprised a 310-L open-topped water collection vessel (1). This container was positioned on a metal grid (2) supported by construction bricks (3) to allow collecting and disposing the outflow.

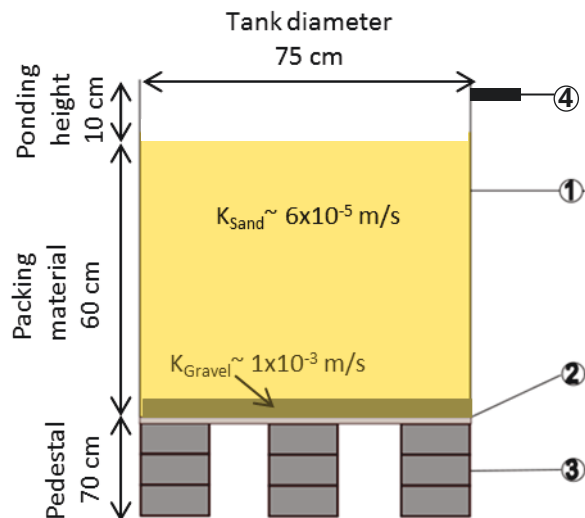


Figure 4.12. Schematic sketch of the spreading infiltration tank, together with the main dimensions of the vessel (1) resting on a metal grid (2), brick pedestal (3) and overflow pipe (4). The hydraulic conductivities of both packing materials are included

Each tank had four outflow points, which were evenly spaced around the midpoint of the base of the unit. The tubing was fed through the metal grid base and led to the outflow collection basin. To prevent the solid contents of the infiltration basin from escaping or blocking the outflow connectors, each of the four outflow points was covered with a geotextile filter. This material allowed fluid flow but restricted the passage of soil particles.

Coarse sand (1×10^{-3} m/s) was placed into the base of the infiltration unit. This coarser material helped to drain the system and formed a barrier between the outlets and the finer soil on the infiltration unit.

The experimental soil was the same fine-grained sand used in the previous field and laboratory experiments in Chapter 4.1. To create an even compaction and density of the sand layers, the filling process was done in several stages. The sand was evenly dispersed in the tank, and afterwards manually compacted.

An overflow pipe was attached to each tank, to prevent flooding of the surface. The outflow pipe consisted of a PVC pipe with a 20 mm diameter and a length of 150 mm. The entry point for the pipe was situated 5 cm below the 60 cm height line, allowing the pipe to be angled upwards to create an efficient drainage of the basin (width: 20 cm; length: 30 cm). The dimensions of the infiltration point in each tank are in the same width: length ratio (2:3) as the rapid infiltration unit in the field (see Chapter 4.1.1). Tank 1 basin was designed deeper (15 cm) than the one in Tank 2 (10 cm) anticipating a faster clogging development, since it won't be scraped.

Water supply system

The infiltration water was taken directly from the Elbe River, and as this is a surface water resource, the water quality varies over time due to several reasons. The upstream ecological and lithological processes influence naturally dissolved and suspended solids, and the sediment load in the river water. Depending on seasonal variations or weather situations, which may initiate floods or landslides in the catchment as well as sustained periods of drought, the content of suspended sediments, and organic material may vary (Douglas, 1968; Lehmann and Rode, 2001). Moreover, temperature variations will affect the bacterial content of the water. Böckelmann et al. (2000) describe the seasonal change in lotic microbial aggregates in the Elbe River, which results in a great diversity in bacteria during spring, the predominance of algae in the summer months, and a reduction in the bacteria during the autumn and winter months. Thus, this study was conducted

during the colder winter months when bacterial growth and diversity is expected to be low. The water quality may have been different if the experiment had been conducted during a warmer period.

The water used during the experiment was non-treated river water pumped directly from the Elbe River. However, as it was impractical to pump this water continuously, a water storage and a distribution system were designed and installed in the laboratory (Figure 4.13). Two 1000 L water tanks (4) were connected in a sequence, with one of the containers being raised slightly higher than the other to encourage the flow of water between the two tanks. The Elbe River water within the tanks was continuously mixed by two mixing pumps (5). Water could be transferred from the main tanks into the 500-L tank (6), via a pump (7) operated by a timer (8). This water was thereafter pumped to the constant head reservoir (9), via another pump (7). As the minimum pump rate was higher than the outflow required by the experiment, and to maintain a constant flow rate, a constant head reservoir was installed similar as in the soil column experiments (Chapter 4.1.2). The water level in the constant head reservoir would rise and stabilise at the level of the outlet, and the excess water was returned to the 500-L tank (10). The four 8 mm outlet hoses (11) that fed each infiltration basin were attached to the base of the constant head reservoir outflow connectors.

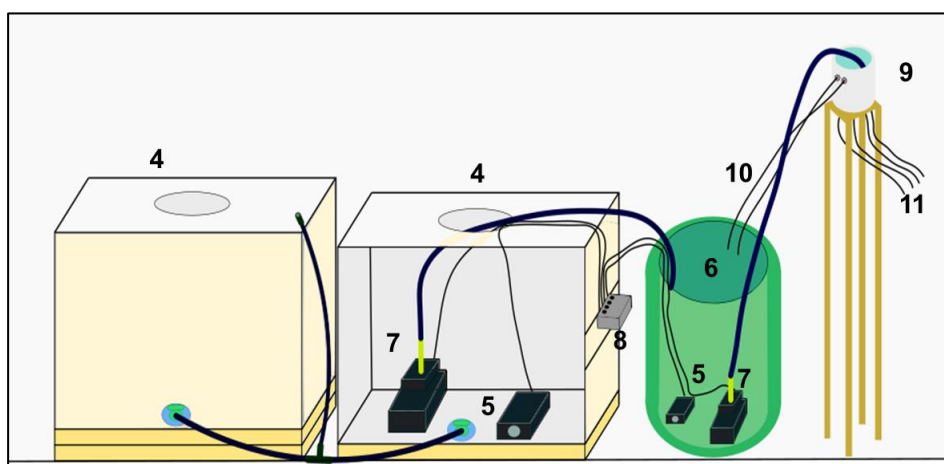


Figure 4.13. Schematic sketch of the water storage and distribution system. (not to scale). (4) primary storage Tanks- (5) mixing pumps- (6) secondary storage tank on top of a pedestal- (7) 400W pumps- (8) timer- (9) constant head reservoir- (10) overflow hoses- (11) inlet hose to spreading basin units

Water drainage system

Elbe River water not only had to be stored, but efficiently and accurately distributed to each infiltration unit at a specific hydraulic loading rate. The water that had infiltrated and passed through each infiltration unit was intercepted; whereby electrical conductivity measurements were taken (Figure 4.14).

Water from the constant head reservoir (9) flowed down the 8 mm tubing (11) towards the infiltration basins. The flow rate of the discharge from the tubing was controlled by the flow rate valve (12), resulting in an accurate level of discharge at point (13) above each basin. The designed HLR corresponds to 300 m/a, which is equivalent to 137 mL/min considering the basin surface area. Water left the infiltration basins (1) at the outflow connectors and flowed down the 10mm tubing. This tubing discharged the outflow water from the experiment into the soil EC probe apparatus. This apparatus comprised a clamp (14) which held a 5 cm diameter PVC tube (15) containing sandy soil and soil EC meters (16). This apparatus recorded changing levels of EC of the water infiltrating through it. This water drained out of the bottom of the PVC tube into a 70 L outflow reservoir (17). Basin overflow pipes (19) installed into the side of the basin, drained each

basin when the basin water level exceeded 10 cm. This water was drained directly into the outflow reservoir through a 10 mm hose (20).

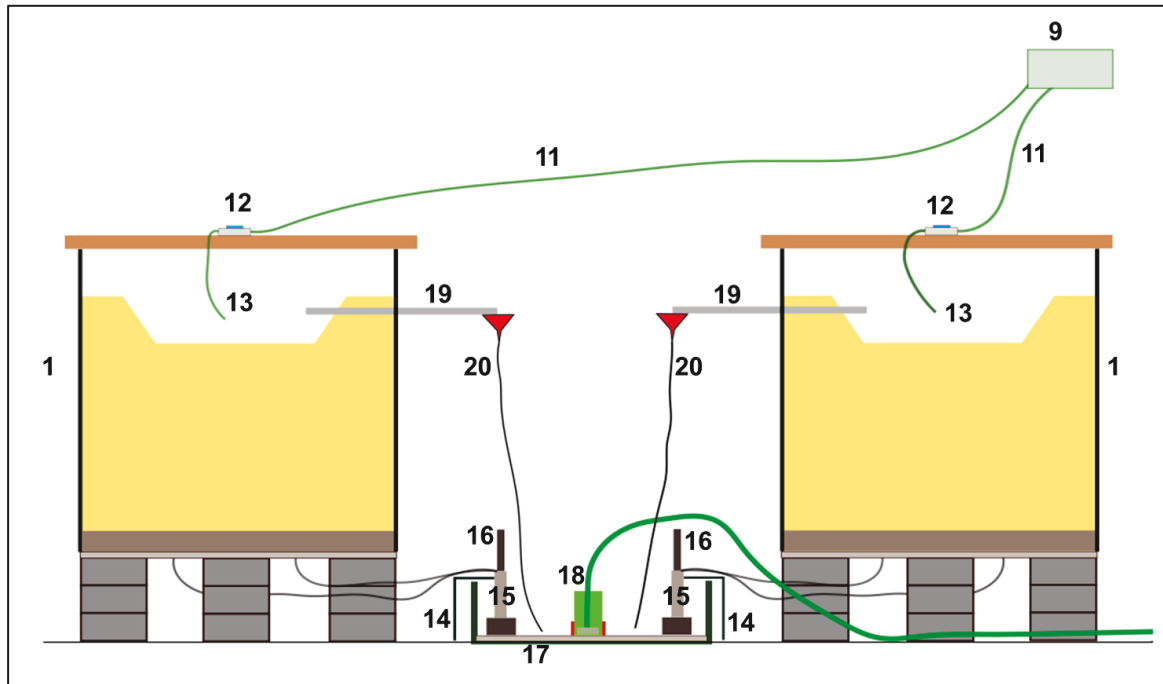


Figure 4.14. Schematic sketch of water distribution, drainage system and EC monitoring apparatus. (not to scale) (1) infiltration basin tank – (9) constant head reservoir – (11) inlet hoses to spreading basin – (12) flow rate valve – (13) discharge point – (14) clamp – (15) PVC chamber for EC measurement – (16) soil EC meters – (17) outflow reservoir – (18) self-regulating pump – (19) basin overflow pipe – (20) overflow collector

Scraping

This chapter investigates the differences in the infiltration capacity of the medium between a unit with regular scraping events and a second unit without them. Therefore, in Tank 2 a scraping procedure was conducted every time an overflow occurred in the basin. The scraping procedure consisted in the removal of the upper 2 cm of the basin surface with a small spatula. The material was not exchanged, resulting in a deeper infiltration basin. First, the infiltration in Tank 2 was interrupted, the basin was drained for 2 or 3 days (to avoid mobilization of fine particles), and finally the upper 1 - 3 cm of the basin surface were scraped and the infiltration was restarted without replacing the removed soil. It is important to note that only the bottom surface of the infiltration basin was scraped and that the infiltration basin walls were left untouched. This was done to maintain the structural integrity of the infiltration basin itself, as removing material from the sidewalls of the basin may have had a detrimental effect and caused the slumping of the basin walls into the base of the infiltration basin. Tank 1 was in contrary operated without any scraping measure to reflect how the infiltration capacity would have decreased with no management plan.

Salt tracer test method

The determination of clogging in the infiltration ponds was done by calculating the reduction of the infiltration rate, similar as in the experiments in the rapid infiltration unit in the field (Chapter 4.1.1) and the soil columns in the laboratory (Chapter 4.1.2). Salt tracer solutions (NaCl) with electrical conductivities between 3.5 mS/cm and 11.5 mS/cm were prepared in the storage tank (6 in Figure 4.13) and the t_{50} times were measured for both tanks.

The data from the salt tracer tests were obtained using manual readings, an automatic water EC meter and a soil EC meter. The infiltration velocities (m/s) were calculated using equation (4), where

the distance between the bottom of the tank and the infiltration basin is divided by the t_{50} time in seconds. The flow distance (Δh) in Tank 2 decreased by 1 cm after each scraping event.

Since Tank 2 had to be set in an infiltration pause a couple of times to allow the draining and scraping of the basin, the actually infiltrated volume was divided by the area of the infiltration basin (600 cm²) so that the volume of water could be presented with the unit m³/m².

4.3 DETERMINATION OF INFILTRATION CAPACITY USING WATER CONTENT

This chapter together with chapter 5.3 include the results from the publication with title: *Methods of In Situ Assessment of Infiltration Rate Reduction in Groundwater Recharge Basins*. in Water Journal 2019, 11(4), 784. Therefore, the citation of Barquero et al. (2019) was suppressed in its content.

The objective of this chapter was to compare a tracer test method with new methods calculating the reduction of the infiltration rate over time based on instantaneous profile method (IPM) data. IPM consists in the simultaneous determination of specific parameters at different depths (Askarinejad et al., 2012). These methods are able to track fluctuations in the infiltration rate (e.g. due to clogging of the basin surface) over time, without influencing the conditions of the experimental setup for the subsequent infiltration cycles. Especially for laboratory experiments, it is very important to keep the same soil structure over time. As representative input data for tracking the decrease of the hydraulic conductivity over time after the infiltration of river water, water content of two MAR experimental units (field- and laboratory scale) were selected.

The infiltration experiments were run in the field scale infiltration unit (Chapter 4.1.1) as well as in a laboratory scale infiltration unit (1.5 m × 1.0 m × 1.0 m); which was filled with the same sandy soil as used in the field ($K_s \approx 6 \times 10^{-5}$ m/s) with a bulk density of 1.6 - 1.7 kg/m³. The observation points are located in both units at a depth of 28 cm. The water used in both units was from the Elbe River and was mixed at the beginning of each infiltration cycle with NaCl (2.5 – 5.0 mS/cm) for tracer experiments. River water was pumped into the infiltration basins with the configuration of Scenario 1: an annual hydraulic loading rate of 300 m/a under wet:dry cycles of 1:3 (24 h infiltration followed by 72 h dry period). In total, nine infiltration cycles were run and analyzed. They encompass a total specific volume of approximately 29 000 L/m² during 30 days. Both units were equipped with UMP sensors, which measured volumetric water content (vol%), electrical conductivity (mS/cm), and temperature (°C) at two minutes intervals. Further details of the description of the laboratory scale infiltration unit are presented by Fichtner et al. (2019).

4.3.1 Tracer method

The tracer method implemented in Chapter 4.1.1 for Run 8 (Scenario 1 Climate 3) was used as a standard and already established method to determine the hydraulic conditions of a porous medium. Several tracer experiments were performed, introducing NaCl at a concentration of 1 g/L into the river water during the first six hours of each infiltration cycle, to determine the time for solute transport through the infiltration unit by means of the installed monitoring sensor, located 28 cm below the infiltration pond. For the calculation of the decrease of the infiltration rate, equation (4) was used.

4.3.2 Libardi method

Considering the basics of the Richards and the Darcy-Buckingham equation (Buckingham, 1907; Darcy, 1856; Richards, 1931), Hillel (1972) set a finite difference based analytical model to calculate the hydraulic conductivity using water content (θ) changes in flooding or draining systems. Therefore, θ was smoothed with time t in a semi-log model subtracting it from the initial water content (θ_0):

$$\theta_0 - \theta = A_L \ln(t) + B_L \quad (5)$$

In order to define the fitting parameters A_L and B_L at depth L (Figure 4.15), by integrating the Richard's equation from soil surface ($z = 0$) down to depth $z = L$, the hydraulic conductivity can be

calculated (see Equation (6)). A_L is represented by the inverse of the slope γ , whereas B_L is the multiplication of A_L with the natural logarithm of the fraction of slope γ times initial hydraulic conductivity (K_o) over parameter a times depth z .

$$K(\theta)_L = \int_0^L \frac{\partial \theta}{\partial t} dz / \left(\frac{\partial H}{\partial z} \right)_L \quad (6)$$

With H = matric potential.

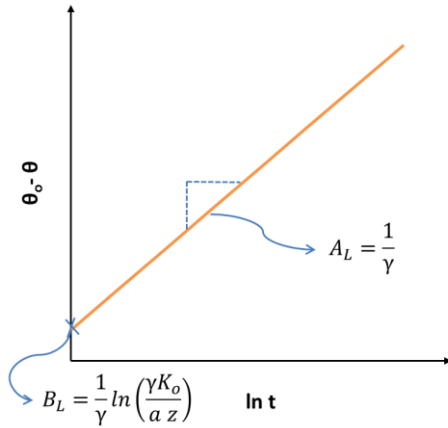


Figure 4.15. Adapted smoothed semi-log model designed by Hillel and Libardi (1972) for the empirical determination of hydraulic conductivity.

The smoothed semi-log model equation (5) was analyzed with finite differences for depth z and approximated the integral in n measurements in Δz intervals and using L as upper limit of the integral. This antiderivate resulted in Equation (7).

$$q = \int_0^L \frac{\partial \theta}{\partial t} dz \cong - \sum_{i=1}^n \frac{A_L}{t} \Delta z \quad (7)$$

The matric potential gradient $\left(\frac{\partial H}{\partial z} \right)_L$ can either be measured with tensiometers or must be assumed to have a value of 1 (valid for short time steps). However, using the finite difference can develop a gap after n measurements.

Libardi et al. (1980) worked on an empirical equation without integration based on Hillel's previous investigations. Libardi came up with Equation (8).

$$K(\theta) = K_o e^{-\gamma(\theta_o - \theta)} \quad (8)$$

where $K(\theta)$ is hydraulic conductivity (m/s) dependent on the water content, K_o , and θ_o are the initial values of hydraulic conductivity and water content, respectively. The fitting parameters $\gamma \left[\frac{1}{A_L} \right]$ and $K_o \left[\frac{za}{\gamma} e^{\gamma B_L} \right]$ were determined using the linear semi log model of Hillel (see Figure 4.15) which yields Equation 9.

$$\theta_o - \theta = \frac{1}{\gamma} \ln(t) + \frac{1}{\gamma} \ln \left(\frac{\gamma K_o}{a z} \right) \quad (9)$$

Sisson (1980) further assumed a homogenous soil by setting the parameter $a = 1$, which represents a constant water content change over depth. The Libardi method can calculate an absolute value for hydraulic conductivity and not only the relative linear velocity in contrast to normal tracer breakthrough curves.

4.3.3 Root mean square method

The root mean square displacement (D_{RMS}) indicates hydraulic properties variations of the soil analyzing water content data during the infiltration periods from the IPM system. The D_{RMS} defines the deviation distribution of the whole time series in a single representative value (Chai and Draxler, 2014). The D_{RMS} values give back the factor of reduction of the infiltration capacity to infer an absolute rate of it.

The first infiltration cycle of the scenario was used as a reference cycle. D_{RMS} are calculated between the i -th infiltration cycle ($i = 1, 2, \dots, 9$) and the first infiltration cycle of time step t_x (see Equation (10)). This describes the change of the averaged water content of each cycle in comparison to the initial state.

$$D_{RMS} = \frac{\sum (WC_{cycle\ i, t_x} - WC_{cycle\ 0, t_x})^2}{n} \quad (10)$$

A model was developed to make this method analogous to tracer curves (Equation (11)). A quadratic regression analysis between the obtained values from the tracer experiments and those from D_{RMS} from Equation (10) was executed.

$$Tracer_i = a + b \times [D_{RMS\ i}] + c \times [D_{RMS\ i}]^2 \quad (11)$$

where $Tracer_i$ represents the calculated infiltration capacity reduction at the i -th infiltration cycle ($i = 1, 2, \dots, 9$) determined with the tracer experiment; $D_{RMS\ i}$ is the calculated D_{RMS} value (%) at the i -th infiltration cycle; whereas a , b , and c are fitting parameters for the linear regression model. Once the parameters were fitted, the results from Equation (11) were inserted and analyzed against the tracer curve data.

4.3.4 Water content method

The water content (WC) method works similar to the D_{RMS} method. The main difference is that D_{RMS} calculates the root mean square difference, whereas the water content method calculates the average water content of each infiltration cycle. Therefore, the infiltration time parameter of each infiltration cycle loses relevance. A linear regression model was also created and determined with the obtained data using the tracer test's results as reference (Equation (12)).

$$Tracer_i = a + b \times \left[\frac{\sum WC_i}{n_i} \right] + c \times \left[\frac{\sum WC_i}{n_i} \right]^2 \quad (12)$$

where $Tracer_i$ represents the calculated infiltration capacity reduction in the i -th infiltration cycle ($i = 1, 2, \dots, 9$) determined with the tracer experiment; $\frac{\sum WC_i}{n_i}$ is the averaged water content value (%) at the i -th infiltration cycle; n_i is the amount of measured data in the i -th infiltration cycle; and a , b , and c are fitting parameters for the linear regression model. This model was used afterwards to be compared to the tracer curve that works as reference.

4.3.5 Trigger time method

There are other potential basic indicators that can determine the infiltration capacity reduction of the infiltration basin. The "trigger time" (TT) is the time that the sensor needs to register the first rise of the water content/tension. This time gives for example a hint on the delay of the infiltration water. This method is primarily dependent on the advection and dispersion properties of the soil, ignoring any diffusion effects. A third linear regression model (Equation (13)) was created to correlate the tracer curve results with the information obtained from the trigger time method.

$$\text{Tracer}_i = a + b \times [\text{TT}_i] + c \times [\text{TT}_i]^2 \quad (13)$$

where Tracer_i represents the calculated infiltration capacity reduction in the i -th infiltration cycle of the given scenario ($i = 1, 2, \dots, 9$) determined with the tracer experiment method; TT_i is the trigger time, given in min, at the i -th infiltration cycle, as the water content started to increase and a , b , and c are fitting parameters of the given linear regression model. Similar to the other models, the obtained model was analyzed against the tracer curve.

5 RESULTS AND DISCUSSION

5.1 INFLUENCE OF CLIMATE ON INFILTRATION BASINS

In the following sections, the results of the infiltration tests in the field and the laboratory are presented. These experiments should clarify the influence that temperature and climate have on the reduction of the infiltration capacity of recharge basins.

The wind velocity and direction at the investigation site eases the transport of fine particles coming from the Elbe River. This were considered of minimal influence for the field experiments since the duration of each scenario was not longer than one month.

5.1.1 Temperature

Temperature and solar irradiance vary with the seasons. Figure 5.1 shows how temperatures can reach values above 35 °C in summer (Run 18 – July 2018, See Table 5.1), whereas the basin was operated even below -10 °C during winter (Run 11 – February 2018). Nevertheless, the changes of temperature are smaller when considering at the medians (day and night values). Taking into consideration the given medians, the lower and upper boundaries of the mild category were defined as 10.8 °C and 14.8 °C, respectively. Runs 2 - 4, 10 - 13, and 20 were conducted under cold conditions, whereas Runs 6 - 8 and 16 - 18 exhibited warm conditions (See climate categories in Table 5.2). The remaining runs had a mild temperature range. Values for Run 12 are missing because of an interruption of measurement at the weather station in Jessen after cyclone Friederike in February 2018.

Figure 5.1 shows the solar irradiance including the night hours. A difference between summer and winter climate can be clearly identified due to the change of the daily sun incidence hours. Median values in winter remained below 34.3 W/m²/h, whereas in summer the medians were higher than 63.7 W/m²/h and the peak irradiance reached up to 900 W/m²/h when the sun was in the zenith. Runs 1-4, 9-11, 13, and 19-20 were all under cold climate conditions, whereas Runs 6-7 and 15-18 exhibited warm climate conditions. All remaining runs had a medium solar irradiance range.

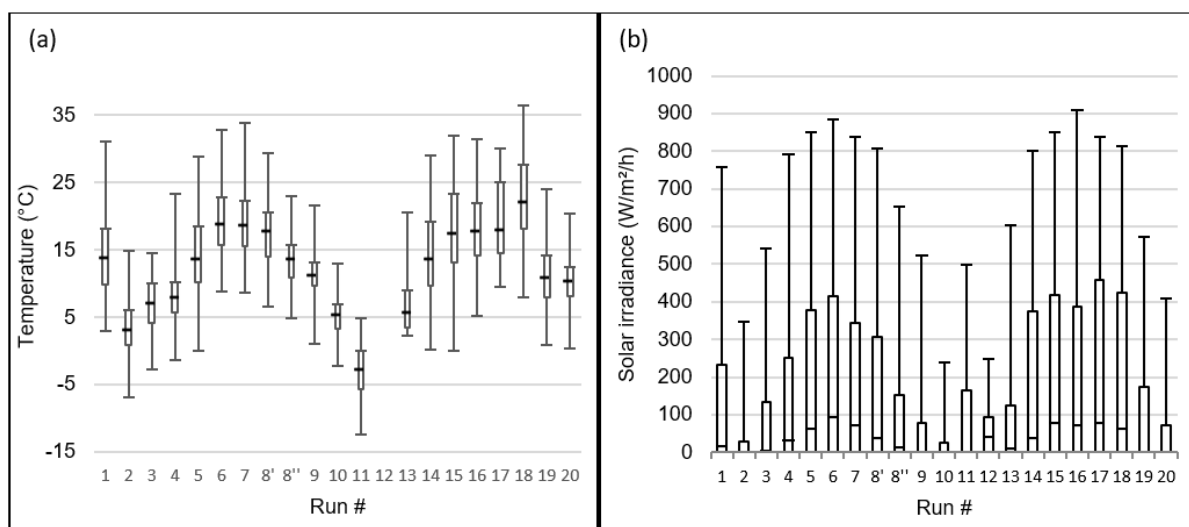


Figure 5.1. Variation of the temperature (a) and solar irradiance (b) during the experiments

Temperature and solar irradiance were analysed using the median values in a specific period of time. Extremes values (e.g. hottest days, coldest day) would have deepened the analysis of this thesis. Nevertheless, it would have been challenging to manage the measurement of the hydraulic conductivity state (meaning clogging development) in a frequency matching to the extreme climatic events. Therefore, medians should englobe all mean and extreme conditions occurring in the time as tracer experiments were performed.

An overview of the climatic description of each Run are shown in Table 5.1.

Table 5.1. Climatic description of the 20 infiltration Runs

Year	Months	Duration of scenario (days)	Run #	Median temperature (°C)	Median solar irradiance (W/m ²)
2016	Aug/Sept	44	1	13.7	18.0
	Nov/Dec	40	2	2.8	0.0
2017	March	16	3	6.9	5.0
	April	6	4	7.9	33.0
	May	35	5	13.6	62.0
	June/July	27	6	18.7	93.0
	July	20	7	18.5	72.0
	August	25	8'	17.7	37.0
	September	25	8''	13.4	13.5
	October	32	9	11.2	0.0
	November	33	10	5.3	0.0
	February	30	11	-2.9	0.0
2018	March	1	12	n.d.	n.d.
	March	5	13	n.d.	n.d.
	April	35	14	3.7	39.3
	May	18	15	4.1	79.2
	June	29	16	3.4	71.4
	July	12	17	3.3	78.2
	July/Aug	30	18	3.7	64.3
	Sept /Oct	18	19	3.1	0.0
	October	10	20	2.1	0.0

Note: 8' refers to the first part of the scenario with a warmer climate and 8'' to the second part with a milder climate

n.d. – no data available

A summary of the boundaries of each interval is presented in Table 5.2. Since the temperature data does not have a restriction for the lower limit, this was used as the main parameter for classifying each Run. Solar irradiance during the night and cloudy days was set to a value of 0 W/m².

Table 5.2. Climate category's intervals

Climate	Median temperature [°C]	Median Solar irradiance [W/m ²]
1 (cold)	< 10.8	< 34.3
2 (mild)	10.8 - 14.8	34.3 - 63.7
3 (warm)	> 14.8	> 63.7

A summary of the performed runs and its classification is presented in Table 5.3. Each row is filled with the corresponding color of the climate category. The HLR, HLC, and pumping rate of each scenario can be found in Table 4.2.

Table 5.3. Runs and their corresponding climate characterization

Category	Scenario 1	Scenario 2	Scenario 3	Scenario 4
1 (cold)	Run 3	Run 4	Run 10	Run 11
2 (mild)	Run 9	Run 14	Run 5	Run 19
3 (warm)	Run 8	Run 7	Run 16	Run 6

The defined climate categories are also evident in sensors installed in the experimental unit. Figure 5.2 presents the soil temperature data for Scenario 1 for the 3 different climatic conditions (red: warm, green: mild, and blue: cold) in the 3 different layers (28 cm – Sensor 1.2, 70 cm – Sensor 2.2, and 140 cm – Sensor 3.2). Night and day are responsible for the temperature peaks. This influence is softened in deeper layers. The natural daily changes of soil temperature are in the shallow layer between 4 and 6 °C, in the middle layer between 1 and 3 °C and in the deep layer between 0 and 2 °C. As Racz et al. (2012) also described, the daily temperature fluctuations propagate downward into the subsurface as thermal waves by conduction, advection, and dispersion. The magnitude of the reduction of the amplitude and the phase shift between layers are in direct dependence to the infiltration rate.

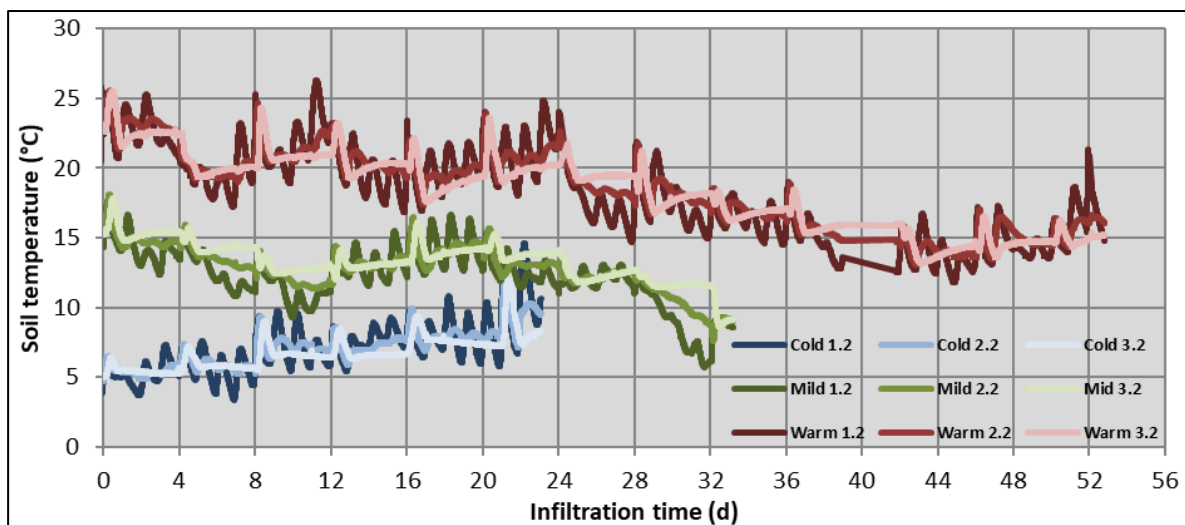


Figure 5.2. Soil temperature at Scenario 1 depths in the 3 climate scenarios.

Infiltration capacity reduction in different hydraulic scenarios

Figure 5.3 shows the reduction of the infiltration capacity based on the tracer tests under the influence of different climatic conditions for different scenarios (a: Scenario 1, b: Scenario 2, c: Scenario 3, and d: Scenario 4). Each diagram contains the infiltration capacity reduction curve (ICRC) for cold, mild, and warm climates at the depth of 28 cm (Sensor 1.2). In summer climatic conditions (Climate 3), higher rates of biological - mechanical and physical clogging occur in all scenarios. Sequentially, infiltration performance decreases the most (up to 40 % more than in colder conditions). Nevertheless, the duration of these scenarios was sometimes much longer than those of the colder climates (up to 3x longer). A high TSS concentration in the feed water (typical for summer season ~ warm climate) led to a faster physical blocking of the pores. In combination with low temperatures, which increase the viscosity of the water and reduces the infiltration capacity, this resulted in a faster overflow of the infiltration basin and a stop of the scenarios. Lower infiltration capacity during colder months was also validated by Clark et al. (2005) in El Rio spreading grounds (USA), where they determined twofold higher percolation rates during the spring/summer months in comparison to the winter months.

In scenarios 1, 2, and 4, a clear difference between the behavior of the curves in mild and warm climates is not observed. This suggests that the reduction of infiltration capacity is strongly influenced whether the temperatures are below or above 11 °C (temperature boundary between cold and mild climate). This might be a decisive threshold temperature where significant differences in bacterial growth occur and, additionally, in the viscosity properties of the water. In the only scenario without drying phase (Scenario 3), the ICRC of the mild climate shows similar as in a cold climate. The permanent absence of oxygen combined with lower biological activity leads here to a smaller reduction in infiltration capacity than in warm climates.

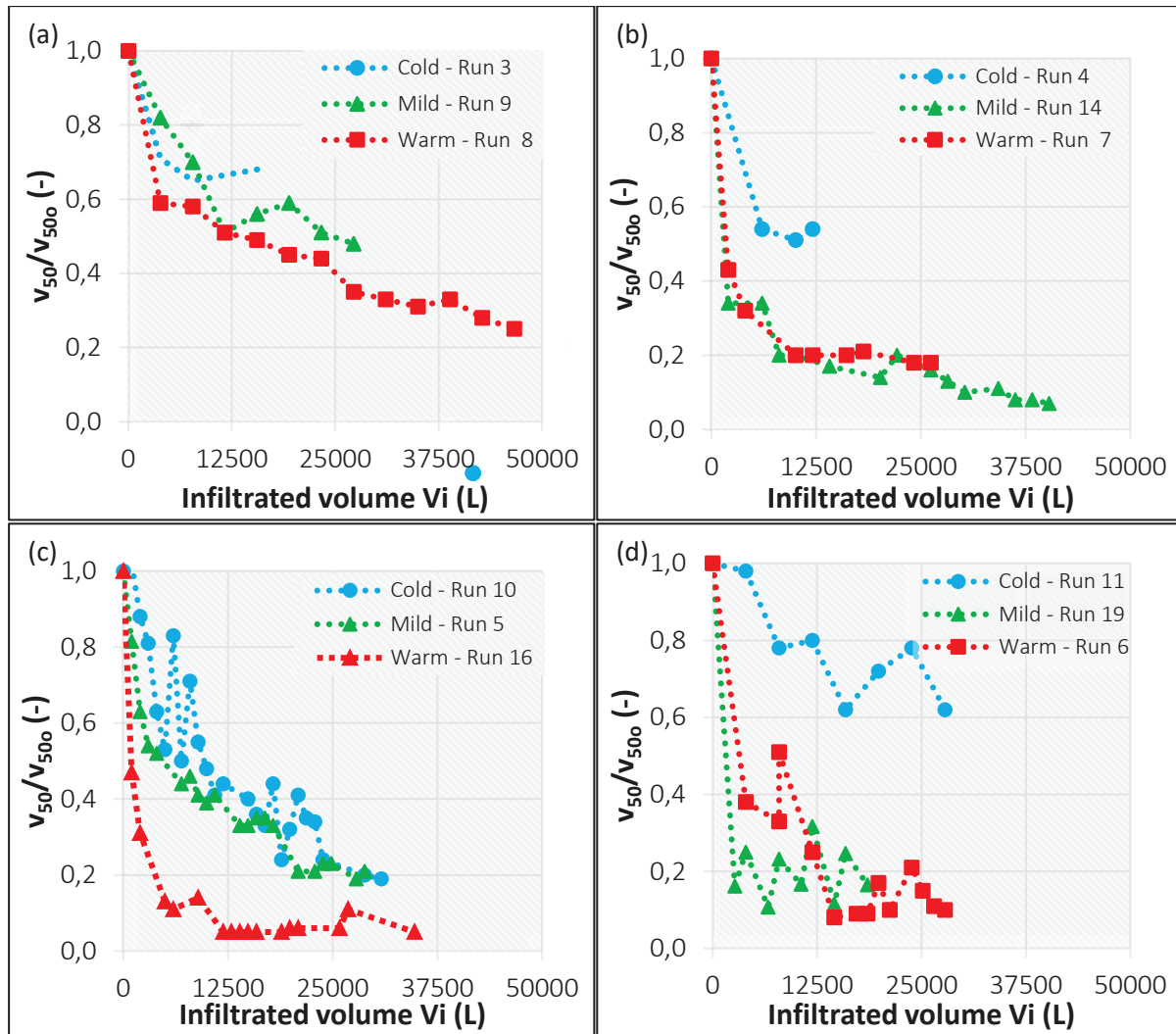


Figure 5.3. Overview of the ICRC change in different climates for the (a) Scenario 1, (b) Scenario 2, (c) Scenario 3, and (d) Scenario 4.

Excluding Scenario 3, the infiltration capacity under cold conditions reached their strongest reduction ($< 50\%$) after 12 m^3 of infiltrated water. All these Runs were stopped because the basin was overflowing. This suggests that viscosity has a higher relevance than clogging development. For Scenario 3, the infiltration capacity continued reducing after 13 m^3 of infiltrated river water, reaching a final reduction of 80% of the initial conditions. Scenario 3 was run with the lowest pumping rate and thus did not overflow as in the other three scenarios.

The reduction of the infiltration capacity in Climate 2 and Climate 3 was higher than in Climate 1 after the first 12 m^3 of infiltrated water in Scenario 1 (49%), Scenario 2 (80%), and Scenario 4 (75%). As more water was infiltrated, the infiltration capacity was reduced by half of the capacity at 12 m^3 . This difference suggests the development of biological clogging, which is dependent on the bacterial and algae growth rate.

Relation between climate and hydraulic conductivity

If the daily air temperature drastically changes during an infiltration scenario, the influence of viscosity on the reduction of infiltration capacity can be tracked. For example, in Run 8 (Scenario 1 Climate 3), there was a change in air temperature and solar irradiance that caused a change in the velocity of the infiltrated water (Figure 5.4). This change has been examined in more detail for the following three time periods: 7th - 31st August; 1st -15th September and 16th - 25th September in

2017. Figure 5.5a shows the change of the average hourly temperature for one day in the specified time period. The difference of the maxima between the first and second periods is 5 °C (23 °C to 18 °C), while between the second and third periods it is 2 °C (18 °C to 16 °C).

Figure 5.5b contains the theoretical calculation of the hydraulic conductivity as a function of the temperature change. The temperature influences the dynamic viscosity μ (Eq. 2) and density ρ (Eq. 3) which in turn are parameters necessary to determine the hydraulic conductivity (Eq. 1). Based on the relationship between hydraulic conductivity and dynamic viscosity, which does not consider changes due to biological or physical clogging, it is possible to estimate how large the change in infiltration capacity should be as a result of the temperature change. With the values extracted from Figure 5.5, a theoretical reduction of 11 % between the first and second time period and 5 % between the second and third period was calculated. The actual reductions obtained from the ICRC of Run 8 are 9 % and 5 %, respectively (Figure 5.4). Such calculations are only valid assuming that the influence of external factors (e.g. clogging) remains constant.

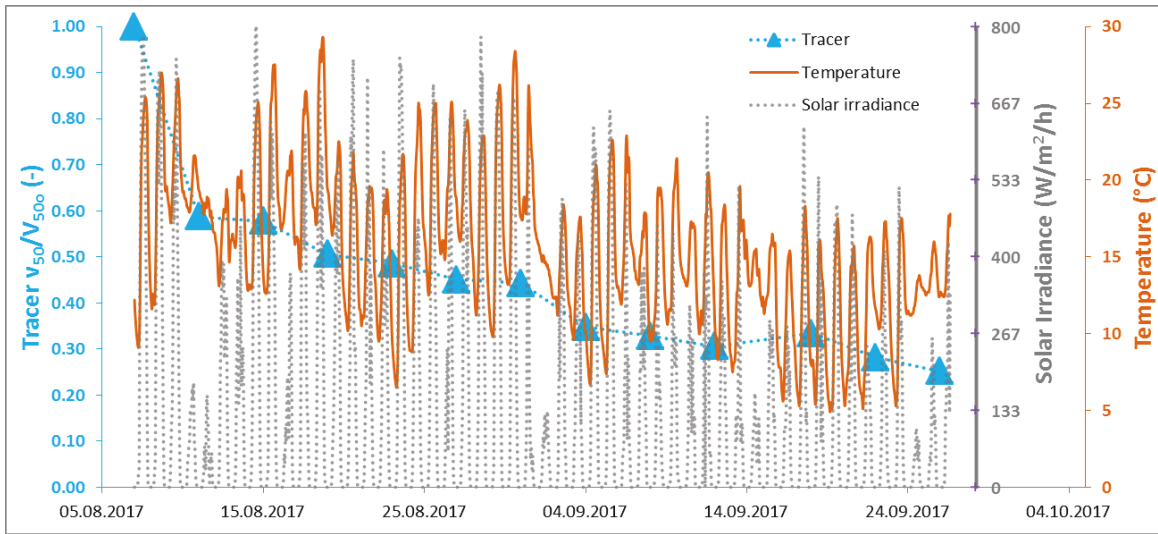


Figure 5.4. Monitoring of the solar irradiance and air temperature during Run 8 (Scenario 1 Climate 3) in a phase of decreasing breaks (see 1.9.17 & 15.9.17) and its graphical comparison with the ICRC. (v_{50}/v_{500})

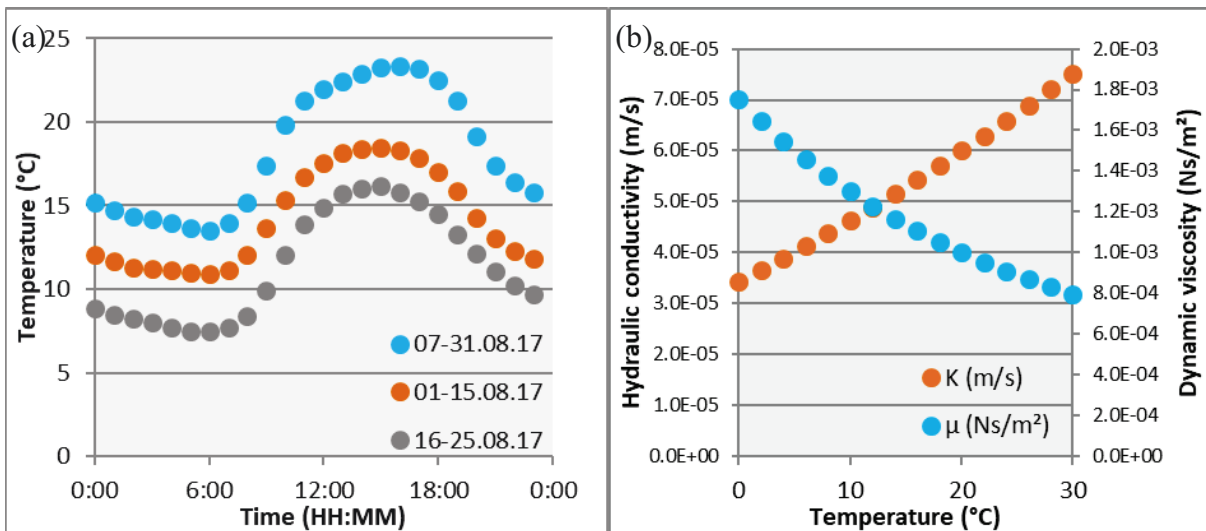


Figure 5.5. (a) Hourly air temperature during the infiltration in Run 8 during 3 periods of time and (b) theoretical influence of the dynamic viscosity in the hydraulic conductivity

Infiltration capacity reduction in different climates

Figure 5.6 presents the ICRC categorized by the climate classes. This enables an analysis of the reduction of the infiltration capacity in each climatic condition depending on the HLC scenario. Note that the diagrams have as abscissa (x-axis) the infiltrated volume to avoid conflict of variable dry period lengths between the scenarios. According to the tracer tests (Figure 5.6a), infiltrating without any drying period under cold conditions, reduces the infiltration capacity the most (up to 80 % of the initial capacity). However, there are low probabilities of an basin overflow because the flow rates are lower (0.35 L/min) than for the rest of scenarios. In mild and warm conditions (Figure 5.6b and c) the infiltration capacity remains the highest with an HLC of 1:3 (Scenario 1). Long periods of infiltration (Scenario 2: 7 days and Scenario 3: continuous) have a drastic effect on the reduction of the infiltration capacity at the beginning. After approximately 2000 L of infiltrated water the infiltration capacity is already reduced more than 60 % in both scenarios, whereas in the scenarios with shorter flooding periods (Scenario 1 and Scenario 4) the infiltration capacity is reduced less than 40 % after the first 2000 L of infiltrated water. If the time that it is needed to infiltrate the given volumes of water is considered, Scenario 1 presents the best conditions in which water is infiltrated faster and simultaneously maintaining the infiltration capacity the highest.

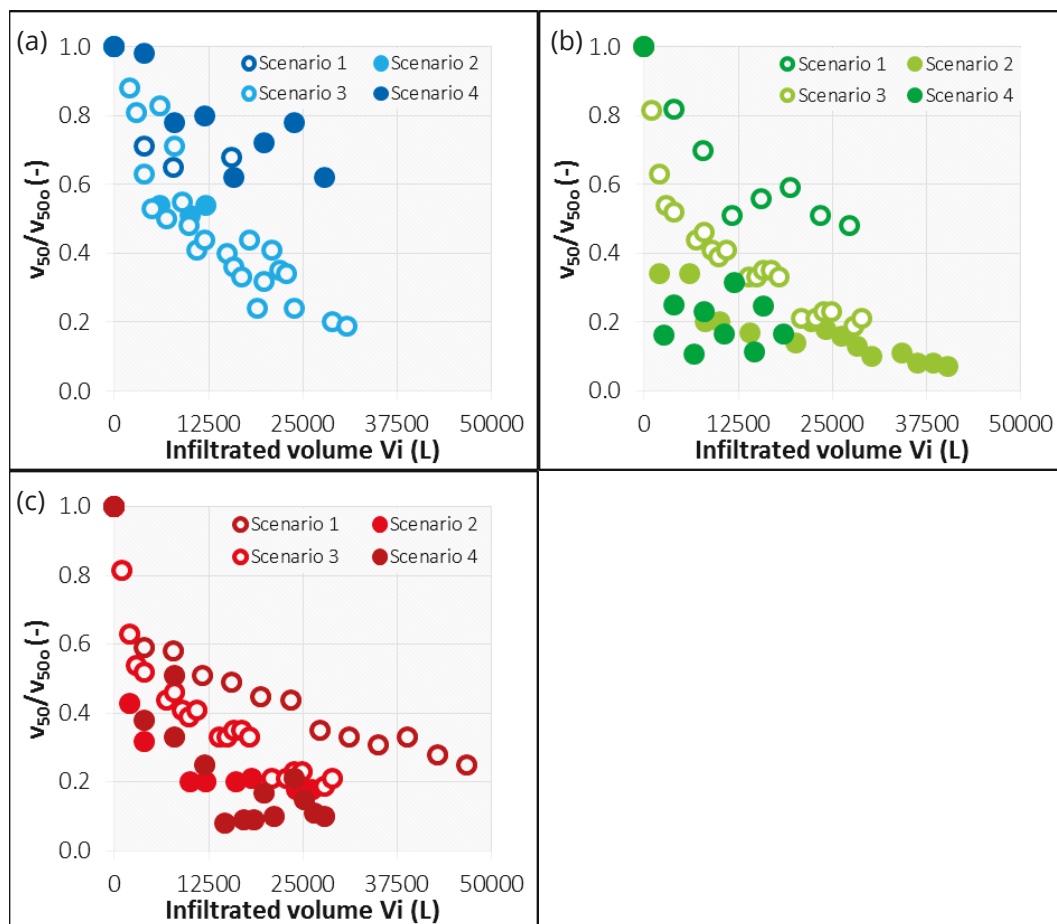


Figure 5.6. Overview of the ICRC change in different HLC scenarios for the climatic conditions (a) Cold, (b) Mild, and (c) Warm

Infiltration capacity reduction in depth

Scenario 1 and Scenario 4 were selected to apply an analysis of the climatic influence of the conditions on the trigger time in which the water content sensors below the infiltration basins (1.2, 2.2, and 3.2) detect a rise for the first time after the start of an infiltration cycle. Scenario 2 had only

three infiltration cycles starting with dry conditions, whereas Scenario 3, due to its configuration of continuous flow, had only one single infiltration cycle.

Figure 5.7, displays a comparison of the velocity to trigger a rise in the water content sensors in the three layers in the three climate scenarios. Trigger times in the two bottom layers do not vary in all climates (Layer 2: 10 min & Layer 3: 40 min). The shallow layer (Layer 1) shows an increase in trigger time from 100 min to 140 min in all climates until the sensor detects the incoming water front. For a further analysis of the influence of seasonal climate, the trigger velocities for each layer were calculated and are represented in Figure 5.7a (categorized by climates) and in Figure 5.7b (categorized by layers). The linear flow velocity decreases in depth in the soil profile (Figure 5.7a). Reason for this is, on one hand, the infiltration plume spread with depth and on the other hand, the extra compaction because of the weight of the soil above in lower soil layers. Comparing the flow velocity in each layer in the different climates (Figure 5.7b), it can be stated that no influence of climate on clogging occurs in the deep layer (velocity reduction lower than 0.3 mL/min)). In the middle layer (2nd layer) there is a slight decrease of the velocity (maximum reduction of 0.5 mL/min), which is similar for all climate scenarios. In the first layer, most of the clogging occurs and therefore also the flow speed is reduced the most (from 3.5 cm/min to 0.5 cm/min in Climate 3). Nevertheless, the change seems to be independent of the climate conditions.

The results of Scenario 4 (Figure 5.8) are clearer, with regard to the development of clogging in the warm conditions. A longer shift of the trigger time occurs in the upper and mid layer, 1.7 mL/min and 0.8 mL/min, respectively. However, in cold and mild conditions the velocities just slightly change in the middle and deep layer. The flow speed in the deep layer keeps in all climates the same rate and is not influenced by clogging processes or climate related issues. Additionally, the pumping rate in Scenario 4 was three times lower than in Scenario 1 due to its HLC. Thus, it takes also longer for the water front to reach the sensors in Scenario 4.

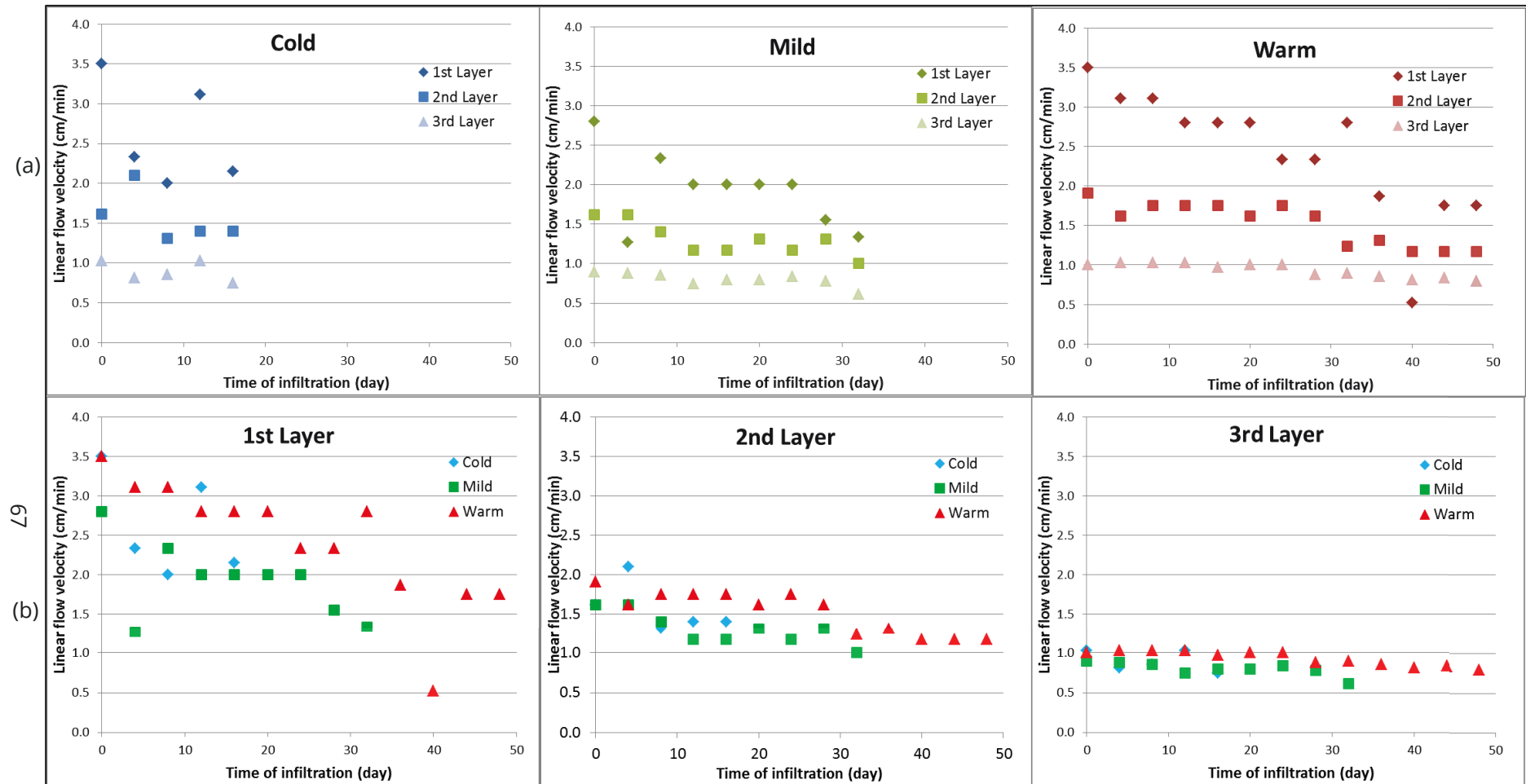


Figure 5.7. Water content trigger velocity for the Layer 1, Layer 2, and Layer 3 for Scenario 1 (1 day infiltration, 3 days dry period) in the three experimental climates (Blue: Cold, Green: Mild, and Red: Warm) grouped in (a) by climate, and in (b) by layer

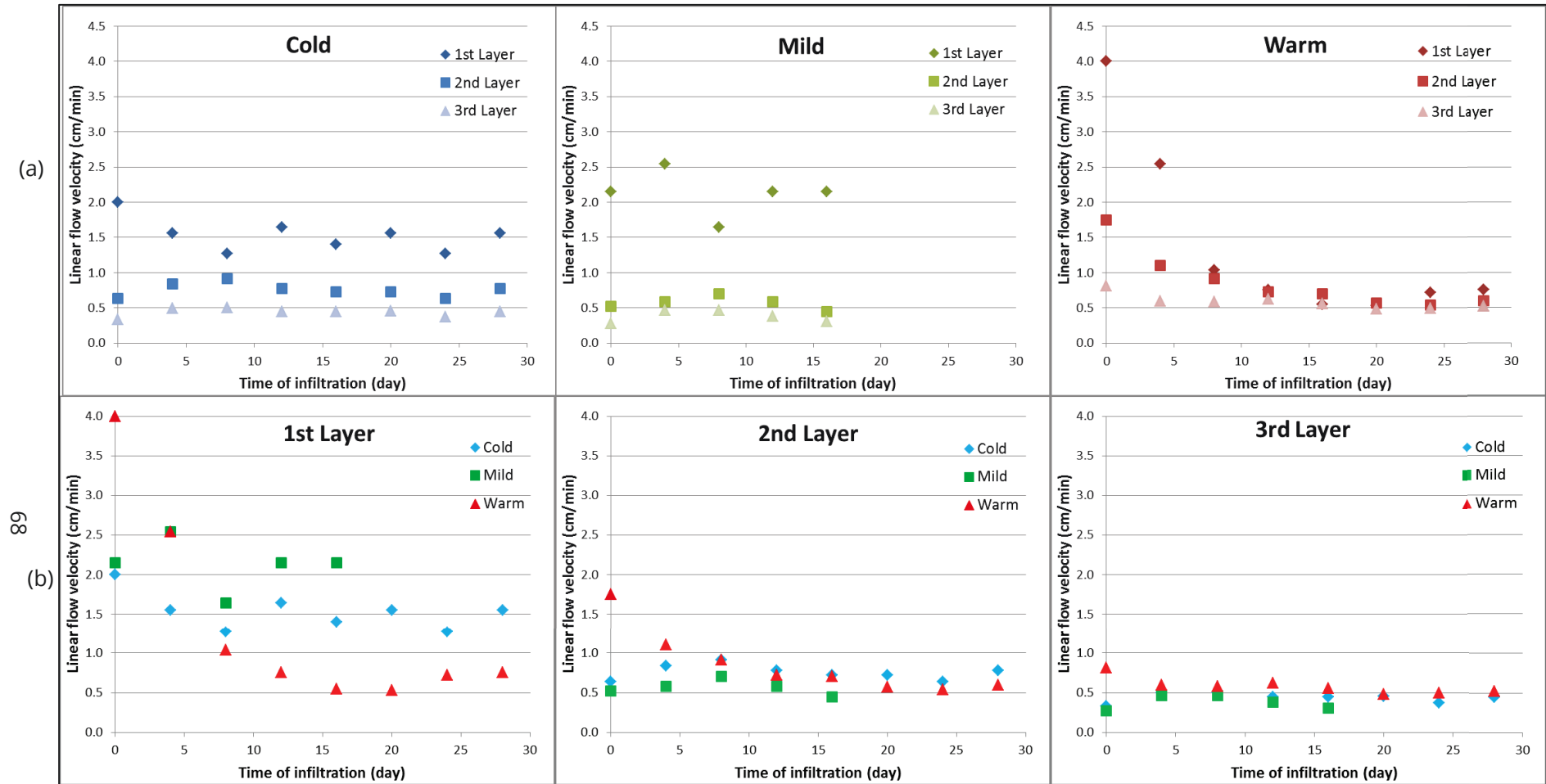


Figure 5.8. Water content trigger velocity for the Layer 1, Layer 2, and Layer 3 for Scenario 4 (3 days infiltration, 1 day dry period) in the 3 experimental climates (Blue: Cold, Green: Mild, and Red: Warm)

The results of the shallow layer in Figure 5.7 and Figure 5.8 were merged in Figure 5.9, since is the upper layer the one that exhibits clearer variations because of the reduction of the infiltration capacity. The linear flow velocities in the shallow layer during Scenario 1 (HLC 1:3) are up to six times higher than in Scenario 4 (HLC 3:1) in warm climatic conditions (see Figure 5.9c). The difference with mild and low temperatures are much lower. Despite higher pumping rates, clogging develops slower if the aereation time is long enough during warm climates. 20 days after the infiltration start, the velocity in Scenario 1 is 2.80 cm/min, whereas in Scenario 4, it is only 0.53 cm/min. These results in a higher infiltration volume of water in Scenario 1 in comparisson to Scenario 4. However, the difference of the velocities becomes smaller with decreasing temperatures (Climate 2). Here, a clear distinction of the reduction of the infiltration capacity can be made, since after 18 days the velocities are in both scenarios around 2.0 cm/min. In Climate 1, the velocity of the water front to reach the sensor 1.2 is additionally influenced by the extreme cold conditions. For example, the results for Scenario 4 (Run 11, February 2018) were obtained during colder conditions than in Scenario 1 (Run 3, March 2017), resulting sometimes even in a frozen surface of the infiltration basin.

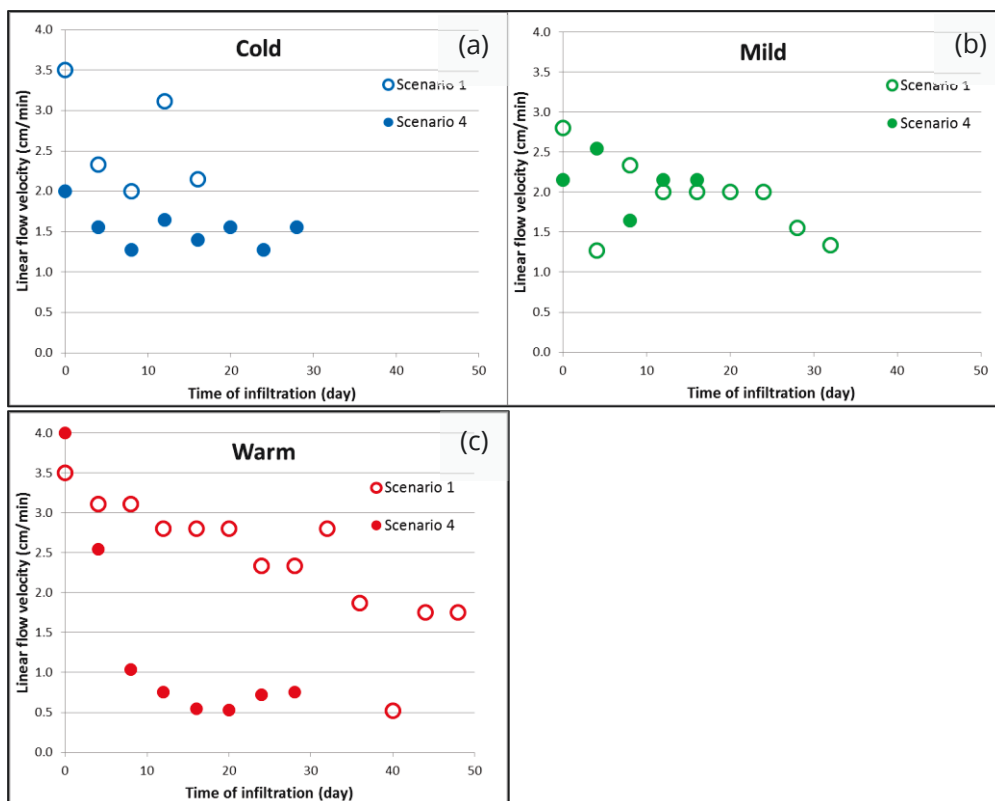


Figure 5.9. Water content trigger velocity for Layer 1 (28 cm depth; Sensor 1.2) for Scenario 1 (1 day infiltration, 3 days dry period), and Scenario 4 (3 days infiltration, 1 day dry period) in the 3 experimental climates (a - Blue: Cold, b - Green: Mild, and c - Red: Warm)

The influence of seasonability on the temperature in the subsoil is also detectable. Figure 5.10 shows the temperature data below the basin in the three monitoring depths (Layer 1: 28 cm; Layer 2: 70 cm; and Layer 3: 140 cm) for Scenario 1 during the warm climate (Climate 3) and separated for each infiltration cycle. Cycle 7 is missing due to a disruption of the data logger. The shift of the maximum peak in the lower layer is clear. The buffer capacity of the soil in infiltration sites with constant water level conditions (continuous flow) increases with depth, resulting in a reduction of the temperature amplitude in the lower layers (Hatch et al., 2006). However, in this experimental setup the infiltrated water comes only in intervals dictated by the hydraulic loading cycles. This results in similar soil temperatures at different depths.

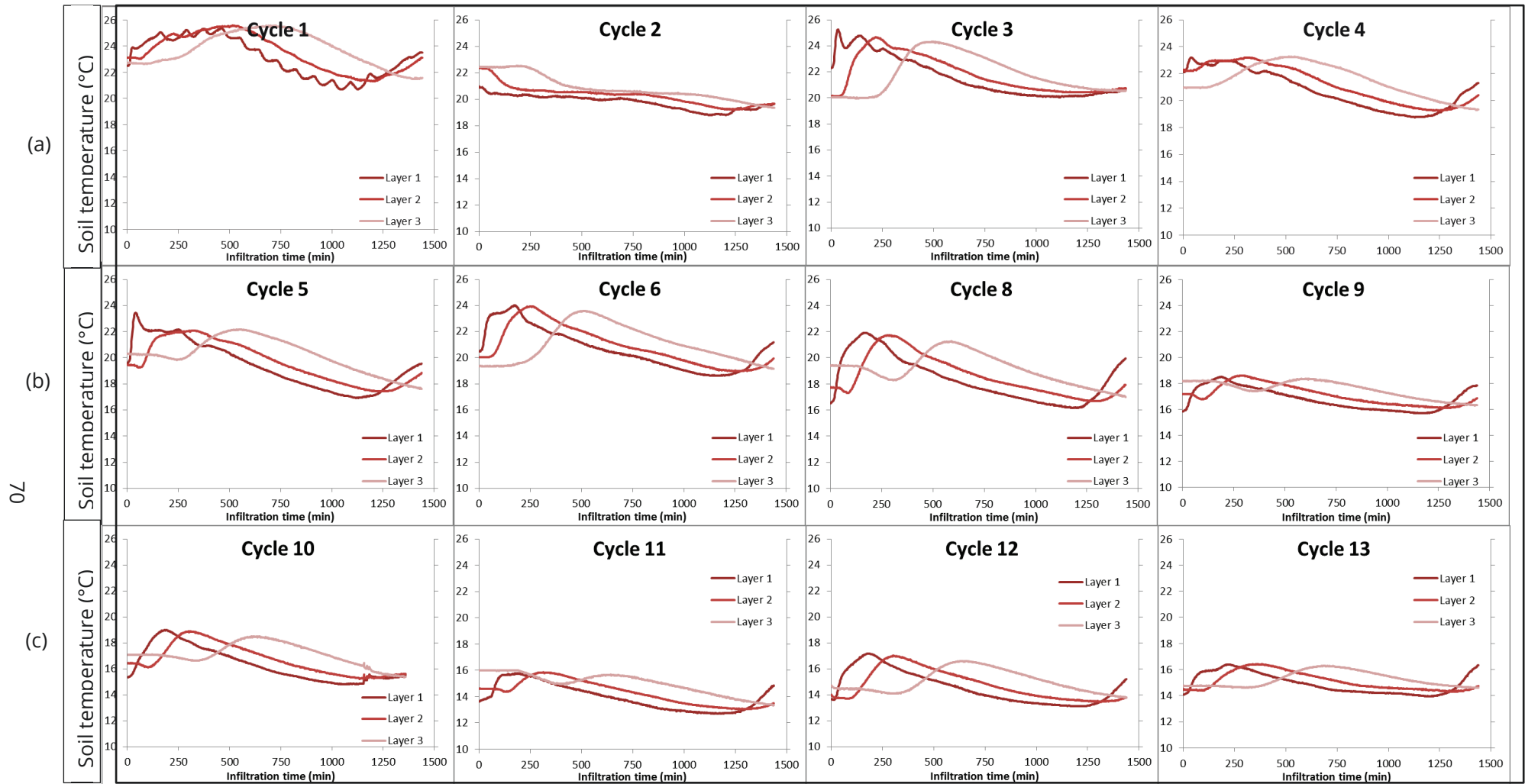


Figure 5.10. Soil temperature at depth of 28 cm (Layer 1), 70 cm (Layer 2), and 140 cm (Layer 3) for each infiltration cycle during Scenario 3 Climate 3 (Run 8)

Figure 5.11 shows the result applying the same procedure of Figure 5.10 to Climate 1 and Climate 2. The time to reach the temperature peak is shorter during Climate 3 (faster flow rate) in comparison to the cold and mild experiments, which is in accordance with the tracer experiment. Unfortunately, this information can be only used as a trend and not as absolute output, because of the thermic and unconservative properties of using temperature as a flow signature. Nevertheless, it also confirms the effect that the seasonality might exert on the subsurface flow patterns.

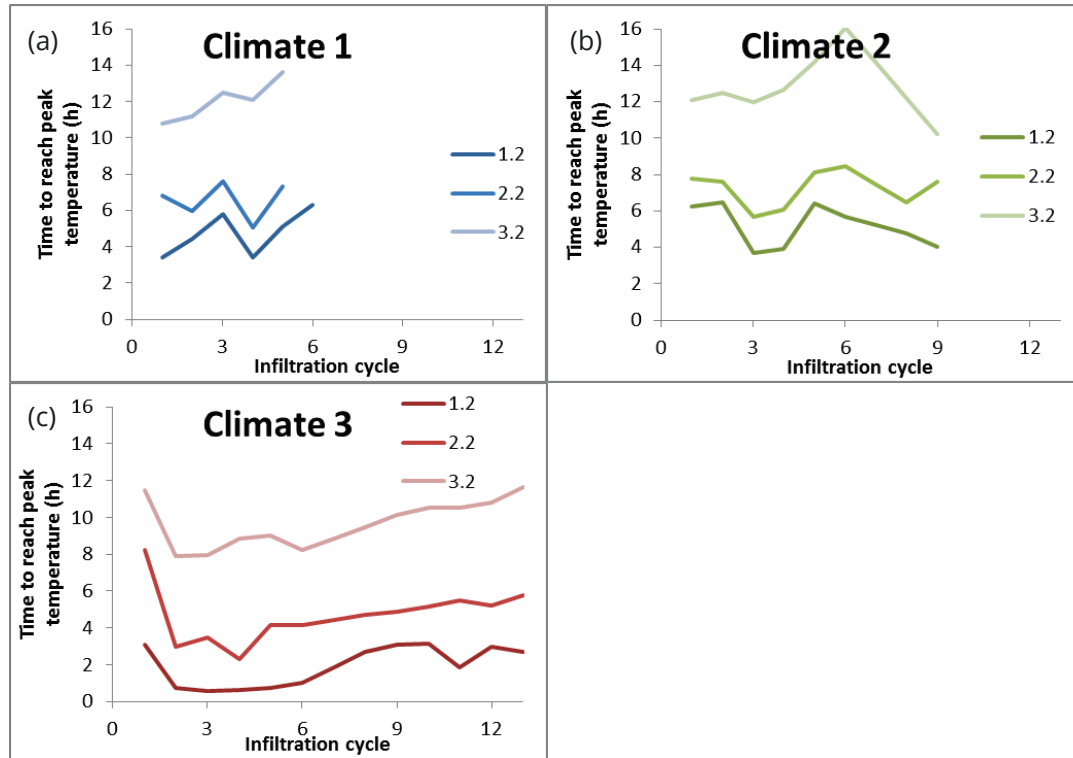


Figure 5.11. Time to reach maximum temperatures after each infiltration cycle at different depths during Scenario 1 (1 day infiltration and 3 days dry period) for Climate 1 (a), Climate 2 (b), and Climate 3 (c)

Infiltration capacity reduction and TOC

Another approach to determine the influence of climate on the clogging process is the analysis of TOC in the basin surface. With higher algae growth the total organic content in soil increases (Holm-Hansen, 1969). The concentration of organic carbon on the surface of the basin at the end of each scenario is higher with warmer conditions (Figure 5.12). The increase of TOC from Climate 1 to Climate 3 is for Scenario 1: 44 mg/kg, Scenario 2: 12 mg/kg, Scenario 3: 41 mg/kg, and Scenario 4: 27 mg/kg. The relatively low difference in Scenario 3 is given due to the high algae growth (56 mg/kg) in Climate 1. Figure 5.13 illustrates the visual difference of the basin at the end of Scenario 1 during Climate 1 and Climate 3. Under warm conditions, the growth of an algae layer was predominant, whereas in colder conditions, there was only a thin layer of cake formation (darker color). With cold climatic conditions the TOC values remain lower than 10 mg/kg in Scenarios 1, 2, and 4, and 36 mg/kg in Scenario 3. The results under warmer conditions (Climate 3) of TOC (Figure 5.12) with the tracer tests (Figure 5.3) were linked. The high TOC concentration of Scenario 3 fits with the highest reduction rate of the ICRC. Nevertheless, Scenario 1 has the second highest TOC and yet is the scenario that presents the lowest reduction of the infiltration capacity according to the tracer test. This suggests that TOC does not indicate the complete reduction of the infiltration capacity, but rather a fraction of the biological clogging.

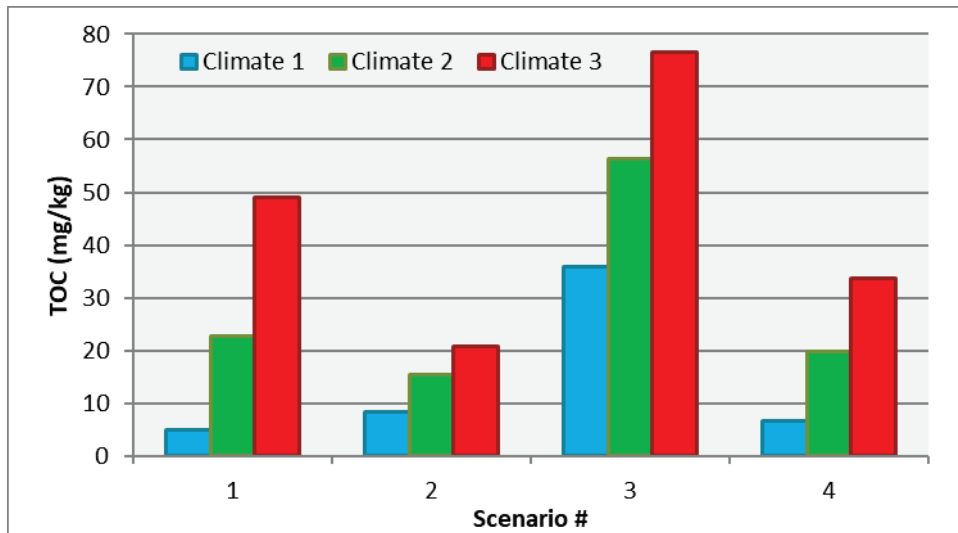


Figure 5.12. TOC in the surface of the infiltration basin grouped by scenarios

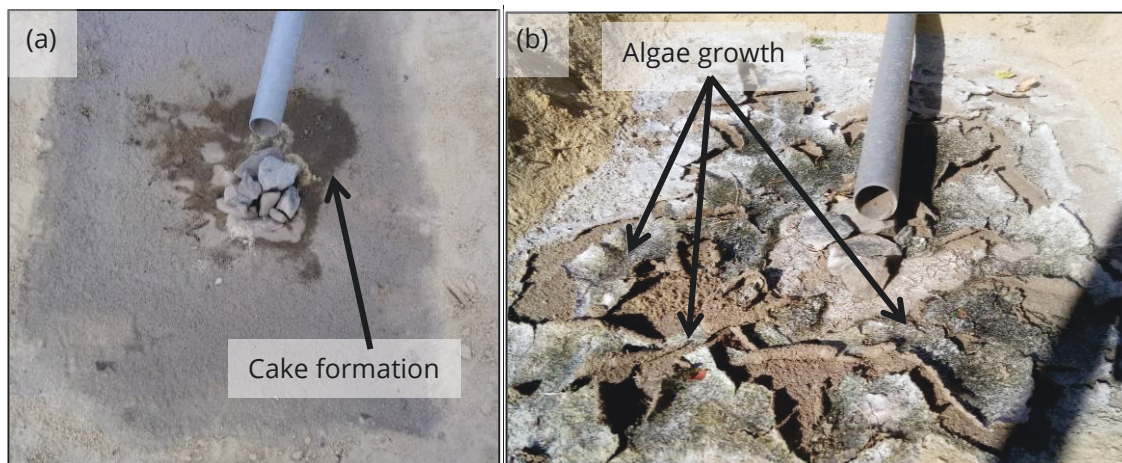


Figure 5.13. Clogging of the surface of the infiltration basin at the end of the Scenario 1 in Climate 1 (a), and Climate 3 (b)

The TOC values presented in Figure 5.12 reflect the conditions at the surface (1-2 cm depth) of the basin bed. Additional samples were taken at depths of 5 cm, 10 cm, and 20 cm (not shown). At 5 cm, the concentration of organic carbon sinks to a mean value of 2 mg/kg and at 20 cm depth, the original TOC was measured (0.2 mg/kg). This denotes the influence of mainly solar irradiance on the growth of algae in the topsoil.

Arnosti et al. (1998) stated that the oxygen consumption increases the conditions for algae growth. Hulthe et al. (1998) indicated that the extent of long-term oxidation decreases by oxygenated or anoxic conditions alone and improves when the medium is exposed to the activity of oxic and anoxic organisms together. Scenario 2 involves a homogeneous ratio of flooded and dry conditions (1:1) and the TOC values are also low in comparison to the concentrations in the other three scenarios in Climate 2 and Climate 3 (see Figure 5.14). Whereas, Scenario 3 is characterized by anoxic conditions due to its continuous infiltration, and the TOC values are the highest in each of the climate categories. Mixing of oxic-anoxic states becomes more relevant under higher temperatures and solar incidence. The concentration of organic carbon in the surface varies in Climate 1 from 5 to 36 mg/kg, in Climate 2 from 15 to 56 mg/kg, and in Climate 3 from 21 to 77 mg/kg.

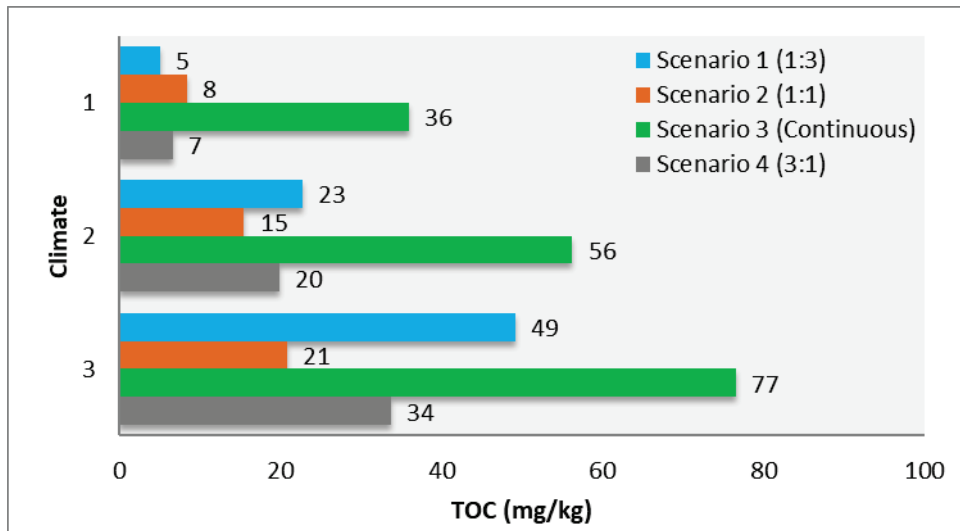


Figure 5.14. TOC in the surface of the infiltration basin grouped by climates

Impact of clogging to the aquifer recharge at test field site

The hydrogeological characteristics of the field site did not allow an analysis of the infiltration capacity reduction of the basin on the residence time or the mounding height of the recharge plume. The main reason for this was that the recharge rate was in comparison to the aquifer hydraulic conductance very low. The recharged water volume with salt tracer was not enough to activate a change in the water column in the monitoring well or detect any change in the dissolved oxygen or electrical conductivity. Figure 5.15 illustrates the groundwater conditions (water column, dissolved oxygen (LDO) and electrical conductivity) in the monitoring well I-2 (located next to the infiltration basin) together with the cumulative volume of infiltrated water during Scenario 4 Climate 3 (3 days infiltration and 1 day drying period). In total, 31 m³ were infiltrated within 32 days and there was no clear reaction in the monitoring sensors. The infiltrated water volume was not significant when considering a small infiltration area of 1.17 m² and adding the factor of the travel distance through the vadose zone (approx. 8 m) where the salt concentration could have gotten completely diluted.

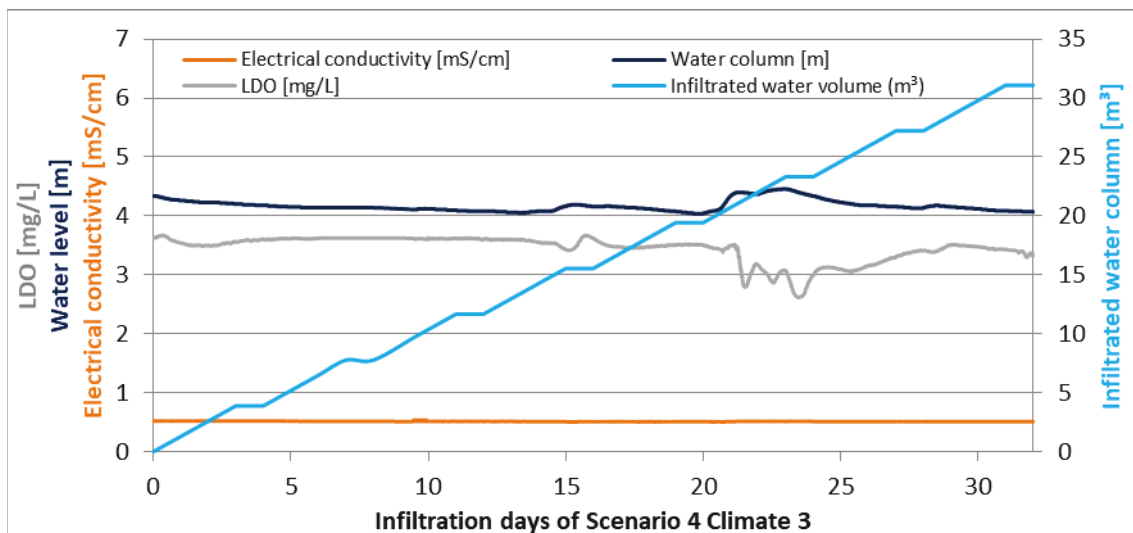


Figure 5.15. Effect of recharged water in the monitoring well water level (m), dissolved oxygen (mg/L) and electrical conductivity (mS/cm) during Scenario 4 Climate 3 (3d:1d)

Therefore, the analysis efforts were directed to the infiltration capacity reduction occurring in the vadose zone (up to 1.5 m depth). Furthermore, another challenge of this investigation was the very varying natural solar irradiance on the test field site. This issue can also have had an influence on the growth rate of the algae and microorganisms in the basin causing the reduction of the infiltration capacity. Thus, the experiment with the soil columns should further assess the influence of solar irradiance.

5.1.2 Solar irradiance

The presentation of results from the soil column experiments are divided in river water and tap water runs, followed by the main outcomes from the TOC analysis.

Reduction of infiltration capacity by using river water

The decrease of the infiltration capacity was tracked using tracer tests. It is analyzed as a function of reducing infiltration rates.

Time values (min) for the 90 % salt recovery during the tracer test were measured to compute the infiltration rates (m/min) for each tracer test using the respective lengths of the soil columns (m), as the 50 % concentration of the EC already was measured within the first 10 min of the experiment and only two 20 mL samples could be taken until that time, due to low outflow rates (6 mL/min). The subsequent values of infiltration rates were normalized with the initial infiltration rate. The reduction in the infiltration rates for each column varies based on different light conditions within the experimental setup. The degree of clogging can be set by the ratio of hydraulic conductivity to the initial hydraulic conductivity.

The variation of infiltration rates in the soil columns is divided into three phases; the initial decrease of hydraulic conductivity is followed occasionally by a small increase which is succeeded by a gradual decrease of the infiltration rates (Figure 5.16). According to Christiansen (1944), slow dissolution of entrapped air leads to an increase in the infiltration rates. During the early stages of the experiment, water infiltrates through the soil column by displacing the soil air which becomes compressed ahead of the wetting front. This compressed air is believed to result in decreased infiltration rates at the beginning of the experiment (Jalali-Farahani et al., 1993; Wang et al., 1998). Moreover, increased compression leads to high air pressure within the column which pushes the air out of the soil surface. Consequently, the air pressure decreases resulting in a sharp increase of infiltration rates (McWhorter, 1971; Wang et al., 1998).

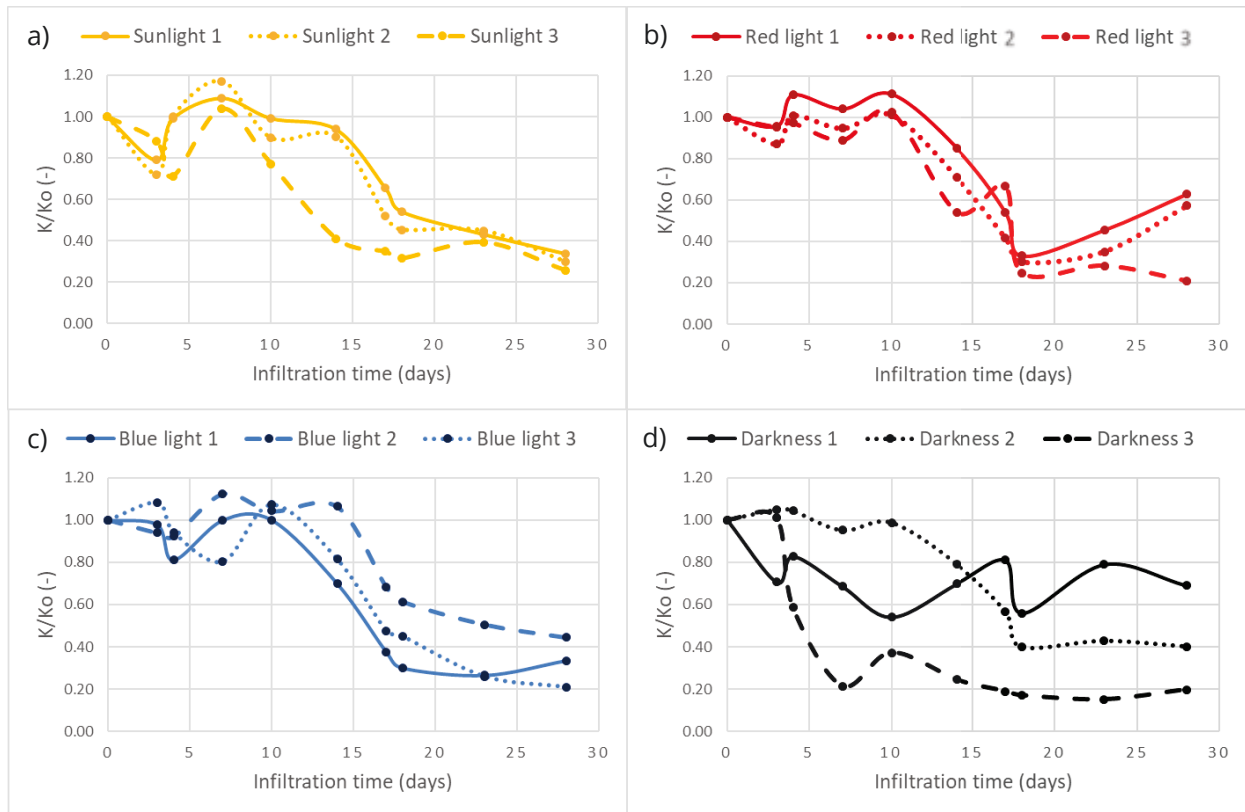


Figure 5.16. Variation in the infiltration rates of Elbe River water for 90 % salt recovery for a period of one month in (a) sunlight scenario (b) red light scenario (c) blue light scenario, and (d) darkness. Each scenario was investigated by triplicated soil columns (1 - 3)

The delayed start of the decrease of the infiltration rate also suggests that biological clogging was the main clogging process. Okubo and Matsumoto (1983) showed the increase in microorganisms during the initial aerobic growth phase and the decrease in the transient phase due to the degradation of aerobic microorganisms. The slow microorganism growth rate at the beginning of the infiltration together with the escape of entrapped air explains the ups and downs of the infiltration rates during the first 10 days. Later on, anaerobic growth governed, and the infiltration rate began to decrease gradually (Okubo and Matsumoto, 1983). The exponential decrease in the infiltration rates after the initial 10 days can be associated with the exponential microbial growth rate. Thereafter, the infiltration rates became quasi-steady which corresponds to the stationary phase of the microbial growth curve (Cunningham and Ross, 2006).

However, the results of Figure 5.16 do not show clearly which light scenario lead to the greatest or least reduction in the hydraulic conductivities, in other words, which scenario had the greatest or least degree of clogging. Therefore, the mean of the hydraulic conductivity values for the triplicates in each scenario was computed (Figure 5.17). For the darkness Scenario, the curve of the column number 2 was not considered in the average because it was considered an outlier. During one month, the sunlight scenario had maximum reduction in infiltration rates of 70 % whereas the darkness scenario had the lowest with 57 %. The difference between both scenarios was about 13 %. Furthermore, there was no clear difference between red and blue lights, which represent cloudy days. The relative difference in the clogging behavior between red and the blue light was only 4 % at the end of the experiment, which suggests that varying spectral power of light does not have a major impact on the clogging (Figure 5.18).

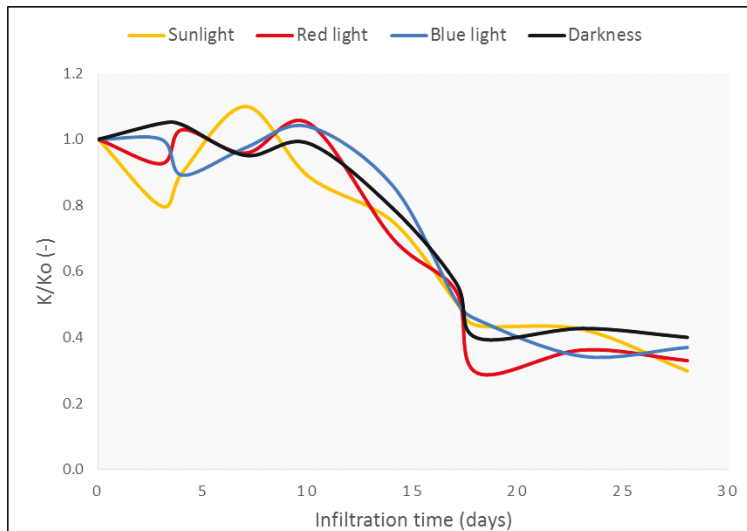


Figure 5.17. Mean infiltration rates for 90% recovery using Elbe River water in sunlight, red light, blue light, and darkness after 30 days of infiltration

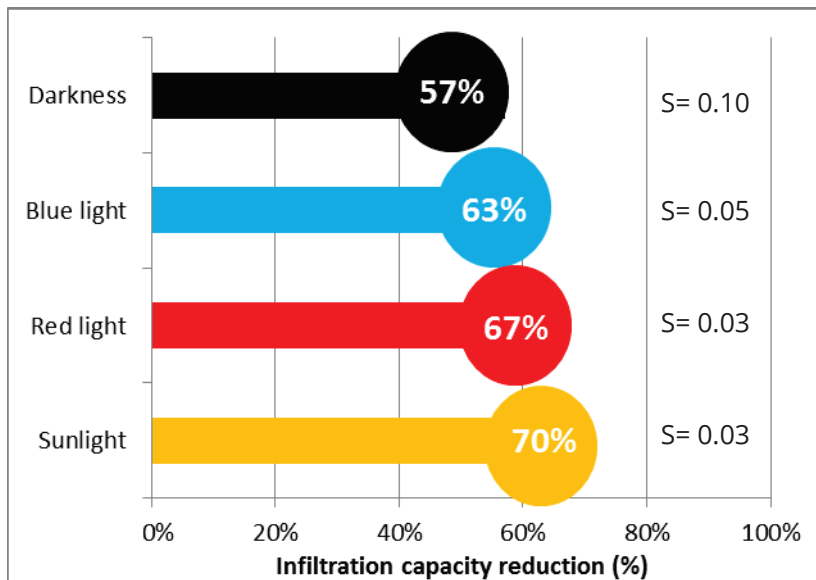


Figure 5.18. Relative difference in clogging between sunlight, red light, blue light, and darkness scenarios based on the results of the last tracer test

In addition to tracer tests, outflow rates also provided an indication of biological clogging. The outflow rates decreased slightly for the initial ten days followed by an exponential decrease and then became constant towards the end of the experiment (Figure 5.19). Such a behavior is associated with the lag phase, exponential growth phase and stationary phase of the microbial growth rate curve (Warren and Bekins, 2015).

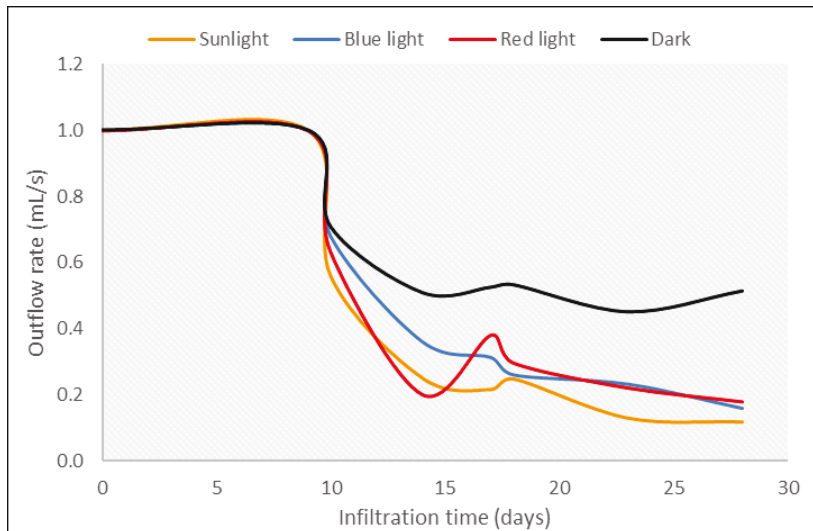


Figure 5.19. Variations in the outflow rates of the soil columns with Elbe river water under different light scenarios

The infiltration rate in the darkness scenario was higher by the end of the experiment with a difference of approximately 30 % to the other three scenarios. This indicates that the degree of clogging under darkness is significantly lower.

Reduction of infiltration capacity by using tap water

The results from the tracer test with 90 % salt recovery using tap water shows less variation in hydraulic conductivities compared to Elbe River water (Figure 5.20 vs. Figure 5.17). There is a general decreasing trend, suggesting that clogging has occurred, which could be due to a combination of chemical and mechanical clogging. Oxidic conditions in the tap water columns, especially in the top layers lead to the formation of Fe (III) oxide which left a reddish-brown stain on the walls of the columns. However, the reddish-brown stain was not visible in the darkness scenario indicating little or no formation of Fe (III) oxide. Besides, any biological clogging taking place in the tap water scenario is most probably due to the microorganisms present in the soil and not in the tap water itself. Soil columns with the visible difference in the color were sampled and tested for iron and manganese presence. A sample of original soil (oven-dried) is also compared. The conditions under sunlight are most conducive for chemical clogging leading to iron and manganese oxidation which can be evidenced from the percentage increase, which was between 23 % and above 170 %, respectively (Table 5.4).

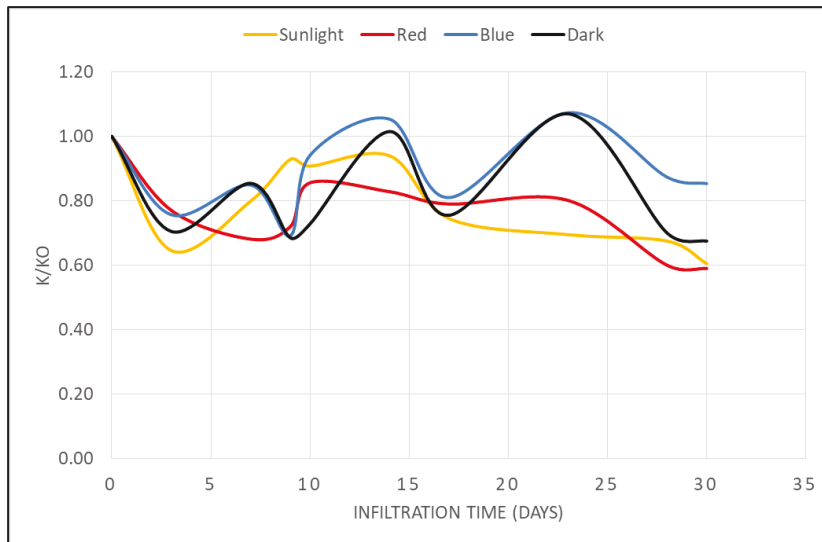


Figure 5.20. Mean infiltration rates for 90% recovery of tap water in sunlight, red light, blue light, and darkness

Table 5.4. Summary of iron and manganese mean concentrations and their respective standard deviation under various light conditions compared to the blank soil sample

	Total Fe [mg/kg]	Total Mn [mg/kg]	Relative increase in Fe [%]	Relative increase in Mn [%]
Sunlight	1344.5 ± 7.1	26.6 ± 0.2	23.1	171.3
Red light	1269.9 ± 91.7	17.2 ± 0.6	16.3	75.7
Blue light	1064.2 ± 15.2	17.4 ± 0.4	-2.6	77.6
Blank soil	1092.1 ± 5.0	9.8 ± 0.7	-	-

It can be concluded that although the quality of tap water meets drinking water standards (Fe: <0.20 mg/L; Mn: <0.05 mg/L) in the Free State of Saxony, Germany (Bundesministerium der Justiz und für Verbraucherschutz, 2001), the chemical clogging can still be caused by certain chemicals especially iron and manganese. Zhang et al. (2019) identified iron oxides, hydroxides, and calcium carbonate as the main forms of geochemical clogging, which are dependent to the presence of oxygen and nitrates in the recharge water. Du et al. (2013) stated that even lower concentrations of these chemicals can result in notable decrease in hydraulic conductivities. The tap water in the laboratory was analyzed for these two cations, resulting in concentrations of $286.1 \pm 7.8 \mu\text{g/L}$ and $2.7 \pm 0.2 \mu\text{g/L}$ for iron and manganese, respectively. Additionally, the concentration of both cations was also analyzed in the Elbe River water. These were $522.1 \pm 68.5 \mu\text{g/L}$ for iron and $41.1 \pm 0.8 \mu\text{g/L}$ for manganese. Unfortunately, no analysis of iron and manganese could be done in the surface soil of the set of columns, where Elbe River was infiltrated, because all the material was used for the TOC analysis.

Total Organic Carbon (TOC)

Once the infiltration scenario was concluded, the soil columns with Elbe River water were tested for TOC to link the proportion of clogging with the illumination scenario. The highest value of TOC was on the shallow layer of each soil column. This is supported by Anderson et al. (2006) in which the vertical distribution of chlorophyll a (Chl a) is shown with significant higher algae growth in the

upper sand layer than in the lower. Also, Benamar (2013) stated that the main TOC storage in the subsurface occurs in the top layer and is dependent on the suspension concentration, pore size, and flow rates.

The values for the triplicates in each of the scenarios were averaged to obtain a single value of TOC for the corresponding layer depths (Table 5.5). The amount of TOC in the sunlight scenario is the highest with 94 % TOC in the top layer, followed by red light, blue light, and darkness scenario, respectively. This confirms the results from the tracer tests and outflow rates, suggesting a higher degree of clogging in the sunlight scenario.

Table 5.5. Mean TOC and the respective standard deviation corresponding to each scenario in different depths of the soil columns under sunlight, red light, blue light, and darkness scenarios

Total Organic Carbon in mg/L				
Soil depth in cm	Sunlight	Red light	Blue light	Dark
0 - 5	6.5 ± 0.97	4.5 ± 0.93	3.2 ± 0.31	2.7 ± 0.24
5 - 10	0.1 ± 0.02	0.1 ± 0.02	0.3 ± 0.09	0.2 ± 0.04
10 - 20	0.1 ± 0.02	0.1 ± 0.02	0.2 ± 0.05	0.2 ± 0.04
20 - 35	0.1 ± 0.04	0.1 ± 0.02	0.1 ± 0.02	0.1 ± 0.01
Total TOC (mg/L)	7.0 ± 0.97	4.9 ± 0.93	3.8 ± 0.31	3.2 ± 0.32
% of TOC in top layer	94.1	92.3	85.4	84.8

Over 80 % of the clogging-driving carbon is located in the upper section (5 cm) of the soil column, which confirms why the scraping of the top soil in infiltration basins can represent a positive effect for the improvement of the infiltration capacity of the site. The results of the scraping investigation follow in the next chapter.

5.2 MANAGEMENT OF CLOGGING IN SPREADING BASINS

5.2.1 Recovery of infiltration capacity by scraping in field unit

During the first scenario with the soil of *Stein und Erden* (Scenario 1), the bottom of the pond was scraped with a shovel two times after the basin was overflowing. The first overflow occurred after 39 days of infiltration under the flooding regime of 1 day infiltration followed by 3 days of dry period. The infiltration capacity recovered by scraping, as it was expected, but the infiltration rate decreased faster and after 14 days an overflow of the basin occurred again. The basin was scraped again, and the basin was overflowing once again after only 7 days. An overview of the infiltration days before the basin overflow is shown in Figure 5.21 and a tendency becomes clear: The fact that the overflow of the basin takes place earlier after each scraping indicates that clogging not only occurs in the upper layer of the basin surface but also in deeper layers. In Figure 5.22a, b a photograph of the clogging layer before and after scraping is shown. In Figure 5.22c, the upper soil profile is shown together with the extension in depth of the clogging layer.

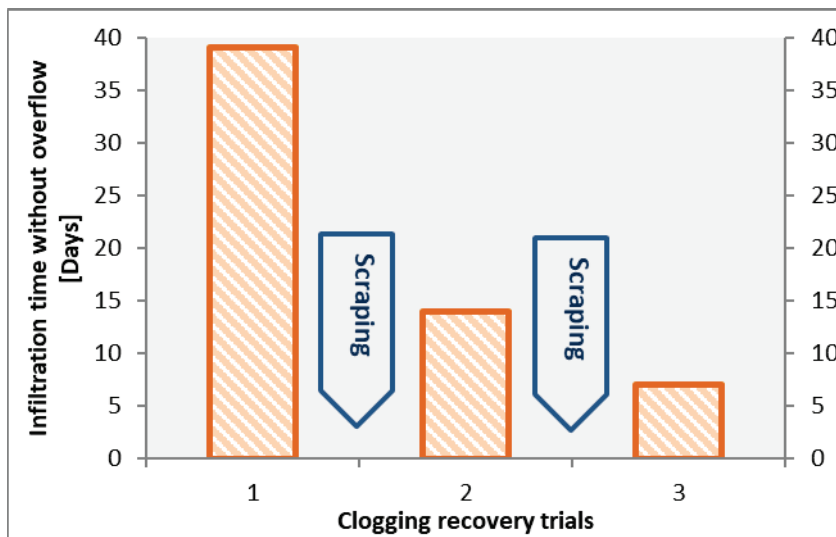


Figure 5.21. Days of infiltration before occurrence of basin overflow and scraping intervals during a test scenario running with an HLC of 3:1 during cold conditions

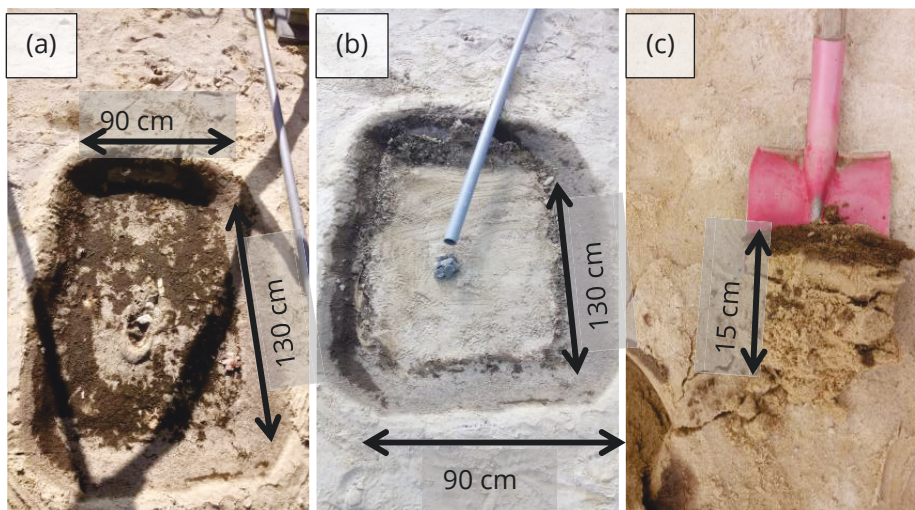


Figure 5.22. State of the basin (a) before scraping, (b) after the scraping, and (c) a sample of the upper 15 cm of the basin to examine the depth of the clogged layer

Given this outcome, it was decided to study more in depth the efficiency of repeated scraping procedures in a recharge basin in the controlled laboratory environment. The development of the clogging layer is influenced by several factors, such as climatic conditions, which complicate the interpretation of scraping on clogging.

5.2.2 Recovery of infiltration capacity by scraping in lab units

The water quality data of infiltration water used for both laboratory infiltration basins (described in Chapter 4.2) is presented in Table 5.6. The concentration of total suspended solids (TSS) for the Elbe River water was in average 4.7 mg/L.

Table 5.6. Total suspended solids concentration in the Elbe River Water.

Date	TSS (mg/L)
10.12.2018	2.3
04.01.2019	5.4
07.01.2019	1.8
08.01.2019	6.5
10.01.2019	5.0
17.01.2019	7.3

The reduction of dissolved organic carbon (DOC) in the effluent from the infiltration tanks (Table 5.7) was very low, since the organic particles in the river water (6 mg/L DOC) are not retained or degraded in the given soil filter depth. The average for the two tanks outflow was 5.5 mg/L DOC.

Table 5.7. DOC data in the inflow and outflow of the infiltration tanks

Sample	Tank	DOC	DOC
		Inflow (mg/L)	Outflow (mg/L)
1	Tank 1 start	6.85	6.71
2	Tank 2 start	5.56	5.39
3	Tank 1 end	4.71	4.54
4	Tank 2 end	5.45	5.36

Note: Samples for DOC analysis were taken from the inflow and from the outflow at the beginning and at the end of the infiltration experiment of both tanks.

In Figure 5.23, the infiltration capacity reduction for both infiltration units was normalized in respect to the initial conditions. The percolation rate reduces with increased clogging layer thickness and ponding stage (Houston et al., 1999). Tank 1 (no scraping) experienced a decrease of the infiltration capacity right from the start and kept the decreasing tendency until the basin was overflowing after approximately 100 m³ of infiltrated river water per square meter of basin area. The overflowing event happened during night hours and the fine particles were mobilized, blocking the outflow cavity of the tank and leaving the infiltration unit unusable, since the infiltration basin was not draining any water in the outflow.

In comparison to Tank 1, the surface of Tank 2 was scraped four times, which increased the infiltration capacity temporarily. After the first two maintenance works, the infiltration recovered almost completely, showing an increase of about 40 %. Nevertheless, the next tracer test evidenced that the infiltration velocity sank once again at a very steep rate. After the second scraping event, the decrease of the infiltration capacity was higher. A third scraping event managed to recover only 23 % of the infiltration capacity, and the last scraping yield 30 %. After 210 m³/m², the Tank 2 unit experienced a malfunction in the outflow, which necessitated termination of the experiment.

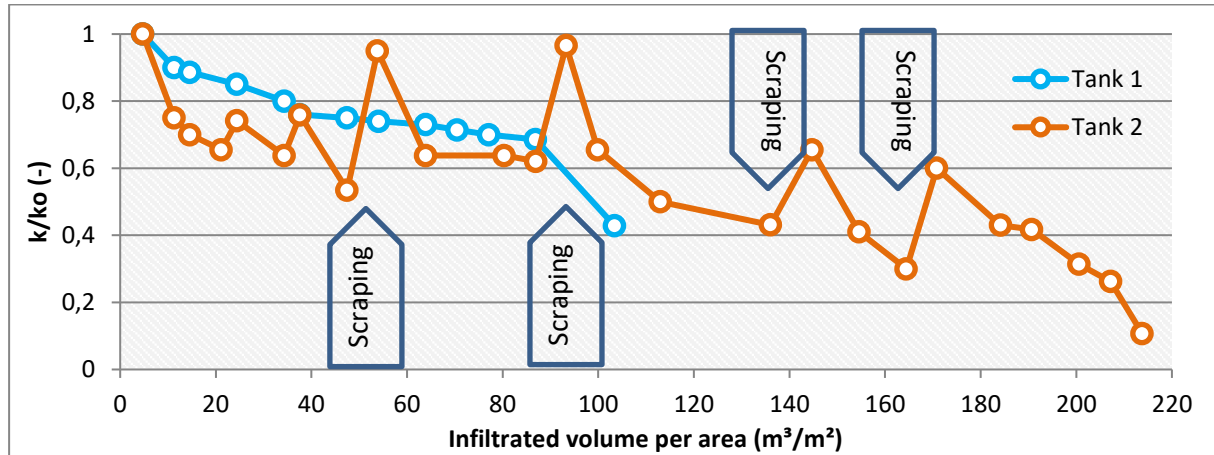


Figure 5.23. Infiltration capacity reduction in Tank 1 (no scraping) and Tank 2 (with scraping)

Scraping was defined during the experiment as the removal of the surface clogging layer. This was done by stopping the inflowing water and allowing the infiltration basin surface to dry for a minimum of 24 hours. This is important since by scraping the basin whilst it was under saturated conditions, the fine particles may mobilize. Once the basin surface was dry, an edged tool such as a ruler or spatula was used to remove the surface clogging layer. Clogging was classified via a visual inspection of the infiltration surface. The clogging layer is of a different color and texture to the native infiltration soil. Thus, it can be easily identified and removed. The scraping procedure was complete when the whole clogging layer has been extracted. This was typically reached between the 0-3 cm clogging material removal during each scraping procedure. It is important to note that the walls of the infiltration basin were not scraped to maintain the structural integrity of the infiltration basin. Removing material from the sidewalls of the basin may have had a detrimental effect, and could cause the slumping of the basin walls down to the bottom of the infiltration basin.

As commented before, the infiltration rate decreased immediately after the first day of flooding. The infiltration capacity reduction of Tank 2, shown in Figure 5.23, was divided into five sections, namely when the basin was scraped, a new section was selected. An exponential trend line was drawn for each section and the resulting equations are given in Figure 5.24. The exponential equations follow the structure by Phipps (2007):

$$y = \alpha * e^{\beta x} \quad (14)$$

where y is the estimated reduction of the infiltration capacity, x the infiltrated volume per square meter of basin area, α is the initial infiltration capacity and β is the factor that determines the steepness of the decay. When comparing β between the different sections, a significant decrease (two times higher) can be observed between sections 3 and 4. This decrease can be interpreted as a steeper decrease of the infiltration capacity, which is equivalent to a faster developing clogging layer. Additionally, it can be noted that the initial state (factor α) after the third scraping event does not reach the values as at the beginning of the experiment.

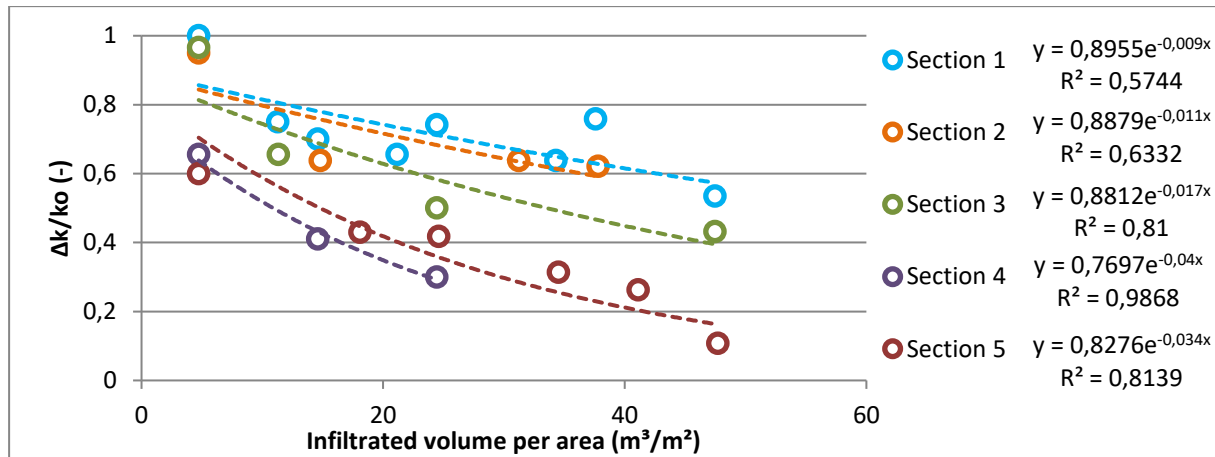


Figure 5.24. Infiltration capacity reduction in Tank 2 after each scraping event

These different equations can be related to the work done by Phipps et al. (2007) where they proposed that the reduction of infiltration velocities can be described by the log decay expression:

$$Q = Q_0 e^{-(rL)} \quad (15)$$

where Q_0 is the initial percolation rate, L is the total foulant per unit of area, deposited at the sediment or water interface, Q is the percolation observed at l foulant loading and r is a sediment / foulant interaction coefficient.

Phipps et al. (2007) based their analysis on how the percolation rate changes while a given amount of deposits builds up a clogging layer on the surface. In this study, the height of the fouling layer could not be quantified, which is the reason to use the total volume of water that percolated per square meter of basin area.

Two types of clogging processes may have occurred in Tank 2:

The clogging of the upper layer was the visually apparent layer of particulate matter, algae and bacterial growth. TSS are considered the prime determinant in surface clogging (Harpaz, 1971; Hutchinson, 2007; Siegrist and Boyle, 1987; Winter and Goetz, 2003).

The clogging of the lower layer is the mechanical movement of the native sediment formed of organic and inorganic solids becoming trapped in pore spaces and thus reducing hydraulic conductivity (Duryea, 1997). This is shown in the lower recovery rates after each of the scraping events. The first two scraping procedures allowed full recovery of the infiltration velocities. However, with every subsequent scraping event shown in Figure 5.23, there is a decreasing effect on the recovery of the infiltration velocity. As each scraping event removed the clogging layer in the basin surface, e.g. between 2-3 cm, this layer had minor effects upon hydraulic conductivity. This suggests that clogging in the lower layer within the main infiltration soil could be responsible for these decreases in infiltration velocity. Ponding within the infiltration basins may also have caused local increases in soil saturation. This could lead to mobilization of fine particles causing a natural compaction of the soil. This compaction reduces the pore space and size, which in return reduces the infiltration velocities.

The high salt concentrations of the infiltrating water during salt tracer tests may have reduced the hydraulic conductivity of the infiltration soils by several mechanisms. The high EC in the tracer solution can chemically precipitate salts directly within the pore of the infiltration soil, and reduce the hydraulic conductivity (Platzer and Mauch, 1997). Particle size distribution analysis shows that the soil contains a clay fraction ($< 0.002\text{mm}$) of 1.22 %. At high salt concentrations, swelling of the clay fraction of the native infiltration sediment can lead to a reduction in hydraulic conductivity and therefore velocity decreases (Pupisky and Shainberg, 1979). At lower salt concentrations,

dispersion of the clay fraction can be expected (Shainberg et al., 1981; Yousaf et al., 1987). This dispersion and the possible subsequent flocculation could have contributed to the mobilization of fine particles recorded throughout the study. Therefore, it is plausible to assume that infiltrating high salinity, EC salt tracer solutions into the infiltration basins may have been instrumental in reducing hydraulic conductivities and therefore, infiltration velocities during the experiment. High EC, saline salt tracer infiltration tests may also have hindered the growth of some bacterial species (Hotchkiss, 1923) and therefore may have reduced the effect of biological clogging processes.

Due to the challenges faced by using a salt tracer and its possible influence on the development of biological clogging, alternative methods for tracking the flow infiltration velocity were investigated. The next chapter focuses on the results of self-developed methods based on water content measurements, which are inexpensive in operation compared to using isotopes as tracers, for example.

5.3 DETERMINATION OF INFILTRATION CAPACITY USING WATER CONTENT

This chapter together with chapter 4.3 include the main findings from the publication with title: *Methods of In Situ Assessment of Infiltration Rate Reduction in Groundwater Recharge Basins*. in Water Journal 2019l, 11(4), 784. Therefore, the citation of Barquero et al. (2019) was suppressed in its content.

A description of the results of the methods introduced in chapter 4.3 was done using the raw data of Scenario 1 (1 day infiltration and 3 days drying period) in warm climatic conditions, followed by a comparison of the methods with other relevant hydraulic scenarios.

5.3.1 Tracer method

Figure 5.25 contains the set of t_{50} (time to recover 50 % of the tracer concentration) of each infiltration cycle against the infiltration time and gives an indication of the reduction of the infiltration rate during Scenario 1 (Run 8 Climate 3; HLR 300 m/a; HLC: 1:1). Moreover, it reflects the lowest infiltration rate after nine infiltration cycles. This is relevant information for the managers of infiltration basin plants for scheduling maintenance programs. The tracer test gave the reference data to analyze the fit of the other methods and determine their capacity to identify the variations of the soil's hydraulic conductivity.

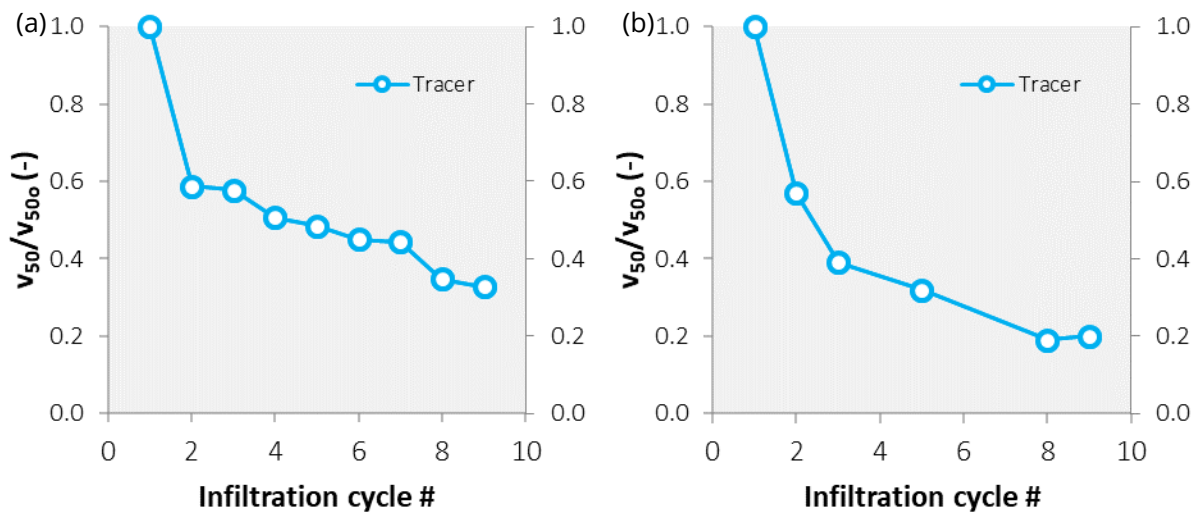


Figure 5.25. Infiltration capacity curve determined by tracer experiments in (a) field scale and (b) laboratory scale. Infiltration modus: 24 h infiltration / 72 h dry period

5.3.2 Libardi method

The time series data at the end of each infiltration cycle were selected to introduce the change of water content data into the Libardi equation (8). Because the maximum water content is obtained fast with the designed pumping rate (2.7 L/min in the field and 0.9 L/min in the laboratory) at the beginning of the infiltration cycle, it does not allow to take enough water content measurements and makes it inadequate for applying the Libardi equation. Therefore, the initial water content, θ_o , was set as the water content value started to decline and θ was set as the water content at time t_i , which is included in the abscissa of the smoothed model in Figure 4.15 as natural logarithm $[\ln(t)]$. Parameters A_L and B_L represents the slope and ordinate intercept, respectively.

The starting conditions of each drying cycle presented lower initial water content values as the number of infiltration cycles increased. Additionally, its decrease is less steep every time in comparison to the subsequent drying cycles (see Figure 5.26). After the 1440 min (3 days) dry period, the difference between all cycles is very low (about 1 %). During the first 100 min of the draining period, the main difference of the water content reduction between cycles is clearly identifiable.

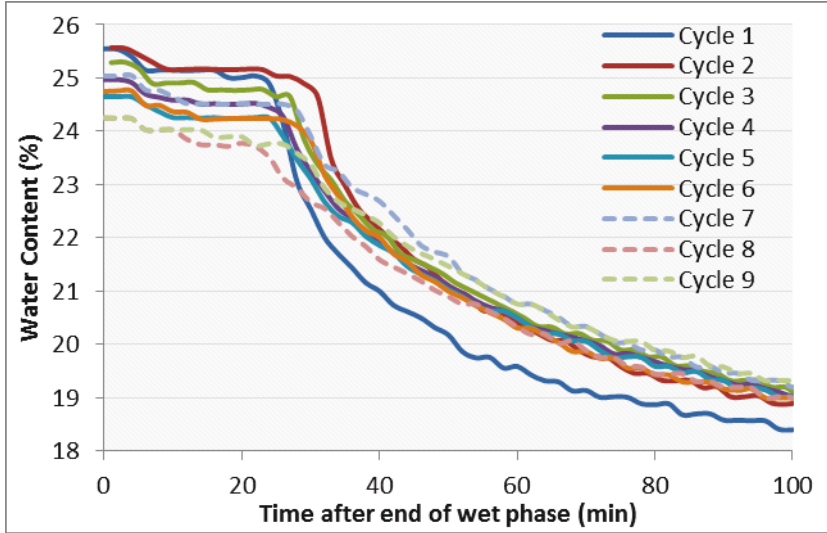


Figure 5.26. Water content decrease during the drying cycles in the first 100 min in field experiment. Infiltration modus: 24 h infiltration/72 h dry period

Figure 5.27 shows the results of the obtained infiltration reduction curve after applying equation (8) with the drying period data series, together with the tracer test results (reference). The Libardi method presents an overestimation of the final reduction of the infiltration capacity in comparison to the tracer test method. However, the trend remains similar in both techniques. The linear regression root mean square error (RMSE) of the values of the Libardi curves in laboratory and in field scale against to the tracer curve values are 0.40 and 0.55, respectively.

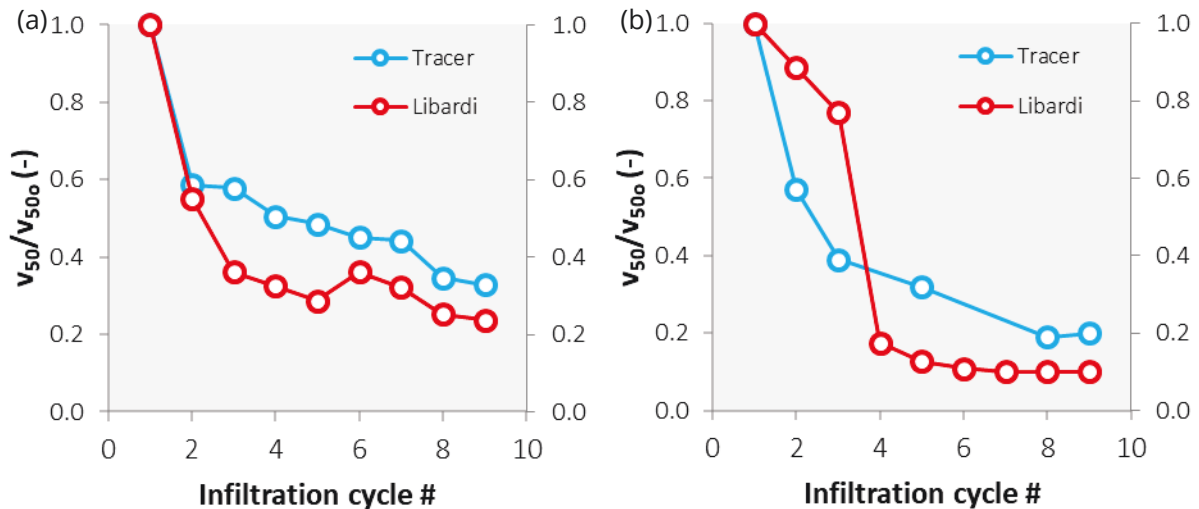


Figure 5.27. Infiltration capacity curve comparison between Libardi method and Tracer curve in (a) field scale, and (b) laboratory scale. Infiltration modus: 24 h infiltration / 72 h dry period

The Libardi method is based on the data of the drying phase of each cycle (1440 min) and is strongly dependent on the water level in the infiltration basin at the end of the infiltration. With higher

water levels above the basin surface, it will be necessary that the sensor detects a steep reduction of the water content. The estimation of the hydraulic conductivity after Libardi changed faster at the beginning of the scenario, since the water head draining occurred faster. The results suggest that the clogging layer on the surface of the infiltration basin has a stronger influence in drying conditions than during the wetting events and therefore using Libardi calculations lead to higher rates of infiltration rate reduction compared to the tracer methodology.

5.3.3 Root mean square method

Overlapping all the water content readings of each cycle during the wet regime, as it was done with the drying cycles in Figure 5.27, results in a decrease of water content after each infiltration cycle. Equation (10) was applied between cycle 1 (set as the reference cycle for the starting conditions without clogging) and the remaining eight infiltration cycles, obtaining a continuous decrease of the infiltration capacity until cycle 8. The change pattern of the D_{RMS} values and of the tracer curve are very similar. Applying the calculated D_{RMS} in the linear regression model (Equation (11)), results in the following equations for field and laboratory, respectively:

$$\text{Tracer}_{\text{Field}} = 0.9583 - 0.6084 \times D_{RMS \text{ Field}} + 0.1270 \times D_{RMS \text{ Field}}^2 \quad (16)$$

$$\text{Tracer}_{\text{Lab}} = 0.8974 - 0.2055 \times D_{RMS \text{ Lab}} + 0.0144 \times D_{RMS \text{ Lab}}^2 \quad (17)$$

The fitting of the calculated D_{RMS} -based infiltration capacity reduction curve, and the tracer-based curve gave good results, resulting in an RMSE value of 0.14 (Figure 5.28a). However, the D_{RMS} -based curve in the laboratory experiment presented an abrupt sink of the infiltration capacity at the third infiltration cycle, similarly as it occurred in the Libardi method. Therefore, the RMSE between the curves (0.23) was much higher compared to the field experiment.

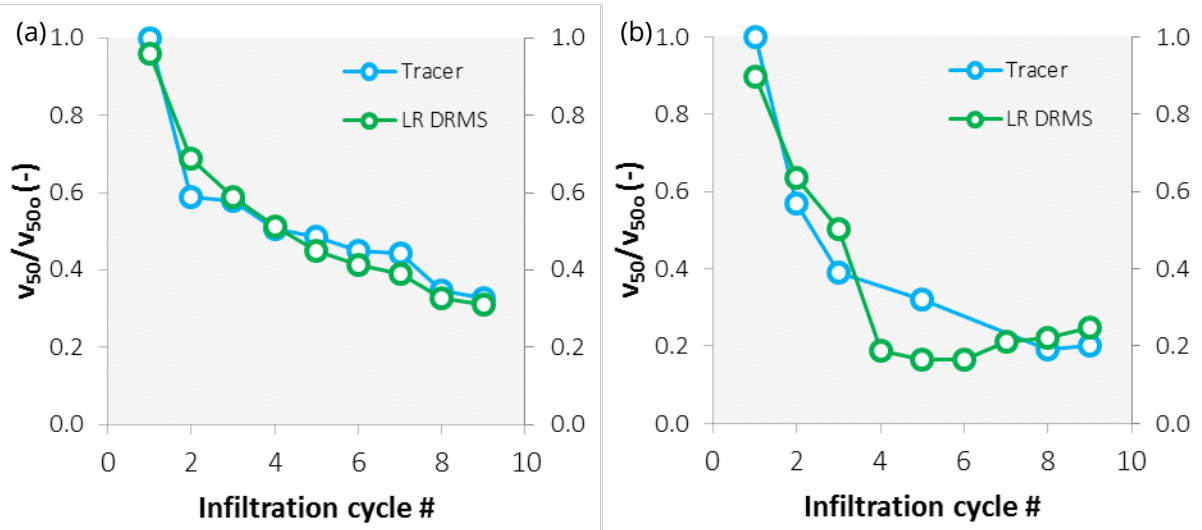


Figure 5.28. Comparison between tracer curve and linear regression (LR) DRMS-based curve in (a) field scale, and (b) laboratory scale

5.3.4 Water content method

The determination of infiltration capacity reduction curve using the average water content of each infiltration cycle was done using Equation (12):

$$\text{Tracer}_{\text{Field}} = 101.3208 - 8.4626 \times \left[\frac{\sum WC_i}{n} \right]_{\text{Field}} + 0.1771 \times \left[\frac{\sum WC_i}{n} \right]_{\text{Field}}^2 \quad (18)$$

$$\text{Tracer}_{\text{Lab}} = 0.5372 - 0.0683 \times \left[\frac{\sum \text{WC}_i}{n} \right]_{\text{Lab}} + 0.0029 \times \left[\frac{\sum \text{WC}_i}{n} \right]_{\text{Lab}}^2 \quad (19)$$

The RMSE values between the reference tracer curve and constructed linear regression water content (LR WC) curve were 0.21 in the field and 0.26 in the laboratory. The fit of the curve in the field was acceptable along the whole infiltration cycles (Figure 5.29a), whereas for the laboratory the model it improves after the fourth infiltration cycle. This stage is the one where the hydraulic conductivity reduction is not steep anymore, having changes below 10 %.

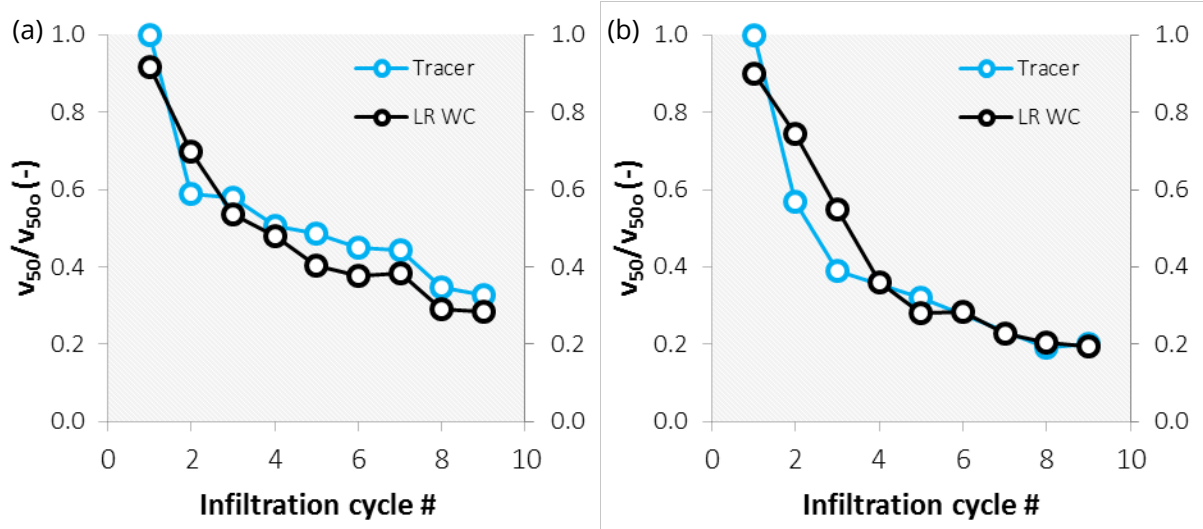


Figure 5.29. Comparison between tracer curve and LR WC-based curve in (a) field scale, and (b) laboratory scale

The results coming from tracer tests show the flow dynamics during the first stage of each infiltration (for this study's experiment about 4 hours). D_{RMS} and water content methods are not only representing the wetting process and infiltration velocities at the beginning of the infiltration cycle, but also include the complete 24 h infiltration cycle water content data. The D_{RMS} method represents a more elaborate analysis relating the water content values between infiltration cycles in time. This may be the reason for the difference between both methods in the laboratory experiment. A lag phase of the water content in the infiltration cycles 4, 5 and 6 was analyzed by the D_{RMS} method as a reduction of the infiltration capacity. On the other hand, the water content method calculates an overall mean water content of each infiltration cycle and does not identify differences in time. This results in more stable data.

5.3.5 Trigger time method

The parameters for the trigger time method equations 20 and 21 were obtained using the linear regression model of Equation (10):

$$\text{Tracer}_{\text{Field}} = 2.8854 - 0.3112 \times \text{TT}_{\text{Field}} + 0.0093 \times \text{TT}_{\text{Field}}^2 \quad (20)$$

$$\text{Tracer}_{\text{Lab}} = 1.4748 - 0.1279 \times \text{TT}_{\text{Lab}} + 0.0030 \times \text{TT}_{\text{Lab}}^2 \quad (21)$$

The tracer curve in the field scale was best reproduced by the trigger time of the water content sensor with an RMSE of 0.06 (Figure 5.30a); while in the laboratory the results did not fit with the tracer curve, resulting in one of the highest RMSE values (0.37) of the here analyzed regression models.

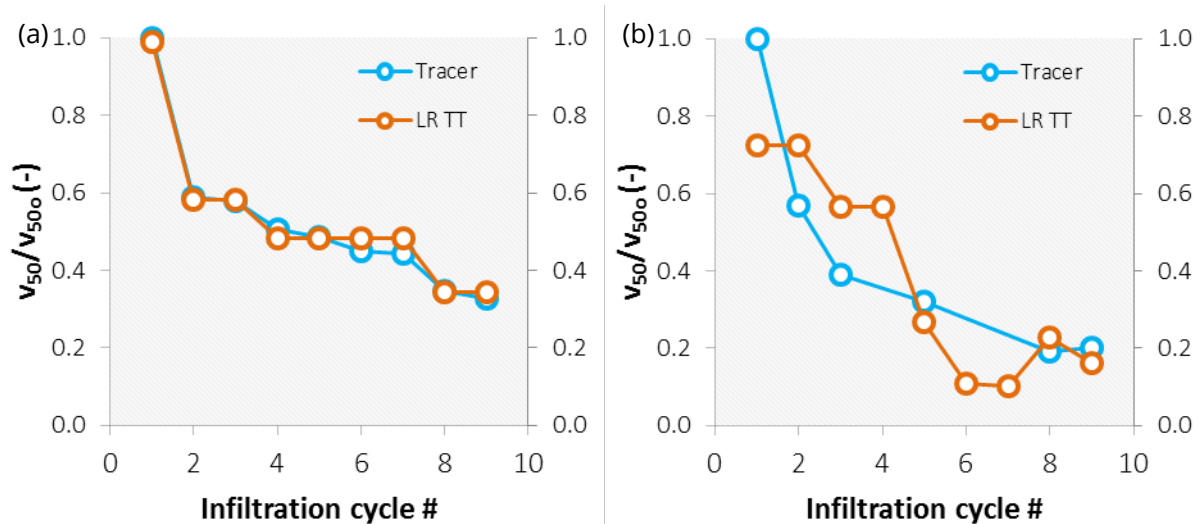


Figure 5.30. Comparison between tracer curve and LR TT-based curve in (a) field scale, and (b) laboratory scale

The trigger time method resulted in an precise estimation of the reduction of the infiltration capacity in the field scale. However, the step-shape decrease of the infiltration capacity is mainly due to the coarse resolution of the measured data (2 min). Furthermore, similar to the tracer experiment, the trigger time method produced a value obtained from the early stage of the infiltration cycle and does not really represent the conditions throughout the wet period. In the laboratory scale, the calculated values were very different all along the tracer curve. This suggests that sidewall flow of the experimental setup may have interfered in the estimation of the ICRC using the trigger method, which is based only on the first increase of the water content. Gibert (2015) stated that a preferential flowpath within vicinity to the inner tank walls may result in more water flowing in comparison to field conditions.

5.3.6 Validation process

A notable limitation of the linear regression methods (D_{RMS} , WC, and TT) is that a validation of the obtained equations is only possible in constrained conditions. Namely, the linear regression equations are only able to simulate the reduction of the infiltration capacity if the input data are within the limits that were used for the reference run. For example, in the analyzed field experiment (Scenario 1 Climate 3), the variation of water content was between 26 and 24 % (Table 5.8). When approaching colder conditions, this variation becomes larger (Climate 2: 27 % to 24 %; climate 1: 29 % to 22 %). The saturated water content also varies with different soil types (total porosity), the hydraulic operation of the infiltration (HLR & HLC), and the climate (fluid viscosity).

Table 5.8. Summary of D_{RMS} (%), WC (%), TT (min) raw data and tracer test (-) values for Scenario 1 (Climate 1, 2, and 3) and Scenario 4 (Climate 3). By changing hydraulic and climatic conditions the D_{RMS} and WC values change in their magnitude (look at max and min). The TT method is more sensible to hydraulic changes.

Inf. cycle #	Sc. Clim.	D_{RMS} (%)				WC (%)				TT (min)				Tracer (-)			
		1	1	1	4	1	1	1	4	1	1	1	4	1	1	1	4
		Cold	Mild	Warm	Warm	Cold	Mild	Warm	Warm	Cold	Mild	Warm	Warm	Cold	Mild	Warm	Warm
1		0.00	0.00	0.00	0.00	29.83	27.21	25.87	25.87	8	10	8	10	1.00	1.00	1.00	1.00
2		4.76	1.99	0.49	0.86	25.04	25.28	25.52	25.41	12	12	11	10	0.71	0.82	0.59	n.d.*
3		6.76	2.58	0.71	2.01	24.54	24.71	25.22	24.14	14	12	11	26	0.65	0.7	0.58	0.51
4		7.07	2.91	0.91	3.59	25.45	24.48	25.09	22.39	11	14	12	40	0.665	0.51	0.51	0.25
5		7.38	3.25	1.08	4.73	22.43	24.13	24.89	21.27	13	14	12	50	0.68	0.56	0.49	n.d.*
6		n.d.*	3.21	1.20	3.99	n.d.*	24.14	24.82	22.00	n.d.*	14	12	52	n.d.*	0.59	0.45	0.17
7		n.d.*	3.09	1.27	4.01	n.d.*	24.25	24.84	21.85	n.d.*	14	12	48	n.d.*	0.51	0.44	0.21
8		n.d.*	3.14	1.52	3.99	n.d.*	24.25	24.49	21.90	n.d.*	16	14	36	n.d.*	0.48	0.35	n.d.*
9		n.d.*	3.41	1.60		n.d.*	24.06	24.47		n.d.*	21	14		n.d.*	0.12	0.33	

*n.d.: No data: No tracer experiment conducted.

Thus, Equations 16 - 21 cannot be used for the data base of other scenarios with varying HLC or a different climate. For a validation step, the raw data of Scenario 1 Climate 2 (change in climate) and Scenario 4 Climate 3 (change in HLC) sorted in Table 5.8 were set in a multi-axis diagram (Figure 5.31) to confirm that the trend of the different methods coincide with the tracer results.

With a decreasing infiltration capacity of the soil, the water content value (black line in Figure 5.31) also becomes smaller. The magnitude of the decrease is proportional when comparing the drop in the Figure 5.31a, b. After the first four infiltration cycles, the infiltration capacity in Scenario 1 Climate 2 was reduced by 41 %, whereas the mean water content decreased by 2.7 %. The decline of the infiltration capacity in Scenario 4 Climate 3 is much stronger (75 %) and also the mean water content described this trend by registering a change of 4.6 %.

On the other hand, D_{RMS} and TT work inversely proportional to the infiltration capacity reduction. For the same first 4 infiltration cycles, the change of D_{RMS} is 2.91 % and 3.59 % for the low and high infiltration capacity drop, respectively. The trigger time also increases from 14 min to 40 min (note that the TT axis scale differs in Figure 5.31b).

Once the consistency of the methods is proven for different scenarios, their applicability is the conclusive part of this section. The methods can be used in sites with infiltration basins to monitor the development of clogging during the infiltration period. The time trigger and Libardi methods are not useful for sites operating with a continuous infiltration setup, since there is no drying period to feed the model with data. D_{RMS} and Water Content method can be set to indicate the clogging magnitude for a whole infiltration cycle or for a fraction of the cycle. This becomes handy, especially when the infiltration cycles are long (e.g. 7 days). Due to the constraints of the linear regression methods analyzed in this study, the recharge site should have at least three different analyzing equations for changing climate conditions (cold, mild, and warm). If the mean daily temperature variation on the site is greater than 20 °C, more linear regression equations should be considered.

The developed methods ease the determination of infiltration capacity of the soil without making use of salt tracers in laboratory experiments. This becomes relevant when the scope of the study is the growth rate of biological clogging, which might be sensible to sudden changes of electrical conductivity or salinity. These methods become more attractive since the operational costs are lower compared to isotope analysis. Furthermore, notable is the feasibility of using this type of methods in in unsaturated media, which is a key condition when studying surface spreading methods.

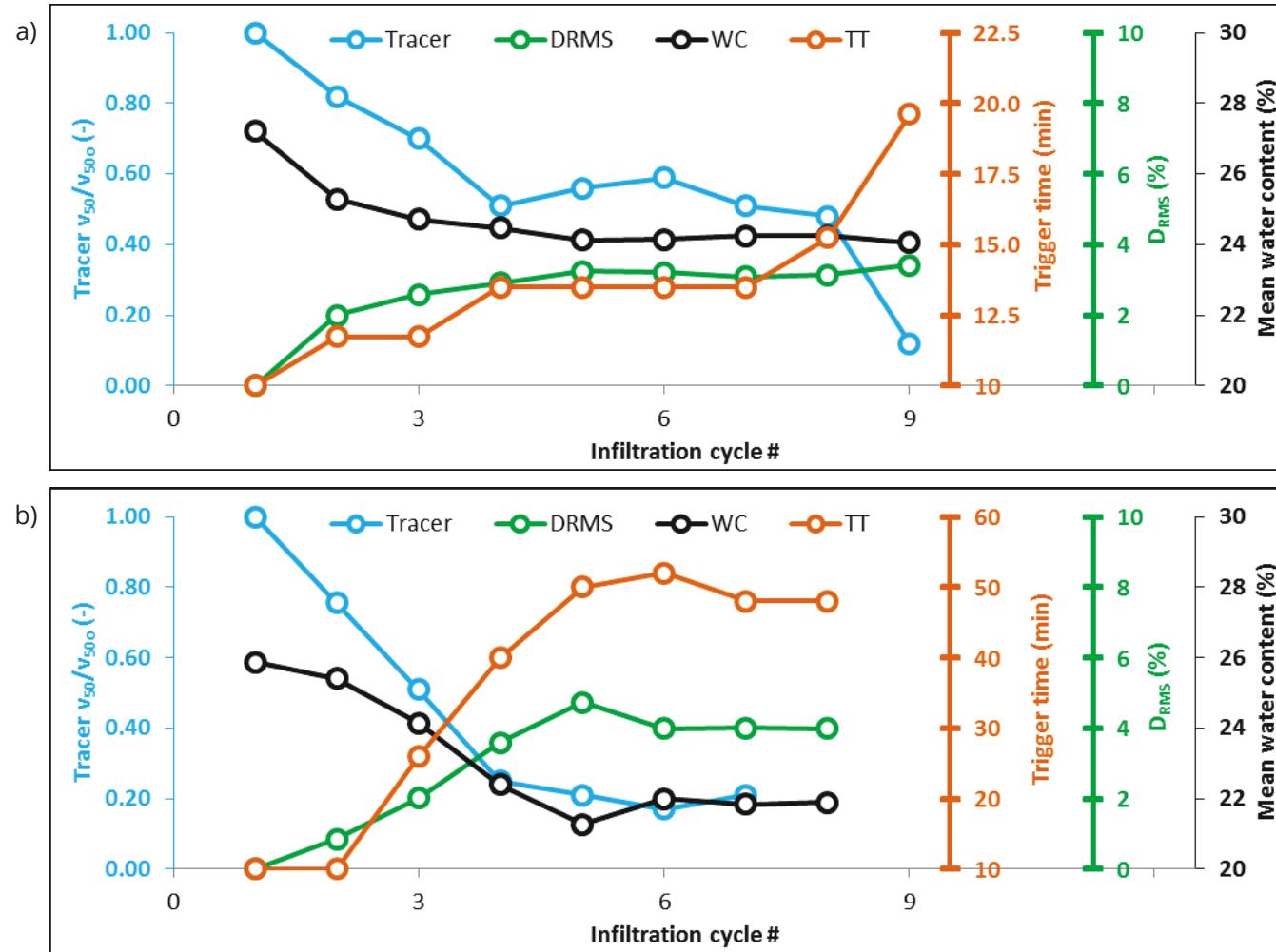


Figure 5.31. Correlation between the raw data of the infiltration capacity reduction curves for (a) Scenario 1 Climate 2, and (b) Scenario 4 Climate 3 for Tracer, Displacement Root Mean Square (DRMS), Mean Water Content (WC), and Trigger Time (TT) methods. Tracer and WC work proportional, whereas the relation is inversely proportional for the DRMS and TT methods. These trends keep valid under variable hydraulic and climatic conditions

6 CONCLUSIONS

Climate is under constant modification in short terms (daily and seasonal variation) as well as in long terms (climate change). Therefore, it is imperative to better understand how the phenomenon of clogging reacts under different climatic situations.

The experiments run in the field under seasonally varying climate represent conditions present in real world infiltration sites, especially because they also consider the natural variation of the Elbe River water quality. The set of 12 investigation batches (four hydraulic scenarios in three climatic conditions) confirms that colder conditions (mean temperature lower than 10 °C) are the most resistant to infiltration flow, forcing the system operation to stop infiltration earlier. This is not mainly due to clogging, but rather because of the water quality and viscosity changes of the fluid. The latter can be responsible for reduction of the infiltration velocity of up to 40 % due to drastic temperature changes of 30 °C, or 17 % by moderate changes of 10 °C. The results with a mild or warm climate indicated that under warmer conditions, the development of clogging is the main driver of the infiltration capacity reduction of the soil. Furthermore, the continuous infiltration mode was set as the most sensible one to seasonal climate variations. During warmer conditions, the development of clogging was 40 % higher than in colder conditions.

The air temperature of 10 °C was identified as the main temperature threshold that represents a significant change in the reduction of the infiltration capacity of the soil. Especially, the upper 20 cm of the soil are sensitive to the seasonality effects during infiltration, whereas the hydraulic conditions below 1 m in depth remain constant. The results of the TOC sampling of the upper soil layer after each scenario confirmed that the algae growth always gets intensified in warmer conditions (especially due to more intense solar incidence) and the oxygen consumption is better regulated in oxic-anoxic shifting phases. This is a disadvantage for the use of continuous infiltration modes, when trying to avoid blocking of pores because of the accumulation of the organic cake layer on the basin surface.

In recharge sites that are vulnerable to changes in air temperature, because of the regional climate fluctuation by 2050, the operators can, for example, adjust their operational system either to a higher recharge capacity or to an increased frequency of clogging maintenance in time (under warmer conditions).

The solar irradiance effect could not be studied in the field investigation unit without the effect of climate variability and therefore, soil columns with controlled conditions were tested. The results suggest that the sun effects in the development of biological clogging of up to about 30 %. Therefore, shifting to night time infiltration intervals should prolong the operation of the infiltration basin at its maximum capacity and also reduces the evaporation rate. The fractions of the solar irradiance during cloudiness (450 nm and 650 nm) did not exhibit a special difference in the development of the organic cake layer.

The field and the laboratory experiments reveal that the most affected section of the infiltration basin to the clogging formation is the upper surface layer (1–3 cm). Like real world infiltration sites, this indicates that scraping may be the best maintenance procedure. Nevertheless, performing several scraping procedures might decrease its effectiveness in the long-term. The investigation under continuous infiltration showed that in laboratory conditions after the fourth maintenance event, the recovery of the infiltration rate corresponds only to a recovery of 60 %. This suggests that the site should invest, for example, in deep ploughing procedures after certain operation time with the scraping procedure. This allows also deeper layers to recover their initial infiltration capacity. The frequency will depend on the site operation mode (HLC), the recharge rate, water source and quality, and size of the basin.

To sum up, the relevance of clogging was presented, and therefore, developing alternative methods to determine it becomes also important. During this investigation, new methods were suggested to monitor the infiltration capacity reduction in recharge sites without using invasive determination methods like infiltration rings. The methods were based on water content measurements in 2 minutes intervals during the complete infiltration cycle. Applying these techniques in recharge facilities can enhance the understanding of the hydraulic behavior changes and its organic as well as inorganic components during the flooding cycles. This could maximize the time in which the infiltration basin can be operated and the best time for its maintenance can be defined. The suggested methods are not meant to substitute any other already existing analytical or numerical tools, but rather to foster and complement the knowledge of the involved processes.

The method of Libardi reproduced an accurate pattern of the infiltration capacity reduction, analyzing the water content decline during the drying period after every infiltration cycle. Higher number of drying periods allows an increased traceability of the decrease in the infiltration capacity. The sensor trigger time method showed an accurate representation of the reduction in infiltration rate in the field conditions only. Nevertheless, this method is completely dependent upon the time measurement interval in which the data was logged, and represents only the conditions at the beginning of the infiltration cycle (analogous to tracer methods). The D_{RMS} method and the Water Content method were the most accurate approaches for data management in MAR basins to determine the actual state of the infiltration capacity. In addition, these methods calculate a value that represents the complete infiltration cycle and not just a fraction of it.

D_{RMS} , water content, and the trigger time methods feature linear regression models to correlate the raw data with the results of tracer experiments. The obtained equations can only be used within each experiment, and in the analyzed intervals. If the hydraulic and climatic boundary conditions remain constant, the given empirical equation could also be applied in different experiments.

Summing up all the results, this thesis offers to the scientific community related to MAR, a list of tools and facts that can be used to enhance the management of infiltration basins taking into consideration the variability of climate: (1) controlling the clogging state of the basin with the water content based calculations, (2) implementing design parameters to reduce the clogging rate in time given the site climate condition, and (3) once the clogging state is advanced, applying recovery measures to the basin to improve the infiltration capacity.

7 LIMITATIONS AND OUTLOOK

This last section of the thesis refers to the limitations and research perspectives to the topic of clogging management in a changing climatic system:

The main limitation of the field rapid infiltration unit was that its size and location were not adequate for studying the connection between the vadose zone and the saturated zone, since the hydraulic processes were completely influenced by the strong dynamics between the aquifer and Elbe River. The question of the effect of the changing climatic conditions on the saturated zone remains still open. The following aspects could be further investigated to better characterize the influence of climate variation in the dynamics between vadose zone and saturated zone: (1) monitoring the water table mounding, (2) observing physicochemical changes of the groundwater, as well as (3) to include production wells to extract the recharge water.

Many measurements were taken but this was not enough to enable the possibility of building a numerical model. The major hindrance was the access to a software that is capable not only to incorporate changes of hydraulic conductivity of the soil media in time but also to independently calculate this variation under given scenario conditions.

Three years were needed to collect the results of each scenario in all climate conditions. This investigation time was challenging due to the uncertainty of the climatic forecast in a monthly step and the barrier of being unable to control the climate conditions. This thesis could be the reference for further research for the connection between climate and clogging in a more detailed approach. For instance, in the chemical perspective: Which organic matter compound is the main driver for the formation of the cake layer under a specific climate condition? Or which microorganisms manage to better adapt to the river water conditions either in oxic or in anoxic conditions?

The field investigations could be resumed by using a water source that chemically brings more stress to the system, such as treated wastewater. It has some parameters that should be further treated before disposal. The major challenge of this source of water has been the local permits to allow the introduction of this water into the vadose zone.

The soil column experiments considered a continuous flow condition only. It is worth to evaluate an extension of the investigation with scenarios with hydraulic cycles, namely with night flooding events to evaluate the development of the clogging layer and determine the avoided evaporated water.

A key issue is the transfer of the valuable knowledge from the pilot scale investigation units to a large scale infiltration sites. Applying the output of this thesis to an ongoing recharge site would ease the quantification of the advantages of the applied clogging management tools.

8 BIBLIOGRAPHY

- Abdalla, O.A.E., Al-Rawahi, A.S., 2013. Groundwater recharge dams in arid areas as tools for aquifer replenishment and mitigating seawater intrusion: example of AlKhod, Oman. *Environ. Earth Sci.* 69, 1951–1962. <https://doi.org/10.1007/s12665-012-2028-x>
- Abrantes, J.R.C.B., Moruzzi, R.B., Silveira, A., de Lima, J.L.M.P., 2018. Comparison of thermal, salt and dye tracing to estimate shallow flow velocities: Novel triple-tracer approach. *J. Hydrol.* 557, 362–377. <https://doi.org/10.1016/j.jhydrol.2017.12.048>
- Achilleos, M., Ourania, T., Antunes, I., Ribeiro, M., 2019. Monitoring of the managed aquifer recharge (MAR) system by treated wastewater reuse (Akrotiri Limassol, Cyprus), in: *Proceedings of the 10th International Symposium on Managed Aquifer Recharge (ISMAR 10)*. Madrid, Spain, 20-24 May 2019. pp. 107–113.
- Adger, W.N., Arnell, N.W., Tompkins, E.L., 2005. Successful adaptation to climate change across scales. *Glob. Environ. Change* 15, 77–86. <https://doi.org/10.1016/j.gloenvcha.2004.12.005>
- Aguilera, J., Karsten, U., Lippert, H., Vögele, B., Philipp, E., Hanelt, D., Wiencke, C., 1999. Effects of solar radiation on growth, photosynthesis and respiration of marine macroalgae from the Arctic. *Mar. Ecol. Prog. Ser.* 191, 109–119. <https://doi.org/10.3354/meps191109>
- Ahfir, N.-D., Wang, H.Q., Benamar, A., Alem, A., Massei, N., Dupont, J.-P., 2007. Transport and deposition of suspended particles in saturated porous media: hydrodynamic effect. *Hydrogeol. J.* 15, 659–668. <https://doi.org/10.1007/s10040-006-0131-3>
- Ahrens, L., Felizeter, S., Sturm, R., Xie, Z., Ebinghaus, R., 2009. Polyfluorinated compounds in waste water treatment plant effluents and surface waters along the River Elbe, Germany. *Mar. Pollut. Bull.* 58, 1326–1333. <https://doi.org/10.1016/j.marpolbul.2009.04.028>
- Alados, I., Foyo-Moreno, I. y, Alados-Arboledas, L., 1996. Photosynthetically active radiation: measurements and modelling. *Agricultural and Forest Meteorology*, 78, 121–131. [https://doi.org/10.1016/0168-1923\(95\)02245-7](https://doi.org/10.1016/0168-1923(95)02245-7)
- Alexowsky, W., 1997. *Geologische Karte des Freistaates Sachsen 5049, 5049., Landesvermessungsamt Sachsen, Dresden.*
- Allen, M.R., Dube, O.P., Solecki, W., Aragon-Durand, F., Cramer, W., Humphreys, S., Kainuma, M., Kala, J., Mahowald, N., Mulugetta, Y., Perez, R., Wairiu, M., Zickfeld, K., 2018. Framing and Context. In: *Global Warming of 1.5°C. An IPCC Special Report on the impacts of global warming of 1.5°C above pre-industrial levels and related global greenhouse gas emission pathways, in the context of strengthening the global response to the threat of climate change, sustainable development, and efforts to eradicate poverty.* URL <https://www.ipcc.ch/sr15/chapter/chapter-1/> (accessed 10.22.19).
- Al-Senafy, M., Sherif, M., 2006. Proposed scheme for a natural soil treatment system in Kuwait, in: *Recharge Systems for Protecting and Enhancing Groundwater Resources; Proceedings of the 5th International Symposium on Management of Aquifer Recharge ISMAR5*, Berlin, Germany, 11–16 June 2005, IHP-VI Series on Groundwater. Presented at the 5th International Symposium on Management of Aquifer Recharge ISMAR5, UNESCO document, Berlin, pp. 174–178.
- Anderson, M., Dewhurst, R., Jones, M., Baxter, K., 2006. Characterisation of turbidity and well clogging processes in a double porosity Chalk aquifer during the South London Artificial Recharge Scheme trials, in: *UNESCO (Ed.), Recharge Systems for Protecting and Enhancing Groundwater Resources - Proceedings of the 5th International Symposium on Management of Aquifer Recharge ISMAR 5*, Berlin, Germany, 11–16 June 2005, ISMAR Proceedings. pp. 593–598.
- Ansems, N., Khaka, E., Villholth, K.G., 2014. *Ecosystem-based Adaptation in Groundwater Management.* UNEP, IGRAC, IWMI, UNESCO.

- <https://www.un-igrac.org/sites/default/files/resources/files/Ecosystem%20Based%20Adaptation%20in%20Groundwater%20Management.pdf> (accessed 22.10.19)
- Armbruster, H., Mors, K., Eiswirth, M., Hoetzel, H., Merkler, G.-P., Naegelsbach, E., 1992. Leakage detection of sewing pipes by combined geophysical and tracer techniques. KITopen-ID: 111692 <https://publikationen.bibliothek.kit.edu/111692> (accessed 10.10.19)
- Arnosti, C., Jørgensen, B.B., Sagemann, J., Thamdrup, B., 1998. Temperature dependence of microbial degradation of organic matter in marine sediments: polysaccharide hydrolysis, oxygen consumption, and sulfate reduction. *Marine Ecology Progress Series*. 165, 59–70. <https://doi.org/10.3354/meps165059>
- Arshad, M., Guillaume, J., Ross, A., 2014. Assessing the Feasibility of Managed Aquifer Recharge for Irrigation under Uncertainty. *Water* 6, 2748–2769. <https://doi.org/10.3390/w6092748>
- Asano, T., Burton, F.L., Leverenz, H., Tsuchihashi, R., Tchobanoglous, G., 2007. *Water reuse - Issues, Technologies, and Applications*. McGraw-Hill Professional Publishing. ISBN: 9780071459273
- Askarinejad, A., Beck, A., Casini, F., Springman, S.M., 2012. Unsaturated Hydraulic Conductivity of a Silty Sand with the Instantaneous Profile Method, in: Mancuso, C., Jommi, C., D'Onza, F. (Eds.), *Unsaturated Soils: Research and Applications*. Springer Berlin Heidelberg, pp. 215–220.
- Assouline, S., Or, D., 2014. The concept of field capacity revisited: Defining intrinsic static and dynamic criteria for soil internal drainage dynamics. *Water Resour. Res.* 50, 4787–4802. <https://doi.org/10.1002/2014WR015475>
- Avnimelech, Y., Nevo, Z., 1964. BIOLOGICAL CLOGGING OF SANDS. *Soil Sci.* 98, 222.
- Barquero, F., Fichtner, T., Stefan, C., 2019. Methods of In Situ Assessment of Infiltration Rate Reduction in Groundwater Recharge Basins. *Water* 11, 784. <https://doi.org/10.3390/w11040784>
- Barry, K., Dillon, P., Pavelic, P., 2013. Domestic scale rainwater ASR observations of clogging and effectiveness of its management. *Clogging Issues Assoc. Manag. Aquifer Recharge Methods IAH Commission Manage Aquifer Recharge* 184.
- Barry, K., Vanderzalm, J., Miotlinski, K., Dillon, P., 2017. Assessing the Impact of Recycled Water Quality and Clogging on Infiltration Rates at A Pioneering Soil Aquifer Treatment (SAT) Site in Alice Springs, Northern Territory (NT), Australia. *Water* 9, 179. <https://doi.org/10.3390/w9030179>
- Baveye, P., Vandevivere, P., Hoyle, B.L., DeLeo, P.C., de Lozada, D.S., 1998. Environmental Impact and Mechanisms of the Biological Clogging of Saturated Soils and Aquifer Materials. *Crit. Rev. Environ. Sci. Technol.* 28, 123–191. <https://doi.org/10.1080/10643389891254197>
- Bekele, E., Toze, S., Higginson, S., Patterson, B., Blair, P., Heitz, A., Browne, A.L., Leviston, Z., Po, M., Nancarrow, B., others, 2008. Determining requirements for managed aquifer recharge in Western Australia: progress report. CSIRO: Water for a Healthy Country National Research Flagship. (<http://www.clw.csiro.au/publications/waterforahealthycountry/2008/wfhc-DeterminingRequirementsManagingAquiferRechargeWA.pdf>). (accessed 10.22.19)
- Bekele, E., Toze, S., Patterson, B., Fegg, W., Shackleton, M., Higginson, S., 2013. Evaluating two infiltration gallery designs for managed aquifer recharge using secondary treated wastewater. *Journal of Environmental Management*. 117, 115–120. <https://doi.org/10.1016/j.jenvman.2012.12.018>
- Bekele, E.B., Donn, M.J., Barry, K.E., Vanderzalm, J.L., Kaksonen, A.H., Puzon, G.J., Wylie, J., Miotlinski, K., Cahill, K., Walsh, T., Morgan, M., McFarlane, D., Dillon, P.J., 2015. *Managed Aquifer Recharge and Recycling Options: understanding clogging processes and water quality impacts*. Australian Water Recycling Center of Excellence: Brisbane, Australia.
- Benamar, A., 2013. Soil clogging phenomena in vertical flow. *Clogging Issues Assoc. Manag. Aquifer Recharge Methods IAH Comm. Manag. Aquifer Recharge Aust.* 77–83.

- Bennani, A.C., Lary, J., Nrhira, A., Razouki, L., Bize, J., Nivault, N., 1992. Wastewater treatment of greater Agadir (Morocco): an original solution for protecting the bay of Agadir by using the dune sands. *Water Sci. Technol.* 25, 239–245. <https://doi.org/10.2166/wst.1992.0355>
- Bennion, D.B., Bennion, D.W., Thomas, F.B., Bietz, R.F., 1998. Injection Water Quality-A Key Factor to Successful Waterflooding. *J. Can. Pet. Technol.* 37. <https://doi.org/10.2118/98-06-06>
- Bernhofer, C., Matschullat, J., Bobeth, A., 2009. Das Klima in der REGKLAM-Modellregion Dresden. Rhombos-Verlag. ISBN: 978-3-941216-22-8
- Bishop, J.K.B., Rossow, W.B., 1991. Spatial and temporal variability of global surface solar irradiance. *J. Geophys. Res. Oceans* 96, 16839–16858. <https://doi.org/10.1029/91JC01754>
- Bista, A., 2015. Implementation of heterogeneous high-resolution saturated groundwater flow and mass transport model for the test site Pirna for analyzing multiple tracer tests (Master thesis). Technische Universität Dresden, Germany.
- Böckelmann, U., Manz, W., Neu, T.R., Szewzyk, U., 2000. Characterization of the microbial community of lotic organic aggregates ('river snow') in the Elbe River of Germany by cultivation and molecular methods. *FEMS Microbiology and Ecology* 33, 157–170. <https://doi.org/10.1111/j.1574-6941.2000.tb00738.x>
- Bothwell, M.L., Sherbot, D.M., Pollock, C.M., 1994. Ecosystem response to solar ultraviolet-B radiation: influence of trophic-level interactions. *Science* 265, 97–100. <https://doi.org/10.1126/science.265.5168.97>
- Bouwer, H., 2002. Artificial recharge of groundwater: hydrogeology and engineering. *Hydrogeology Journal*. 10, 121–142. <https://doi.org/10.1007/s10040-001-0182-4>
- Bouwer, H., 1996. Issues in artificial recharge. *Water Sci. Technol., Wastewater Reclamation and Reuse* 1995 33, 381–390. [https://doi.org/10.1016/0273-1223\(96\)00441-6](https://doi.org/10.1016/0273-1223(96)00441-6)
- Bouwer, H., Pyne, R., Brown, J., St Germain, D., Morris, T.M., Brown, C.J., Dillon, P., Rycus, M.J., 2009. Design, operation, and maintenance for sustainable underground storage facilities. Water Environment Research Foundation. USA. ISBN: 978-60573-041-7
- Bouwer, H., Rice, R.C., 1989. Effect of water depth in groundwater recharge basins on infiltration. *J. Irrig. Drain. Eng.* 115, 556–567. [https://doi.org/10.1061/\(ASCE\)0733-9437\(1989\)115:4\(556\)](https://doi.org/10.1061/(ASCE)0733-9437(1989)115:4(556))
- Brecht, S., 2015. Abschätzung der Grundwasserneubildung mit Hilfe eines Tracerversuches in Pirna, Deutschland (Master Thesis). Technische Universität Dresden, Germany.
- Bromly, M., Hinz, C., Aylmore, L.A.G., 2007. Relation of dispersivity to properties of homogeneous saturated repacked soil columns. *European Journal of Soil Science*. 58, 293–301. <https://doi.org/10.1111/j.1365-2389.2006.00839.x>
- Buckingham, E., 1907. Studies on the movement of soil moisture. US Department of agriculture Bureau of soils no 38. <https://archive.org/details/studiesonmovemen38buck> (accessed 11.18.19)
- Bundesministerium der Justiz und für Verbraucherschutz, 2001. Verordnung über die Qualität von Wasser für den menschlichen Gebrauch, (Trinkwasserverordnung - TrinkwV) Anlage 3 (zu §7 und §14 Absatz 3) Indikatorparameter. URL https://www.gesetze-im-internet.de/trinkwv_2001/anlage_3.html (accessed 11.11.19).
- Camacho, J., 2017. Engineering fluid-mechanics. Fluid dynamics <https://www.slideshare.net/JavierICamacho/engineering-fluidmechanics-71386864> (accessed 21.10.19).
- Casanova, J., Devau, N., Pettenati, M., 2016. Managed Aquifer Recharge: An Overview of Issues and Options, in: Jakeman, A.J., Barreteau, O., Hunt, R.J., Rinaudo, J.-D., Ross, A. (Eds.), *Integrated Groundwater Management*. Springer International Publishing, pp. 413–434. https://doi.org/10.1007/978-3-319-23576-9_16
- Chai, T., Draxler, R.R., 2014. Root mean square error (RMSE) or mean absolute error (MAE)? – Arguments against avoiding RMSE in the literature. *Geoscience Model Dev.* 7, 1247–1250. <https://doi.org/10.5194/gmd-7-1247-2014>

- Chaieb, H., 2014. Tunisian Experience in Artificial Recharge using Treated Waste Water, in: Regional Conference on "Sustainable Integrated Wastewater Treatment and Reuse". Sharm El Sheikh, Egypt. 1-2 December 2014.
- Chaieb, H., Moncef, R., Ouerfelli, N., Laghi, M., Magagnini, L., Tosatto, O., De Angelis, A., Sollazzo, F., Teatini, P., 2013. On the effectiveness of reusing treated wastewater by infiltration ponds in coastal farmlands. Preliminary investigation on insights from the Korba site, Tunisia, in: 1st CIGR Inter-Regional Conference on Land and Water Challenges.
- Christiansen, J.E., 1944. Effect of entrapped air upon the permeability of soils. *Soil Science*. Vol. 58, p 355–366. <https://doi.org/10.1097/00010694-194411000-00002>
- Clark, J.F., Hudson, G.B., Avisar, D., 2005. Gas transport below artificial recharge ponds: Insights from dissolved noble gases and a dual gas (SF₆ and ³He) tracer experiment. *Environmental Science Technology*. 39, 3939–3945. <https://doi.org/10.1021/es049053x>
- Corwin, D.L., Yemoto, K., 2017. Salinity: Electrical Conductivity and Total Dissolved Solids. *Methods Soil Analysis* <https://doi.org/10.2136/mta2015.0039>
- Council, N., 1994. Ground water recharge using waters of impaired quality. National Academies Press. Washington, DC: The National Academies Press. <https://doi.org/10.17226/4780>
- Crites, R.W., Middlebrooks, E.J., Bastian, R.K., 2014. Natural wastewater treatment systems. CRC Press, Taylor & Francis Group, Boca Raton, Florida.
- Cunningham, A.B., Ross, R.J., 2006. Biofilms: the hypertextbook. Mont. State Univ. Bozeman MT.
- Darcy, H., 1856. Les fontaines publiques de la ville de Dijon: Exposition et Application des Principes a Suivre et des Formules a Employer dans les Questions de Distribution d'Eau. Paris, 647 p.
- De Zwart, A.H., 2007. Investigation of clogging processes in unconsolidated aquifers near water supply wells. Ponaen Looyen BV Delft.
- der, G., Jac van, 2012. The United Nations World Water Development Report – N° 4 – Groundwater and Global Change: Trends, Opportunities and Challenges. UNESCO.
- Dietze, M., Dietrich, P., 2012. Evaluation of Vertical Variations in Hydraulic Conductivity in Unconsolidated Sediments. *Ground Water* 50, 450–456. <https://doi.org/10.1111/j.1745-6584.2011.00854.x>
- Dillon, P., 2005. Future management of aquifer recharge. *Hydrogeology Journal*. 13, 313–316. <https://doi.org/10.1007/s10040-004-0413-6>
- Dillon, P., Pavelic, P., Page, D., Behringen, H., Ward, J., 2009. Managed aquifer recharge: An introduction (No. 13), Waterlines Report Series. National Water Commission, Canberra, Australia.
- Dillon, P., Stuyfzand, P., Grischek, T., Lluria, M., Pyne, R.D.G., Jain, R.C., Bear, J., Schwarz, J., Wang, W., Fernandez, E., Stefan, C., Pettenati, M., van der Gun, J., Sprenger, C., Massmann, G., Scanlon, B.R., Xanke, J., Jokela, P., Zheng, Y., Rossetto, R., Shamrukh, M., Pavelic, P., Murray, E., Ross, A., Bonilla Valverde, J.P., Palma Nava, A., Ansems, N., Posavec, K., Ha, K., Martin, R., Sapiano, M., 2019. Sixty years of global progress in managed aquifer recharge. *Hydrogeol. J.* 27, 1–30. <https://doi.org/10.1007/s10040-018-1841-z>
- Domenico, P.A., Schwartz, F.W., 1998. Physical and chemical hydrogeology. Wiley New York.
- Douglas, I., 1968. The effects of precipitation chemistry and catchment area lithology on the quality of river water in selected catchments in eastern Australia. *Earth Science Journal*, 2(2), 126–144.
- Du, X., Wang, Z., Ye, X., 2013. Potential Clogging and Dissolution Effects During Artificial Recharge of Groundwater Using Potable Water. *Water Resour. Manag.* 27, 3573–3583. <https://doi.org/10.1007/s11269-013-0365-5>
- Duryea, P.D., 1997. Clogging layer development and behavior in infiltration basins used for soil aquifer treatment of wastewater. Doctoral Dissertation. Arizona State University, Tempe, Arizona.
- Dutta, T., Carles-Brangarí, A., Fernández-García, D., Rubol, S., Tirado-Conde, J., Sanchez-Vila, X., 2015. Vadose zone oxygen (O₂) dynamics during drying and wetting cycles: An artificial

- recharge laboratory experiment. *Journal of Hydrology* 527, 151–159. <https://doi.org/10.1016/j.jhydrol.2015.04.048>
- Einsiedl, F., 2005. Flow system dynamics and water storage of a fissured-porous karst aquifer characterized by artificial and environmental tracers. *Journal of Hydrology*. 312, 312–321. <https://doi.org/10.1016/j.jhydrol.2005.03.031>
- El Ayni, F., Cherif, S., Jrad, A., Trabelsi-Ayadi, M., 2011. Impact of treated wastewater reuse on agriculture and aquifer recharge in a coastal area: Korba case study. *Water Resource Management*. 25, 2251–2265 (2011). <https://doi.org/10.1007/s11269-011-9805-2>
- Endler, J.A., 1993. The Color of Light in Forests and Its Implications. *Ecol. Monogr.* 63, 2–27. <https://doi.org/10.2307/2937121>
- Fernandez, E., Navarro, J., 2019. Clogging map for Santiuste basin MAR site, Los Arenales Aquifer, Spain. ultivariable analysis to correlate types of clogging and groundwater quality, in: *Proceedings of the 10th International Symposium on Managed Aquifer Recharge (ISMAR 10)*. Madrid, Spain, 20-24 May 2019. pp. 450–463.
- Fernández Escalante, E., González Herrarte, F.B., San Sebastián Sauto, J., 2015. Recarga gestionada de acuíferos: multifuncionalidad en la zona regable de Santiuste, in: *XXXIII CONGRESO NACIONAL DE RIEGOS*. Valencia 16-18 June 2015. Editorial Universitat Politècnica de València.
- Fichtner, T., Barquero, F., Sallwey, J., Stefan, C., 2019. Assessing Managed Aquifer Recharge Processes under Three Physical Model Concepts. *Water* 11, 107. <https://doi.org/10.3390/w11010107>
- Figuerola, F., Salles, S., Aguilera, J., Jiménez, C., Mercado, Viñegla, Flores-Moya, A., Altamirano, M., 1997. Effects of solar radiation on photoinhibition and pigmentation in the red alga *Porphyra leucosticta*. *Marine Ecology Progress Series* 151, 81–90. <https://doi.org/10.3354/meps151081>
- Fodor, N., Sándor, R., Orfanus, T., Lichner, L., Rajkai, K., 2011. Evaluation method dependency of measured saturated hydraulic conductivity. *Geoderma* 165, 60–68. <https://doi.org/10.1016/j.geoderma.2011.07.004>
- Fondriest Environmental, Inc., 2014. Solar Radiation & Photosynthetically Active Radiation. Environmental Measurement Systems. URL <https://www.fondriest.com/environmental-measurements/parameters/weather/photosynthetically-active-radiation/> (accessed 7.9.19).
- Friedman, S.P., 2005. Soil properties influencing apparent electrical conductivity: a review. *Computers and electronics in agriculture- Applications of Apparent Soil Electrical Conductivity in Precision Agriculture* 46, 45–70. <https://doi.org/10.1016/j.compag.2004.11.001>
- Gibert, O., Hernandez, M., Vilanova, E., Cornella, O., 2015. Guidelining protocol for soil column experiments assessing fate and transport of trace organics. *Demeau European Union* 54.
- Glass, J., 2019. New advances in the assessment of managed aquifer recharge through modelling (Doctoral dissertation). TU Dresden, Pirna.
- Google, n.d. Satellite view of Institut für Abfall- und Kreislaufwirtschaft in Pirna.
- Goren, O., Burg, A., Gavrieli, I., Negev, I., Guttman, J., Kraitzer, T., Kloppmann, W., Lazar, B., 2014. Biogeochemical processes in infiltration basins and their impact on the recharging effluent, the soil aquifer treatment (SAT) system of the Shafdan plant, Israel. *Appl. Geochem.* 48, 58–69. <https://doi.org/10.1016/j.apgeochem.2014.06.017>
- Greco, R., 2006. Soil water content inverse profiling from single TDR waveforms. *J. Hydrol.* 317, 325–339. <https://doi.org/10.1016/j.jhydrol.2005.05.024>
- Grischek, T., Bartak, R., 2016. Riverbed clogging and sustainability of riverbank filtration. *Water* 8, 604. <https://doi.org/10.3390/w8120604>
- Gunkel, G., Hoffmann, A., 2006. Gunkel, Günter, and Anja Hoffmann. "Clogging processes in a bank filtration system in the littoral zone of Lake Tegel (Germany).", in: *Recharge Systems for*

- Protecting and Enhancing Groundwater Resource - Proceedings of the 5th International Symposium on Management of Aquifer Recharge - ISMAR 5. United Nations Educational, Scientific and Cultural Organization, Berlin, Germany, pp. 10–16.
- Haaken, K., 2018. Applied Hydrogeophysics for Managed Aquifer Recharge (Doctoral dissertation). Rheinische Friedrich-Wilhelms-Universität Bonn.
- Händel, F., Binder, M., Dietze, M., Liedl, R., Dietrich, P., 2016. Experimental recharge by small-diameter wells: the Pirna, Saxony, case study. *Environ. Earth Sci.* 75, 1–8. <https://doi.org/10.1007/s12665-016-5701-7>
- Harbaugh, A.W., 2005. MODFLOW-2005, the US Geological Survey modular ground-water model: the ground-water flow process (No. 6-A16), U.S. Geological Survey Techniques and Methods. US Department of the Interior, US Geological Survey Reston, VA, USA.
- Harpaz, Y., 1971. Artificial Ground-Water Recharge by Means of Wells in Israel. *Journal of the hydraulics division*. Volume 97. Pg. 1947–1964.
- Hatch, C.E., Fisher, A.T., Revenaugh, J.S., Constantz, J., Ruehl, C., 2006. Quantifying surface water–groundwater interactions using time series analysis of streambed thermal records: Method development. *Water Resour. Res.* 42. <https://doi.org/10.1029/2005WR004787>.
- Hazen, A., 1892. Some physical properties of sands and gravels. Mass. State Board of Health. 24th Annu. Rep. 539–556.
- Heilweil, V.M., Marston, T., 2013. Evaluation of potential gas clogging associated with managed aquifer recharge from a spreading basin, Southwestern Utah, USA. *Clogging Issues Assoc. Manag. Aquifer Recharge Methods IAH Comm. Manag. Aquifer Recharge Aust.* 84–94.
- Hernandez, M., Tobella, J., Ortuno, F., Armenter, J.L., 2011. Aquifer recharge for securing water resources: the experience in Llobregat river. *Water Science and Technology*. 63, 220–226. <https://doi.org/10.2166/wst.2011.036>
- Hernández-Aguilar, M.H. Recarga artificial en el acuífero del valle de San Luis Río Colorado a través de lagunas de infiltración. In *Manejo de la recarga de acuíferos: Un enfoque hacia Latinoamérica*, 1st ed.; Escolero, O., Gutiérrez-Ojeda, C., Mendoza, E.Y., Eds.; Instituto Mexicano de Tecnología del Agua, Universidad Nacional Autónoma de México: Morelos, México, 2017; pp. 431–462.
- Hida, N., 2009. Managed aquifer recharge by using spreading basin methods on alluvial fans: a general overview of the situation in Japan. *Bol. Geológico Min.* 120, 311–320. ISSN: 0366-0176
- Hillel, D., Hatfield, J.L., 2005. *Encyclopedia of Soils in the Environment*. Elsevier Amsterdam.
- Hillel, D., Krentos, V.D., Stylianou, Y., 1972. Procedure and test of an internal drainage method for measuring soil hydraulic characteristics in situ. *Soil Science: Volume 114 - Issue 5*, p 395–400.
- Hoffmann, A.A., Sgro, C.M., 2011. Climate change and evolutionary adaptation. *Nature* Vol. 470 (7335), 479–485. <https://doi.org/10.1038/nature09670>
- Hoffmann, R., Dietrich, P., 2004. Geoelektrische Messungen zur Bestimmung von Grundwasserfließrichtungen und -geschwindigkeiten. *Grundwasser* 9, 194–200. <https://doi.org/10.1007/s00767-004-0045-8>
- Holländer, H.M., Hinz, I., Boochs, P.W., Billib, M., 2006. Experiments to determine clogging and redevelopment effects at laboratory scale., in: *Recharge Systems for Protecting and Enhancing Groundwater Resource - Proceedings of the 5th International Symposium on Management of Aquifer Recharge - ISMAR 5*. United Nations, Berlin, Germany, pp. 11–16.
- Holm-Hansen, O., 1969. Algae: amounts of DNA and organic carbon in single cells. *Science* 163, 87–88. <https://doi.org/10.1126/science.163.3862.87>
- Hotchkiss, M., 1923. Studies on Salt Action: VI. The Stimulating and Inhibitive Effect of Certain Cations upon Bacterial Growth 1. *Journal of bacteriology*. Vol. 8 (2), 141. URL: <https://jb.asm.org/content/jb/8/2/141.full.pdf> (accessed 7.9.19)

- Houston, S.L., Duryea, P.D., Hong, R., 1999. Infiltration considerations for ground-water recharge with waste effluent. *Journal of irrigation and drainage engineering*. 125, 264–272. [https://doi.org/10.1061/\(ASCE\)0733-9437\(1999\)125:5\(264\)](https://doi.org/10.1061/(ASCE)0733-9437(1999)125:5(264))
- Huff, G.F., Wald, J.D., 1989. Geochemistry of artificial-recharge tests in the Oakes aquifer near Oakes, southeastern North Dakota (USGS Numbered Series No. 89–4122), *Water-Resources Investigations Report*. U.S. Geological Survey.
- Hulthe, G., Hulth, S., Hall, P.O.J., 1998. Effect of oxygen on degradation rate of refractory and labile organic matter in continental margin sediments. *Geochim. Cosmochim. Acta* 62, 1319–1328. [https://doi.org/10.1016/S0016-7037\(98\)00044-1](https://doi.org/10.1016/S0016-7037(98)00044-1)
- Hutchinson, A.S., 2013. Report on Groundwater Recharge in the Orange County Groundwater Basin 2011-2012. Orange County Water District, Fountain Valley, CA, USA.
- Hutchinson, A.S., 2007. Challenges in optimizing a large-scale managed aquifer recharge operation in an urbanized area. *P Fox Ed Manag. Aquifer Recharge Sustain*. Phoenix 346–354.
- Hutchinson, Adam and Milczarek, Mike, 2018. Design and Operations Considerations - State of the Art Techniques in Characterizing, Constructing and Operating Optimum Surface Spreading Groundwater Recharge Projects. Presented during the 16th Biennial Symposium on Managed Aquifer Recharge, San Diego, USA (March 2018).
- Hutchinson, A.S., Milczarek, M., Banerjee, 2013. Clogging Phenomena Related to Surface Water Recharge Facilities, in: Martin, R. (Ed.), *Clogging Issues Associated with Managed Aquifer Recharge Methods*. IAH Commission on Managing Aquifer Recharge, Australia, pp. 95–106.
- Ilyas, A., 2012. Microwave dielectric sensing of moisture in MSWibottom ash – Comparison of frequency vs. time domain reflectometry. URL <https://www.tidskriftenvatten.se/tsv-artikel/microwave-dielectric-sensing-of-moisture-in-mswibottom-ash-comparison-of-frequencyvs-time-domain-reflectometry-fukthaltsmatning-i-bottenaska-med-dielektriska-metoder-en-jamfore/>.
- Irving, J., Singha, K., 2010. Stochastic inversion of tracer test and electrical geophysical data to estimate hydraulic conductivities. *Water Resources Research*, 46(11). <https://doi.org/10.1029/2009WR008340>
- Jalali-Farahani, H.R., Heermann, D.F., Duke, H.R., 1993. Physics of Surge Irrigation II. Relationship between Soil Physical and Hydraulic Parameters. *Trans. ASAE* 36, 45–50. <https://doi.org/10.13031/2013.28312>
- Jilali, A., El Harradji, A., 2017. Study of Managed Aquifer Recharge and Climate Change, Using a Numerical Model: The Figuig Aquifer (Eastern High Atlas, Morocco), in: *Water and Land Security in Drylands*. Springer, pp. 35–42.
- Jokinen, R.E., Langwaldt, J.H., Puhakka, J.A., 2006. Changes of water quality and bacterial community structure during artificial groundwater recharge with humic lake water, in: *Recharge Systems for Protecting and Enhancing Groundwater Resource - Proceedings of the 5th International Symposium on Management of Aquifer Recharge - ISMAR 5* (June 2005). Berlin, Germany, pp. 617–623.
- Karimov, A., Mavlonov, A., Miryusupov, F., Gracheva, I., Borisov, V., Abdurahmonov, B., 2012. Modelling policy alternatives toward managed aquifer recharge in the Fergana Valley, Central Asia. *Water Int.* 37, 380–394. <https://doi.org/10.1080/02508060.2012.706432>
- Karsten, U., Lembcke, S., Schumann, R., 2007. The effects of ultraviolet radiation on photosynthetic performance, growth and sunscreen compounds in aeroterrestrial biofilm algae isolated from building facades. *Planta* 225, 991–1000. <https://doi.org/10.1007/s00425-006-0406->
- Kollmann, W., Meyer, J.W., Supper, R., 1992. Geoelectric surveys in determining the direction and velocity of groundwater flow using introduced salt tracer. *Tracer Hydrology*, Balkema, Rotterdam, 109–113.
- Kürschner, A., 2018. Einfluss von Infiltrationsraten und Wasserqualität auf stattfindende Prozesse während der künstlichen Grundwasseranreicherung. BSc. thesis. TU Dresden, Dresden.

- Laws, B.V., Dickenson, E.R.V., Johnson, T.A., Snyder, S.A., Drewes, J.E., 2011. Attenuation of contaminants of emerging concern during surface-spreading aquifer recharge. *Sci. Total Environ.* 409, 1087–1094. <https://doi.org/10.1016/j.scitotenv.2010.11.021>
- Lee, T.-C., Williams, A.E., Wang, C., 1992. An artificial recharge experiment in the San Jacinto basin, Riverside, southern California. *Journal of Hydrology* 140, 235–259. [https://doi.org/10.1016/0022-1694\(92\)90242-N](https://doi.org/10.1016/0022-1694(92)90242-N)
- Lehmann, A., Rode, M., 2001. Long-term behaviour and cross-correlation water quality analysis of the river Elbe, Germany. *Water Res.* 35, 2153–2160. [https://doi.org/10.1016/S0043-1354\(00\)00488-7](https://doi.org/10.1016/S0043-1354(00)00488-7)
- Leibundgut, C., Maloszewski, P., Külls, C., 2011. *Tracers in Hydrology*. John Wiley & Sons.
- Lewis, J., Sjöström, J., 2010. Optimizing the experimental design of soil columns in saturated and unsaturated transport experiments. *Journal of Contaminant Hydrology*. 115, 1–13. <https://doi.org/10.1016/j.jconhyd.2010.04.001>
- Li, C., 2014. Conception of a high-resolution saturated model for the test site Pirna (Master Thesis). Technische Universität Dresden, Germany.
- Libardi, P.L., Reichardt, K., Nielsen, D.R., Biggar, J.W., 1980. Simple field methods for estimating soil hydraulic conductivity. *Soil Sci. Soc. Am. J.* 3–7. <https://doi.org/10.2136/sssaj1980.03615995004400010001x>
- Liou, K.-N., 1976. On the absorption, reflection and transmission of solar radiation in cloudy atmospheres. *J. Atmospheric Sci.* 33, 798–805. [http://journals.ametsoc.org/jas/article-pdf/33/5/798/3419504/1520-0469\(1976\)033_0798_otarat_2_0_co_2.pdf](http://journals.ametsoc.org/jas/article-pdf/33/5/798/3419504/1520-0469(1976)033_0798_otarat_2_0_co_2.pdf)
- Liu, S., Wang, W., Shisong, Q., Zheng, Y., Wenliang, L., 2019. Specific types and adaptability zoning evaluation of managed aquifer recharge for irrigation in the North China Plain, in: *Proceedings of the Symposium ISMAR 10*. Madrid, Spain, p. 223.
- Lobell, D.B., Burke, M.B., Tebaldi, C., Mastrandrea, M.D., Falcon, W.P., Naylor, R.L., 2008. Prioritizing Climate Change Adaptation Needs for Food Security in 2030. *Science* 319, 607–610. <https://doi.org/10.1126/science.1152339>
- Mahmood, H., Iqbal, M.M., Binte Delwar, R., 2019. Solar Irradiance Dependence in Clogging of Managed Aquifer Recharge Basins (Study Project WS 18/19). TU Dresden, Dresden.
- Maliva, R., 2014. Economics of Managed Aquifer Recharge. *Water* 6, 1257–1279. <https://doi.org/10.3390/w6051257>
- Mao, N., 2016. Methods for characterisation of nonwoven structure, property, and performance, in: *Advances in Technical Nonwovens*. Elsevier, pp. 155–211. Woodhead Publishing Series in Textiles
- Markovic, D., Koch, M., 2015. Stream response to precipitation variability: a spectral view based on analysis and modelling of hydrological cycle components: BASIN LOW-FREQUENCY RESPONSE TO PRECIPITATION FORCING. *Hydrology Processes*. 29, 1806–1816. <https://doi.org/10.1002/hyp.10293>
- Martin, 2013. Clogging issues associated with managed aquifer recharge methods (scientific, technical). IAH.
- McCutcheon, S.C., Martin, J.L., Barnwell, T.O.J., 1993. Water density as function of temperature and concentration, “Water Quality”, in Maifment, D.R., “Handbook of Hydrology”, McGraw-Hill. New York, NY, USA. Source: <http://web.colby.edu/ch217public/files/2012/04/density-of-water.xlsx>
- McWhorter, D.B., 1971. Infiltration affected by flow of air. *Hydrol. Pap. Colo. State Univ.* No 49.
- Mendoza, A., Palma, A., Gonzalez Villareal, F., 2012. Ante proyecto de recarga artificial de acuíferos en la cuenca del Rio Sonora. XXII Congreso Nacional de Hidraulica. Acapulco, Mexico <https://fddocuments.net/document/anteproyecto-de-recarga-artificial-de-acuiferos-en-la-cuneca-del-rio-sonora.html> (accessed 11.11.19)
- Mendoza, B., 2005. Total solar irradiance and climate. *Adv. Space Res., Fundamentals of Space Environment Science* 35, 882–890. <https://doi.org/10.1016/j.asr.2004.10.011>

- Mengemann, S., n.d. Pirna-Wetter.de. Pirna-Wetterde. URL <http://pirna-wetter.de/indexDesktop.php> (accessed 24.10.19).
- Moreno, M., 2015. Methods for characterization of soil hydraulic properties and sub-surface stratigraphy with application at an infiltration site in Pirna, Germany. MSc. thesis. Technische Universität Dresden, Germany.
- Murray, R., Harris, J., 2010. Water banking: a practical guide to using artificial groundwater recharge Department of Water Affairs, Pretoria, South Africa.
- Nadee, S., Trelo-ges, V., Pavelic, P., Srisuk, K., 2012. Effect of water quality on infiltration rates from the ponding method of Managed Aquifer Recharge: A case study from Ban Nong Na, Phitsanulok, Thailand. Environmental natural Resource. J. 10, 68–77. www.ennrjournal.com/2012_v10_n1/6_suwanchai.pdf
- Nann, S., Riordan, C., 1991. Solar Spectral Irradiance under Clear and Cloudy Skies: Measurements and a Semiempirical Model. J. Appl. Meteorol. 30, 447–462. [https://doi.org/10.1175/1520-0450\(1991\)030<0447:SSIUCA>2.0.CO;2](https://doi.org/10.1175/1520-0450(1991)030<0447:SSIUCA>2.0.CO;2)
- Navarro, R., Fernandez, E., 2017. Implementacion de mas de 500 pozas de recarga artificial para la sostenibilidad del regadio en el acuífero de Ica (Peru), Chapter 17. ed. IMTA, Mexico. ISBN: 978-607-9368-91-3
- Negev, I., Schechter, T., Rozenbach, H., Livne, A., 2019. The Effect of Soil Tillage Equipment on the Recharge Capacity of Infiltration Ponds, in: Proceedings of the Symposium ISMAR 10. Madrid, Spain, pp. 430–431 (May 2019).
- Niebuhr, B., Wilmsen, M., 2014. Kreide-Fossilien in Sachsen, Teil 1. Geologica Saxonica Journal of central European geology 60 (2): 330 – 331. ISBN 978-3-910006-53-9
- Nikolaou, A., Meric, S., Fatta, D., 2007. Occurrence patterns of pharmaceuticals in water and wastewater environments. Analytical and bioanalytical chemistry. 387, 1225–1234. <https://doi.org/10.1007/s00216-006-1035-8>
- Nitschke, L., Schüssler, W., 1998. Surface water pollution by herbicides from effluents of waste water treatment plants. Chemosphere 36, 35–41. [https://doi.org/10.1016/S0045-6535\(97\)00286-5](https://doi.org/10.1016/S0045-6535(97)00286-5)
- Noborio, K., 2001. Measurement of soil water content and electrical conductivity by time domain reflectometry: a review. Comput. Electron. Agric. 31, 213–237. [https://doi.org/10.1016/S0168-1699\(00\)00184-8](https://doi.org/10.1016/S0168-1699(00)00184-8)
- NRMMC, E., 2009. AHMC, Australian Guidelines for Water Recycling Managed Aquifer Recharge. Nat. Resour. Minist. Manag. Counc. Environ. Prot. Herit. Counc. Aust. Health Minist.
- Okubo, T., Matsumoto, J., 1983. Biological clogging of sand and changes of organic constituents during artificial recharge. Water Res. 17, 813–821. https://webcms.pima.gov/UserFiles/Servers/Server_6/File/Government/Flood%20Control/Engineering/Planning/Lower%20Santa%20Cruz%20River%20Living%20River%20Project/okubo-and-matsumoto-1983.pdf (accessed 11.11.19)
- Parsons, S., Cook, P., Irvine, E., Holland, G., Kaufman, C., 2012. Progress in managed aquifer recharge in Australia (No. 73). National Water Commission, Canberra.
- Passadore, G., Monego, M., Altissimo, L., Sottani, A., Putti, M., Rinaldo, A., 2010. Artificial recharge of the aquifer system of Central Vento (Italy): modelling and forced infiltration experiments though dismissed quarries. ISMAR 7 – International symposium on managed aquifer recharge. Abu Dhabi, United Arab Emirates.
- Pavelic, P., Dillon, P.J., Mucha, M., Nakai, T., Barry, K.E., Bestland, E., 2011. Laboratory assessment of factors affecting soil clogging of soil aquifer treatment systems. Water Res. 45, 3153–3163. <https://doi.org/10.1016/j.watres.2011.03.027>
- Pavelic, P., Mucha, M., Dillon, P., Barry, K.E., 2005. Laboratory column study on the effect of ponding depth on infiltration rate during SAT. In: Proc. ISMAR5; June 2005; Berlin. 2005. 624-9. <http://hdl.handle.net/102.100.100/181966?index=1>

- Phipps, D.W., Lyon, S., Hutchinson, A.S., 2007. DEVELOPMENT OF A PERCOLATION DECAY MODEL TO GUIDE FUTURE OPTIMIZATION OF SURFACE WATER RECHARGE BASINS, in: Fox, P. (Ed.), Management of Aquifer Recharge for Sustainability: Proceedings of the 6th International Symposium on Managed Artificial Recharge of Groundwater, ISMAR6, Phoenix, Arizona USA October 28 - November 2, 2007, ISMAR Proceedings. Acacia Publishing Incorporated, Phoenix Arizona, pp. 433–446.
- Platzer, C., Mauch, K., 1997. Soil clogging in vertical flow reed beds – mechanisms, parameters, consequences and solutions? *Water Sci. Technol.* 35, 175–181.
<https://doi.org/10.2166/wst.1997.0191>
- Pollock, D., Cirpka, O.A., 2010. Fully coupled hydrogeophysical inversion of synthetic salt tracer experiments. *Water Resource Research* 46. <https://doi.org/10.1029/2009WR008575>
- Pupisky, H., Shainberg, I., 1979. Salt Effects on the Hydraulic Conductivity of a Sandy Soil1. *Soil Sci. Soc. Am. J.* 43, 429. <https://doi.org/10.2136/sssaj1979.03615995004300030001x>
- Racz, A.J., Fisher, A.T., Schmidt, C.M., Lockwood, B.S., Huertos, M.L., 2012. Spatial and Temporal Infiltration Dynamics During Managed Aquifer Recharge. *Groundwater* 50, 562–570.
<https://doi.org/10.1111/j.1745-6584.2011.00875.x>
- Rast, H., 1959. *Geologischer Führer durch das Elbsandsteingebirge*. Bergakademie Freiberg.
- Rice, R.C., 1974. Soil clogging during infiltration of secondary effluent. *J. Water Pollut. Control Fed.* 708–716. <https://www.jstor.org/stable/25038184>
- Richards, L.A., 1931. Capillary conduction of liquids through porous mediums. *Physics* 1, 318.
<https://doi.org/10.1063/1.1745010>
- Ruijuan, C., Xueyan, Y., Xinqiang, D., Ying, L., 2019. Effects of ionic strength on the formation of bioclogging in MAR, in: Proceedings of the Symposium ISMAR 10. Madrid, Spain, pp. 428–429 (May 2019).
- Rupérez-Moreno, C., Pérez-Sánchez, J., Senent-Aparicio, J., Flores-Asenjo, P., Paz-Aparicio, C., 2017. Cost-Benefit Analysis of the Managed Aquifer Recharge System for Irrigation under Climate Change Conditions in Southern Spain. *Water* 9, 343. <https://doi.org/10.3390/w9050343>
- Ryer, A., Light, V., 1997. *Light measurement handbook, international light*. Newburyport, MA, 6, 28–30. ISBN 0-9658356-9-3
- Sächsisches Staatsministerium für Umwelt und Landwirtschaft, n.d. Aktuelle Wasserstände und Durchflüsse, Vorhersagen: Pegel Pirna. Wasser Wasserwirtsch. URL <https://www.umwelt.sachsen.de/umwelt/infosysteme/hwims/portal/web/wasserstand-pegel-501040> (accessed 10.30.19).
- Sallwey, J., Glass, J., Stefan, C., 2018. Utilizing unsaturated soil zone models for assessing managed aquifer recharge. *Sustain. Water Resour. Manag.* 4, 383–397.
<https://doi.org/10.1007/s40899-018-0214-z>
- San Sebastián Sauto, J., Fernandez, E., 2019. Three-in-one uses of a managed aquifer recharge system: the triplets in Los Arenales (Spain), in: Proceedings of the Symposium ISMAR 10. Madrid, Spain, pp. 636–647 (May 2019).
- Schlamminger, C., Klein, J., Schieblich, E., 2014. Infiltration in den oberflächennahen Untergrund unter Verwendung von Direct-Push-Brunnen (Projektarbeit). TU Dresden, Dresden, Germany.
- Shainberg, I., Rhoades, J.D., Suarez, D.L., Prather, R.J., 1981. Effect of Mineral Weathering on Clay Dispersion and Hydraulic Conductivity of Sodict Soils. *Soil Sci. Soc. Am. J.* 45, NP. <https://doi.org/10.2136/sssaj1981.03615995004500020051x>
- Sheehan, L., 2009. Summary of costs and benefits of water supply alternatives. Calif. Coastkeeper Alliance.
- Siegrist, R.L., Boyle, W.C., 1987. Wastewater-induced soil clogging development. *J. Environ. Eng.* 113, 550–566. [https://doi.org/10.1061/\(ASCE\)0733-9372\(1987\)113:3\(550\)](https://doi.org/10.1061/(ASCE)0733-9372(1987)113:3(550))

- Šimůnek, J., van Genuchten, M.T., Šejna, M., 2016. Recent Developments and Applications of the HYDRUS Computer Software Packages. *Vadose Zone Journal* (2016) 15 (7): vzj2016.04.0033. <https://doi.org/10.2136/vzj2016.04.0033>
- Singha, K., Gorelick, S.M., 2005. Saline tracer visualized with three-dimensional electrical resistivity tomography: Field-scale spatial moment analysis. *Water Resource Research* Volume 41 Issue 5. <https://doi.org/10.1029/2004WR003460>
- Sisson, J.B., Ferguson, A.H., van Genuchten, M.T., 1980. Simple Method for Predicting Drainage from Field Plots 1. *Soil Sci. Soc. Am. J.* 44, 1147–1152. <https://doi.org/10.2136/sssaj1980.03615995004400060004x>
- Skoček, V., Valečka, J., 1983. Paleogeography of the Late Cretaceous Quadersandstein of Central Europe. *Palaeogeogr. Palaeoclimatol. Palaeoecol.* 44, 71–92. [https://doi.org/10.1016/0031-0182\(83\)90005-6](https://doi.org/10.1016/0031-0182(83)90005-6)
- Snehota, M., Sobotkova, M., Cislerova, M., 2008. Impact of the entrapped air on water flow and solute transport in heterogeneous soil: Experimental set-up. *Journal of Hydrology and Hydromechanics* 56, 247–256. https://www.researchgate.net/publication/262373931_Impact_of_the_entrapped_air_on_water_flow_and_solute_transport_in_heterogeneous_soil_experimental_set-up/link/00b7d5378814a07e43000000/download (accessed 11.11.19)
- Soares, C., 2015. Chapter 7 - Gas Turbine Fuel Systems and Fuels, in: Soares, C. (Ed.), *Gas Turbines* (Second Edition). Butterworth-Heinemann, Oxford, pp. 317–411. <https://doi.org/10.1016/B978-0-12-410461-7.00007-9>
- Soni, P., Dashora, Y., Maheshwari, B., Dillon, P., Singh, P.K., 2019. Managed Aquifer Recharge at a Farm Level: Evaluating the Performance of Direct Well Recharge Structures, in: *Proceedings of the Symposium ISMAR 10*. Madrid, Spain, pp. 169–184 (May 2019).
- Sparks, D.L., Page, A.L., Helmke, P.A., Loeppert, R.H., Rhoades, J.D., 1996. Salinity: Electrical Conductivity and Total Dissolved Solids, in: *SSSA Book Series*. Soil Science Society of America, American Society of Agronomy. <https://doi.org/10.2136/sssabookser5.3.c14>
- Sprenger, C., Hartog, N., Hernández, M., Vilanova, E., Grützmacher, G., Scheibler, F., Hannappel, S., 2017. Inventory of Managed Aquifer Recharge sites in Europe - historical development, current situation and perspectives. *Hydrogeology Journal*. 25, 1909–1922. <https://doi.org/10.1007/s10040-017-1554-8>
- Stefan, C., Ansems, N., 2018. Web-based global inventory of managed aquifer recharge applications. *Sustain. Water Resour. Manag.* 4(2), 153–162. <https://doi.org/10.1007/s40899-017-0212-6>
- Stibinger, J., Univerzita J.E. Purkyně v Ústí nad Labem, Fakulta životního prostředí, 2014. Examples of determining the hydraulic conductivity of soils: theory and applications of selected basic methods: university handbook on soil hydraulics. Jan Evangelista Purkyně University, Faculty of the Environment, Ústí nad Labem.
- Su, X., Xu, W., Du, S., 2014. In situ infiltration test using a reclaimed abandoned riverbed: managed aquifer recharge in Shijiazhuang City, China. *Environmental Earth Science*. 71, 5017–5025. <https://doi.org/10.1007/s12665-013-2893-y>
- UGT GmbH, 2018. Operating manual Tensio 152. <https://www.ugt-online.de/produkte/bodenkunde/tensiometer/tensio-152/> (accessed on 1.6.19)
- UGT GmbH, 2014. Operating instructions UMP-1. <https://manualzz.com/doc/4558239/bedienungsanleitung-ump-1---ugt> (accessed on 1.6.19)
- Uličný, D., Laurin, J., Čech, S., 2009. Controls on clastic sequence geometries in a shallow-marine, transtensional basin: the Bohemian Cretaceous Basin, Czech Republic. *Sedimentology* 56, 1077–1114. <https://doi.org/10.1111/j.1365-3091.2008.01021.x>
- United Nations, 2019. Sustainable Development Knowledge Platform. URL <https://sustainabledevelopment.un.org/> (accessed 10.9.19).

- US EPA, 2006. Process Design Manual: Land Treatment of Municipal Wastewater Effluents (No. EPA/625/R-06/016). U.S. Environmental Protection Agency, Cincinnati, Ohio, USA.
- U.S. EPA, 2002. The QTRACER2 program for tracer-breakthrough curve analysis for tracer tests in karstic aquifers and other hydrologic systems. National Center for Environmental Assessment-Washington Office, Office of Research and Development, U.S. Environmental Protection Agency, Washington, DC, USA.
- V. Bagarello, M. Iovino, D. Elrick E., 2004. A simplified falling-head technique for rapid determination of field-saturated hydraulic conductivity. *Soil Science Society of America Journal*. 68(1), 66–73. <https://doi.org/10.2136/sssaj2004.6600>
- Vařilová, Z., 2016. Elbe Sandstones, in: Pánek, T., Hradecký, J. (Eds.), *Landscapes and Landforms of the Czech Republic*. Springer International Publishing, Cham, pp. 123–137. https://doi.org/10.1007/978-3-319-27537-6_11
- Vienken, T., Dietrich, P., 2011. Field evaluation of methods for determining hydraulic conductivity from grain size data. *UFZ Helmholtz Center for Environmental research Journal of Hydrology* 400 (2011) 58–71. Leipzig, Germany. <https://doi.org/10.1016/j.jhydrol.2011.01.022>
- Vigneswaran, S., Ronillo, B.S., 1987. A detailed investigation of physical and biological clogging during artificial recharge. *Water, Air, and Soil Pollution*, 35(1-2), 119–140. <https://doi.org/10.1007/BF00183848>
- Villanueva, V.D., Font, J., Schwartz, T., Romani, A.M., 2011. Biofilm formation at warming temperature: acceleration of microbial colonization and microbial interactive effects. *Biofouling* 27, 59–71. <https://doi.org/10.1080/08927014.2010.538841>
- Vink, R., Behrendt, H., Salomons, W., 1999. Development of the heavy metal pollution trends in several European rivers: An analysis of point and diffuse sources. *Water Sci. Technol.* 39, 215–223. [https://doi.org/10.1016/S0273-1223\(99\)00338-8](https://doi.org/10.1016/S0273-1223(99)00338-8)
- Wagner, B., Tarnawski, V.R., Hennings, V., Müller, U., Wessolek, G., Plagge, R., 2001. Evaluation of pedo-transfer functions for unsaturated soil hydraulic conductivity using an independent data set. *Geoderma* 102, 275–297. [https://doi.org/10.1016/S0016-7061\(01\)00037-4](https://doi.org/10.1016/S0016-7061(01)00037-4)
- Walther, G.-R., Post, E., Convey, P., Menzel, A., Parmesan, C., Beebee, T.J.C., Fromentin, J.-M., Hoegh-Guldberg, O., Bairlein, F., 2002. Ecological responses to recent climate change. *Nature* 416, 389–395. <https://doi.org/10.1038/416389a>
- Wang, Z., Feyen, J., van Genuchten, M.T., Nielsen, D.R., 1998. Air entrapment effects on infiltration rate and flow instability. *Water Resources Research*. 34, 213–222. <https://doi.org/10.1029/97WR02804>
- Warren, E., Bekins, B.A., 2015. Relating subsurface temperature changes to microbial activity at a crude oil-contaminated site. *Journal of Contaminant Hydrology*. 182, 183–193. <https://doi.org/10.1016/j.jconhyd.2015.09.007>
- Weather Spark, n.d. Durchschnittswetter in Pirna, Deutschland. URL <https://de.weatherspark.com/y/75744/Durchschnittswetter-in-Pirna-Deutschland-das-ganze-Jahr-%C3%BCber> (accessed 11.18.19).
- Whalley, W.R., Ober, E.S., Jenkins, M., 2013. Measurement of the matric potential of soil water in the rhizosphere. *J. Exp. Bot.* ert044. <https://doi.org/10.1093/jxb/ert044>
- Wiegel, S., Aulinger, A., Brockmeyer, R., Harms, H., Löffler, J., Reincke, H., Schmidt, R., Stachel, B., von Tümpling, W., Wanke, A., 2004. Pharmaceuticals in the river Elbe and its tributaries. *Chemosphere* 57, 107–126. <https://doi.org/10.1016/j.chemosphere.2004.05.017>
- Winter, K.-J., Goetz, D., 2003. The impact of sewage composition on the soil clogging phenomena of vertical flow constructed wetlands. *Water Sci. Technol.* 48, 9–14. <https://doi.org/10.2166/wst.2003.0268>
- Xia, L., Gao, Z., Zheng, X., Wei, J., 2018. Impact of recharge water temperature on bioclogging during managed aquifer recharge: a laboratory study. *Hydrogeology Journal*. 26, 2173–2187. <https://doi.org/10.1007/s10040-018-1766-6>

- Yiou, P., Ribereau, P., Naveau, P., Nogaj, M., Brázdil, R., 2006. Statistical analysis of floods in Bohemia (Czech Republic) since 1825. *Hydrology Science Journal* 51, 930–945. <https://doi.org/10.1623/hysj.51.5.930>
- Yousaf, M., Ali, O.M., Rhoades, J.D., 1987. Clay Dispersion and Hydraulic Conductivity of Some Salt-Affected Arid Land Soils. *Soil Science Society of America Journal*. 51, 905. <https://doi.org/10.2136/sssaj1987.03615995005100040013x>
- Zellweger, G.W., 1994. Testing and comparison of four ionic tracers to measure stream flow loss by multiple tracer injection. *Hydrol. Process.* 8, 155–165. <https://doi.org/10.1002/hyp.3360080206>
- Zhang, H., Xinqiang, D., Xueyan, Y., 2019. Laboratory Research on the Laws of Fe(III) Clogging during Urban Storm-water Groundwater Recharge, in: *Proceedings of the Symposium ISMAR 10*. Madrid, Spain, pp. 432–439.
- Zieschang, J., 1961. Zur zulässigen Höchstbelastung eines Brunnens. *Z Angew Geol* 7, 580–582. Berlin, Germany.
- Zou, Z., Shu, L., Min, X., Chifuniro Mabedi, E., 2019. Clogging of Infiltration Basin and Its Impact on Suspended Particles Transport in Unconfined Sand Aquifer: Insights from a Laboratory Study. *Water* 11, 1083. <https://doi.org/10.3390/w11051083>

A.1. LIST OF PUBLICATIONS

A.1.1 LIST OF PEER REVIEWED JOURNAL ARTICLES

Barquero, F.; Fichtner, T.; Stefan, C. *Methods of In Situ Assessment of Infiltration Rate Reduction in Groundwater Recharge Basins*. Water 2019, 11(4), 784; <https://doi.org/10.3390/w11040784>.

Fichtner, T.; **Barquero, F.;** Sallwey, J.; Stefan, C. *Assessing Managed Aquifer Recharge Processes under Three Physical Model Concepts*. Water 2019, 11(1), 107; <https://doi.org/10.3390/w11010107>.

Sallwey, J.; **Barquero, F.;** Fichtner, T.; Stefan, C. *Planning MAR Schemes Using Physical Models: Comparison of Laboratory and Field Experiments*. Appl. Sci. 2019, 9(18), 3652; <https://doi.org/10.3390/app9183652>.

A.1.2 LIST OF CONFERENCE PROCEEDINGS (ONLY FIRST AUTHOR)

Barquero, F. and Stefan, C.; 2017. *Impact of climate variations on managed aquifer recharge infiltration basins*. Poster presentation at the EGU Congress 2017 in Vienna, Austria.

Barquero, F.; Fichtner, T.; and Stefan, C.; 2018. Managed aquifer recharge through surface spreading methods: Optimization of infiltration process by means of physical models. Oral presentation at the BSMAR Symposium 2018 in San Diego, USA.

Barquero, F. and Stefan, C.; 2018. A novel technique to estimate infiltration capacity reduction in unsaturated soil media in managed aquifer recharge surface spreading methods. Oral presentation at the EGU Congress 2018 in Vienna, Austria.

Barquero, F. and Stefan, C.; 2018. Assessment of infiltration rate reduction in managed aquifer recharge facilities under variable climate scenarios. Oral presentation at the IAH Conference 2018 in Daejeon, South Korea.

Barquero, F. and Stefan, C.; 2019. *Laboratory investigation for management of clogging in managed aquifer recharge infiltration basins*. Poster presentation at the EGU Congress 2019 in Vienna, Austria.

Barquero, F.; Binte, R.; Mahmood, H.; Iqbal, M. and Stefan, C.; 2019. *Laboratory experiments for the assessment of the impact of solar irradiance on clogging of MAR basins*. Oral presentation at the ISMAR Symposium 2019 in Madrid, Spain.

A.2 GEOLOGY OF THE ELBTAL GROUP

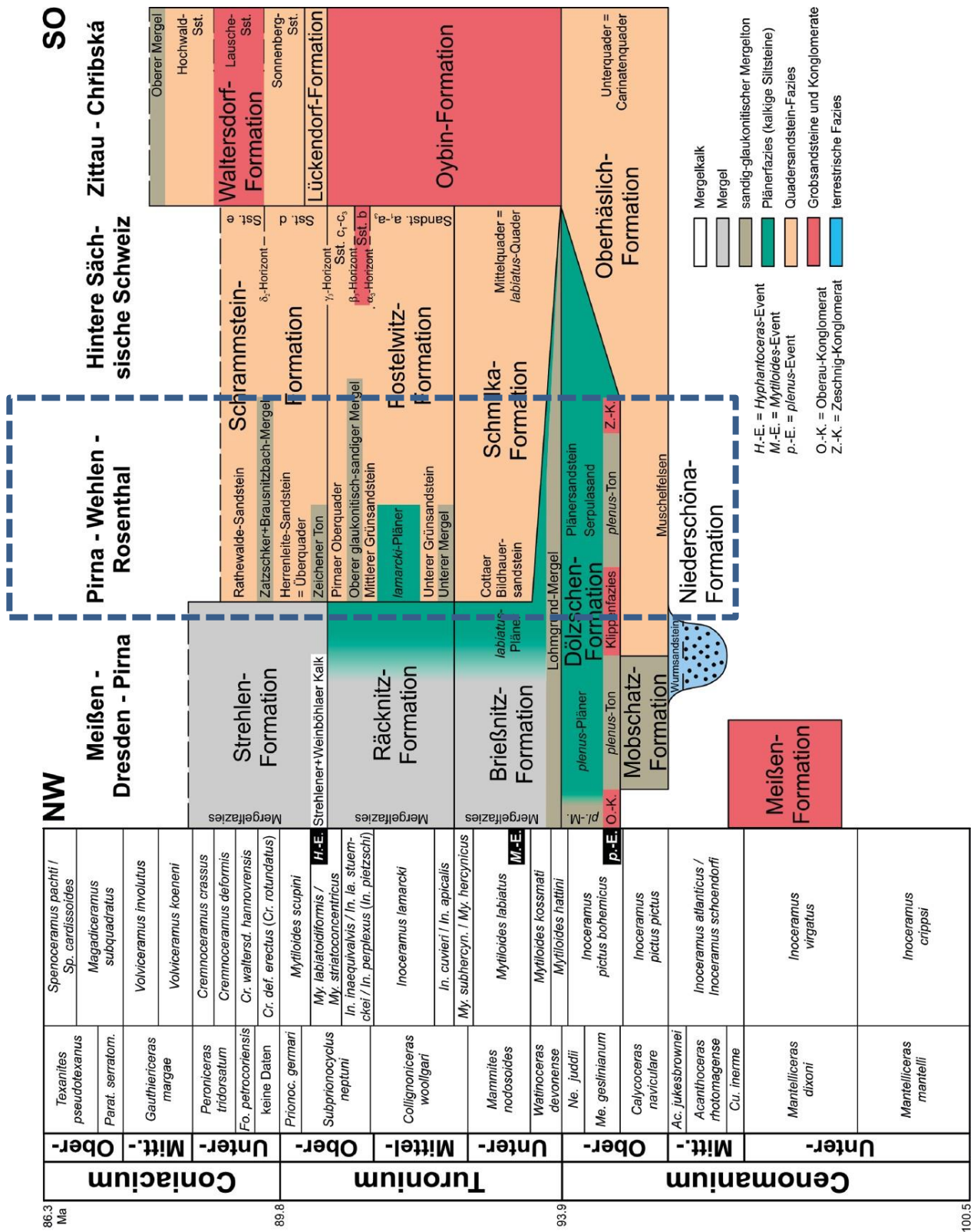


Figure 0.1. Chrono-, bio and lithostratigraphy of the Saxonian Cretaceous (Elbtal Group). Source: Niebuhr and Wilmsen (2014)

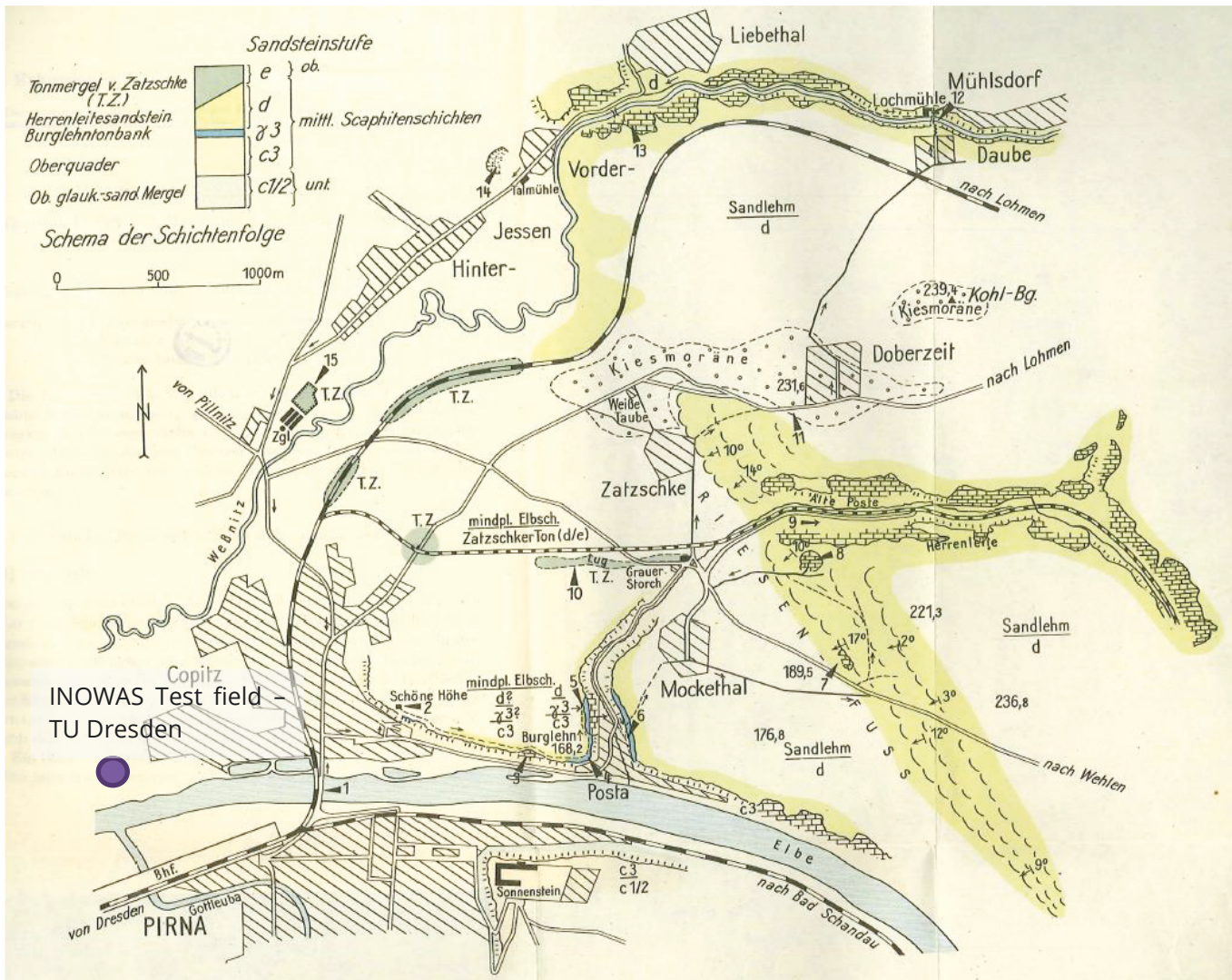


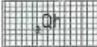

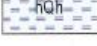


Figure 0.2. Sketch of sandstone structures (marked in yellow and green) in the region of Pirna - Mocketal - Zatschke - Doberzeit - Weßnitztal. Source: Rast (Rast, 1959)

Legende

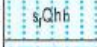
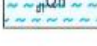
KÄNOZOIKUM Quartär

Holozän

Anthropogene Bildungen

- 1  Müll, Bauschutt, Auffülle unbekannter Herkunft
- 2  Bergbauhalde, Abraum, Gesteinsmassen
- 3  Organogene Bildungen: Torf, Ton und Schluff, stark humos
- 4  Fluß- und Bachablagerungen (fluviatil)
- 5  Tiefere (rezente) Aue der Elbe: Jüngerer Auenlehm, lokal Kies und Sand


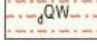


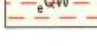
Höhere (ältere) Aue der Elbe

- 5  Auenlehm (über vorwiegend hochweichselzeitlichem Kies)
- 6  Sand (über vorwiegend hochweichselzeitlichem Kies)
- 7  Auenlehm über Kies (z.T. hochweichselzeitlich) der Elbnabenflüsse
- 8  Bildungen kleiner Täler („Alluvionen“, deluvial-fluviatil): Sand, Kies, Schluff, z.T. humos; junge Abschwemmassen; (z.T. Weichsel)

Pleistozän


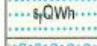


Weichsel-Kaltzeit

Früh-, Hoch- und Spätweichsel: Periglazial-Komplex Umlagerungen (deluvial und deluvial-fluviatil)

- 9  Schluff in Trockentälern (z.T. Holozän): umgelagerter Löß
- 10  Solifluktsdecken >2m: Gehängelehm, Solifluktslöß, häufig über Schuttdecken (z.T. älter als Weichsel)
- 11  Windablagerungen (äolisch)
- 12  Dünen, Flugsand (z.T. Holozän)
- 13  Löß, meist Lößlehm, z.T. krypturbat verändert

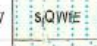


Hochweichsel

Flußablagerungen der Tieferen Niederterrasse

- 13  Taltehm über Sand und Kies der Elbe und ihrer Nebenflüsse
- 14  Sand über Kies der Elbe und ihrer Nebenflüsse
- 15  Kies der Elbe
- 16  Kies der Elbnabenflüsse





Frühweichsel

Flußablagerungen der Höheren Niederterrasse

- 17  Sand und Feinkies der Elbe
- 18  Sand der Elbe mit viel Wesenitzmaterial (vorwiegend umgelagerter Heidesand)
- 19  Kies und Sand der Gottleuba (QWfG), Müglitz (QWfM), Seidewitz und Bahre (QWfS)

Saale-Kaltzeit



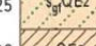
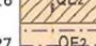
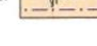
Älterer Eisvorstoß (Drenthe-Stadium)

- 20  Schmelzwasserbildungen (glazifluviatil), Sander: „Heidesand“
- 21  Flußablagerungen
- 22  Kies der Gottleuba (QSG), Müglitz (QSM), Seidewitz und Bahre (QSS)
- 23  Kies des Berliner Elbelaufes (Spätelster bis Frühsaale QES-SfE)

Elster-Kaltzeit

2. Eisvorstoß

Schmelzwasserbildungen (glazifluviatil)


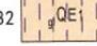
- 23  Kies
- 24  Kies, mit viel aufgearbeitetem Elbmateriale
- 25  Sand
- 26  Grundmoräne (glazigen): Geschiebelehm, oft sehr stark sandig-kiesig
- 27  Beckenbildungen (glazilimnisch): Schluff und Feinsand

Flußablagerungen der Mittleren Mittelterrasse

- 28  Kies der Elbe
- 29  Kies der Gottleuba (QE2G), Lockwitz (QE2L), Müglitz (QE2M)

1. Eisvorstoß

Schmelzwasserbildungen (glazifluviatil): Kies mit viel Lokalmateriale

- 30  Grundmoräne (glazigen): Geschiebemergel, Geschiebelehm
- 31  Beckenbildungen (glazilimnisch): Bänderton und Schluff

Frühester (z.T. bis Cromer-Komplex)

Flußablagerungen der Höheren Mittelterrasse

- 33  Kies der Elbe: Streumener Elbelauf
- 34  Kies der Gottleuba (QEfG), Müglitz (QEfM), Seidewitz und Bahre (QEfs)


Menap- (bis Bavel) Kaltzeit

Flußablagerungen der Tieferen Hochterrasse (Nebenflüsse des Schmiedeberger Elbelaufes)

- 35  Kies der Gottleuba (QMpG), Müglitz (QMpM), Seidewitz und Bahre (QMps)

Tegelen-Komplex

Flußablagerungen der Höheren Hochterrasse

- 36  Kies der Elbe: Bautzener Elbelauf

Quartär (ungegliedert)

Lesestein-Bestreung:

Schwarzer Kieselchiefer / Gangquarz


- 37  Einzelne Feuersteine / Gerölle unterschiedlicher, z.T. unsicherer Herkunft (Tertiär bis Pleistozän)

Figure 0.3. Legend of geologic map of the region of Pirna of Free State of Saxony, Sheet 5059 of Figure 3.10. Source: Alexowsky (1997)

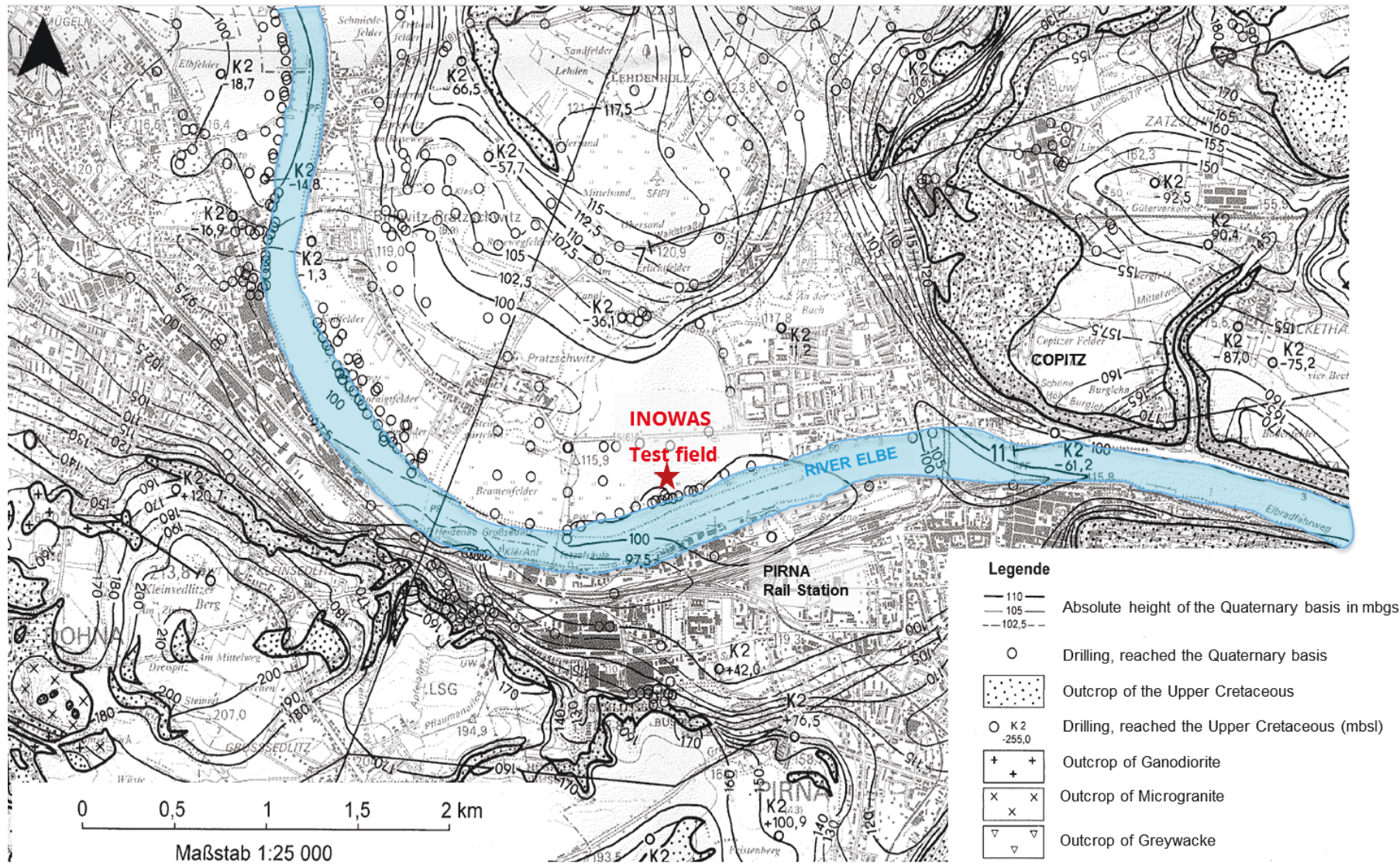


Figure 0.4. Isolines of the absolute height of the Quaternary basis in meters below sea level (mbgs). Source: Alexowsky (1997)

A.3 SUPPLEMENTARY MATERIAL

All the supplementary material is in a soft copy in the server of the INOWAS Research Group with the following address:

Netzwerk/INOWAS-PC/INOWAS Data/PhD/Felix/Phd. Thesis

The supplementary material consists in the text files exported from every data logger in the field experiment sorted by every hydraulic scenario and climate.

1. Logger 263 (WC, Temp and EC)
 - 1.1. Scenario 1 (S1_300ma_HLC_1d3d)
 - 1.2. Scenario 2 (S1_300ma_HLC_6h18h)
 - 1.3. Scenario 3 (S2_300ma_HLC_1d3d)
 - 1.3.1. Climate 1
 - 1.3.2. Climate 2
 - 1.3.3. Climate 3
 - 1.4. Scenario 4 (S2_300ma_HLC_7d7d)
 - 1.4.1. Climate 1
 - 1.4.2. Climate 2
 - 1.4.3. Climate 3
 - 1.5. Scenario 5 (S2_300ma_HLC_continuous)
 - 1.5.1. Climate 1
 - 1.5.2. Climate 2
 - 1.5.3. Climate 3
 - 1.6. Scenario 6 (S2_300ma_HLC_3d1d)
 - 1.6.1. Climate 1
 - 1.6.2. Climate 2
 - 1.6.3. Climate 3
 - 1.7. Scenario 7 (S2_600ma_HLC_1d3d)
 - 1.8. Scenario 8 (S2_450ma_HLC_1d3d)
2. Logger 264 (Tension)
 - 2.1. Scenario 1 (S1_300ma_HLC_1d3d)
 - 2.2. Scenario 2 (S1_300ma_HLC_6h18h)
 - 2.3. Scenario 3 (S2_300ma_HLC_1d3d)
 - 2.3.1. Climate 1
 - 2.3.2. Climate 2
 - 2.3.3. Climate 3
 - 2.4. Scenario 4 (S2_300ma_HLC_7d7d)
 - 2.4.1. Climate 1
 - 2.4.2. Climate 2
 - 2.4.3. Climate 3
 - 2.5. Scenario 5 (S2_300ma_HLC_continuous)
 - 2.5.1. Climate 1
 - 2.5.2. Climate 2
 - 2.5.3. Climate 3
 - 2.6. Scenario 6 (S2_300ma_HLC_3d1d)
 - 2.6.1. Climate 1
 - 2.6.2. Climate 2
 - 2.6.3. Climate 3
 - 2.7. Scenario 7 (S2_600ma_HLC_1d3d)

- 3. Tracer experiments
 - 3.1. Scenario 1 (S1_300ma_HLC_1d3d)
 - 3.2. Scenario 2 (S1_300ma_HLC_6h18h)
 - 3.3. Scenario 3 (S2_300ma_HLC_1d3d)
 - 3.3.1. Climate 1
 - 3.3.2. Climate 2
 - 3.3.3. Climate 3
 - 3.4. Scenario 4 (S2_300ma_HLC_7d7d)
 - 3.4.1. Climate 1
 - 3.4.2. Climate 2
 - 3.4.3. Climate 3
 - 3.5. Scenario 5 (S2_300ma_HLC_continuous)
 - 3.5.1. Climate 1
 - 3.5.2. Climate 2
 - 3.5.3. Climate 3
 - 3.6. Scenario 6 (S2_300ma_HLC_3d1d)
 - 3.6.1. Climate 1
 - 3.6.2. Climate 2
 - 3.6.3. Climate 3

In der Schriftenreihe „Beiträge zu Abfallwirtschaft/Altlasten“ des Institutes für Abfall- und Kreislaufwirtschaft sind folgende Bände erschienen:

		Preis EUR zzgl. Porto und Versand
	Erstes Abfall- und Altlastenkolloquium – Altholzseminar	vergriffen
Band 1	Möglichkeiten und Grenzen der Verbrennung von landwirtschaftlichen Reststoffen und Nebenprodukten für die Kalkproduktion	vergriffen
Band 2	Steuerungsmöglichkeiten abfallwirtschaftlicher Gebühren	vergriffen
Band 3	Prozeßbezogene Silberbilanzierung bei der Diafilmentwicklung im Fotogroßlabor	begrenzt kostenlos
Band 4	Langzeitverhalten von Deponien	vergriffen
Band 5	Steuerungsmöglichkeiten abfallwirtschaftlicher Gebühren in Großwohnanlagen	vergriffen
Band 6	6 Jahre Verpackungsverordnung – eine Zwischenbilanz	vergriffen
Band 7	Anaerobe biologische Abfallbehandlung	begrenzt kostenlos
Band 8	125 Jahre geordnete Müllabfuhr in Dresden	vergriffen
Band 9	Thermische Abfallbehandlung Co-Verbrennung	vergriffen
Band 10	Ein Simulationsmodell des Kompostierungsprozesses und seine Anwendung auf Grundfragen der Verfahrensgestaltung und Verfahrensführung	vergriffen
Band 11	Auswirkungen der Konzentratrückführung nach der Membranfiltration auf die Sickerwasserneubildung von Hausmülldeponien	vergriffen
Band 12	Anaerobe biologische Abfallbehandlung Erfahrungen – Konzepte – Produkte	vergriffen
Band 13	Stoffstrommanagement für Abfälle aus Haushalten	vergriffen
Band 14	Langzeitemissionsverhalten von Deponien für Siedlungsabfälle in den neuen Bundesländern	vergriffen
Band 15	Untersuchungen zum Säurepufferungsverhalten von Abfällen und zur Stofffreisetzung aus gefluteten Deponien	begrenzt kostenlos
Band 16	Brennstofftechnische Charakterisierung von Haushaltsabfällen	vergriffen
Band 17	Einfluss von Deponien auf das Grundwasser - Gefährdung, Prognose, Maßnahmen -	vergriffen
Band 18	Analytical Workshop on Endocrine Disruptors	vergriffen

Band 19	Anaerobe biologische Abfallbehandlung Grundlagen – Probleme – Kosten	begrenzt kostenlos
Band 20	Thermische Abfallbehandlung 2002	vergriffen
Band 21	Einfluss der getrennten Sammlung von graphischem und Verpackungspapier auf den Schadstoffgehalt im Altpapier am Beispiel von Pentachlorphenol und Polycyclischen Aromatischen Kohlenwasserstoffen	vergriffen
Band 22	Die „ökologische Wertigkeit der Entsorgung“ unter Berücksichtigung des Transportaspektes am Beispiel Altkühlgeräte im Land Brandenburg	vergriffen
Band 23	Endokrin wirksame Substanzen in Abwasser und Klärschlamm Neueste Ergebnisse aus Wissenschaft und Technik	begrenzt kostenlos
Band 24	Ökologische Bilanzierung von Verwertungsverfahren für Trockenbatterien	vergriffen
Band 25	Untersuchungen zur Verdichtung von Restabfall mittels Kompaktoren	vergriffen
Band 26	Ein neues Probenahmemodell für heterogene Stoffsysteme	begrenzt kostenlos
Band 27	Schwermetalle in Haushaltsabfällen – Potenzial, Verteilung und Steuerungsmöglichkeiten durch Aufbereitung	vergriffen
Band 28	Third International Conference on Water Resources and Environment Research (3 Bände)	vergriffen
Band 29	Mikrobielles Abbaupotential im Untergrund	begrenzt kostenlos
Band 30	Endokrin aktive Stoffe im Klärschlamm	begrenzt kostenlos
Band 31	First European Conference on MTBE	vergriffen
Band 32	Anaerobe biologische Abfallbehandlung – Neue Entwicklungen –	vergriffen
Band 33	Potenzial technischer Abwasser- und Klärschlammbehandlungsverfahren zur Elimination endokrin aktiver Substanzen	26,00
Band 34	Verhalten der endokrin wirksamen Substanz Bisphenol A bei der kommunalen Abwasserentsorgung	26,00
Band 35	Trockene Tonne – Neue Wege und Chancen einer gezielten stofflichen Verwertung	15,00
Band 36	Comparative Evaluation of Life Cycle Assessment Models for Solid Waste Management	10,00

Band 37	Abfallkennzahlen für Neubauleistungen im Hochbau	10,00
Band 38	Endokrin aktive Stoffe in Abwasser und Klärschlamm	30,00
Band 39	Handbook on the implementation of Pay-As-You-Throw as a tool for urban waste management	vergriffen
Band 40	Thermische Abfallbehandlung 2005	vergriffen
Band 41	Anforderungen an die Aufbereitung von Siedlungs- und Produktionsabfällen zu Ersatzbrennstoffen für die thermische Nutzung in Kraftwerken und industriellen Feuerungsanlagen	30,00
Band 42	Perspektiven von Deponien – Stilllegung und Nachnutzung nach 2005	30,00
Band 43	Verfahren zur Herstellung und zum Einbau Kornskelett-integrierter-Erdstoffabdichtungen unter Vakuum einfluss	30,00
Band 44	Restabfallmengen aus privaten Haushalten in Sachsen – Entwicklung eines abfallwirtschaftlichen Simulations- und Prognosemodells	30,00
Band 45	Effizienz-Modell zur Bewertung der Transportlogistik in der Abfallwirtschaft	30,00
Band 46	Anaerobe biologische Abfallbehandlung - Entwicklungen, Nutzen und Risiken der Biogastechnologie -	30,00
Band 47	Analytik und Freisetzungsverhalten von Chlor in abfallstämmigen Brennstoffen	30,00
Band 48	Das ElektroG und die Praxis Monitoring – Erstbehandlung – Technik	30,00
Band 49	Resource Efficiency Strategies for Developing Countries	30,00
Band 50	Thermische Abfallbehandlung 2007	30,00
Band 51	Untersuchungen zur Qualifizierung der Grundwasserimmission von polyzyklischen aromatischen Kohlenwasserstoffen mithilfe von passiven Probennahmesystemen	30,00
Band 52	Abfallwirtschaft und Klimaschutz Emissionshandel-Emissionsminderung-Klimaschutzprojekte	30,00
Band 53	Wirbelschichttechnik in der Abfallwirtschaft	30,00
Band 54	EBS – Analytik – Anforderungen – Probleme – Lösungen	30,00
Band 55	Improvements of Characterization of Single and Multisolute Absorption of Methyl tert-Butyl Ether (MTBE) on Zeolites	30,00

Band 56	Proceedings MGP 2008 Redevelopment, Site Management and Contaminant Issues of former MGP's and other Tar Oil Polluted Sites	30,00
Band 57	Anaerobe biologische Abfallbehandlung -Neue Tendenzen in der Biogastechnologie	30,00
Band 58	Leitfaden Natürliche Schadstoffminderung bei Teerölastlasten. KORA-Themenverbund 2	begrenzt kostenfrei
Band 59	VON NANO-TECH BIS MEGA SITES. Forschung am IAA	30,00
Band 60	II. EBS – Analytik Workshop - Qualitätssicherung und Inputkontrolle -	30,00
Band 61	4. Symposium Endokrin aktive Stoffe in Abwasser, Klärschlamm und Abfällen	30,00
Band 62	Brennpunkt ElektroG Umsetzung - Defizite - Notwendigkeiten	30,00
Band 63	Umweltverträgliches und kosteneffizientes Bodenmanagementsystem	30,00
Band 64	Untersuchungen zur Quellstärke verschiedener Abfallstoffe	30,00
Band 65	15. Fachtagung Thermische Abfallbehandlung 2010	39,00
Band 66	III. EBS – Analytik Workshop	30,00
Band 67	Anaerobe biologische Abfallbehandlung - Aktuelle Tendenzen, Co-Vergärung und Wirtschaftlichkeit -	30,00
Band 68	Untersuchungen zum anaeroben Abbau proteinreicher Reststoffe	30,00
Band 69	Schwermetalle aus Elektroaltgeräten und Batterien im kommunalen Restabfall	30,00
Band 70	German-Vietnamese Platform for Efficient Urban Water Management	kostenlos als CD erhältlich
Band 71	Siloxane in mechanisch-biologischen Abfallbehandlungsanlagen	30,00
Band 72	Charakterisierung und Verbrennung von Shredderleichtfraktionen in einer stationären Wirbelschicht	30,00
Band 73	Integrated Water Resources Management in Vietnam – Handbook for a sustainable approach	30,00
Band 74	Quản lý tích hợp tài nguyên nước ở Việt Nam – Sách hướng dẫn tới phát triển bền vững	30,00
Band 75	Bereitstellung von Bioabfall für die BtL-Produktion durch eine nassmechanische Aufbereitung	30,00

Band 76	Nutzung von NA-Prozessen zur Sanierung MTBE-belasteter Grundwässer am Beispiel des Referenzstandortes Leuna, Sachsen –Anhalt	30,00
Band 77	Vermeidung von Treibhausgasemissionen durch Steigerung der Energieeffizienz deutscher Müllverbrennungsanlagen	30,00
Band 78	Strategic Directions and Policy Options for Hazardous Waste Management in Thailand	30,00
Band 79	20 Jahre Abfallwirtschaft, Herstellerverantwortung, Produktpolitik / 20 years Waste Management, Producer Responsibility, Product Policy	30,00
Band 80	SILOXANE - Siliziumorganische Verbindungen in der Abfallwirtschaft	30,00
Band 81	8. Biogastagung Dresden - Biogas aus Abfällen und Reststoffen	30,00
Band 82	Biogas and Mineral Fertiliser Production from Plant Residues of Phytoremediation	30,00
Band 83	Guidelines for a sustainable restoration, stabilisation and management of lakes in the tropics	30,00
Band 84	Entwicklung eines Schnelltestsystems zur Bestimmung brennstoffrelevanter Parameter von Ersatzbrennstoffen	30,00
Band 85	A Laboratory Simulation of Municipal Solid Waste Biodegradation in Landfill Bioreactors	30,00
Band 86	Potentials and Limitations of Energy Recovery from Municipal Solid Waste in Vietnam	30,00
Band 87	Risk-Based Management of Chemicals and Products in a Circular Economy at a Global Scale	30,00
Band 88	Biokunststoffe in Verwertung und Recycling	30,00
Band 89	The effect of sediment removal on selected processes of nitrogen cycle in Hoan Kiem Lake (Hanoi, Vietnam)	30,00
Band 90	Nachhaltiger Umgang mit nicht erneuerbaren Ressourcen - Stoffstrommanagement als Verbindung zwischen Abfallwirtschaft und Chemiepolitik	30,00
Band 91	Evaluation of informal sector activities in Germany under consideration of electrical and electronic waste management systems	30,00
Band 92	9. Biogastagung Dresden - Anaerobe Biologische Abfallbehandlung 2013	30,00
Band 93	Recycling von PVC aus Kunststoffabfällen mit Hilfe des Carbidprozesses	30,00
Band 94	Modellierung von Strömungs- und Stofftransportprozessen bei Kombination der ungesättigten Bodenzone mit technischen Anlagen.	30,00
Band 95	Untersuchungen zur Biofiltration flüchtiger Methylsiloxane	30,00

Band 96	Desintegration und anaerobe Verwertung bioabbaubarer Biokunststoffe	30,00
Band 97	10. Biogastagung Dresden - Anaerobe Biologische Abfallbehandlung 2015	30,00
Band 98	n.n. (Veröffentlichung folgt)	
Band 99	Entwicklung und Implementierung einer Methodik zur Erfassung der Grünschnittpotenziale von Siedlungs- und Verkehrsflächen in kommunale Verwertungsstrukturen	30,00
Band 100	Review of arsenic contamination and human exposure through water and food in rural areas in Vietnam Hanoi	30,00
Band 101	11. Biogastagung Dresden (21./22. September 2017): Anaerobe biologische Abfallbehandlung – Innovationen und Internationalisierung	30,00
Band 102	Modellgestütztes Monitoring von Störungen der Prozessbiologie in Biogasanlagen	30,00
Band 103	Managed Aquifer Recharge Assessment to Overcome Water Scarcity During the Dry Season in Costa Rica	30,00
Band 104	Abfallvergärungstagung 11.-13. März 2019 in Dresden	30,00
Band 105	The Impact of Membrane Fouling on the Removal of Trace Organic Contaminants from Wastewater by Nanofiltration	30,00
Band 106	New advances in the assessment of managed aquifer recharge through modelling	30,00
Band 107	Institutions, Groundwater Resources and Climate Change Adaptation in Northern Ghana	30,00

Die vergriffenen Bände 16, 27, 31, 32 und 39 können als CD zum Preis von 15,- € + Porto und Verpackung versendet werden.

Bestelladresse: Forum für Abfallwirtschaft und Altlasten e. V.

c/o Technische Universität Dresden
 Pratzschwitzer Straße 15
 01796 Pirna
 Germany
 Tel.: +49 351 463 441 38
 Fax: +49 351 463 441 17
 E-Mail: forum@mail.zih.tu-dresden.de

